

UNCLASSIFIED

AD NUMBER
AD865505
NEW LIMITATION CHANGE
TO Approved for public release, distribution unlimited
FROM Distribution authorized to U.S. Gov't. agencies and their contractors; Critical Technology; Nov 1969. Other requests shall be referred to Air Force Weapons Lab., Attn: WLRX, Kirtland AFB. NM 87117.
AUTHORITY
Air Force Weapons Lab ltr dtd 30 Nov 1971

THIS PAGE IS UNCLASSIFIED

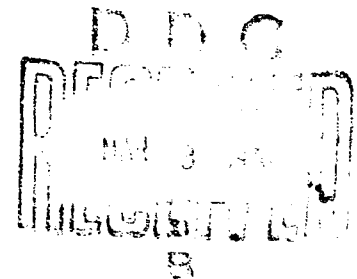
AFWL-TR-69-96

AFWL-TR-  
69-96

AD 865505

## CLASSIFICATION OF MATERIALS BY SHOCK PROPERTIES

L. Seaman  
R. F. Williams  
J. T. Rosenberg  
D. C. Erlich  
R. K. Linde



Stanford Research Institute  
Menlo Park, California 94025  
Contract F29601-67-C-0087

TECHNICAL REPORT NO. AFWL-TR-69-96

November 1969

AIR FORCE WEAPONS LABORATORY

Air Force Systems Command  
Kirtland Air Force Base  
New Mexico

Reproduced by the  
CLEARINGHOUSE  
for Federal Scientific & Technical  
Information Springfield Va. 22151

This document is subject to special export controls and each transmittal to foreign governments or foreign nationals may be made only with prior approval of AFWL (WLRX) , Kirtland AFB, NM, 87117.

AFWL-TR-69-96

ACCESSION FOR	
CPRT	WHITE SECTION <input type="checkbox"/>
DDG	BUFF SECTION <input checked="" type="checkbox"/>
UNCLASSIFIED	<input type="checkbox"/>
IDENTIFICATION	
BY	
DISTRIBUTION AVAILABILITY CODES	
DIST.	AVAIL. AND/OR SPECIAL
2	

AIR FORCE WEAPONS LABORATORY  
Air Force Systems Command  
Kirtland Air Force Base  
New Mexico

When U. S. Government drawings, specifications, or other data are used for any purpose other than a definitely related Government procurement operation, the Government thereby incurs no responsibility nor any obligation whatsoever, and the fact that the Government may have formulated, furnished, or in any way supplied the said drawings, specifications, or other data, is not to be regarded by implication or otherwise, as in any manner licensing the holder or any other person or corporation, or conveying any rights or permission to manufacture, use, or sell any patented invention that may in any way be related thereto.

This report is made available for study with the understanding that proprietary interests in and relating thereto will not be impaired. In case of apparent conflict or any other questions between the Government's rights and those of others, notify the Judge Advocate, Air Force Systems Command, Andrews Air Force Base, Washington, D. C. 20331.

DO NOT RETURN THIS COPY. RETAIN OR DESTROY.

CLASSIFICATION OF MATERIALS BY SHOCK PROPERTIES

L. Seaman  
R. F. Williams  
J. T. Rosenberg  
D. C. Erlich  
R. K. Linde

Stanford Research Institute  
Menlo Park, California 94025  
Contract F29601-67-C-0087

TECHNICAL REPORT NO. AFWL-TR-69-96

This document is subject to special export controls and each transmittal to foreign governments or foreign nationals may be made only with prior approval of AFWL (WLRX), Kirtland AFB, NM, 87117. Distribution is limited because of the technology discussed in the report.



FOREWORD

This report was prepared by Stanford Research Institute, Menlo Park, California, under Contract F29601-67-C-0087. The research was performed under Program Element 61102H, Project 5710, Subtask RAS1114 (previously 15.018 and 15.025), and was funded by the Defense Atomic Support Agency (DASA).

Inclusive dates of research were May 1967 to March 1969. The report was submitted 10 October 1969 by the Air Force Weapons Laboratory Project Officer, Lt Mark Ferdman (WLRX). The former project officer was Captain G. P. Crotwell (WLRP).

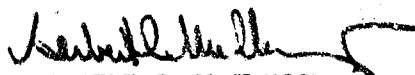
Information in this report is embargoed under the US Export Control Act of 1949, administered by the Department of Commerce. This report may be released by departments or agencies of the US Government to departments or agencies of foreign governments with which the United States has defense treaty commitments, subject to approval of AFWL (WLRX), Kirtland AFB, NM, 87117.

The contractor's account reference number is SRI Project PGU 6736.

This technical report has been reviewed and is approved.



MARK A FERDMAN  
Lt, USAF  
Project Officer



HERBERT C. McCLAMMY  
Major, USAF  
Chief, X-Ray Branch



HARRY F. RIZZO  
Lt Colonel, USAF  
Chief, Radiation Division

## ABSTRACT

(Distribution Limitation Statement No. 2)

A new experimental technique was developed for determining loading and unloading stress-volume paths directly from gage measurements; theoretical models were formulated for stress relaxation and the Bauschinger effect; Hugoniot information was generated from impact experiments on aluminum alloys, titanium alloys, and a woven quartz-phenolic; and the new experimental technique and Bauschinger calculations were applied to the aluminum alloys. The new experimental technique provides for measurement of complete loading and unloading paths (in  $\sigma$ - $v$  stress-particle velocity and stress-volume planes) rather than the discrete Hugoniot or release points previously obtained. The technique is applicable to the examination of nonsteady-state, nonisentropic flow, yield point phenomena, strain-hardening, the Bauschinger effect and strain-rate (or stress-relaxation) effects. The technique is based on the entire stress or particle-velocity records obtained from a series of gages embedded in a specimen. Four stress relaxation models were implemented in the SRI PUFF wave propagation code, and computations were made to obtain representative results. Criteria were suggested for selecting a model based on the precursor attenuation and separation of precursor and main wave. The Bauschinger model implemented in the SRI PUFF code exhibits the smooth unloading adiabat and high rarefaction velocity observed in our experiments on 6061-T6 and 2024-T8 aluminum alloys. The marked differences between the wave shapes and attenuation rate from the Bauschinger model and those obtained with the usual elastic-plastic model makes use of the Bauschinger model imperative if unloading and attenuation are of interest. Experiments with Ti-50A, Ti-6Al-4V, and Ti-13Cr-11V-3Al titanium served to map Hugoniots from 15 to 750 kbar, indicate Hugoniot elastic limits, and show an  $\alpha \rightarrow \omega$  phase transformation at 50 kbar in Type 50A. Preliminary experiments on a three-dimensional woven quartz phenolic resulted in Hugoniot data from 10 to 200 kbar and indicated a shock-wave structure that is very different from that observed in homogeneous solids.

# CONTENTS

<u>Section</u>	<u>Page</u>
I INTRODUCTION	1
1. Scope	1
2. Material Behavior Under Study	2
3. Materials	4
4. Background on Stress Relaxation Models	5
5. Background on Rate-Independent Models	11
II THEORETICAL MODEL DEVELOPMENT	15
1. Introduction	15
2. Nature of the SRI PUFF Computer Code	15
3. Stress Relaxation Models	24
4. Bauschinger Model	41
III EXPERIMENTAL METHODS	49
1. Theory of Data Reduction for Multiple Embedded Gages	49
2. Experimental Techniques	55
IV STUDY OF ALUMINUM	69
1. Introduction	69
2. Dynamic Experiments	70
3. Calculations for 2024-T8 Aluminum	82
4. Calculations for 6061-T6 Aluminum	88
5. Summary of Results	92
V STUDY OF TITANIUM	99
1. Introduction	99
2. Dynamic Experiments	101
3. Initial and Terminal Observations of Shocked Titanium Specimens	110
VI STUDY OF WOVEN QUARTZ PHENOLIC	115
1. Introduction	115
2. Material Description	115
3. Gas Gun and HE Experiments	117
4. Theoretical Calculations	125
VII SUMMARY AND RECOMMENDATIONS	129
1. Summary	129
2. Recommendations	130

## CONTENTS (Concl.)

<u>Section</u>	<u>Page</u>
APPENDIX I: TEST RUNS AND LISTING OF THE SRI PUFF 2 COMPUTER CODE	133
APPENDIX II: QUASI-STATIC AND ACOUSTIC DATA	257
REFERENCES	273
DISTRIBUTION	278

## FIGURES

<u>Figure</u>	<u>Page</u>
1 A Distance(X) - Time(t) Diagram Showing Coordinate Layout and Order of Calculations in the SRI PUFF Code	17
2 Common Forms of Pressure and Stress Hugoniots	20
3 Stress Profiles Following Impact in a Material Represented by Model 1 (Simple Anelastic)	31
4 Stress Profiles Following Impact in a Material Represented by Model 4 (Two Parameter)	32
5 Stress Profiles Following Impact in a Material Represented by Model 2 (Band)	38
6 Stress Profiles Following Impact in a Material Represented by Model 3 (Gilman)	39
7 Relationship Between Deviatoric Stress and Specific Volume Obtained from 50-kbar Tests in 2024-T8 Aluminum	44
8 Experimental Arrangement for Gas Gun Attenuation Shots	56
9. Side View of HE Flyer Systems B, D. and E for Generating Uniaxial Strain Loading and Unloading States	59
10 A Distance(X) - Time(t) Diagram Showing Shock and Rarefaction Waves Caused by Impact	60
11 Symmetrical Impact Experiment (HE System E) to Determine Hugoniot Data and Shock Wave Profiles	62
12 Measured Unloading Calibration of Manganin Element in Soda-Lime Glass	67
13 Stress-Particle Velocity Hugoniot Data for 2024-T8 and 6061-T6 Aluminum	71
14 Stress-Volume Hugoniot Data for 2024-T8 and 6061-T6 Aluminum	72
15 Typical Manganin Transducer Records Obtained from Impacts in 6061-T6 Aluminum	75
16 Interface Stress Histories Recorded by Manganin-Glass Gages Behind Aluminum Targets (50 kbar Impacts)	76
17 Interface Stress Histories Recorded by Manganin-Glass Gages Behind Aluminum Targets (20 kbar Impacts)	77
18 Comparison of Stress Histories Recorded at Aluminum-Glass and Aluminum-Aluminum Interfaces	78
19 Average Instantaneous Impedance $\rho_0 D_0$ as a Function of Axial Stress from 50-kbar Experiments in Aluminum	79
20 Stress-Particle Velocity Compression and Release Paths from 50-kbar Experiments in Aluminum	80

# FIGURES (Cont.)

<u>Figure</u>		<u>Page</u>
21	Stress-Volume Compression and Release Paths from 50-kbar Experiments in Aluminum	80
22	Stress-Volume Path Reduced from Data for 2024-T8 Aluminum and a Computed Pressure-Volume Relation	84
23	Comparison of Computed and Recorded Stress Histories from Impacts with 2024-T8 Aluminum at 50 kbar	86
24	Comparison of Computed and Recorded Stress Histories from Shot 13,532 in 4.48-mm-Thick 2024-T8 Aluminum Target	89
25	Comparison of Computed and Recorded Stress Histories from Shot 13,532 in 8.96-mm-Thick 2024-T8 Aluminum Target	90
26	Comparison of Computed and Recorded Stress Histories from Shot 13,529 in 25.42-mm-Thick 2024-T8 Aluminum Target	91
27	Stress-Volume Path Reduced from Data on 6061-T6 Aluminum and A Computed Pressure-Volume Relation	92
28	Relationship Between Deviatoric Stress and Specific Volume Obtained from 50 kbar Tests in 6061-T6 Aluminum	93
29	Comparison of Computed and Recorded Stress Histories From Impacts with 6061-T6 Aluminum at 50 kbar	94
30	Comparison of Computed and Recorded Stress Histories from Shot 13,559 in 8.21-mm-Thick 6061-T6 Aluminum Target	95
31	Comparison of Computed and Recorded Stress Histories from Shot 13,559 in 4.86-mm-Thick 6061-T6 Aluminum Target	96
32	Comparison of Computed and Recorded Stress Histories from Shot 13,530 in 25-mm-Thick 6061-T6 Aluminum Target	97
33	Stress-Particle Velocity Hugoniot and Release Data for Titanium Alloys	102
34	Stress-Volume Hugoniot Data for Titanium Alloys	103
35	Stress-Particle Velocity Hugoniot Data at Low Stresses for Titanium Alloys	104
36	Stress-Volume Hugoniot Data at Low Stresses for Titanium Alloys	105
37	Manganin Stress Records from Test G589 on Type 50A Titanium and Test G791 on Ti-6Al-4V Titanium	108
38	Photomicrograph of Type 50A Titanium Sample After Being Shocked to 56 kbar	111

# FIGURES (Concl.)

<u>Figure</u>		<u>Page</u>
39	Photomicrograph of Ti-13V-11Cr-3Al Titanium Specimen After Being Shocked to 70 kbar	113
40	Shock Velocity-Particle Velocity Hugoniot Data for 3-D Weave Quartz Phenolic	119
41	Stress-Particle Velocity Hugoniot Data for 3-D Weave Quartz Phenolic	120
42	Recovered 3-D Weave Quartz Phenolic Target and Aluminum Gas Gun Projectile Head Which Impacted It. Impact Velocity = 0.85 mm/ $\mu$ sec, Impact Stress = 37 kbar	122
43	Comparison of Computed and Recorded Stress Histories for Shot 13,422	124
44	Typical manganin wire/C-7 Transducer Records of Stress-Time Profiles Induced in C-7 by High-Stress (HE) and Low-Stress (Gas Gun) Shock in 3-D Weave Quartz Phenolic	126
45	Test 1c: Sample Plot of Stress Deviator (Curves plotted by computer from calculated results)	158
46	Test 1c: Summary Plot of All Time Edits	159
47	Test 1c: Summary of Stress Histories at Four Jedit Locations	160
48	Test 2: Summary Plot of Time Edits	168
49	Test 2: Summary of Stress Histories at Three Jedit Locations	169
50	Test 2: Sample Plot of Stress Deviator	170
51	Test 3: Summary Plot of Time Edits	178
52	Test 3: Summary of Stress Histories at Six Jedit Locations	179
53	Test 3: Sample Plot of Stress Deviator	180
54	Test 4: Summary Plot of Time Edits	188
55	Test 4: Summary of Stress Histories at Six Jedit Locations	189
56	Test 4: Sample Plot of Stress Deviator	190

# FIGURES (Concl.)

<u>Figure</u>		<u>Page</u>
57	Test 5: Summary Plot of Time Edits	198
58	Test 5: Summary of Stress Histories at Six Jedit Locations	199
59	Test 5: Sample Plot of Stress Deviator	200
60	Test 6: Summary Plot of Time Edits	208
61	Test 6: Summary of Stress Histories at Six Jedit Locations	209
62	Test 6: Sample Plot of Stress Deviator	210



# TABLES

<u>Table</u>	<u>Page</u>
1 Parameters of Explosively Launched Flyer Plate Systems	58
2 Measured Static Properties of Aluminum Alloys	70
3 Hugoniot Data for 6061-T6 Aluminum	73
4 Hugoniot Data for 2024-T8 Aluminum	74
5 Aluminum Peak Rarefaction Velocities	83
6 Parameters for the Bauschinger Model for 2024-T8 and 6061-T6 Aluminum	87
7 Properties of Tested Titanium Alloys	100
8 Hugoniot Data for Titanium	106
9 Comparison of Static and Dynamic Yield Strength in Titanium	107
10 Rarefaction and Shock Velocities in Titanium Alloys	110
11 Detailed Material Description of 3-D Quartz Phenolic	116
12 "Hugoniot" Data for 3-D Quartz Phenolic	118
13 Aluminum: Number of Specimens Tested	144
14 Titanium: Number of Specimens Tested	145
15 Titanium Data from Static Tests (Average Values)	147
16 Aluminum Data from Static Tests (Average Values)	148
17 Static Test Parameter Variation for Titanium	149
18 Static Test Parameter Variation for Aluminum	150
19 Acoustic Velocity Measurements	153
20 Illustration of Variability of Elastic Constants Derived from Acoustic Velocity Measurements	154
21 Manufacturer's Data for Type 50A Titanium	155
22 Manufacturer's Data for Ti-6Al-4V Titanium	156
23 Manufacturer's Data for Ti-13Cr-11V-3Al Titanium	156

# NOMENCLATURE

$A'$	$(2\mu/3)/(K+4\mu/3)$ , an attenuation factor
$A'$	$(2\mu/3) \rho/(K+4\mu/3)^3$
$A_1, A_2$	functions of $\xi$ in Eq. 34
$B$	damping coefficient
$B_g$	fictitious gage velocity associated with propagation of a constant particle velocity level
$b$	Burger's vector
$C$	bulk modulus, EQSTC in program; a relaxation constant in Gilman's model
$C_0$	coefficient of quadratic artificial viscosity
$C_1$	coefficient of linear artificial viscosity
$C_L$	acoustic velocity, longitudinal
$C_R$	rarefaction velocity
$C_S$	acoustic velocity, shear
$D$	density; coefficient in Eq. 27, EQSTD in program
$D_g$	fictitious gage velocity associated with propagation of a constant stress level
$E$	Young's modulus; internal energy
$E_H$	internal energy on the Hugoniot
$E_{rad}$	radiated energy
$E_{ref}$	reference energy
$E_s$	sublimation energy, EQSTE in program
EQSTG	Gruneisen ratio in program
EQSTC	bulk modulus at zero stress
$F$	$(8/3\mu)(\partial\gamma/\partial t)$ , the stress relaxation function
$g$	stress relaxation function; a constant in Band's relaxation model
$H$	$\gamma-1$ , EQSTH in program
$K$	bulk modulus
$k$	constant
$k_0$	constant
$M$	constant in Eq. 4; mass between gages; shear modulus
$M_0$	initial shear modulus

$M_1$	strain-hardening modulus during loading
$M_2$	initial unloading shear modulus
$M_3$	strain-hardening modulus during unloading
$MU$	shear modulus in the computer program
$MUUN$	unloading shear modulus in the computer program
$MU_0$	initial value of shear modulus
$MU_1, MU_2$	coefficients in series expansion of shear modulus
$N_1, N_2$	exponent in equation for shear modulus during unloading
$N$	number of dislocations; $C/(E_s \rho_0)$ , EQSTN in program
$N_0$	initial number of dislocations
$N_m$	number of mobile dislocations
$N_{m0}$	initial number of mobile dislocations
$N_t$	total number of dislocations
$N_{t0}$	initial total dislocations
$N'_m$	value of $N_m$ at $t = t_0 + \Delta t$
$N'_t$	value of $N_t$ at $t = t_0 + \Delta t$
$n$	constant in Eq. 8
$P$	pressure
$P_H$	Hugoniot pressure
$P_{ref}$	reference pressure
$R$	resultant or total stress
$S$	coefficient in Eq. 27, EQSTS in program
$SD_f$	deviatoric stress at end of time increment
$SD_{ii}$	deviatoric stress in $i^{th}$ direction
$SD_0$	deviatoric stress at beginning of time increment
$S_{ii}$	principal stress in the $i^{th}$ direction
$T_1, T_2$	relaxation times
$T_y$	yield relaxation time constant
$T_{rlx}$	relaxation time
$t$	time
$t_0$	time at beginning of calculation cycle
$t_1, t_2$	arrival times of a stress level at positions $X_1$ and $X_2$
$t_a$	arrival time of the shock wave

$U$	particle velocity
$U_s$	shock velocity
$u$	particle velocity
$u_0$	initial particle velocity
$V$	specific volume
$V_0$	initial specific volume
$V_H$	specific volume on the Hugoniot
$v$	dislocation velocity
$v_m$	maximum dislocation velocity
$W$	slope in $x, t$ plane of line of constant particle velocity
$X$	position
$XPO$	exponent, $N_1$ , in the computer program
$XP$	exponent, $N_2$ , in the computer program
$x_1, x_2$	gage locations
$Y$	yield strength
$Y_0$	initial yield strength
$Y_1, Y_2$	yield strength at yielding during loading and unloading respectively
$Y_{avg}$	average of $Y_f$ and $Y_{old}$
$Y_f$	final value of $Y$ at end of time increment
$Y_{old}$	value of $Y$ at beginning of time increment
$YADD$	strain-hardening modulus in the program
$YADF$	ratio of strain-hardening moduli during unloading and loading in the program
$Y_0$	$Y_0$ in the program
$Z$	mass of a finite difference cell
$\alpha$	constant in Eq. 6
$\beta$	dislocation damping constant
$\Gamma$	Gruneisen's ratio
$\Gamma_0$	initial Gruneisen's ratio
$\gamma$	ratio of specific heats; plastic shear strain
$\epsilon$	strain; a constant in Band's relaxation model
$\epsilon_s$	static strain
$\epsilon_p$	plastic strain component

$\theta$	$SD/ SD $
$k$	Heaviside constant
$\lambda$	Lame's constant, a modulus
$\mu$	Lame's shear modulus; $\rho/\rho_0 - 1$ , strain
$\mu_m$	strain at maximum stress
$\nu$	Poisson's ratio
$\xi$	$ SD  - 2/3Y$ , excess of deviatoric stress above shear strength
$\rho$	density
$\rho_0$	initial density
$\rho_1$	density at yield during loading
$\rho_2$	density at unloading
$\rho_m$	density at maximum stress
$\sigma$	stress
$\sigma_0$	constant in Eq. 8; HEL after stress relaxation
$\sigma_{Hel}$	Hugoniot elastic limit
$\sigma_1$	Hugoniot elastic limit as a function of time
$\sigma_0$	initial amplitude of precursor
$\tau$	$3/4 SD$ , shear stress
$\tau_b$	$Y/2$ , shear stress to cause yielding
$\tau_0$	constant in Eq. 5
$\phi$	constant in Eq. 4; work-hardening coefficient in Gilman's model

AFWL-TR-69-96

This page intentionally left blank.

## SECTION I

### INTRODUCTION

#### 1. Scope

The gross features of shock wave propagation in solids appear to be fairly well understood. These features generally include an elastic precursor, a main (or plastic) shock wave, and a rarefaction or unloading wave. The simplest and most common model incorporating these effects is the model of ideal plasticity. For precise quantitative prediction of these waves, however, theoretical calculations based on the model of ideal plasticity are inadequate. The behavior of real materials is modified by stress-relaxation (time-dependent) effects, Bauschinger effect (difference in load and unload response), a nonlinear transition from elastic to plastic behavior, strain or work hardening, etc. (These terms are explained more fully later in this chapter.) Each of these effects is important for some materials. Each leaves its imprint on some portion of the wave profile and leads to a modification of the attenuation of a short-duration shock pulse.

The main objective of the present program was to develop methods for characterizing materials by their shock propagation behavior. These characterizations fall into two major categories:

- . Rate dependent: stress relaxation effect.
- . Rate independent: Bauschinger effect on unloading and a nonlinear transition from linear elastic to plastic behavior on loading.

Specific objectives were to:

- . Study the nature of stress relaxation effects in shock waves.
- . Investigate unloading or Bauschinger effects.
- . Relate shock properties to quasi-static and acoustic material properties.
- . Improve methods to experimentally study rate-dependent and rate-independent effects.
- . Develop or improve theoretical models for both rate-dependent and rate-independent effects and implement them in a wave propagation computer code.

- . Develop guidelines for ascertaining the relative importance of the several effects studied.

These objectives were pursued in an experimental study of three materials: aluminum (2 alloys), titanium (3 alloys), and a woven quartz phenolic. The theoretical study, which was directed mainly to the aluminum, led to the exploration of five computational models, which were incorporated into the SRI PUFF computer code.

The two main developments of this program are the theoretical models implemented in the SRI PUFF code and the development of a new method for obtaining complete loading and unloading paths from experimentally recorded stress-time profiles. These two topics occupy the Sections II and III of this report. Sections IV, V, and VI contain descriptions of each material studied. In the materials sections the experiments are described, the data analyzed, and comparisons are made with the theoretical models.

## 2. Material Behavior Under Study

The kinds of behavior studied in this program fall into the two broad categories: rate-dependent and rate-independent. The rate-dependent phenomena are associated with an apparent softening of a loaded material with time. If the material is loaded with a stress that remains at a constant level for some time, there is an instantaneous strain followed by a gradually increasing strain as long as the load remains: this response is called creep.<sup>\*</sup> Alternatively, one may observe that the instantaneous stress required to produce a constant strain in the material gradually decreases with time: this response is called stress relaxation. When the material is loaded at different strain rates, the successive states describe different stress-strain paths: this behavior is referred to as strain rate effects. Stress relaxation, creep, and strain rate effects are just different (but relatively interchangeable) descriptions of the basic time-dependent phenomena.

<sup>\*</sup> The term "creep" is usually associated with very long time intervals and slow loading rates. However, the concept of time-dependent increasing strain at constant stress is also applicable to shock loading rates. In fact, some analytical creep functions (such as Gilman (Ref. 5)) have been successfully used to predict time-dependent phenomena in shocks.



These time-dependent phenomena lead to predictable variations in the shape of shock waves. A common effect is the attenuation of the amplitude of a flat-topped wave or a precursor with distance. Another effect is the variation of wave front shape with propagation distance, particularly a broadening of the shock front and general rounding of the stress-time profiles. While the presence of this latter effect may suggest time-dependence of the material properties, this effect is not conclusive evidence of time-dependent material response. Time-independent material properties can also cause such an effect to occur.

Time-independent phenomena of particular interest are work hardening, the elastic-plastic transition, and the Bauschinger effect. The term work hardening (or strain hardening) refers to the tendency of the yield strength of a material to increase as the material is strained. The hardening is often characterized by a work-hardening modulus relating the yield stress to the strain. The elastic-plastic transition refers to the region of the stress-strain curve where the material behavior is not linearly elastic nor purely plastic but is a mixture of nonlinear elastic and plastic. In a material such as aluminum in which no sharp yield point occurs the elastic-plastic transition describes the "gradual yielding" observed. This transition region is convex upward on the stress-volume plane and therefore leads to dispersion of compressional waves, an apparent decrease in the Hugoniot elastic limit\* (HEL) with distance, and a nonsteady transition region between a precursor and a main wave. (These are some of the same effects usually attributed to time-dependent material properties.)

The Bauschinger effect refers to a change in the stress-strain relations that occurs when the sign of the stress is reversed after partial loading. Usually this effect is interpreted as simply a reduction in yield strength, although bulk and shear moduli may also be affected. The present study of shock wave propagation has indicated that in fact, the entire shapes of the stress-strain relations may change when unloading occurs after shock compression. Because the Bauschinger effect comes into play only on unloading in the present case, it does not modify wave fronts. Instead the effect modifies the arrival time of rarefaction waves, the attenuation rate of stress waves, and the shape of the "back,"

\* The HEL is the maximum axial stress that the material can support (in uniaxial strain and under shock loading conditions) with a linearly elastic response. Such a limit of elastic behavior under static test conditions is referred to as the "proportional limit."

or unloading portion of the waves.

Hugoniot data may be considered part of the time-independent phenomena of interest to us on this project. A Hugoniot point is the final equilibrium state (hence, time-independent) of a material that has been traversed by a steady-state shock wave. For convenience, we have adopted the common practice of generalizing the definition to include any approximately steady-state stress wave, such as the gradually rising stress waves seen in porous materials, composites and rate-dependent media.

Real materials exhibit complex behavior that is a mixture of time-dependent and time-independent phenomena. Hence, some materials may show a combination of all the above effects.

### 3. Materials

Three materials were used in this study as the basis for theoretical model development and investigation of shock properties. The primary material was aluminum, with preliminary studies being performed also on titanium and a woven quartz phenolic.

Two alloys of aluminum--6061-T6 and 2024-T8--were selected especially to study stress relaxation phenomena. On the basis of earlier work, it was expected that the 2024-T8 would show significant stress relaxation and that 6061-T6 would not. In addition, we planned to investigate in detail the unloading behavior of these alloys because of its relevance to experimental studies on other materials. Considerable information on the loading behavior of these alloys was available so that we were able to deal immediately with unloading phenomena and precursor decay.

The preliminary study of titanium was undertaken to map the low-pressure (under 500 kbar) Hugoniot, to look for possible high-pressure phase transitions, to investigate strain-rate sensitivity, and to study release waves and attenuation. Three titanium alloys were selected: Ti-50A, commercially pure titanium all in the alpha phase; Ti-6Al-4V, an alloy with mixed alpha and beta phases; and Ti-13Cr-11V-3Al, an alloy that is entirely beta phase. The Ti-6Al-4V alloy was selected because it is a material of practical importance that has already been studied at intermediate strain-rates, where it exhibited strain-rate sensitivity. The Ti-50A and Ti-13Cr-11V-3Al alloys were chosen to study independently the behavior of each of the constituent phases of the Ti-6Al-4V alloy.

The quartz phenolic was supplied to SRI by the Air Force Weapons Laboratory for a preliminary investigation. Although the effort with this material was much more limited, the purpose was essentially the same: to perform a series of experiments and attempt to establish which shock phenomena are important.

#### 4. Background on Stress Relaxation Models

Early work on stress-relaxation was presented by Malvern in 1951 (Ref. 1). He derived basic relaxation equations that are essentially the same as those currently used. His formulation, which is for a rod with stress-free sides, is

$$\frac{\partial \sigma}{\partial t} = \frac{E \partial \epsilon}{\partial t} - g(\sigma, \epsilon) \quad (1)$$

where

$\sigma, \epsilon$  = stress and strain in the direction of the shock motion

$E$  = Young's modulus

$g$  = the relaxation function

$t$  = time

Malvern solved a simple impact problem using

$$g = k [\sigma - f(\epsilon)] \quad (2)$$

where  $k$  is a constant. This model is one form of the standard linear anelastic model described by Zener in 1948 (Ref. 2). In Malvern's model the relaxation time is proportional to  $1/k$ , a constant, and is therefore independent of stress level.

In 1963, Taylor (Ref. 3) performed a series of impact experiments on Armco iron. The results showed that relaxation was very rapid at high stresses and slower at low stresses. The variation of precursor amplitude with distance of travel was independent of the initial impact stress except for distances less than 2 mm. These experimental data did not correlate well with predictions of the standard model that uses a constant relaxation rate independent of initial stress level. Taylor constructed a stress-relaxing model by making  $k$  in Eq. 2 a function of the square of the impact velocity. The predictions of this model were in reasonable agreement with his data.

In 1964 Lubliner (Ref. 4), presented a general discussion of methods for solving wave propagation problems in rate-dependent and rate-independent

materials. He noted that characteristic lines are usually curved for rate-dependent materials, and for both types of materials there is a discontinuity in slope between loading and unloading characteristics.

In 1965 a basic paper on the formulation of a dislocation model for stress relaxation was presented by Gilman (Ref. 5). The model of the stress relaxation term is presented as  $\dot{\gamma}$ , the plastic shear strain rate. He introduced

$$\dot{\gamma} = bNv \quad (3)$$

where

$N$  = the number of dislocations per square centimeter

$b$  = the Burger's vector

$v$  = the dislocation velocity

and then derived equations for  $N$  and  $v$  from the available experimental data. These equations are

$$N = (N_0 + M\gamma) e^{-\phi\gamma} \quad (4)$$

$$v = v_0 e^{-\tau_0/\tau} \quad (5)$$

where

$N_0$  = the number of initial dislocations

$v_0$  = the maximum velocity

$\tau$  = the shear stress

$M$ ,  $\phi$  and  $\tau_0$  = constants

The model was intended to be applicable to both creep and shock front behavior. Computations showed that, according to the model, there is an incubation time during which dislocations multiply but no significant yielding occurs. Subsequently, the yielding occurs rapidly for a time and then reaches a third, or equilibrium, state when yielding ceases.

Taylor (Ref. 6) reanalyzed his data of 1963 two years later with the aid of Gilman's model above. He augmented the model to include work hardening, using

$$\dot{\gamma} = bNv = b(N_0 + \alpha\gamma) v_0 e^{-(\tau_0 + \phi\gamma)/\tau} \quad (6)$$

where

$\gamma$  = the plastic shear strain

$\alpha, \tau_0$  = constants

$\phi$  = a work-hardening coefficient

The constitutive equation for the material was written in the form

$$\dot{\sigma} = (\lambda + 2\mu) \dot{\epsilon} - 8/3\mu \dot{\gamma} \quad (7)$$

where

$\lambda, \mu$  = Lamé's constants

$\sigma, \epsilon$  = stress and strain

The first term on the right-hand side represents elastic strain; the second is the plastic strain. With the use of Eq. 6 for  $\dot{\gamma}$ , Eq. 7 became a stress-relaxing constitutive relation. With this equation for  $\dot{\sigma}$ , the relaxation time decreases exponentially with stress and therefore has the appropriate form to fit Taylor's data on Armco iron. Taylor considered only the rate of precursor decay, not the changes in the entire wave form.

In 1965, Dorn, Mitchell, and Hansen (Ref. 7) presented a summary of current information on athermal, thermally activated, viscous, and relativistic effects associated with dislocation mechanisms. For each of the first three effects they suggested several possible micromechanisms. It seems likely that at relatively low strain rates ( $< 100/\text{sec}$ ) thermally activated mechanisms govern dislocation velocity. But at higher strain rates the velocity is proportional to the excess of shear stress above the static limit: this proportionality suggests a viscous damping mechanism. While it was theoretically predicted that dislocation velocities could approach but not exceed the shear wave velocity, there was no experimental evidence to support this view. No dislocation velocities had yet been measured above half the shear velocity.

Maiden and Green in 1966 (Ref. 8) reported results of an experimental study of rate sensitivity in 6061-T6 and 7075-T6 aluminum, annealed Ti-6Al-4V titanium, and several other materials. The testing rates ranged from  $10^{-3}$  to  $10^4$  in./in./sec. A comparison of stress-strain curves derived from tests up to  $10^3$  in./in./sec showed no rate sensitivity in either aluminum alloy but considerable rate sensitivity in titanium. In the titanium, the strain rate effect was described by equations of two forms:

$$\sigma - \sigma_s = k_0 \log (\dot{\epsilon}/\dot{\epsilon}_s) \quad (8)$$

$$\sigma - \sigma_s = k_1 (\dot{\epsilon})^n \quad (9)$$

where

- $\sigma$  = stress at a given strain
- $\sigma_s$  = the static stress at the same strain
- $\dot{\epsilon}$  = the strain rate
- $\dot{\epsilon}_s$  = the "static" strain rate
- $n, k$  = constants

The data fit the second form best, with  $n = 1/5$ . The corresponding forms of  $g$  (see Eq. 1) are

$$g = k_2 e^{(\sigma - \sigma_s)/\sigma_0} \quad (8a)$$

$$g = k_3 (\sigma - \sigma_s)^5 \quad (9a)$$

where the  $k$ 's and  $\sigma_0$  are constants. Both of these forms indicate a relaxation time which is very short for high stresses, longer for low stresses. Equation (8a) is reminiscent of Gilman's model, (Eq. 5), while Eq. 9a exhibits a time constant inversely proportional to stress to the fourth power.

In 1966, Ahrens and Duvall (Ref. 9) reported some stress relaxation studies in Sioux quartzite. They derived a complex form for  $g$  from their data. The precursor appeared to attenuate linearly with distance in the rather narrow range for distances which they used.

Butcher and Munson in 1967 (Ref. 10) conducted tests on 1060 aluminum and 4340 steel, both of which are known to be rate-sensitive. Results showed precursor decay and separation of the precursor and main wave. In several stress-time records there was a dip in stress between the two waves. The attenuation appeared to be approximately exponential with distance. Approximate theoretical computations of precursor decay were made using several possible relaxation models. Best results were obtained using Gilman's model with plastic shear strain rate in the form

$$\dot{\sigma} = bNv = bN_0 (1 + \alpha\gamma) e^{-\phi\gamma} v_0 e^{-T_0/T} \quad (10)$$

In 1966 Johnson (Ref. 11) investigated three models: the standard anelastic model, Gilman's model, and a model suggested by Band (Ref. 12). Johnson provided a derivation of each model and modified them appropriately for application to a material with a specified static yield strength. His basic equation, corresponding to Eq. 7, for one-dimensional flow is

$$\frac{\partial \sigma'}{\partial t} = 4/3 \frac{\mu}{\rho} \frac{\partial \rho}{\partial t} - 8/3 \mu \frac{\partial \gamma}{\partial t} \quad (11)$$

where

$\sigma'$  =  $\sigma - p$ , the deviatoric stress

$\rho$  = the density

$\mu$  = the shear modulus

$\gamma$  = the plastic shear strain

The form of Eq. 11 emphasizes the fact that only the deviatoric stress is being relaxed; the pressure component follows an elastic, rate-independent, law. Johnson showed that for many forms of  $\gamma$ , the precursor decay could be found simply from

$$\frac{d\sigma}{dt} = - 4/3 \mu \frac{\partial \gamma}{\partial t} \quad (12)$$

where

$\sigma$  = the stress at the precursor

$t$  = the arrival time of the precursor

$\gamma$  = plastic shear strain evaluated from the unshocked state

In the modified Gilman model presented by Johnson, dislocation velocity is

$$v = v_0 \exp ( - \tau_0 / (\tau - Y/2) ) \quad (13)$$

where  $Y$  = the static yield strength. Band's model, as presented by Johnson, has a form identical to the modified one of Gilman, except that the number of mobile dislocations is given by a set of simultaneous equations. These equations express rates of growth, pinning, and annihilation of mobile and total dislocations.

In 1967 Anderson et al., (Ref. 13) conducted impact experiments on 2024 aluminum and polyethylene and measured precursor attenuation in the aluminum. The experimental results were compared with predictions based on four models: the three treated by Johnson plus a new two-parameter model. The new model was based on the constitutive relations

$$\frac{\partial \sigma}{\partial t} = K(\rho) \frac{\partial \rho}{\partial t} - \frac{\sigma - \sigma_1}{T_1} \quad (14)$$

$$\frac{\partial \sigma_1}{\partial t} = - \frac{\sigma_1 - \sigma_0}{T_2} \quad (15)$$

where

$T_1, T_2$  = relaxation times

$K(\rho)$  = the elastic modulus function

$\sigma_1$  = the Hugoniot elastic limit, a function of time

$\sigma_0$  = the Hugoniot elastic limit after complete relaxation.

This model was formulated to provide both for the phenomenon of precursor decay and for separation of the two waves.

In 1967, Wilkins (Ref. 14) described several possible stress-relaxation functions. He presented typical results from one- and two-dimensional wave propagation calculations.

Historically, the first matter of interest was the rate of precursor decay. This could be measured quantitatively and was clearly an indication of strain rate effects. Stress-relaxation models from various other applications were brought in to explain the decay. As more information became available from dislocation dynamics, more appropriate models were developed to predict precursor decay. Interest was then kindled in describing the entire wave front: precursor, main wave, and region between these waves. At present, models are just being developed to represent all these phenomena.



## 5. Background on Rate-Independent Models

Attenuation of shock waves occurs when the unloading or rarefaction portion of the wave overtakes the shock front. Therefore, the relative magnitudes of the shock velocity and rarefaction velocity govern the attenuation. Early studies of attenuation considered only a hydrodynamic model. In later studies, which are discussed below, it was presumed that the rarefaction behavior is a function of both elastic and plastic effects.

The groundwork for considering elastic-plastic behavior of materials was laid by Morland (Ref. 15) with his analysis of wave propagation in rods. He used the ideal plastic model for his work.

In 1960, Al'tshuler et al., (Ref. 16) used plate slap experiments to study rarefaction velocities up to pressures of 3 Mbar. They employed the stress attenuation rate as a means of measuring the rarefaction velocity. Even at the highest stresses, they noted the presence of initial elastic rarefaction waves. However, they disregarded these waves and concentrated on the slower-moving plastic rarefactions.

Curran (in 1963, Ref. 17) conducted a series of plate slap experiments at lower stress than Al'tshuler et al. used to study specifically the elastic rarefaction waves. His results showed clearly that elastic-plastic effects led to much higher attenuation rates than predicted by hydrodynamic models. He was able to match the attenuation rate in computations by assuming a large (tenfold) increase in yield strength during compression.

Barker, Lundergan, and Herrmann (Ref. 18) used plate slap experiments up to 20 kbar to determine the loading and unloading stress-strain relation. They noted a small strain rate effect during loading and a significant Bauschinger effect during unloading. Even at the low stress of 10 kbar, the elastic rarefaction velocity was some 5 percent higher than the initial loading velocity. Under static loading, the Bauschinger effect in aluminum had been well documented by Buckley and Entwistle in 1956 (Ref. 19). In the static work there was an elastic unloading to zero stress. Reloading in the opposite sense followed a stress-strain relation with a much reduced slope. The shapes of these static reloading waves appeared to be geometrically similar for different yield strength levels.

Jones and Holland (in 1964) conducted plate slap experiments with SAE 1018 steel in both the annealed condition and with 20 percent cold work (Ref. 20). The precursor (and hence the yield strength) was about half as large in the cold-worked material as in the annealed: this was interpreted as evidence of a strong Bauschinger effect.

Further evidence that static stress-strain data are pertinent to dynamic studies was gained by Butcher and Canon (Ref. 21) in 1964. They performed plate impact tests on 4340 steel to determine the loading stress-strain relation. There were important effects of work hardening and some stress-relaxation effects, but the authors concluded that the static and dynamic constitutive relations could be taken as identical without serious error.

In 1967, Erkman and Christensen (Ref. 22) conducted plate slap experiments on aluminum at 110 and 340 kbar to study unloading velocities and attenuation. Calculations were made with the ideally plastic model and with an elastoplastic model in which shear modulus and yield strength varied with density. The best correlation with experimental attenuation rates was obtained by assuming a yield strength that increased threefold. A sharp step in the unloading wave (which is predicted by the elastoplastic model) was not observed in the experiments.

In 1968, Barker (Ref. 23) presented a discussion of plate slap experiments in which a more refined rear-surface measurement technique was used. The data led him to the formulation of a Bauschinger model in which there was an initial elastic release to zero deviatoric stress. Then for continued unloading, the yield stress was allowed to increase gradually according to the expression

$$Y = 4/3Y_0 (1 - e^{-800\epsilon_p}) \quad (16)$$

where

- $Y$  = the initial yield strength
- $\epsilon_p$  = the plastic strain component

Calculations with this model compared well with experimentally recorded wave shapes.

The history of attenuation studies shows a gradual realization of the complexity of rarefaction waves. First, hydrodynamic calculations were

used, found inadequate, and replaced by ideally plastic models. The next step was to construct ad hoc models that would exhibit some type of Bauschinger effect. In this report we present a Bauschinger model in a general form that should be applicable to a wide range of materials.

This page intentionally left blank.

## SECTION II

### THEORETICAL MODEL DEVELOPMENT

#### 1. Introduction

Four models for stress-relaxation and one model constituting a Bauschinger effect are outlined in this section. All of the models are sufficiently complex that it is necessary to implement them in a wave propagation computer program to study their effects. The models were inserted into the SRI PUFF code, an artificial viscosity code originally developed for the study of porous materials. These models affect only the computation of deviatoric stress; so the basic program remains unaffected. As background for the introduction of the models, the nature of the code is presented in this section; the models are then described.

#### 2. Nature of the SRI PUFF Computer Code

##### a. Introduction

The SRI PUFF code is a program for analyzing one-dimensional wave propagation caused either by the deposition of radiation in the materials or by the impact of two materials. The code contains a novel integration scheme for solving the governing equations of motion. The equations of state for solid, porous, liquid, and gaseous materials are provided. In the present project, the available equation of state routines were augmented to include stress-relaxation and Bauschinger effects. As background for the discussion of these effects, brief descriptions of the integration procedure and of the equation of state for a solid are given.

##### b. Integration Scheme

The solution procedure for the governing equations of motion is called the method of artificial viscosity. With this method no discontinuous shock fronts occur, but a shock is represented by a stress wave front spread over 3 to 5 cells. Hence, the equations of continuous flow are applicable throughout the flow field.

The continuous flow equations are the one-dimensional Lagrangian equations of motion. These equations are reduced to a form in which only first-order derivatives occur. To improve accuracy and stability, integral

statements of the equations are used in preference to differential equations wherever possible.

The following set of Lagrangian equations are merely presented; they were derived by Richtmyer (Ref. 24) and many other authors.

$$X_1 = X_0 + 1/2 (U_0 + U_1) \Delta t \quad (\text{velocity}) \quad (17)$$

$$U_1 = U_0 + \frac{\Delta R}{D \Delta X} \Delta t \quad (\text{momentum}) \quad (18)$$

$$D_1 = \frac{Z}{\Delta X + \Delta U \Delta t} \quad (\text{mass}) \quad (19)$$

$$E_1 = E_0 + R (1/D_0 - 1/D_1) + E_{\text{rad}} \quad (\text{energy}) \quad (20)$$

$$R_1 = F(E_1, D_1, \dots) \quad (\text{equation of state}) \quad (21)$$

where

$X$  = coordinate location

$U$  = coordinate velocity

$D$  = density

$E$  = internal energy

$R$  = total mechanical stress

$\Delta U = (\partial U / \partial X) \Delta X$

$t$  = time

$E_{\text{rad}}$  = internal energy added by radiation

$Z$  = cell mass ( $D \Delta X$ )

Subscripts 0 and 1 refer to times  $t_0$  and  $t_1 = t_0 + \Delta t$ . The unsubscripted  $R$  and  $D$  values appearing in the equations are chosen to provide an accurate representation of the conservation laws.

For convenience in visualizing the progress of the computation, and distance-time ( $X-t$ ) plot with coordinate points, cells between coordinates, and time steps is shown in Fig. 1. The computations proceed from left to right, one coordinate at a time, updating coordinate location, velocity, density, etc., to the new time  $t_1$ . (Order of the computations is given by the numbers in Fig. 1.) The integration scheme

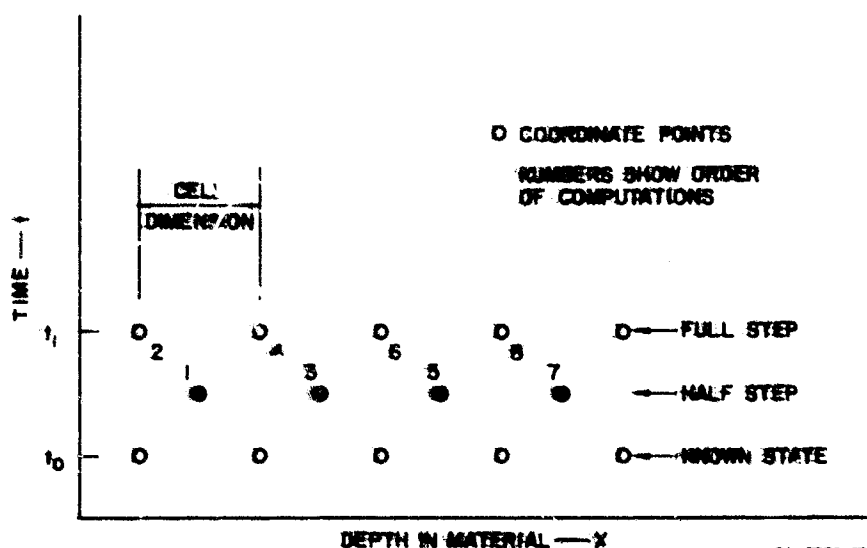


FIGURE 1 A DISTANCE (x)-TIME (t) DIAGRAM SHOWING COORDINATE LAYOUT AND ORDER OF CALCULATIONS IN THE SRI PUFF CODE

used in the SRI PUFF code is a mixture of the leapfrog method proposed by von Neumann and Richtmyer (Ref. 25) and the two-step Lax-Wendroff method (Ref. 24).

In the leapfrog scheme the basic computation cycle proceeds as follows:

$$X_c \rightarrow U_m \rightarrow E_m \rightarrow R_m \rightarrow U_c \rightarrow X_c$$

That is, density is computed from the coordinate position, energy and stress from density, velocity from stress, and coordination location from velocity. The cycle is then repeated in succeeding time steps. The natural procedure, as used in the leapfrog scheme, is to associate  $X$  and  $U$  with the coordinate points and to associate the density, energy, and stress with the midcell points (hence, the subscripts  $c$  and  $m$  in the cycle notation). The midcell quantities are also associated with a time  $1/2 \Delta t$  ahead of the  $X$  and  $U$  values. Thus, the midcell quantities are evaluated at the halfstep locations on the  $X$ - $t$  plot of Fig. 1. In the two-step Lax-Wendroff method, all quantities are computed at both the coordinate and midcell points. Quantities occurring at coordinates

(and full time steps) are treated as primary; the halfstep (midcell) quantities are secondary and are computed by more approximate equations.

In the SRI PUFF code the basic  $X_c - D_m - R_m - U_c - X_c$  cycle is treated as primary. In addition a subsidiary cycle  $x_m - D_c - R_c - U_m - X_m$  is used to generate the other quantities so that all quantities are available at both coordinate and midcell points. The main advantages of the method are (1) elimination of an iterative solution for stress usually required with the leapfrog scheme (thereby decreasing computation time), and (2) diminution of the oscillations in the stress at shock fronts that commonly occur with the Lax-Wendroff method.

### c. Equation of State

The equations of state considered here relate the stress in a material to its internal energy, density, and the previous state. The material may be in solid, liquid, or gaseous states.\*

For convenience in formulating the equations of state for both solid and porous materials, the stress tensor will be defined as the sum of a pressure and a deviator stress tensor. The pressure is defined as

$$P = \frac{1}{3} (S_{11} + S_{22} + S_{33}) \quad (22)$$

where the S's are stresses on any three mutually orthogonal planes. The deviator stress is the variation of any normal stress from the average:

$$SD_{11} = S_{11} - P \quad (i = 1, 2, 3) \quad (23)$$

For the one-dimensional strain case to be treated here, the stresses can be conveniently taken in the directions of principal stresses, so that only normal stresses occur. Furthermore, the deviatoric stresses are simply related as follows

$$SD_{22} = SD_{33} = -\frac{1}{2} SD_{11} \quad (24)$$

\* The code also provides for materials that are initially porous. Spalling, separation, and recombination, and thermal strength reduction are also handled by the code. These provisions, which are not of direct interest here, are discussed in Reference 26.



so that the only stress quantities to be computed are  $SD_{11}$  and  $P$ . The pressure is computed as a function of two or more of the other thermodynamic quantities. The deviator stress is computed from a stress-strain relation. The stress is then found as a simple sum of  $SD_{11}$  and  $P$ . With this separation of stress into two components, the development of an equation of state requires the construction of two relationships, one for pressure and one for deviator stress.

#### (1) Pressure

The equation used here for pressure is of the form

$$P = P(E, V) \quad (25)$$

which says that pressure is a function of specific internal energy and specific volume only. The thermodynamic quantities entropy and temperature are not considered explicitly. Equation 25 defines a surface in E-P-V space.

An equation of state represents equilibrium states. Therefore as a material undergoes gradual changes, such as heating, compression, etc., the successive states describe a path on the equation-of-state surface if there is no heat conduction, stress relaxation, or other nonequilibrium process occurring. If the material is compressed by passing through a steady-state shock front and the initial and final states are equilibrium states, then these states lie on the equation-of-state surface. These initial and final states are connected by a straight line, the Rayleigh line, which lies on or above the surface, for the usual, concave-upward, surfaces. The states of transition within a shock front are not states of thermodynamic equilibrium and hence do not necessarily lie on the surface.

Shock experiments lead to the determination of a Hugoniot or Rankine-Hugoniot curve which is a line on the equation-of-state surface. This line is the locus of final states that can be obtained by a steady-state shock transition from a given initial state. A common form for a pressure-volume Hugoniot is shown in Fig. 2.

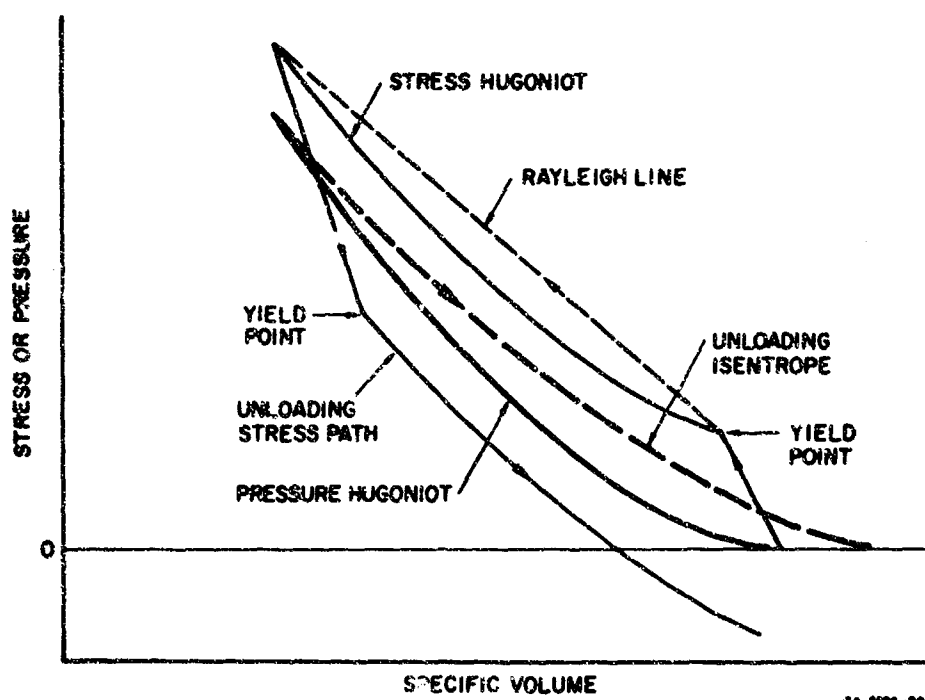


FIGURE 2 COMMON FORMS OF PRESSURE AND STRESS HUGONIOTS

During compression there is some increase in internal energy, so that the Hugoniot does not lie in a single P-V plane.

As a reminder of the role of stress in the compression of the solid, consider the stress-volume Hugoniot of Fig. 2. During compression the stress is greater than the pressure; on unloading, the stress decreases rapidly to yielding and then follows a stress adiabat below the pressure adiabat. The unloading adiabat lies to the right of the Hugoniot for materials that expand during heating. For such materials less internal energy is released by the adiabatic decompression (expansion) than was absorbed during the shock compression.

The pressure equation of state for a solid and the subroutine for calculating it in SRI PUFF are essentially the same as those in PUFF 66 (Ref. 27). The equation of state is described by two analytical equations (one for compression and one for expansion) and is bounded for negative stresses by a spall criterion.

The equation used to describe compression is the Mie-Grüneisen equation

$$P - P_{REF} = \frac{\Gamma(V)}{V} (E - E_{REF}) \quad (26)$$

where

$P_{REF}$  and  $E_{REF}$  = a point on some reference curve at the same specific volume  $V$

$\Gamma(V)$  = the Grüneisen ratio.

Equation 26 has been derived on the assumption that  $\Gamma$  is a function of  $V$  only. Equation 26 provides a means for extrapolating the information of a known P-V relation (such as a Hugoniot) to other values of internal energy. Because the Hugoniot is the P-V relation that is most likely to be known, the computations are constructed so that the Hugoniot is the reference curve used. The Hugoniot P-V equation is presumed to be in the form

$$P_H = C\mu + D\mu^2 + S\mu^3 \quad (27)$$

where

$$\mu = \frac{\rho}{\rho_0} - 1 = \frac{V_0}{V} - 1$$

The internal energy along the Hugoniot is

$$E_H = \frac{1}{2} P_H (V_0 - V_H) \quad (28)$$

Equation 28 is based on the assumption that the initial internal energy is zero and that the Hugoniot is concave upward. In general, the latter assumption excludes consideration of phase changes. Also, the relation is strictly true only if the stress Hugoniot coincides with the pressure Hugoniot; however, at high pressures there is usually little inaccuracy introduced by this approximation. With the aid of Eqs. 27 and 28, the Mie-Grüneisen equation takes the following form in the program:

$$P = (C\mu + D\mu^2 + S\mu^3) * \left(1 - \frac{\Gamma\mu}{2}\right) + \Gamma\rho E \quad (29)$$

In the computer program the Grüneisen ratio  $\Gamma_0$  at initial density is taken as a constant, EQSTG. Then  $\Gamma$  is treated as a function of density such that  $\Gamma\rho$  is constant.

At a constant volume, Eq. 29 is a linear relation between pressure and energy; hence, constant volume lines on the equation-of-state surface are straight lines. The Mie-Grüneisen equation of state is used for densities greater than the initial density. Thus on the equation-of-state surface the straight line  $V = V_0$  is the boundary between the Mie-Grüneisen equation and an expansion equation.

The expansion equation, which is unchanged from PUFF 66 (Ref. 27), meets four requirements:

- It joins smoothly to the Mie-Grüneisen equation along  $V = V_0$ .
- It expands like  $PV = (\gamma - 1)E$  at large expansions (like a gas).
- It provides a linear relation between  $P$  and  $E$  for constant  $V$ .
- It accounts for the partition of internal energy into components for kinetic energy and for intermolecular bond disintegration (sublimation).

An equation that satisfies these requirements is

$$P = \rho \left[ H + (\Gamma - H) \left( \frac{\rho}{\rho_0} \right)^{\frac{1}{2}} \right] * \left\{ E - E_S \left[ 1 - \exp \left( N (1 - \rho_0 / \rho) \rho_0 / \rho \right) \right] \right\} \quad (30)$$

where

$\rho$  = density

$\rho_0$  = initial density

$\Gamma$  = Grüneisen ratio

$H = \gamma - 1 = C_p / C_v - 1$  for expansion at low densities

$N = C / (\Gamma E_S \rho_0)$

$E_S$  = sublimation energy

$C$  = coefficient in Eq. 29, the bulk modulus at low pressures

In the PUFF 66 manual (Ref. 27) a value of 0.25 is suggested for  $H$ .

The sublimation energy as defined there is the difference between the internal energy of the solid material at ambient conditions and the internal energy of the fully expanded vapor at a temperature of absolute zero.

## (2) Deviatoric Stress

The deviatoric stress equation takes a simpler form in the PUFF formulation than does the pressure equation. The deviatoric stress for a perfectly plastic material is

$$SD = \frac{4}{3} \int_{\rho_0}^{\rho} \mu \frac{d\rho}{\rho} \quad \text{for } |SD| < \frac{2}{3} Y \quad (31)$$

otherwise

$$|SD| = \frac{2}{3} Y \quad (32)$$

where

$\mu$  = the shear modulus

$\rho$  = the density

$Y$  = the yield strength

Stress relaxation and Bauschinger effects modify the deviatoric stress computation. These modifications are dealt with in the following subsections.

### 3. Stress Relaxation Models

#### a. Introduction

Materials subjected to shock stresses respond in a manner somewhat different from materials subjected to quasi-static loading. We have attempted to understand and to characterize some aspects of the shock behavior through the use of time-dependent, theoretical models. Attention was focused on materials with no phase change in the stress range being studied. When a shock wave whose amplitude is below a critical over-driving stress traverses such a material, it generally is assumed to proceed initially at the elastic sound speed as a single shock front. As the wave progresses, it breaks into two waves, an elastic precursor and a slower main or plastic wave. The amplitude of the precursor may decrease as the wave proceeds, eventually reaching a steady-state value. The thickness of material through which the shock wave progresses before the precursor reaches its steady-state value varies from material to material. For some materials the thickness is so small (less than 1 mm) that experimental observation of the effect is difficult; for others it is very large.

Three time-dependent phenomena of the shock front were of concern:

- Attenuation of precursor amplitude as a function of distance into a material.
- Degree of separation of main and precursor wave.
- Attenuation of the stress amplitude of the main wave and modification of other state variables.

It was assumed that these effects are caused by time-dependence of the yield strength or deviatoric stress and that there is no time variation in the relationship between volume and hydrostatic pressure. All of the theoretical models we employed are based on the assumption that the deviatoric stress may exceed two-thirds the static yield strength for brief periods of time. Following the passage of a shock front, the deviatoric stress gradually decays back to its static limit.

The four models are introduced by first considering a model with a sufficiently general form to encompass all of the others. This model is

a specification of the stress relaxing function  $F$  in the flow relation presented by Johnson (Ref. 11)

$$\frac{\partial SD}{\partial t} = \frac{4}{3} \frac{\mu}{\rho} \frac{\partial \rho}{\partial t} - \theta F \quad (33)$$

where

$SD$  = the deviatoric stress

$\mu$  = the shear modulus

$\rho$  = density

$F = \frac{8}{3} \mu \frac{\partial \gamma}{\partial t}$ , the relaxation function

$\gamma$  = plastic shear strain

$\theta = \frac{SD}{|SD|}$

In this general model  $F$  is given by

$$F = A_1(\xi) + A_2(\xi)(t - t_a) + A_3(\xi)(t - t_a)^2 + \dots \quad (34)$$

$$= 0 \text{ for } t < t_a$$

where

$\xi = |SD| - \frac{2}{3} Y$ , the excess of deviatoric stress above yielding

$Y$  = the yield strength

$A_i$  = functions of  $\xi$

$t$  = time

$t_a$  = arrival time of the precursor shock front

With the formulation of this model we can now discuss some general results obtainable with all of the models. The deviatoric stress may initially exceed  $2/3 Y$  in the shock front and then decay gradually from the high elastic value to the static value. Because of the decreasing deviatoric stress, the amplitude of the elastic precursor also attenuates as the shock wave proceeds into the material. The first term of Eq. 34 provides for attenuation of the precursor. The second and subsequent terms provide for separation of the precursor and main waves, and for details of the wave shapes. The simple ideally plastic model can be represented by the function  $F$  with  $A_1 = A_3 = \dots = 0$  and

$$A_2 = -\frac{4}{3} \frac{\mu}{\rho} \frac{\partial \rho}{\partial t} \frac{1}{t - t_a} \quad (35)$$

Because  $A_1$  is zero there is no precursor decay. With  $A_2$  as in Eq. 35, there is a clear separation of the wave fronts.

Many physical mechanisms have been proposed as a basis for the formulation of the function  $F$ . Among these are the standard anelastic solid model (Model 1), several dislocation models, and a varying yield strength. The dislocation models considered here are those of Band (Model 2) and Gilman (Model 3) as modified by Johnson (Ref. 11). The yield strength model (Model 4) was suggested by Anderson, et al (Ref. 3). We will first discuss Model 1, then Model 4, and then turn to Models 2 and 3.

#### b. Model 1

The first and simplest stress relaxation model is that of the standard anelastic solid. It is basically a one-parameter mathematical model in which the deviatoric stress  $SD$  is allowed to relax to its static value  $2/3 Y$  exponentially, with an adjustable time constant. Examples of its development are given by Zener (Ref. 2), Kolsky (Ref. 28), Johnson (Ref. 11), and Duvall (Ref. 29). For this model the deviatoric stress satisfied the relations

$$\frac{\partial SD}{\partial t} = \frac{4}{3} \frac{\mu}{\rho} \frac{\partial \rho}{\partial t} - \theta \frac{|SD| - 2/3 Y}{T_{rlx}} \quad \text{for } |SD| > 2/3 Y \quad (36)$$

and

$$\frac{\partial SD}{\partial t} = \frac{4}{3} \frac{\mu}{\rho} \frac{\partial \rho}{\partial t} \quad \text{for } |SD| \leq 2/3 Y \quad (37)$$

where  $T_{rlx}$  is the deviatoric stress decay time parameter and the derivatives are taken at Lagrangian coordinates. In Eq. 36 the first term on the right gives the elastic value of the deviatoric stress, and the second term provides for relaxation to the static value  $2/3 Y$ . For this model the yield strength is assumed constant and  $T_{rlx}$  is the only adjustable parameter in the model.

The current value of the deviatoric stress at each coordinate is computed from Eqs. 36 and 37 in the PUFF code. The finite difference approximation to Eq. 36 for the case where  $|SD| > 2/3 Y$  and  $\partial \rho / \partial t$  is constant throughout the time interval is:



$$SD_f = \frac{2}{3} \theta Y + (SD_o - \frac{2}{3} \theta Y) \exp\left(-\frac{\Delta t}{T_{rlx}}\right) + \frac{4\mu \Delta \rho T_{rlx}}{3 \rho_{avg} \Delta t} \left[1 - \exp\left(-\frac{\Delta T}{T_{rlx}}\right)\right] \quad (38)$$

where

$SD_o$  = deviatoric stress at beginning of the time step of duration  $\Delta t$  and density change  $\Delta \rho$

$SD_f$  = final deviatoric stress

$\rho_{avg}$  = average density during time interval

If  $|SD|$  becomes less than  $\frac{2}{3} Y$  or changes sign during the time interval, then the  $SD - t$  path must be broken into segments. For each segment the correct equation (Eq. 36 or 37) is used.

An alternate physical derivation of the standard anelastic solid can be given from the point of view of dislocation dynamics. For this purpose Eq. 36 is rewritten to emphasize that the third term represents the plastic shear strain rate  $\dot{\gamma}$ :

$$\frac{\partial SD}{\partial t} = \frac{4}{3} \frac{\mu}{\rho} \frac{\partial \rho}{\partial t} - \frac{8}{3} \mu \dot{\gamma} \theta \quad (39)$$

The plastic strain rate is related to the number of mobile dislocations  $N_m$ , the velocity of these dislocations  $v$ , and the Burger's vector  $b$  by

$$\dot{\gamma} = b v N_m \quad (40)$$

The model assumes that the dislocation velocity is governed by phonon viscosity, so that

$$v = \frac{b}{\beta} (\tau - \tau_b) \quad (41)$$

where

$\beta$  = the dislocation damping coefficient

$\tau_b = Y/2$ , the lattice stress that must be exceeded before dislocations can move

$\tau = 3/4 |SD|$ , shear stress

By combining Eqs. 39 through 41 we obtain

$$\frac{\partial SD}{\partial t} = \frac{4}{3} \frac{\mu}{\rho} \frac{\partial \rho}{\partial t} - \frac{24b^2 N_m}{\beta} (SD - \frac{2}{3} \theta Y) \quad (42)$$

Comparison of Eqs. 42 and 36 shows that the two formulations of Model 1 are equivalent if

$$T_{rlx} = \frac{\beta}{2\mu^2 N_m} \quad (43)$$

Model 1 is the only one of the four relaxation models for which the precursor amplitude can be obtained analytically in closed form from the various relaxation parameters. From Zener (Ref. 2), the precursor wave amplitude  $\sigma$  decays in time according to:

$$\sigma = \sigma_{HEL} + (\sigma_o - \sigma_{HEL}) \exp\left(-\frac{At}{T_{rlx}}\right) \quad (44)$$

where

$\sigma_o$  = initial amplitude of the precursor  
 $\sigma_{HEL} = \frac{Y}{2} \left( \frac{K}{\mu} + \frac{4}{3} \right)$ , the Hugoniot elastic limit or final amplitude of the precursor.

$$A = \frac{2\mu/3}{K+4\mu/3}$$

$K$  = bulk modulus

$\mu$  = shear modulus

Using the relationships

$$\frac{\partial \sigma}{\partial x} = \frac{\partial \sigma}{\partial t} \frac{\partial t}{\partial x} \quad \text{and} \quad \frac{\partial t}{\partial x} = \sqrt{\frac{K+4\mu/3}{\rho}} = C_{El}$$

which is the elastic shock velocity, the equation for the precursor amplitude decay in distance can be shown to be

$$\sigma = \sigma_{HEL} + (\sigma_o - \sigma_{HEL}) \exp\left(-\frac{A'x}{T_{rlx}}\right) \quad (45)$$

where

$x$  = distance into the material from the impact interface

$$A' = \frac{2\mu}{3} \sqrt{\frac{\beta}{(K + 4\mu/3)^3}} \quad (46)$$

From either equation, it is evident that decreasing the parameter  $T_{rlx}$  will hasten the decay of the precursor.

c. Model 4

The next model to be discussed is a two-parameter model similar to that of Anderson et al. (Ref. 13). It is identical to Model 1, except that the yield strength is allowed to vary (the yield strength is constant in Model 1). Under rapid loading, the yield strength reaches a high elastic value and then decays exponentially in time until it reaches its initial value. It is governed by the following equation

$$Y = Y_0 \text{ until } |SD| = \frac{2}{3} Y$$

then

$$\begin{aligned} \frac{\partial Y}{\partial t} &= 2 \frac{\mu}{\rho} \left| \frac{\partial \rho}{\partial t} \right| - \frac{Y - Y_0}{T_y} \text{ for } |SD| > 2/3 Y \text{ and } \text{SIGN} \left( \frac{\partial \rho}{\partial t} \right) = \text{SIGN} (SD) \\ &= - \frac{Y - Y_0}{T_y} \text{ for } |SD| > 2/3 Y \text{ and } \text{SIGN} \left( \frac{\partial \rho}{\partial t} \right) = - \text{SIGN} (SD) \\ &= 0 \text{ for } |SD| \leq 2/3 Y \end{aligned} \quad (47)$$

where

$Y_0$  = static yield strength

$T_y$  = yield strength time parameter

Meanwhile, SD obeys Eq. 36 where  $Y$  in that equation is now the current value of the yield strength calculated from Eq. 47, instead of the constant value as in Model 1. In Model 4, therefore, there are two adjustable time parameters, one directly governing the deviatoric stress decay rate ( $T_{rlx}$ ), and another governing the yield strength decay rate ( $T_y$ ), the latter also indirectly affecting the deviatoric stress decay.

In the computer program, Eqs. 36 and 47 are used to calculate current values of yield strength and deviatoric stress. These equations cannot be solved simultaneously in closed form so we approximate a solution to Eq. 47, for  $|SD| > 2/3 Y$ , during a time increment  $\Delta t$

$$Y_f = Y_{old} - (Y_{old} - Y_0) \frac{t}{T_y} + \frac{2\mu \Delta \rho}{\rho} \left( 2 - \frac{\Delta t}{T_y} \right) \quad (48)$$

where

$$k = \text{a constant} = \begin{cases} 1 & \text{if SIGN } (\Delta \rho) = \text{SIGN } (SD) \\ 0 & \text{if SIGN } (\Delta \rho) \neq \text{SIGN } (SD) \end{cases}$$

$Y_{old}$  = yield strength value at beginning of time step  $t_0$

$Y_f$  = yield strength value at  $t = \Delta t + t_0$

In this solution we have used the approximation

$$\exp\left(-\frac{\Delta t}{T_y}\right) \approx 1 - \frac{\Delta t}{T_y} \quad (49)$$

which is valid only  $\Delta t \ll T_y$  (which is the case in all of our PUFF calculations). Inserting  $Y_f$  from Eq. 48 into Eq. 38, we obtain the approximate solution for the deviatoric stress at the end of the time step:

$$\begin{aligned} SD_f = & \frac{2}{3} \theta Y_{avg} + (SD_o - \frac{2}{3} \theta Y_{avg}) \exp\left(-\frac{\Delta t}{T_{rlx}}\right) \\ & + \frac{4\mu \Delta \rho T_{rlx}}{3 \rho_{avg} \Delta t} \left[ 1 - \exp\left(-\frac{\Delta t}{T_{rlx}}\right) \right] \end{aligned} \quad (50)$$

where

$$Y_{avg} = \frac{1}{2} (Y_f + Y_{old})$$

Models 1 and 4 are implemented in the subroutine RELAX. The basic scheme of RELAX is as follows: a tentative value for the deviatoric stress is obtained by using the nonrelaxation Eq. 37. This tentative value and the initial value are compared with  $2/3 Y$  to determine if the deviator is outside the elastic zone. If not, the subroutine returns this tentative value as the new deviatoric stress. Otherwise the time during which the deviator remains outside the elastic zone is calculated and this time value is used to relax the yield strength (for Model 4 only) and to calculate a new deviatoric stress using Eq. 38. This new value for the deviator is again compared with  $2/3 Y$  to see if the relaxation has caused the deviatoric stress to reenter the elastic zone,

in which case a revised relaxation time is determined and used to re-calculate the relaxing quantities. The subroutine then returns with the new value of the deviatoric stress and, for Model 4, the revised value of the yield strength.

The results of a series of representative computations for Model 1 in the SRI PUFF code are shown in Fig. 3. Model 1 yields no distinct separation between the precursor and the main wave until after the precursor has "relaxed" to its Hugoniot elastic limit. As indicated in Fig. 3, there is a gradual rise in stress from the precursor to the main wave peak. The precursor decay curves in Fig. 3 are obtained explicitly using Eq. 41 and they appear to closely match the precursor amplitudes from the PUFF calculations.

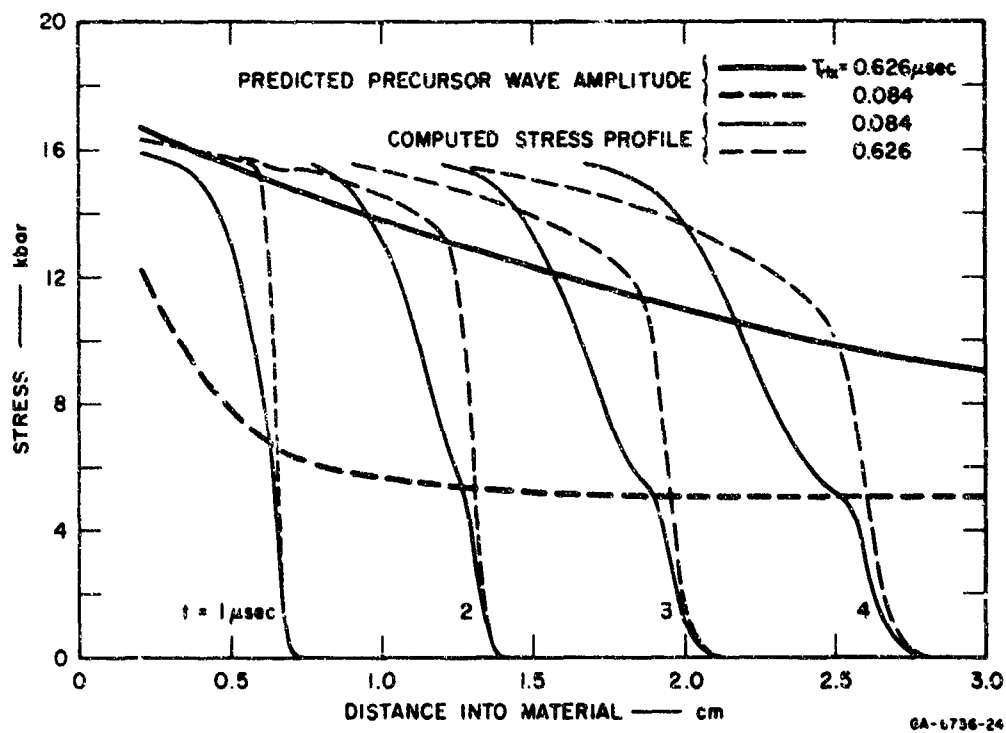


FIGURE 3 STRESS PROFILES FOLLOWING IMPACT IN A MATERIAL REPRESENTED BY MODEL 1 (Simple Anelastic)

The two-parameter variable yield strength model (Model 4) exhibits a distinct two-wave structure, and a noteworthy result of the model is the decrease in stress immediately following the precursor and before the main wave front. Although it has not been possible to derive a closed-form solution for either the precursor amplitude decay or the depth of the trough behind the precursor in terms of the parameters  $T_{rlx}$  and  $T_y$ , the following qualitative information can be obtained from Fig. 4: For a fixed  $T_{rlx}$ , a large  $T_y$  will produce a slowly decaying precursor amplitude and a deep trough behind the precursor. Decreasing  $T_y$  will speed up the precursor decay and decrease the depth of the trough (see curves 2-5 or 6-7 in Fig. 4), until at  $T_y = 0$  (i.e., the yield strength relaxes instantaneously to its static value), the model is identical to Model 1

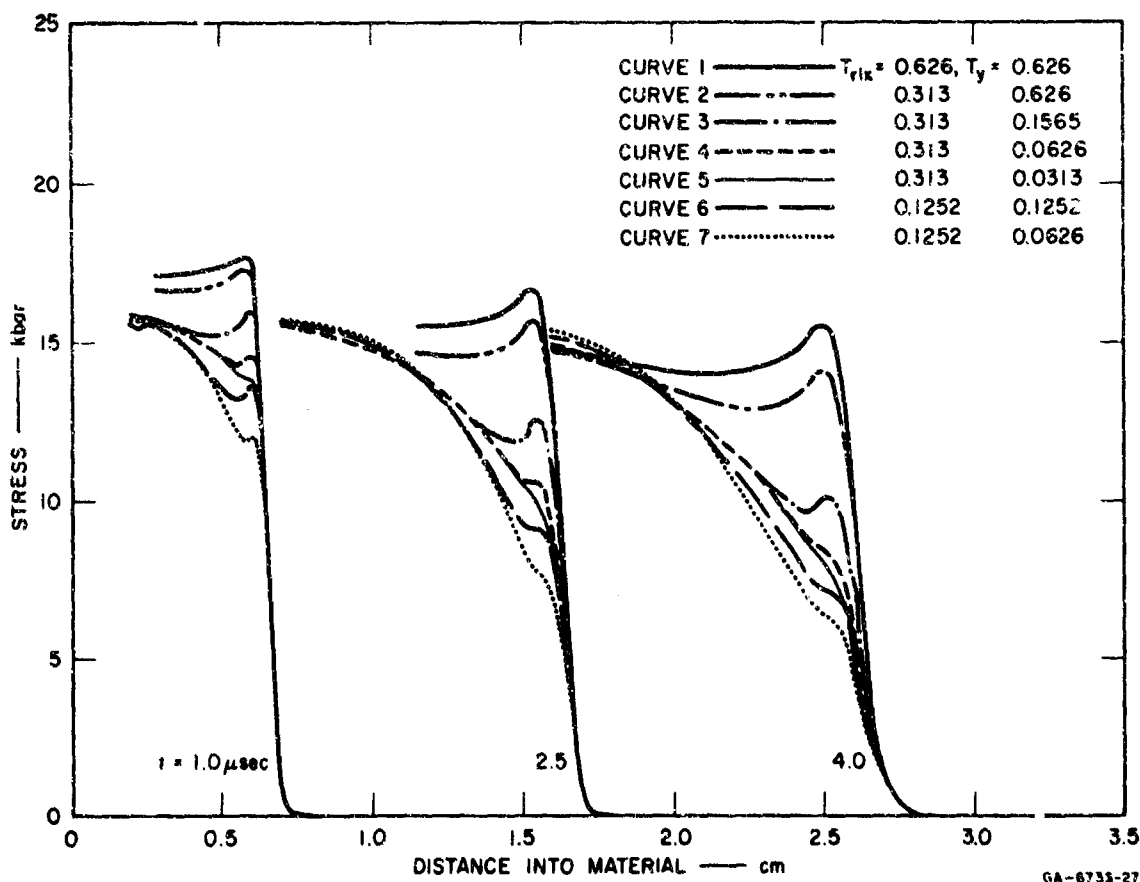


FIGURE 4 STRESS PROFILES FOLLOWING IMPACT IN A MATERIAL REPRESENTED BY MODEL 4 (Two Parameter)

and Eqs. 44 and 45 are valid. If, on the other hand,  $T_y$  is held constant and  $T_{rlx}$  varied (compare curves 1 and 2 or 4 and 7 in Fig. 4), the results show that a decrease in  $T_{rlx}$  will speed up the precursor amplitude decay, but have little or no effect upon the general shape of the shock front. Because no exact equation for precursor attenuation is available, it is not known how much of the precursor decay was caused by the finite difference nature of the calculations.

The two-parameter varying yield model exhibits some of the effects desired of the general two-parameter model described by Eq. 34, but not all of them. In Model 4 the effects of the two parameters are not separable: both affect precursor decay and wave separation. We believe that a more suitable two-parameter model can be generated. The basic purpose of the model is to represent a material with two important stress relaxation mechanisms. In real materials there will generally be a number of mechanisms operating and any two-parameter model will be a simplification of such behavior, intended to represent only the two most important mechanisms.

#### d. Models 2 and 3

The remaining two models were described by Johnson (Ref. 11) and are based on dislocation dynamics. Model 2 (the modified Band model) and Model 3 (the modified Gilman model) both use Eqs. 39 and 40 of the alternate derivation of Model 1, but then depart from Model 1 when relations governing the dislocation velocity and the number of mobile dislocations are considered.

For dislocation velocity, the following equation applies for both Band and Gilman models:

$$v = v_m \exp [-B/(\tau - \tau_b)] = v_m \exp [-B/(\frac{3}{4}|SD| - \frac{1}{2}Y)] \text{ for } |SD| > 2/3 Y$$

$$= 0 \text{ for } |SD| \leq 2/3 Y \quad (51)$$

where

$v_m$  = maximum dislocation velocity  
 $B$  = a constant

The mobile dislocations begin to move when the shear stress exceeds  $\tau_b$  (defined following Eq. 41) and increase in velocity as the shear stress increases. As seen in Eq. 40, the velocity is directly proportional to the relaxation rate of the deviator. From a physical standpoint, the movement of these dislocations relieves the excess shear stress in the material, and the dislocations will continue to move until the shear stress decreases below the lattice strength or until they become pinned.

The difference between the Band and Gilman models arises from the manner in which  $N_m$ , the number of mobile dislocations per unit volume is calculated (see Johnson (Ref. 11), pp. 27-33, for detailed derivation).

In the Band model,  $N_m$  is obtained from the simultaneous solution of:

$$\frac{dN_m}{dt} = g \xi (N_t - N_m) - \left( \frac{1}{T_1} + \frac{1}{T_2} \right) N_m \frac{v}{v_m} \quad (52)$$

and

$$\frac{dN_t}{dt} = \epsilon g \xi (N_t - N_m) - \frac{1}{T_2} N_m \frac{v}{v_m} \quad (53)$$

where

- $N_t$  = total number of dislocations (mobile and pinned) per unit volume
- $\xi$  =  $|\dot{\epsilon}| - 2/3 \dot{\gamma} = \frac{4}{3} (\dot{\epsilon} - \dot{\gamma}_b)$
- $T_1, T_2$  = adjustable time constants
- $\epsilon, g$  = other constants

In Eq. 52 the two terms on the right side represent the rate at which mobile dislocations are created (from pinned dislocations) and destroyed (by being pinned or migrating to a free surface or void), respectively. Similarly, the two terms on the right hand side of Eq. 53 represent the rate at which all dislocations are being created by a Frank-Read multiplication mechanism and destroyed by migration to a free surface or void. To use this model, the initial dislocation densities ( $N_{m0}$  and  $N_{t0}$ ) must



be specified, as well as Burger's vector ( $b$ ), the maximum dislocation velocity ( $v_m$ ), and the adjustable parameters ( $T_1$ ,  $T_2$ ,  $\epsilon$ ,  $g$ , and  $B$ ). Then for every cycle of the PUFF - code calculation,  $N_m$  and  $N_t$  are incremented for each cell in the material by:

$$N'_m = N_m + \left[ g \xi_{avg} (N_t - N_m) - \left( \frac{1}{T_1} + \frac{1}{T_2} \right) N_m \frac{v}{v_m} \right] \Delta t \quad (54)$$

$$N'_t = N_t + \left[ \epsilon g \xi_{avg} (N_t - N_m) - \frac{1}{T_2} N_m \frac{v}{v_m} \right] \Delta t \quad (55)$$

where

$$N'_m \text{ and } N'_t = \text{values of } N_m \text{ and } N_t \text{ at } t = t_0 + \Delta t$$

$$\xi_{avg} = 1/2 \left| SD' + SD \right| - 2/3 Y = \left| SD + \frac{2}{3} \frac{\mu \Delta \rho}{\rho_{avg}} \right| - 2/3 Y$$

$$\approx \xi \Big|_t = t_0 + \frac{\Delta t}{2}$$

$$SD' = \text{value of } SD \text{ at } t = t_0 + \Delta t$$

which is a valid solution to Eqs. 52 and 53 provided that  $N_m$  and  $N_t$  change by only a small fraction during one time step.

In the Gilman model,  $N_m$  is determined by

$$N_m = N_{m0} (1 + C\gamma) \exp(-\emptyset \gamma) \quad (56)$$

where  $C$  and  $\emptyset$  are constants. The mobile dislocation density is increased in proportion to the total plastic shear strain ( $\gamma$ ), which can be obtained from

$$\gamma = 1/2 \left[ \ln \frac{\rho}{\rho_0} - \frac{3}{4} \frac{(SD - 2/3 Y)}{\mu} \right] \quad (57)$$

where  $\rho_0$  = initial density (before shock wave). This equation holds only during initial compression.  $N_m$  decreases at a rate proportional to itself, to account for loss by migration to a surface or pinning. To use the Gilman model, one must specify the mobile dislocation density ( $N_{m0}$ ),

Burger's vector ( $b$ ), the maximum dislocation velocity ( $v_m$ ) and the adjustable constants ( $B$ ,  $C$ , and  $\phi$ ). The plastic shear strain is initialized at zero for all cells, and thereafter, whenever  $|SD| > 2/3 Y$ , the plastic shear strain is increased during a time step by:

$$\Delta \gamma = 1/2 \left| \frac{\Delta \rho}{\rho_{avg}} - \frac{3 \Delta SD}{4 \mu} \right| = \frac{3}{8 \mu} \left| \frac{4}{3} \frac{\mu \Delta \rho}{\rho_{avg}} - \Delta SD \right| \quad (58)$$

Note that the term in the parentheses on the far right hand side is just equal to the amount by which the deviator has been relaxed during the time step, since with no relaxation,  $\Delta SD = \frac{4}{3} \frac{\mu \Delta \rho}{\rho}$ , from Eq. 37. Therefore the total plastic shear strain at any time is just equal to  $3/(8\mu)$  times the total stress relaxation in that cell up to that time. This value for  $\gamma$  is used in Eq. 56 to calculate  $N_m$ , which is then used in Eqs. 39 and 40 to obtain the relaxation for the following cycle, which in turn is used to update  $\gamma$ . The accuracy of this iteration is controlled by the shortness of the time step.

Both Models 2 and 3 are implemented in the subroutine BANDRLX, which operates in a manner similar to that of RELAX insofar as the determination of the location of the stress deviator (in elastic or plastic zones) and calculation of the time during which stress relaxation takes place is concerned. Because of the iterative nature of the Band and Gilman schemes, a feature has been instituted in BANDRLX which enables each cycle of the PUFF calculation to be broken into several shorter time steps and a calculation to be made for each of these smaller times, with a resultant increase in accuracy.

The Band and Gilman models are both based on dislocation dynamics, and unfortunately, this is a field in which little is known quantitatively under the loading conditions of interest. There is little or no experimental data for determining the value of the various dislocation parameters (such as  $v_m$ ,  $\phi$ ,  $C$ ,  $g$ , etc.), some of which like  $N_{to}$  and  $N_{mo}$ , undoubtedly depend upon the history of the material specimen. Therefore, there is at this time no sound reason to expect that the Band or Gilman models will describe the shock phenomena more accurately than Model 4, for example, whose parameters are without real physical basis.

The attenuation rate of the precursor can be predicted analytically for these two models, and in fact, the same equation pertains to both. The equation was derived by Johnson (Ref. 11) as

$$\frac{dS}{dt} = -\frac{4}{3} \mu b v_m N_{mo} \exp \left[ -B / \left( \frac{3}{4} SD - 1/2 Y \right) \right] \quad (59)$$

This equation can be integrated numerically to obtain the precursor amplitude. Obviously, only those parameters that enter Eq. 59 can influence the attenuation rate.

Models 2 and 3 exhibit a fairly distinct two-wave shock front, depending to a large extent on the rate of dislocation multiplication in the material. For the case where there is no increase in the number of dislocations ( $C = 0$  for the Gilman model,  $g = 0$  for the Band model), the shock front is similar to that of Model 1 (see Figs. 5 and 6): a gradual rise in stress from the precursor to the main wave, with no significant change in slope. But when the dislocations are allowed to increase in number ( $C > 0$  for the Gilman model,  $g > 0$  and  $N_{to} > N_{mo}$  for the Band model), the shock front behind the precursor flattens out to some extent before the arrival of the main wave, and thus the two-wave pattern emerges. For the PUFF calculations upon which all of the curves in Figs. 5 and 6 are based, the following values for the various relaxation parameters were used, as suggested by Johnson (Ref. 11). For the Band model:

$$\epsilon = 0.9$$

$$T_1 = 1 \mu\text{sec}$$

$$T_2 = 4 \mu\text{sec}$$

For both Band and Gilman models:

$$B = 1.98 \times 10^{10} \text{ kbar}$$

$$v_m = 3.22 \times 10^5 \text{ cm/sec}$$

$$bN_{mo} = 5 \text{ cm}^{-1}$$

The values for the other parameters are shown in the figures. In addition to the effect of the parameters  $C$  and  $g$  on the shock front appearance, the graphs show that increasing  $N_{to}$  (in the Band model) will

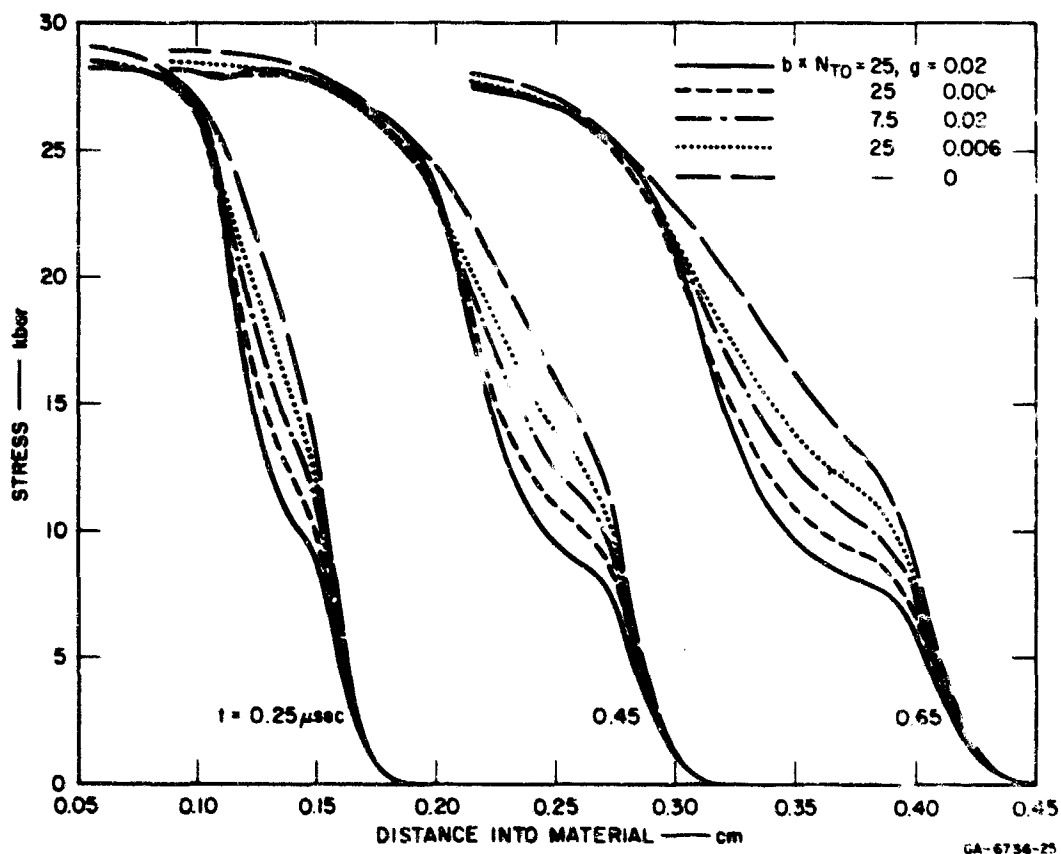


FIGURE 5 STRESS PROFILES FOLLOWING IMPACT IN A MATERIAL REPRESENTED BY MODEL 2 (Band)

increase the separation of the two waves (this is reasonable, since Eqs. 52 and 53 show that the dislocation multiplication rate is also dependent upon  $N_t - N_m$ ), while an increase in  $\phi$  (for the Gilman model) will have the opposite effect ( $\phi$  governs the rate of decrease of the mobile dislocation density). Qualitatively, the Band and Gilman models exhibit a nearly identical shock front appearance.

For both of these models the finite difference calculations have a serious effect on the amplitude of the precursor. According to Johnson's simplified analysis (Ref. 11),  $C$  and  $\phi$  in Gilman's model and  $N_{to}$ ,  $T_1$ ,  $T_2$ ,  $\epsilon$ , and  $g$  in Band's model should have no effect on the precursor decay. In Figs. 5 and 6 it is evident that there is an effect, presumably caused by the artificial viscosity and the finite size of the cells.

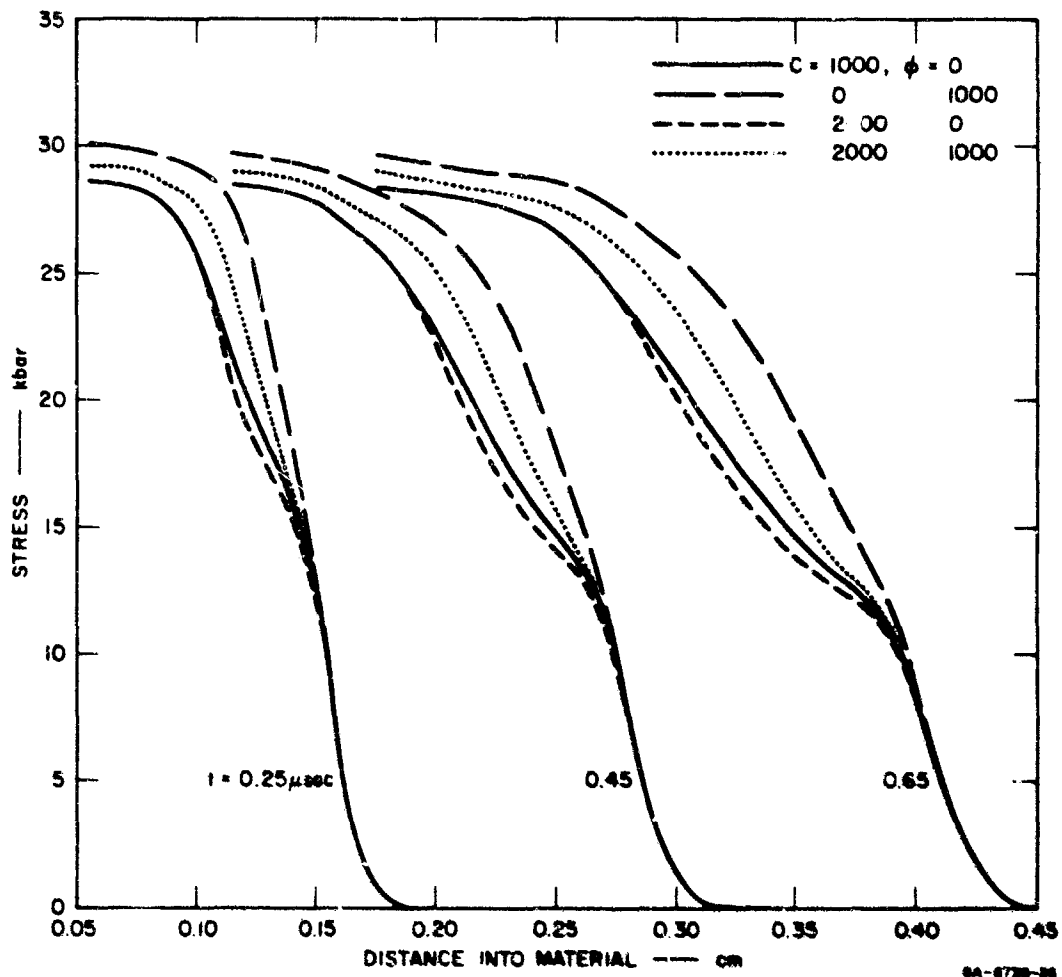


FIGURE 6 STRESS PROFILES FOLLOWING IMPACT IN A MATERIAL REPRESENTED BY MODEL 3 (Gilman)

#### e. Implementation in the Code

In the current version of the SRI PUFF code listed in Appendix I, all four stress relaxation models as well as the Bauschinger model (Model 5) are set up to run through the entire cycle of any impact-induced shock wave: compressive loading, unloading, tension, and reloading. The models are also available for use with shock waves caused by radiation deposition, although no verification test run has been made. A condition indicator is assigned to each cell in the PUFF calculation, to keep track of whether that cell is currently outside of the elastic zone ( $|SD| > 2/3 Y$ ), and hence undergoing relaxation, or within

the elastic zone ( $|SD| \leq 2/3 Y$ ), where relaxation is not applicable. The stress relaxation parameters are read in for each material along with all of the other material properties, so that different stress deviator models, including the elastic-plastic model, the Bauschinger model, and all of the relaxation models, can be used in the same calculation for different materials. In addition, two significant parameters for each model are selected and printed out in the periodic time edits and histories, along with the other shock parameters.

The subroutines for calculating the deviatoric stresses for the five models do not contain any COMMON declaration: All required information is brought in as formal parameters in the calling statement. Thus the subroutines are readily transferable to other types of artificial viscosity codes.

For each of the stress relaxation models, a series of test runs has been made with the SRI PUFF code. These runs are identical within each series, except that one or more of the relaxation parameters for that model are varied to determine the effect of the parameter on the calculation.

The results of the test runs show that all four models are similar in that there is an approximately exponential attenuation (in time or distance into the impacted material) of the precursor wave amplitude. But beyond that, there are significant differences among the various models, in the separation between the precursor and the main wave, and generally in the shape of the wave front.

#### f. Criteria for Choosing a Stress Relaxation Model

The feature of most prominence in studies of stress relaxation often is precursor attenuation. If this is the feature of main interest the model should be chosen first on the basis of the type of precursor attenuation it provides; that is, first choose the form for  $A_1(\xi)$  in Eq. 34. The form for  $A_1(\xi)$  may be chosen on the basis of measurements of precursor decay or from hypothesized dislocation mechanisms. For the latter criteria, it may be noted that only the variation of dislocation velocity with stress level appears to influence precursor attenuation. Some common forms for  $A_1(\xi)$  are provided in Models 1, 2, and 3.

For Model 1,  $A_1(\xi)$  is proportional to  $\xi = SD - 2/3 Y$ . The relaxation time is independent of stress level. In Models 2 and 3,  $A_1(\xi)$  varies as  $e^{-1/\xi}$  so that large stresses decay at a much faster rate than low stresses. Other possible forms for  $A_1(\xi)$  may be found in the literature cited in Section 1.4.

After the form of the precursor attenuation has been selected, then the wave shapes and separation can be considered. They cannot be predicted analytically; therefore, they must be determined by trial computations. We suggest that the first trial should be made for the no-separation case; that is, with  $A_2(\xi) = A_3(\xi) = \dots = 0$  in Eq. 34. This is the automatic form for Model 1. In Band's model this can be accomplished by letting  $\epsilon = g = N_{to} = 0$  and by making  $T_1$  and  $T_2$  very large. For the same effect in Gilman's model, let  $C = \phi = 0$ . This first calculation provides a landmark with which to compare the desired results. If these computed results are inadequate, then the arbitrarily set parameters in Band's or Gilman's model can be given more realistic values. Some estimates of the influence of these parameters were presented in the previous discussion of our computed results.

#### 4. Bauschinger Model

The Bauschinger effect refers to a change in the stress-strain relations which occurs when the sense of loading is reversed after initial loading. For our purposes the effect causes a continuous variation of yield strength and shear modulus from the point at which loading sense changes to the next change of sense.

##### a. Construction of the Model

The recorded stress histories derived from plate impact experiments have usually disagreed with calculations based on the ideally plastic model in three ways: (1) the sharp yield point from the computations is quite gradual in the experimental data, (2) the sharp step in the computed unloading of the stress history is almost entirely absent in the experimental records, and (3) the attenuation of peak stress is significantly faster in experimental observation than is predicted by computed histories. These discrepancies led us to the formulation of a

Bauschinger model to account for the most significant effects. The model is a strain-rate independent, elastoplastic model with an unloading stress-strain relation that can be very different from the loading relation. Specifically, the model provides for computation of the deviatoric stress (total stress minus pressure) using a shear modulus that varies smoothly from some initial value down to the strain-hardening modulus. The values of initial modulus, strain-hardening modulus and the manner in which the modulus varies between these two are not necessarily the same for loading and unloading.

In constructing the Bauschinger model it was desirable to produce a form that would be general enough to be applicable to many materials and would be readily usable by other investigators. With these needs in mind, the following guidelines were adopted as requirements for development of the model:

- As far as possible, the form should be comparable to those developed by other investigators.
- The form should be extendable to other stress levels.
- The data should be closely represented.
- A physical basis or interpretation should be available for the parameters in the analytical relation.

The data of Buckley and Entwistle (Ref. 19), and the analytical form of Barker (Ref. 23) and of Erkman and Christensen (Ref. 22) were useful in constructing our model. To make the model equations extendable to other stress levels it was necessary to separate the stress-volume relationship into pressure-volume and deviatoric stress-volume equations. Only the deviatoric stress equations were modified by the Bauschinger effect. For selecting the particular equations of unloading stress vs. strain and the loading transition at yielding, we closely followed our data of Section IV for 2024 and 6061 aluminum. The parameters required for the model are mostly moduli and yield strengths and hence are easily interpreted physical quantities.



The pressure volume relationship is given in the usual form for the PUFF code:

$$P = C \mu + D \mu^2 + S \mu^3 \quad (60)$$

where

$$\mu = V_0/V - 1$$

The constants C, D, and S are represented by EQSTC, EQSTD, and EQSTS in the code. The stress deviator SD is given by

$$SD = SD_0 + \frac{4}{3} \int_{\rho_1}^{\rho_2} M \frac{d\rho}{\rho} \quad (61)$$

where

$SD_0$  = the value of deviatoric stress at the time corresponding to the lower limit of the integral

$M$  = a shear modulus

If  $|SD|$  exceeds  $2/3 Y$ , then  $|SD|$  is set to  $2/3 Y$ . The form of the required function of deviatoric stress versus volume is shown in Fig. 7 for 2024-T8 aluminum used on this project. This form was achieved by varying the shear modulus  $M$  and yield strength  $Y$  according to the following relations:

$$M = M_0 + (M_1 - M_0) \left( \frac{3SD}{2Y_1} \right)^{N_1} \quad (\text{loading}) \quad (62)$$

$$Y = Y_1 + 2M_1 \int_{\text{yield}}^{\rho} \frac{d\rho}{\rho} \quad (\text{loading, after yielding}) \quad (63)$$

$$M = M_2 + (M_3 - M_2) \left( \frac{1}{2} - \frac{3SD}{4Y_2} \right)^{N_2} \quad (\text{unloading}) \quad (64)$$

$$Y = Y_2 + 2M_3 \int_{\text{yield}}^{\rho} \frac{d\rho}{\rho} \quad (\text{unloading, after yielding}) \quad (65)$$

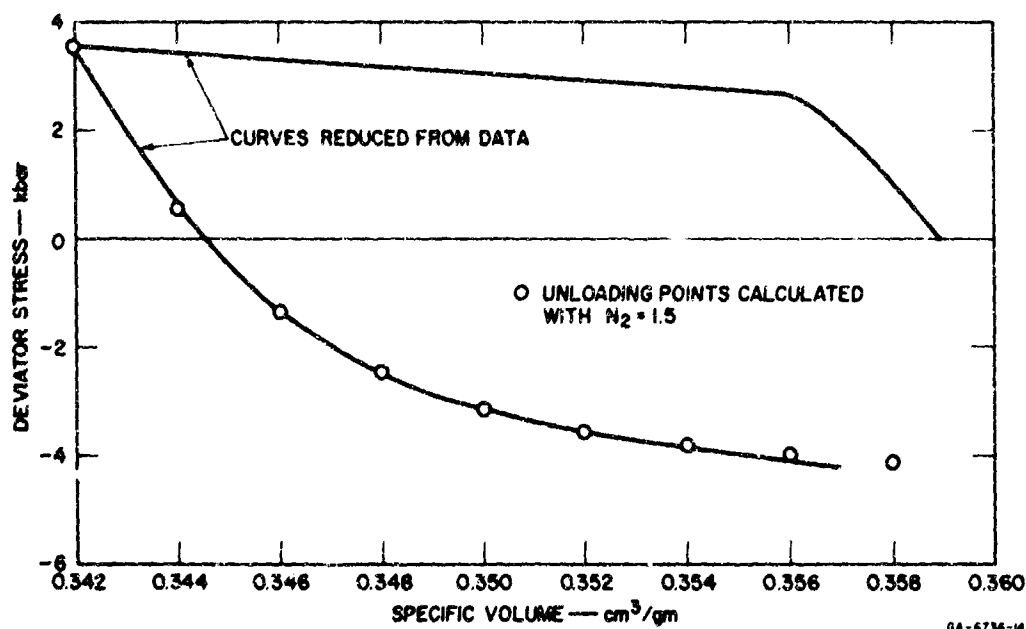


FIGURE 7 RELATIONSHIP BETWEEN DEVIATORIC STRESS AND SPECIFIC VOLUME OBTAINED FROM 50-kbar TESTS IN 2024-T8 ALUMINUM

where

- $Y_1, Y_2$  = yield strengths at yielding on loading and unloading  
 $Y_2$  = the final value of  $Y$  from Eq. 63 before unloading begins  
 $M_0, M_1, M_2, M_3$  = shear modulus at zero stress on loading, strain-hardening modulus for loading, initial unloading shear modulus, and strain-hardening modulus during unloading  
 $N_1, N_2$  = constants.

For  $N = \infty$  the relations of ideal plasticity are obtained. Rounded SD-V relations comparable to those obtained from experiments are obtained for  $N$  between 1 and 10.

#### b. Implementation in the Code

The Bauschinger model is included in the SRI PUFF code as Model 5. The special parameters and yield parameters used in the model are related to the parameters above as follows:

$$\begin{aligned}
MU &= M_0 \\
YADD &= 2M_1/(\rho_1 + \rho_2) \\
MUUN &= M_2 \\
YADF &= M_3/M_1 \\
Y0 &= Y_1 \\
XPO &= N_1 \\
XP &= N_2
\end{aligned}$$

For simplicity in the program and in preparing the data, YADD can be calculated from

$$YADD = \frac{Y_2 - Y_1}{\rho_2 - \rho_1} \quad (67)$$

where subscripts 1 and 2 refer to the yield point and beginning of unloading respectively.

The Bauschinger model reflects considerable detailed knowledge about the loading and unloading character of a material. Therefore, it is probably only worthwhile to use the model if the loading equation of state is well known and some information is available about unloading. Then the moduli can be estimated as follows: MU should be known. YADD can be estimated from static data such as Bridgeman's or dynamic results such as Curran's on work hardening. MUUN is the principle parameter determining the rarefaction velocity; hence it should be carefully determined. The rarefaction velocity  $C_R$  is

$$\begin{aligned}
C_R^2 &= \frac{C + (2D - C\Gamma) \mu_m + (3S - \frac{3}{2} D\Gamma) \mu_m^2}{\rho_0} \\
&+ \frac{\Gamma}{\rho_m} (Cu_m + D\mu_m^2 + S\mu_m^3) + \frac{4}{3} \frac{MUUN}{\rho_m} \quad (68)
\end{aligned}$$

where

$$\mu_m = \frac{\rho}{\rho_0} - 1$$

$\rho_m$  = density at peak stress

$\Gamma$  = Grüneisen's ratio (a constant)

and the other parameters are defined following Eq. 60. YADF may be estimated as 1.0 in the absence of detailed information on the material. The exponent quantities will probably be between 1 and 2 for unloading and about 10 for loading.

Our approach in developing a set of parameters for a material was to calculate as many as possible (i.e., YO, MU, YADD, and MUUN) and then to determine the others by trial. A small computer program was written to compute the stress deviator-volume curves for loading and unloading. The computed values were plotted and compared with the experimental curves. Exponents and YADF parameters were altered until the computed curves were judged satisfactory.

Several computations have been performed with the Bauschinger model to simulate impacts with 2024 and 6061 aluminum. Examples of the output of these calculations are given with the data correlation work of the next section and with the test runs in Appendix I. The results have shown that the model does accurately represent the material behavior. The transition region near the yield point is not required for computations with an artificial viscosity code: the smoothing is caused automatically by the viscosity. Hence XPC should be set  $\geq 100$ . The unloading portion of the calculated stress waves is generally smooth, simulating well the appearance of recorded stress histories.

One defect has appeared in the present model formulation. The fundamental shear modulus MU is read in as a constant (which might be obtained from static tensile or compression tests). In reality, MU should vary with density probably somewhat like the variation in the bulk modulus. In fact, it may be appropriate to write either

$$MU = MU_0 + MU_1\mu + MU_2\mu^2 \quad (69)$$

or

$$MU = (MU_0/EQSTC) K \quad (70)$$

where

- K = the effective bulk modulus provided by Eq. 1
- MU<sub>0</sub> = the initial shear modulus
- MU<sub>1</sub> and MU<sub>2</sub> = constants

Equation 70 reflects the finding of Curran (Ref. 17) that shear modulus appeared to increase in proportion to bulk modulus. Either Eq. 69 or 70 could be used to make a smooth transition from MU to MUUN, the unloading shear modulus. Such a transition is certainly to be expected on physical grounds in place of the jump in modulus from loading to unloading.

Our work with the Bauschinger model and review of the computed results reveal the great importance of correctly computing the rarefaction velocities. Any attenuation computations made without the Bauschinger model for a material with significant strength may be misleading.

Peak rarefaction velocity, i.e., wave velocity of the leading edge of the rarefaction fan, as a function of peak stress level can be used to determine the correct form of the MU function. Our review of the rarefaction velocity data presented in Section IV.2.a has shown that MU increases more rapidly with stress than does the bulk modulus. Hence, Eq. 69 may be preferable.

AFWL-1R-69-96

This page intentionally left blank.

## SECTION III

### EXPERIMENTAL METHODS

#### 1. Theory of Data Reduction for Multiple Embedded Gages

An experimental technique has been developed to measure complete loading and unloading paths (in the stress-particle velocity and stress-volume planes) rather than discrete Hugoniot or release points. The shock or compression need not be steady-state and the release may be nonisentropic. The technique, which requires a special experimental configuration and a corresponding data analysis method, is especially suited to examination of yield point phenomena, strain hardening, the Bauschinger effect, and strain-rate effects. The impact experiments employ a target instrumented with a series of stress and/or particle velocity gages embedded at several depths. During the experiment, stress and particle velocity histories are recorded. The data required from the records are the apparent velocities of propagation of stress and particle velocity states from gage to gage. A rigorous derivation of the theoretical basis for the data analysis procedure follows.

In one-dimensional flow the quantities stress, density, and particle velocity are functions of one cartesian coordinate,  $x$ , and time,  $t$ . The gage analysis is based on apparent wave velocities associated with constant stress or particle velocity states as measured on records from successive gages. We consider two paths in the  $\sigma$ - $u$  plane: a path of constant stress or particle velocity, and a path with a speed equal to the particle velocity (the path of the gage).

In general, for an observer traveling at velocity  $\xi$ , the total change of  $\sigma$  and  $u$  with time will be given by

$$\frac{d\sigma}{dt} = \frac{\partial\sigma}{\partial t} + \xi \frac{\partial\sigma}{\partial x} \quad (71)$$

$$\frac{du}{dt} = \frac{\partial u}{\partial t} + \xi \frac{\partial u}{\partial x} \quad (72)$$

Now consider a path of constant stress in Eq. 71, and a path of constant particle velocity in Eq. 72. In this case  $\xi$  is defined as  $g(\sigma, x, t)$  and  $W(u, x, t)$  respectively and the total derivatives in Eqs. 71 and 72 are zero.

$$\frac{d\sigma}{dt} = \frac{\partial\sigma}{\partial t} + U \frac{\partial\sigma}{\partial x} = 0 \quad (73)$$

$$\frac{du}{dt} = \frac{\partial u}{\partial t} + W \frac{\partial u}{\partial x} = 0 \quad (74)$$

U and W are the velocities of portions of the  $\sigma$  or  $u$  pulses with respect to the fixed or Eulerian coordinates. Hence we have a relationship between the partial derivatives with respect to time and space at a point. Now consider the change of stress or particle velocity at the gage, that is, along a particle path. Then  $\xi = u$ , and

$$\frac{d\sigma}{dt} = \frac{\partial\sigma}{\partial t} + u \frac{\partial\sigma}{\partial x} \quad (75)$$

and

$$\frac{du}{dt} = \frac{\partial u}{\partial t} + u \frac{\partial u}{\partial x} \quad (76)$$

Substitution of Eq. 73 into 75 and Eq. 74 into 76 yields:

$$\frac{d\sigma}{dt} = (u - U) \frac{\partial\sigma}{\partial x} \quad (77)$$

$$\frac{du}{dt} = (u - W) \frac{\partial u}{\partial x} \quad (78)$$

which apply along a particle path. In order to integrate Eqs. 77 and 78 it is necessary to replace the partial derivatives by total derivatives. This can be done using the equations of motion and continuity.

$$\frac{\partial\sigma}{\partial x} = -\rho \frac{du}{dt} \quad (\text{motion}) \quad (79)$$

$$\frac{d\rho}{dt} = -\rho \frac{\partial u}{\partial x} \quad (\text{continuity}) \quad (80)$$

where  $\rho$  = density. Substitution of Eqs. 79 and 80 into Eqs. 77 and 78 yields the following set of differential equations:

$$\frac{d\sigma}{dt} = \rho(U - u) \frac{du}{dt} \quad (81)$$

and

$$\frac{du}{dt} = \frac{(W - u)}{\rho} \frac{d\rho}{dt} \quad (82)$$



By writing Eqs. 81 and 82 in differential form, using the relation  $V = 1/\rho$ , and combining the second equation with the first, the following relations between  $\sigma$ ,  $u$  and  $V$  are obtained.

$$d\sigma = \rho(U - u) du \quad (83)$$

$$du = -\rho(W - u) dV \quad (84)$$

$$d\sigma = -\rho^2(W - u)(U - u) dV \quad (85)$$

The corresponding differential relation for internal energy is derived from the adiabatic relation,  $dE = -\sigma dV$ . With the aid of Eq. 85 the relation for energy is

$$dE = \frac{\sigma d\sigma}{\rho^2(U - u)(W - u)} \quad (86)$$

Equations 83 through 86 are the desired  $\sigma - u$ ,  $u - V$ ,  $\sigma - V$ , and  $E - \sigma$  relationships. The next step is to show how the quantities  $\rho(U - u)$  and  $\rho(W - u)$  are derived from gage records. Consider the case of two thin foil stress or particle velocity gages located in the unstressed material at  $x_1$  and  $x_2$ . If the time at which a particular stress level reaches gage 1 is  $t_1(\sigma)$  then we may define a fictitious (but readily measured) gage velocity  $D_g$  as

$$D_g = \frac{x_2 - x_1}{t_2(\sigma) - t_1(\sigma)} \quad (87)$$

Similarly, for a particular particle velocity, we define the fictitious gage velocity  $B_g$ .

$$B_g = \frac{x_2 - x_1}{t_2(u) - t_1(u)} \quad (88)$$

To relate  $D_g$  and  $B_g$  to actual velocities we make use of the conservation of mass between the gages. The mass traversed along any path with slope  $dx/dt$ , within the  $(x - t)$  plane is given by

$$M = \int_{t_1}^{t_2} \rho \left( \frac{dx}{dt} - u \right) dt$$

where  $dx/dt$  is a velocity with respect to the coordinates and  $(dx/dt - u)$  is velocity relative to the material. In particular, if  $dx/dt = U$ , the velocity associated with a stress  $\sigma$ , and  $t_1$  and  $t_2$  are times at which the stress reaches the two gages, then

$$M = \int_{t_1(\sigma)}^{t_2(\sigma)} \rho(U - u) dt$$

Because mass is conserved between the gages,

$$M = \rho_o (x_2 - x_1) = \rho_o D_g (t_2 - t_1) = \int_{t_1(\sigma)}^{t_2(\sigma)} \rho(U - u) dt \quad (89)$$

where the definition of  $D_g$ , Eq. 87, has also been employed. Evidently  $\rho_o D_g$  is the time average of the quantity  $\rho(U - u)$  between the gages. A similar relationship holds between  $\rho_o B_g$  and  $\rho(W - u)$ .

Because  $\rho_o$  is known and  $D_g$  and  $B_g$  are measurable quantities, we now are able to integrate Eqs. 83 through 86 to obtain the result:

$$u(\sigma, x) = u_o + \int_{\sigma_o}^{\sigma} \frac{d\sigma'}{\rho_o D_g(\sigma', x)} \quad (90)$$

$$V(u, x) = V_o - \int_{u_o}^u \frac{du'}{\rho_o B_g(u', x)} \quad (91)$$

$$V(\sigma, x) = V_o - \int_{\sigma_o}^{\sigma} \frac{d\sigma'}{\rho_o^2 D_g(\sigma', x) B_g(\sigma', x)} \quad (92)$$

$$E(\sigma, x) = E_o + \int_{\sigma_o}^{\sigma} \frac{\sigma' d\sigma'}{\rho_o^2 D_g(\sigma', x) B_g(\sigma', x)} \quad (93)$$

Eqs. 90 through 93 are the relations sought because they provide the  $\sigma - u$ ,  $u - V$ ,  $\sigma - V$ , and  $E - \sigma$  paths during shock and rarefaction regardless of whether the system is steady state or not. As long as suitable gages are available the application of these equations is straightforward, requires no special assumptions, and is capable of determining the entire shock and release paths necessary for computation of propagation and attenuation. In addition the release path measured does not depend on prior knowledge of another material so its accuracy is as good as that of any Hugoniot experiment.

If we consider only simple waves (no wave interactions or rate-dependence) then a line of constant stress is a line of constant particle velocity, and  $U = W$ . In this case  $D_g = B_g$  and the average compression and release paths may be determined with either stress or particle velocity measurements alone. For simple waves the above equations simplify to:

$$u(\sigma) = u_o + \frac{1}{\rho_o} \int_{\sigma_o}^{\sigma} \frac{d\sigma'}{D_g} \quad (94)$$

$$V(u) = v_o - \frac{1}{\rho_o} \int_u^u \frac{du'}{B_g} \quad (95)$$

$$V(\sigma) = v_o - \frac{1}{\rho_o} \int_{\sigma_o}^{\sigma} \frac{d\sigma'}{D_g^2} \quad (96)$$

$$E(\sigma) = E_o + \frac{1}{\rho_o} \int_{\sigma_o}^{\sigma} \frac{\sigma' d\sigma'}{D_g^2} \quad (97)$$

The curves defined by Eqs. 93 to 97 do not necessarily lie on the equation of state surface because no steady-state or equilibrium condition is implied by the equations. The computed loading path for a shock follows the Rayleigh line and therefore lies above the equation-of-state surface. If rate-dependence is important, the equations may lead to a series of noncoincident paths (one path for each pair of gages) for the same material.

The foregoing set of equations readily reduce to the more usual forms when the appropriate simplifying assumptions are made. For example in the case of isentropic flow (as in ideal release behavior) the quantity  $(U - u)$  is equal to the isentropic sound velocity  $C$ . Thus Equation 94 becomes the Riemann integral since in this case  $\rho_0 D = \rho (U - u) = \rho C$ .

For steady state shock the wave profile measured by the gage is unchanging in time. Therefore the measured  $\Delta t$  between gage records is constant and hence  $D = B = \text{constant}$ . Since in general  $D = \frac{\rho}{\rho_0} (U - u)$ , we can evaluate  $D$  at zero stress and  $D$  is therefore equal to  $(U - u_0)$ . By making this substitution Eqs. 94 and 95 simplify to the equations for the Rayleigh line in the  $\sigma - u$  and  $\sigma - V$  planes respectively. If in this simple case Eqs. 94, 95 and 96 are integrated across the shock front, we obtain:

$$\sigma - \sigma_0 = \rho_0 (U - u) (u - u_0) \quad (98)$$

$$1 - \rho_0/\rho = \frac{u - u_0}{U - u_0} \quad (99)$$

$$\sigma - \sigma_0 = - \rho_0^2 (U - u_0)^2 (V - V_0) \quad (100)$$

Integration of Eq. 97 and simplification with the aid of Eq. 100 leads to

$$E - E_0 = - \frac{1}{2} (\sigma + \sigma_0) (V - V_0) \quad (101)$$

Equations 98, 99, and 101 are the usual Hugoniot relations.\*

A sample application of the multiple-gage analysis procedure is presented in Section IV for aluminum.

---

\*Peterson et al., to be published in Geophysical Research.

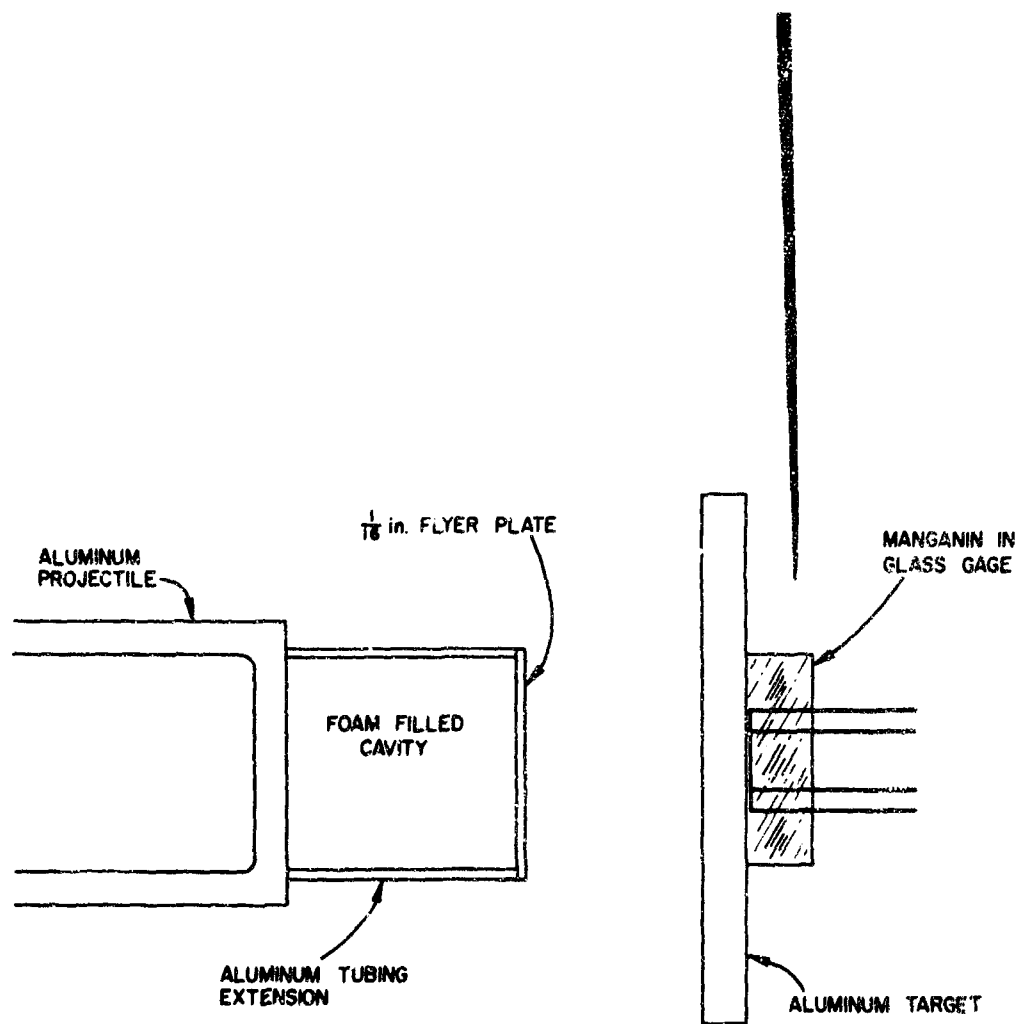
## 2. Experimental Techniques

### a. Gas Gun Experimental Techniques

The SRI light gas gun described by Linde and Schmidt (Ref. 30) is used for impacting samples with flying plates (thin-headed projectiles) to produce plane stress shock waves below 100 kbar traveling into both the target and flyer plate. The projectile material and velocity may be selected for each experiment so that, for example, the projectile head may be of the same material as the target. This "symmetric impact" configuration is often used because it offers a guarantee that the particle velocity in the target at the impact interface will be exactly one half the projectile velocity. If the target exhibits steady state flow, its Hugoniot state is usually determined by measuring the projectile velocity (and thus particle velocity) and the shock velocity in the target and by applying the Rankine-Hugoniot conservation equations (jump conditions) to calculate the other variables.

Figure 8 illustrates the experimental arrangement used in the present study to investigate loading and attenuation in aluminum and titanium alloy at stresses below 50 kbar. The flyer plate may be bonded directly to the projectile or may be supported by a foam material in front of the projectile as in Fig. 8. With the foam backing, the plate behaves approximately as a free flyer and therefore can be used in attenuation studies. The bonded plate configurations are used for shots where only loading is of interest.

When very thin flyer plates were required, a foam backing surrounded by a tubular aluminum extension was added to the projectile to support an aluminum flyer plate (disk) at its circumference. The cavity behind the flyer was filled with a rigid, low-density, high-strength polyurethane foam to ensure that the flyer remained flat while the projectile was accelerated. Tests using an optical flat and a monochromatic light source showed that the foam did not expand when subjected to typical barrel vacuums and the flyers remained flat to better than three microns. The shock impedance of this foam could be neglected compared to that of aluminum although this assumption was not required in the data analysis.



GA-6736-35

**FIGURE 8 EXPERIMENTAL ARRANGEMENT FOR GAS GUN ATTENUATION SHOTS**

The stress history at the back face of the metallic specimens was measured by means of manganin transducers embedded in glass. For the shots with aluminum targets, a soda-lime glass was used with the transducers because this glass has a shock impedance only slightly below that of the aluminum alloys investigated. Therefore, to a good approximation, wave interactions caused by reflections at the aluminum-glass interface could be ignored. To minimize target-gage wave interactions in the tests with titanium, a lead oxide glass was incorporated in the transducers in place of the soda-lime glass. This glass has an impedance only slightly lower than that of titanium. The manganin transducers are discussed further in Section III.3.

#### b. High-Explosive Experimental Techniques

In the present study, specimen stresses between approximately 100 and 700 kbar were generated with high-explosive (HE) driver systems. The three driver systems employed (Table 1) are of one or the other of the two types shown in Fig. 9. The first system propels a thin, high-velocity flyer for attenuation studies. The second, and simpler, type of HE system is used in experiments which require measurement of the loading state but not of attenuation or other unloading properties. Both types of system employ an 8-inch-diameter plane wave generator (P-80) to initiate a plane detonation wave in a cylindrical pad of HE, which either directly or indirectly (see Fig. 7) accelerates the flyer across the flight path to the target. Specimen shock state measurements are made electronically with manganin gages or optically with a smear camera or with a combination of these two techniques.

The first HE system (Fig. 9, System E) was developed by Erkman and Christensen (Ref. 22) to accelerate thin, high-velocity, relatively stress-free, unspalled flyers. Such flyers are required to study shock attenuation and stress release in shocked material resulting from the trailing rarefaction fan originating at the back surface of the flyer (see Fig. 10). Christensen found that when the plane wave generator was in direct contact with an 1/8 in. thick aluminum flyer, the flyer would spall during the experiment. To avoid flyer spalling, the air gap, buffer plate,

Table 1

## PARAMETERS OF EXPLOSIVELY LAUNCHED FLYER PLATE SYSTEMS

Explosive Flyer System*	Driver Free-Surface Velocity <sup>†</sup> $u_{fs}$ (mm/ $\mu$ sec)	Driver Shock Stress <sup>†</sup> $\sigma$ (kbar)	Particle Velocity <sup>†</sup> $u$ (mm/ $\mu$ sec)
<u>System B</u> <sup>‡</sup> P-80 + 4 in. HMX + 1/16 in. air gap + 1/4 in. 2024 Al flyer + 1.0 in. flight + 3/16 in. 2024 Al driver <sup>§</sup>	4.8 $\pm$ 0.1	550 $\pm$ 20	2.3 $\pm$ 0.1
<u>System D</u> <sup>‡</sup> P-80 + 2 in. Baratol + 1/16 in. air gap + 1/2 in. 2024 Al flyer + 1 in. flight + 3/16 in. 2024 Al driver <sup>§</sup>	2.2 $\pm$ 0.1	200 $\pm$ 10	1.1 $\pm$ 0.1
<u>System E</u> <sup>‡</sup> P-80 + 2 in. Comp. B + 1/2 in. air gap + 3/4 in. Al buffer <sup>**</sup> + 1/8 in. sheet explosive + 1/8 in. 2024 Al flyer + 1 in. flight + 3/16 in. 2024 Al driver <sup>§</sup>	3.1 $\pm$ 0.1	310 $\pm$ 15	1.5 $\pm$ 0.1

\* All dimensions are uniform within  $\pm 0.001$  inch and surfaces of all components are flat and parallel within  $\pm 0.0005$  inch.

<sup>†</sup> The tolerances denote the range within which approximately 80 percent of the measurements fall.

<sup>‡</sup> Plane wave generator 8 inches in diameter.

<sup>§</sup> The driver thickness and material were varied in some of the experiments.

\*\* In one experiment the buffer thickness was 1/2 inch.



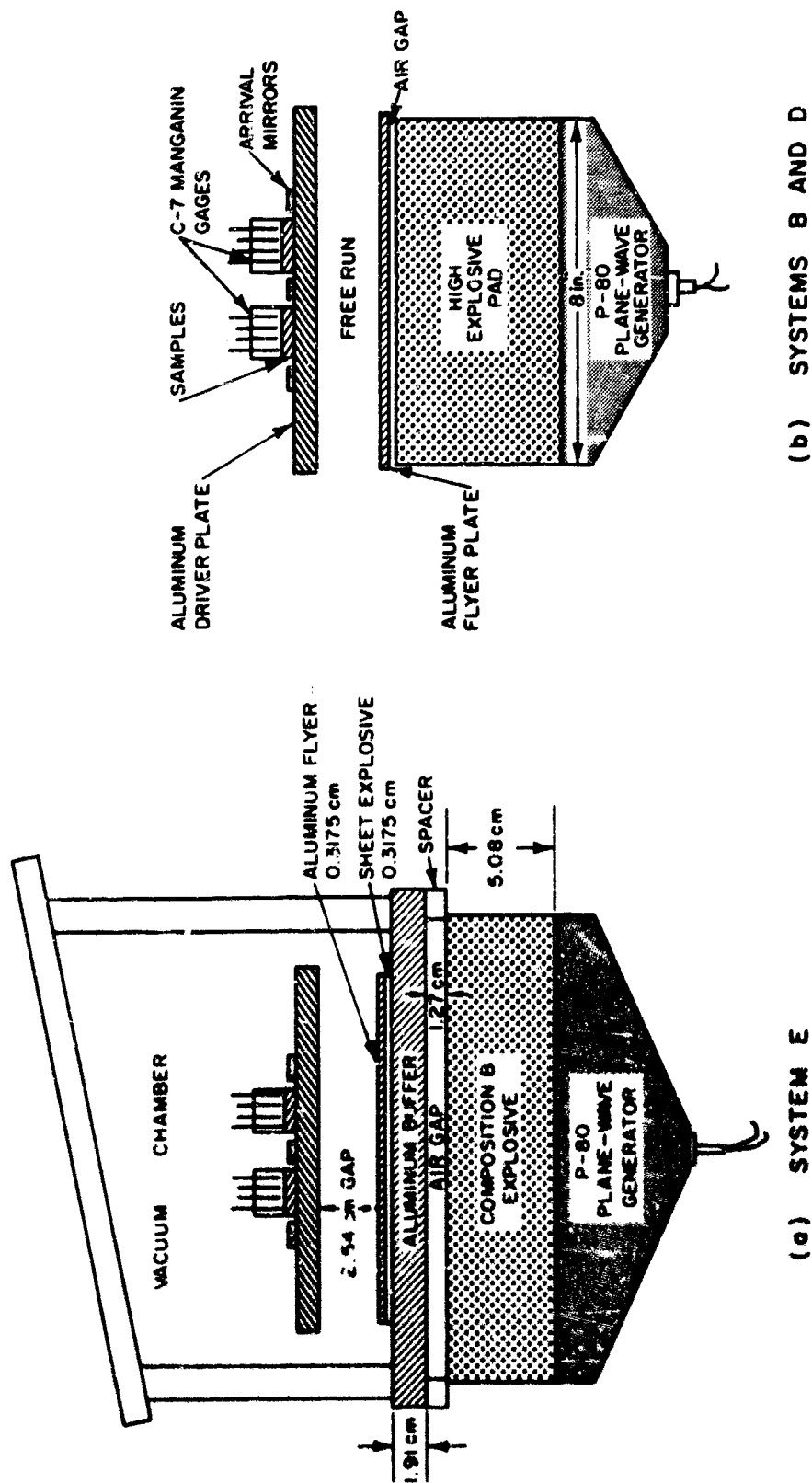
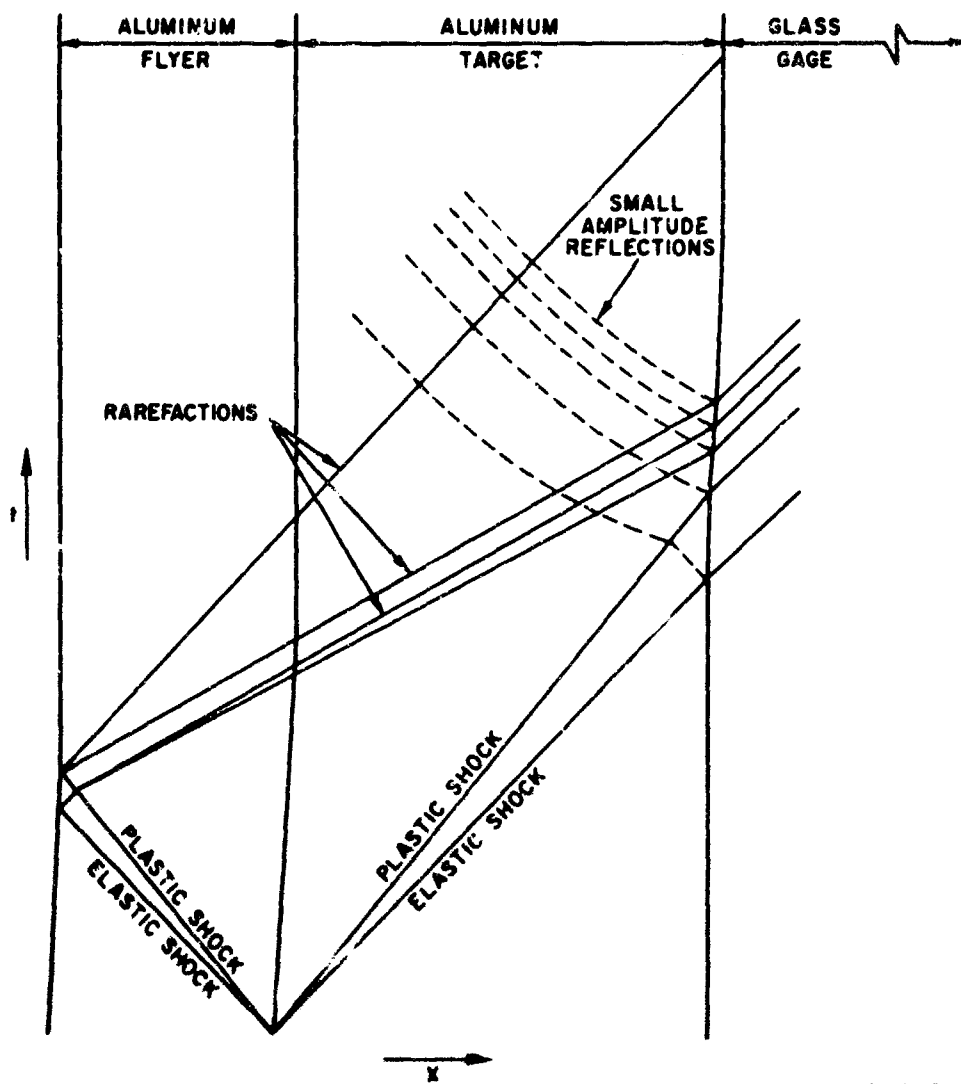


FIGURE 9 SIDE VIEW OF HE FLYER SYSTEMS B, D, AND E FOR GENERATING UNIAxIAL STRAIN LOADING AND UNLOADING STATES

(a) SYSTEM E  
(b) SYSTEMS B AND D  
64-6756-50



60-6726-00

FIGURE 10 A DISTANCE ( $x$ )-TIME ( $t$ ) DIAGRAM SHOWING SHOCK AND RAREFACTION WAVES CAUSED BY IMPACT

and sheet explosive (providing supporting stress at the back of the flyer) were added by Christensen and Erkman (Ref. 22). The resulting flyer velocity is approximately 3 mm/ $\mu$ sec, with planarity (simultaneity of arrival) of 0.04 to 0.06  $\mu$ sec across a 4-inch-diameter impact surface. The vacuum system shown in Fig. 9 is employed to eliminate the air shock which would otherwise precede the impact. A typical experimental configuration using System E is shown in Fig. 11.

The second type of HE system, represented here by Systems B and D (Fig. 9), is characterized by the fact that the high-pressure detonation products act directly on the flyer (usually much thicker than flyers of System E) to accelerate it across the free run gap into the target. Systems B and D were demonstrated not to spall by letting the flying plates impact manganin stress transducers and examining the resulting stress histories. The planarity of the shock front in the target obtained using these systems is of the same order of magnitude as that of System E.

The objectives of the HE experiments in this study were to measure Hugoniot states achieved in the Specimens, and in the case of the thin flyer attenuation shots, to record the stress history during loading and unloading. In all the HE experiments Hugoniot states were determined using optical techniques (Ref. 31,32), and stress histories were obtained electronically using manganin C-7 stress transducers (Ref. 33).

Hugoniot state determinations in the HE experiments were simplified by the observation that the study materials (with the exception of the three-dimensional weave material) supported a single-front, steady-state shock. Therefore, the Rankine-Hugoniot conservation equations apply and the impedance match technique (Ref. 34) is valid. Under these conditions measurement of two shock variables allows the determination of the specimen Hugoniot state. In the present experiments the two variables measured were the driver free-surface velocity (or equivalently the flyer velocity) and the specimen shock velocity. Since these velocities are constant during the experiment (steady-state flow), they were determined from time and distance measurements. Back surface mirrors were positioned

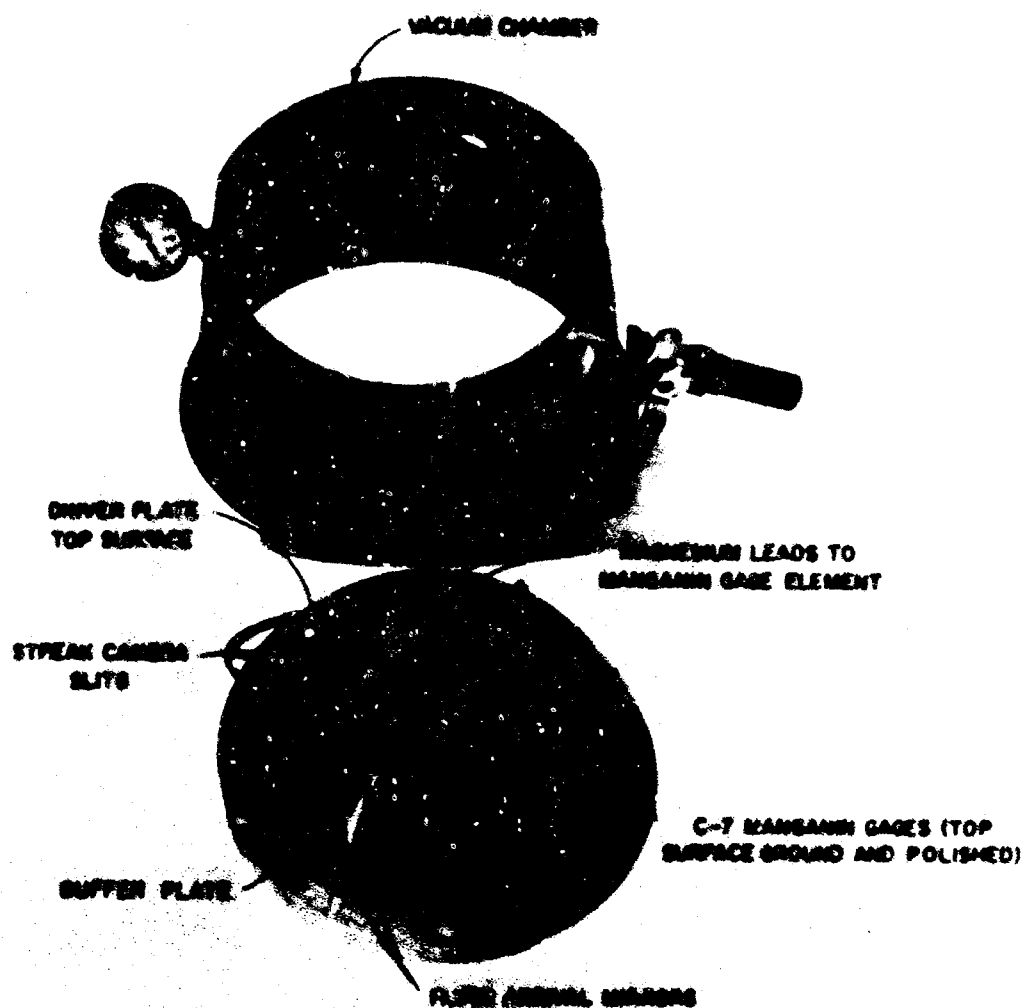


FIGURE 11 SYMMETRICAL IMPACT EXPERIMENT (HE System E) TO DETERMINE HUGONIOT DATA AND SHOCK WAVE PROFILES

at the planes of interest (e.g., the front and back surface of the specimen) and illuminated by a relatively long-duration, shocked argon light bomb. These mirrors were monitored by a time-resolving high-speed streak camera which recorded the relative times of the events of interest (e.g., the shock front arrival at the front and back surfaces of the specimen) by the very rapid (occurring in  $< 10^{-8}$  sec) changes in mirror reflectivities that resulted. With such optical methods velocities can be determined to within 1 percent in a typical experiment.

To determine stress histories in HE experiments, manganin/C-7 gages (Ref.33) were mounted on the specimen. These gages record the entire stress history in C-7 resulting from the shock transmitted across the specimen C-7 interface. Ideally these experiments would employ a transducer medium which closely matched the shock impedance of the specimen, to minimize the waves reflected back into the specimen from the specimen-transducer interface (see Fig. 10). However, manganin/C-7 gages were used in the HE experiments (in spite of being of lower shock impedance than the study materials) because the manganin/C-7 gage is the only one which has been calibrated at these high stresses. It is therefore fortunate that in all HE experiments the study materials support only a single front shock (no elastic precursor or phase transition wave), so interpretations of the gage experiments are not complicated by interactions in the specimen between the rarefaction reflected from the interface and a complex plastic shock front. However, in the region where the rarefacted waves reflected from the gage-target interface intersect the rarefacted waves from the free surface of the flyer (Fig. 10), the stress will become tensile and the specimen may spall. The stress release seen in C-7 is therefore characteristic of the interaction of the two rarefaction fans.

In all HE experiments the transducers were standard 4-terminal 1-ohm gages (Ref.33) with the manganin element (0.002-inch-diameter wire flattened to less than 0.001 inch to minimize response time) set 0.010 inch into the C-7 from the specimen/C-7 interface. It was noted that when this particular manganin/C-7 gage configuration was shocked to ~145 kbar peak pressure in C-7, a 60 to 70 mv signal, commonly termed a polarization signal, occurred.

The signal appeared 30 to 40 nsec before the main pulse, corresponding to the shock transit time through 0.008 to 0.012 inch of C-7, dropped to 10 to 20 m $\mu$  as the shock entered the manganin element, and decayed to zero approximately 1/2  $\mu$ sec later. The signal is believed to be generated by the leakage of induced charge in the C-7 through the active manganin element to ground. In the data analysis this signal was subtracted from the transducer record to obtain the true stress history. To compensate the gage hysteresis during stress release, the observed relative resistance change of the manganin wire is assumed to depend linearly on axial stress (as during loading) but with the proportionality constant decreased during unloading by 12-1/2 percent for peak stresses between 130 and 160 kbar (Ref.33). Thus when  $\Delta R/R$ , the relative resistance change, has decreased to 12-1/2 percent of its peak value, it is assumed that the axial stress has been completely released.

The shock front arrival and planarity at the transducer-specimen interface was monitored optically by looking through the ground and polished top surface of the C-7 transducer at the polished specimen below using the streak camera. For the study of nonmetallic materials, the gage front surface was aluminized. This combined electronic-optical instrumentation proved highly successful and is recommended when detailed shock planarity information is needed in conjunction with stress transducer information.

#### c. Manganin-in-glass Gages

The manganin-glass gage consisted of four terminal  $\pi$  network manganin elements (manganin ribbon 0.0005-inch thick and 0.025-inch wide was used) with mercury-silver dental amalgam leads made by back filling 1/16-inch holes in 1/2-inch-thick glass gage blocks. Aluminum foil disks (0.0004 inch thick by 3/16 inch diameter) were pressed onto the dental amalgam-manganin ribbon juncture and a 0.003-inch-thick cover glass was bonded over the face with C-7 epoxy.\* The aluminum foil disks extend

---

\* C-7 resin with 6 percent activator A by weight, from Armstrong Products, Inc., Warsaw, Indiana.

the recording time (typically 2  $\mu$ sec) of these transducers by maintaining good electrical contact at the ribbon-lead joint during shock loading.

Manganin transducers in soda-lime glass\* were calibrated for peak stresses up to 43 kbar by impacting test glass gages incorporating manganin ribbon elements at two different depths, with either Lucalox\*\* or aluminum flyers. Measurement of shock transit time between the gages yields the shock velocity in the glass. Since the Hugoniot of the projectile material was known, the peak stress could be determined by the impedance match method. The piezoresistive response measured in these tests was linear and equal to 0.9029  $\Omega/\Omega/\text{kbar}$ , identical to that previously obtained in C-7 epoxy.

The Hugoniot and unloading characteristics of the soda-lime glass were also determined from these experiments. The resistance-time records generated by plate impacts revealed that the stress wave in glass was steady state for both the compression and release portions and that the shock velocity was constant up to 43 kbar. The conclusion was that the Hugoniot and the unloading isentrope are a single straight line in the stress-particle velocity plane. The glass shock impedance measured in these experiments was  $\rho_0 U = 14.9 \pm 0.1 \text{ g/cm}^3 \text{ mm}/\mu\text{sec}$ . It is interesting to compare this result with that of Fuller and Price (Ref.35) who investigated a soda-lime glass with a density of  $2.46 \text{ gm/cm}^3$ . The shock impedance of their glass was some 10 percent lower than that of the glass used in this work and their glass displayed strong dispersion of the compressive wave. This indicates that density is not an adequate indicator of dynamic properties in different soda-lime glass. Indeed, discussions with glass suppliers revealed that the composition of soda-lime glass can vary considerably from batch to batch, even from the same supplier. Consequently, all glass used in this work was taken from a single sheet, with the exception of the 0.003-inch-thick cover glass.

\* Soda-lime glass ( $\frac{1}{8}$ -inch-thick plate window glass),  $\rho_0 = 2.52 \text{ g/cc}$ .

\*\* A polycrystalline alumina ( $\text{Al}_2\text{O}_3$ ) produced by General Electric Co., Lamp Glass Department, Los Angeles, California.

Gage hysteresis was measured by impacting test gages with Lucalox flyers. The impedance mismatch between glass and Lucalox causes a series of reverberations in the Lucalox flyer. If all stresses are below the elastic limit of Lucalox, the reverberating waves remain nondispersive and the glass release states are well-defined, thus providing a release calibration of the manganin in glass transducer. The results of release calibrations for peak stress up to 43 kbar are summarized in Fig. 12 which shows that the percentage drop in gage resistance lags the percentage drop in stress during release; i.e., the gage exhibits considerable hysteresis. The recorded stress histories were corrected for release hysteresis according to this curve.

For tests with titanium a lead oxide glass called Hi-D\* was used. The shock impedance of Hi-D is slightly lower than that of titanium. Hugoniot measurements (Ref.36) on Hi-D glass have been performed in this laboratory, and the glass used in these gages came from the same source as that used for the Hugoniot measurements. The Hi-D glass Hugoniot is a straight line up to 150 kbar with  $\rho_0 U = 20.7 \text{ g/cm}^3 \text{ mm}/\mu\text{sec}$ . The previously measured piezoresistive coefficient of the manganin in Hi-D glass transducer, is  $0.0024 \text{ } \Omega/\Omega \text{ kbar}$ . (Ref.37).

---

\* 89 percent PbO glass,  $\rho_0 = 6.2$  supplied by Penberthy Instrument Company, Seattle, Washington.



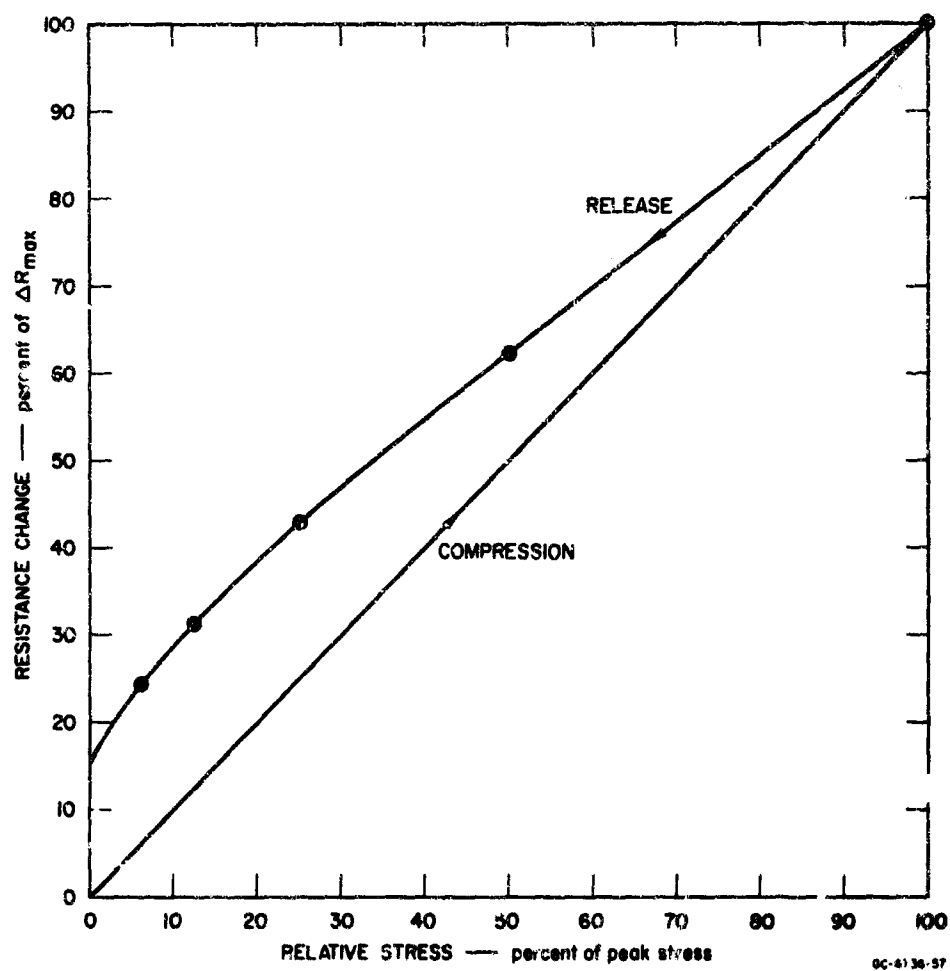


FIGURE 12 MEASURED UNLOADING CALIBRATION OF MANGANIN ELEMENT IN SODA-LIME GLASS

AFWL-TR-69-96

This page intentionally left blank.

## SECTION IV

### STUDY OF ALUMINUM

#### 1. Introduction

For the study of aluminum the objectives were to investigate stress relaxation, unloading effects, and stress attenuation. The design of the experiments was based on the data analysis technique outlined in Section III, a technique which was still being developed. Aluminum was a particularly good choice for the experimental program because many of its properties are well known, and even its unloading characteristics have been studied (Erkman, Christensen, and Fowles (Ref.22) and Barker (Ref.23)). Stress relaxation effects have been observed in some aluminum alloys. Based on results of experiments at low strain rates, it was expected that 2024-T8 would be strain-rate-dependent while 6061-T6 would be relatively rate-independent. Another reason for choosing aluminum was its high experimental reproducibility, a property of special importance in any basic investigation.

The two aluminum alloys selected for study, 6061-T6 and 2024-T8, were supplied by Kaiser Aluminum Company, Department of Metals Research, Spokane, Washington. All sheets of each alloy (from 1/16 inch to 1-1/4 inches thickness) were supplied from a single billet to guarantee uniformity. The heat treatments, ageing, and rolling work hardening were those specified by the standards for T6 and T8 (Ref.38, 39). Table 2 presents a summary of the alloy properties obtained from quasi-static and acoustic measurements. A description of these tests and detailed results are given in Appendix II.

The dynamic study of the two aluminum alloys consisted of:

- Fifteen to 20 experiments on each alloy at four or five nominal pressure levels between 15 and 500 kbar, including two series of impact experiments at stress levels of 50 and 300 kbar with specimens of various thicknesses.
- Reduction of the experimental data to obtain a complete stress-volume relation for loading and unloading.
- Wave propagation calculations to correlate with the experimental stress records.

Table 2

## MEASURED STATIC PROPERTIES OF ALUMINUM ALLOYS

Alloy	Density $\rho$ (g/cm <sup>3</sup> )	Young's Modulus, E (kbar)	Yield Strength (uniaxial tension) (kbar)	Ultimate Strength (uniaxial tension) (kbar)	Poisson's Ratio, $\nu$
2024-T8	2.785	745	4.4	4.9	0.33-0.34
6061-T6	2.709	710	2.8	3.1	0.32-0.34

Notes: Densities are from a series of measurements on each alloy. Moduli and the two strengths are from quasi-static measurements reported in Appendix II. Poisson's ratio is from both acoustic and quasi-static measurements of Appendix II.

## 2. Dynamic Experiments

Both attenuation and Hugoniot-type impact tests were conducted on the two aluminum alloys, 2024-T8 and 6061-T6. The gas gun experiments, which provided considerable detailed information about precursor and rarefaction waves, are described first; then the HE (high explosive) experiments are described. The experimental configurations and the Hugoniot data obtained are summarized in Tables 3 and 4 and Figs. 13 and 14.

### a. Gas Gun Tests

Seventeen gas gun experiments were performed on 2024-T8 and 6061-T6 aluminum using 1/16-inch-thick flyers to examine attenuation in these materials. Four gas gun experiments were performed on 6061-T6 with 1/8-inch-thick flyers to examine shock propagation without attenuation in thick targets. Targets for both sets of experiments were nominally 1/8, 1/4, 3/8, or 1/2 inch thick. The experimental configuration is shown in Fig. 8. A typical set of manganin stress transducer resistance-time records for four different target thicknesses is shown in Fig. 15. (The ratio of target to flyer thickness is given as R in the figure.) The blanking marks on these traces are used for time correlation of stress

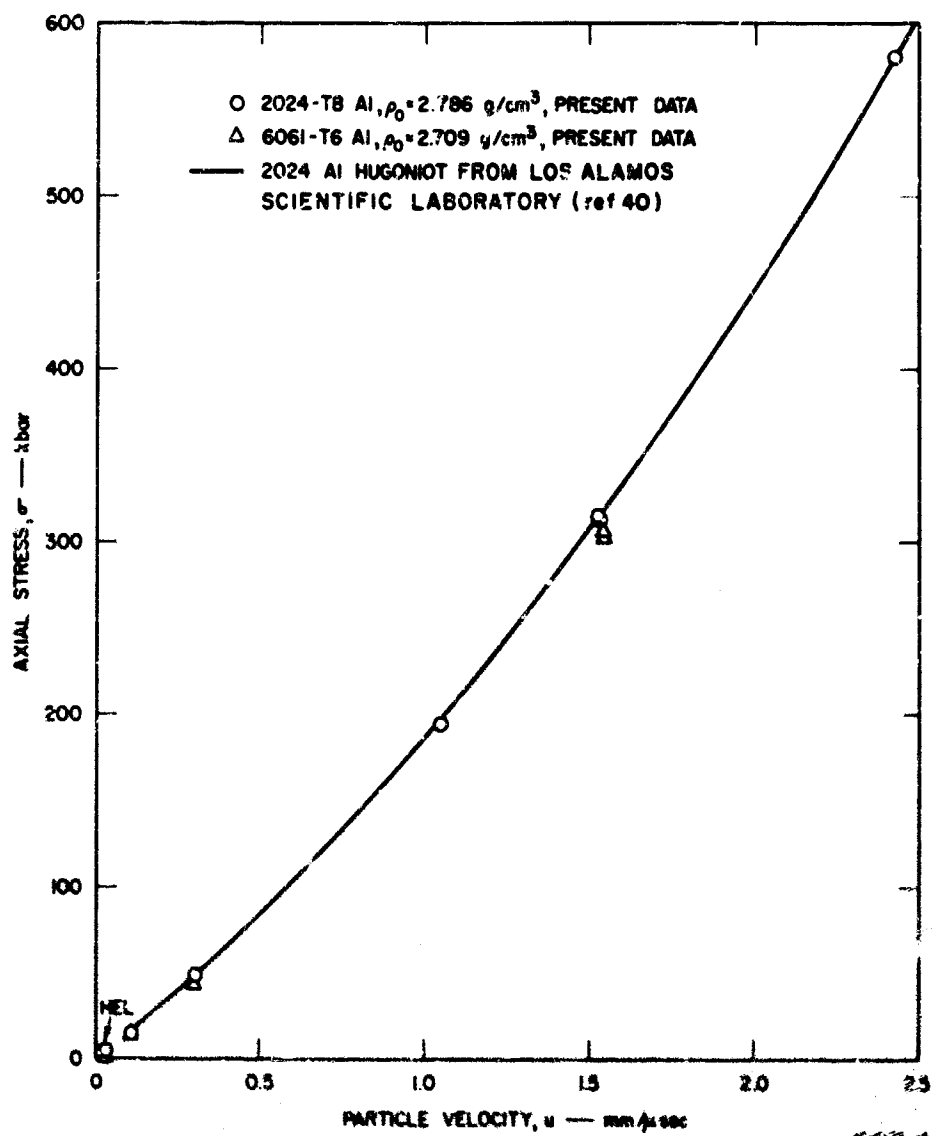


FIGURE 13 . STRESS-PARTICLE VELOCITY HUGONIOT DATA FOR 2024-T8 AND 6061-T6 ALUMINUM

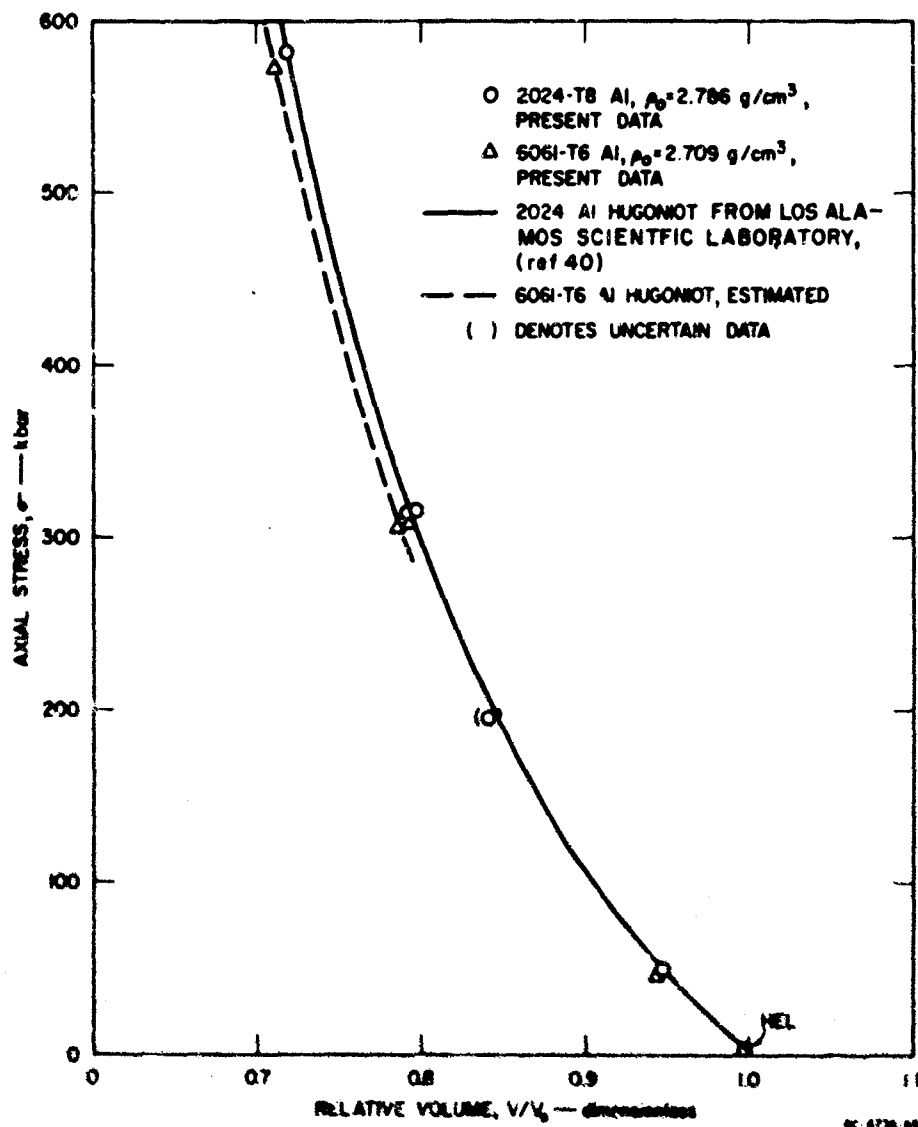


FIGURE 14. STRESS-VOLUME HUGONIOT DATA FOR 2024-T8 AND 6061-T6 ALUMINUM

Table 3

## HUGONIOT DATA FOR 6061-T6 ALUMINUM\*

Shot Number	Driver System			Specimen Thickness (mm)	Hugoniot Elastic Limit†				Final (Hugoniot) State			
	System	Flyer <sup>‡</sup> Velocity (mm/μsec)	Flyer Thickness (mm)		Shock Velocity, U (mm/μsec)	Particle Velocity, U (mm/μsec)	Axial Stress, σ (kbar)	Specific Volume, V (cm <sup>3</sup> /g)	Shock Velocity, U (mm/μsec)	Particle Velocity, U (mm/μsec)	Axial Stress, σ (kbar)	Specific Volume, V (cm <sup>3</sup> /g)
0607	Gun	0.217	1.54	3.16	6.2 <sup>§</sup>	0.025 <sup>§</sup>	4.3 <sup>§</sup>	0.3374 <sup>§</sup>	§	0.108 <sup>§</sup>	17.0 <sup>§</sup>	**
0608	Gun	0.218	1.49									
0609	Gun	0.214	1.35									
0630	Gun	0.217	2.96									
0631	Gun	0.569	2.94	12.56	6.2 <sup>§</sup>	0.025 <sup>§</sup>	4.3 <sup>§</sup>	0.3674 <sup>§</sup>	§	0.303 <sup>§</sup>	45.6 <sup>§</sup>	0.3480
0636	Gun	0.587	2.95									
0637	Gun	0.602	2.94									
0648	Gun	0.580	1.94									
0669	Gun	0.603	1.54									
0666	Gun	0.603	1.54									
0670	Gun	0.603	1.53									
0789	Gun	0.609	1.54									
13,539	E(HI)	3.05	--	4.06	--	--	--	--	7.26	1.55	306	0.290
13,566	E(HI)	3.05	--	8.21	--	--	--	--	7.38	1.54	308	0.292
13,527	E(HI)	4.83	--	4.06	--	--	--	--	8.56	2.46	572	0.263

\* Average initial density = 2.709 g/cm<sup>3</sup> with specimen-to-specimen variation of ±0.005 g/cm<sup>3</sup>. Asterisks (\*) indicate averaged values. ‡ and U, u, and V were obtained from Figs. 13, 14, 24, and 21, respectively.

† Hugoniot elastic limit (HEL) is defined in the text. No HEL was observed in the HE experiments.

‡ Projectile velocity for gun system; flyer velocity or driver free-surface velocity for HE system.

§ Dispersive plastic wave; no unique shock velocity.

\*\* Attenuating wave; no Hugoniot state.

Table 4

## HUGONIOT DATA FOR 2024-T8 ALUMINUM\*

Shot Number	Driver System			Specimen Thickness $d$ (mm)	Hugoniot Elastic Limit†				Final (Hugoniot) State			
	System	Flyer Velocity, $U$ (mm/ $\mu$ sec)	Flyer Thickness (mm)		Shock Velocity, $U$ (mm/ $\mu$ sec)	Particle Velocity, $u$ (mm/ $\mu$ sec)	Axial Stress, $\sigma$ (kbar)	Specific Volume, $v$ ( $\text{cm}^3/\text{g}$ )	Shock Velocity, $U$ (mm/ $\mu$ sec)	Particle Velocity, $u$ (mm/ $\mu$ sec)	Axial Stress, $\sigma$ (kbar)	Specific Volume, $v$ ( $\text{cm}^3/\text{g}$ )
0669	Gun	0.315	1.56	3.12 } 12.00 }	6.4*	0.033	9.9	0.3570	§	0.108**	17.5	††
3095	Gun	0.238	1.55			0.036	6.5	0.3568		**	**	
0664	Gun	0.610	1.56	3.15 } 6.26 } 8.90 } 12.05 }	6.5*	0.031*	5.5*	0.3573*	§	0.304*	49.6*	0.340*
0671	Gun	0.610	1.56									
0663	Gun	0.606	1.57									
0692	Gun	0.610	1.55									
13,525	D(ME)	1.06†	--	4.54	--	--	--	--	6.67‡	1.05‡	193‡	0.302‡
13,566§§	E(ME)	3.05	--	4.48	--	--	--	--	7.36	1.53	314	0.284
13,532	E(ME)	3.05	--	4.48	--	--	--	--	7.44	1.52	316	0.286
13,575	E(ME)	3.05	--	8.96	--	--	--	--	7.43	1.52	316	0.286
13,527	B(ME)	4.25	--	4.72	--	--	--	--	8.65	2.43	583	0.256

\* Average initial density = 2.786 g/cm<sup>3</sup> with specimen-to-specimen variation of  $\pm 0.005$  g/cm<sup>3</sup>. Asterisks (\*) indicate averaged values.  $\sigma$  and  $U$ ,  $u$ , and  $v$  were obtained from Figs. 13, 14, 20, and 21, respectively.

† Hugoniot elastic limit (HEL) is defined in the text. No HEL was observed in the HE experiments.

‡ Projectile velocity for gun system; flyer velocity or driver free-surface velocity for HE systems.

§ Dispersive plastic wave; no unique shock velocity.

\*\* Attenuating wave; no Hugoniot state.

†† Value not calculated.

§§ Mirror cutout time was not sharply defined on smear camera record; hence, precision was low.

¶¶ Specimen mounted on 4.86-mm-thick driver plate of 6061-T6.



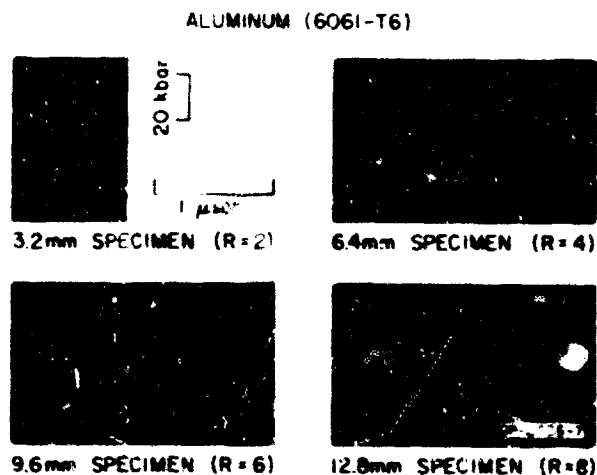
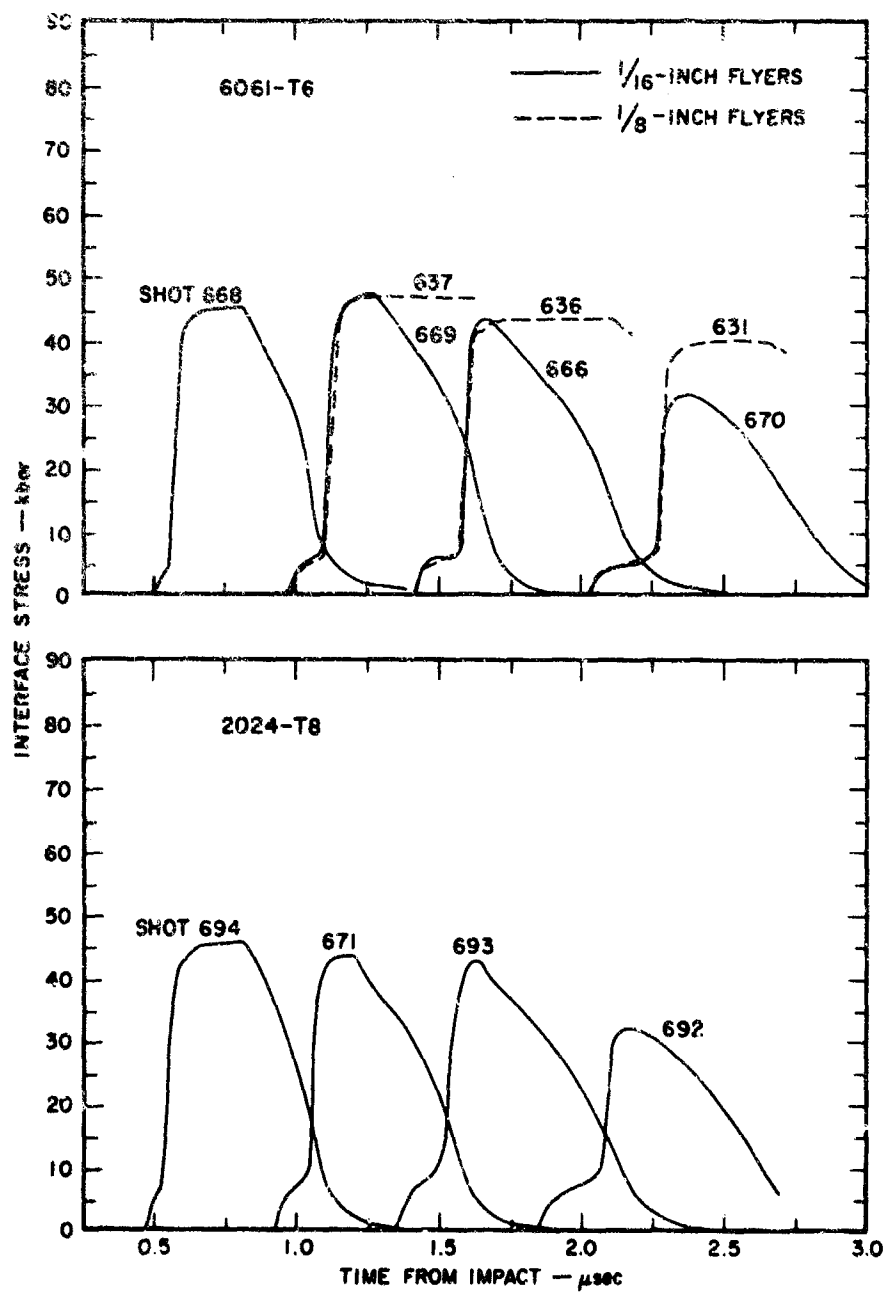


FIGURE 15 TYPICAL MANGANIN TRANSDUCER  
RECORDS OBTAINED FROM  
IMPACTS IN 6061-T6 ALUMINUM

gage data with impact time data. A more precise time base is provided by a separate 10 MHz time mark trace (not shown). Aluminum-glass interface stress-time profiles obtained from transducer records by correcting for gage hysteresis are shown in Figs. 16 and 17. Because of the good impedance match between aluminum and the glass transducers, the effects of reflections from the aluminum-glass interface on later portions of the incoming wave were neglected for the multiple-gage analysis used to compute the continuous stress-volume relations. (This assumption was not made in calculating Hugoniot points nor in the wave propagation computation of the SRI-PUFF code.) The adequacy of the impedance match assumption was checked experimentally with an "in-material" gage in one experiment. In that test a manganin foil gage (0.0002-inch-thick) was sandwiched between two layers of aluminum, using 0.001-inch-thick mica as insulation on each side of the foil (thus producing an "in-material" gage). It is expected that this sandwiched gage disturbs the flow field very slightly, but it is not known how well the gage response follows interface stresses during unloading. The record from this "in-material" gage is in general agreement with the glass transducer record as shown in Fig. 18, although there are differences, particularly in the unloading portion of the wave. These differences show that the reflections from the aluminum-glass interface may not be entirely negligible.

The error bounds of measured impact time were excessive in some experiments due either to tilt or distortion of the flyer. Improvement in the time correlation of the stress-time profiles of Figs. 16 and 17



68-6736-58

FIGURE 1 INTERFACE STRESS HISTORIES RECORDED BY MANGAIN-GLASS BEHIND ALUMINUM TARGETS (50 kbar Impacts)

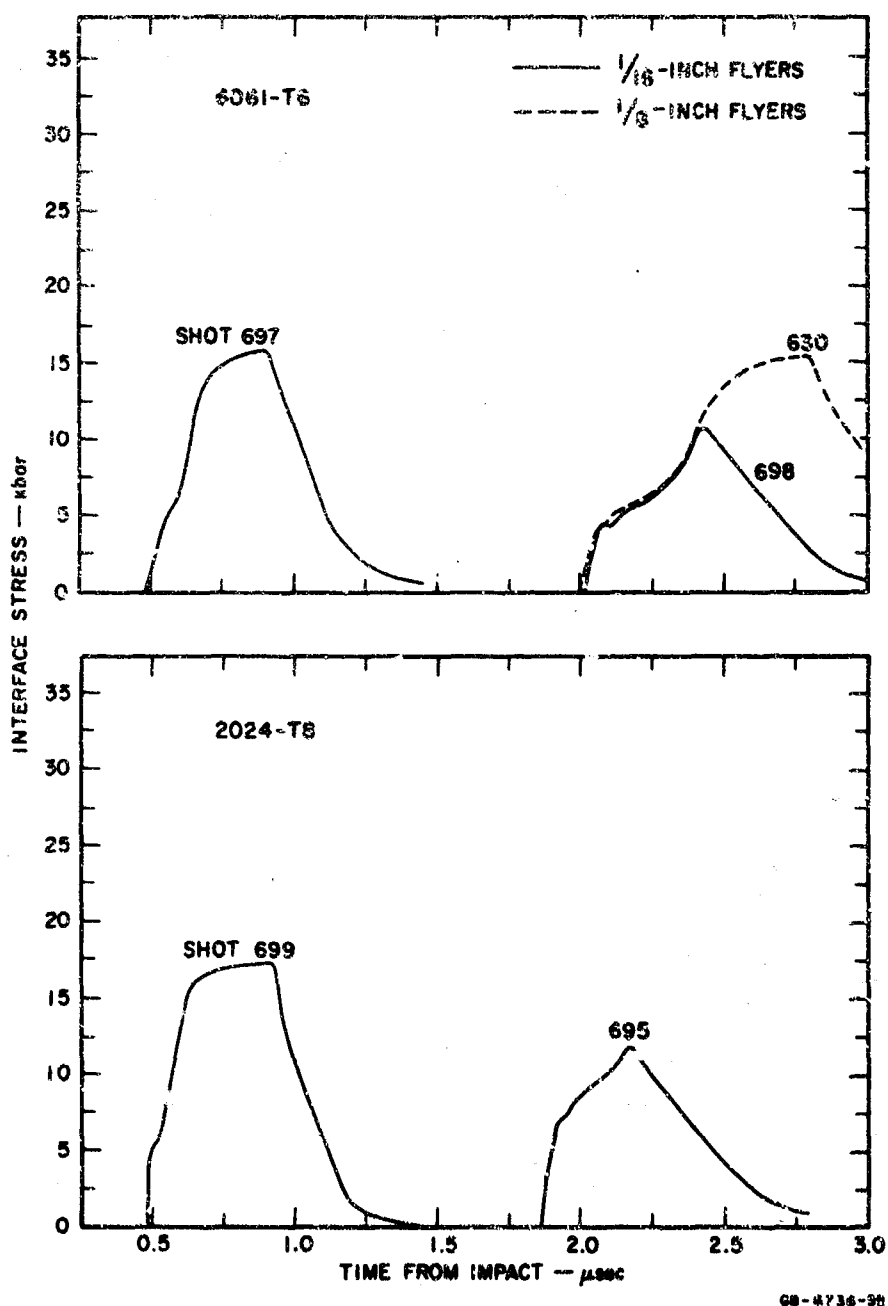


FIGURE 17 INTERFACE STRESS HISTORIES RECORDED BY MANGANIN-GLASS GAGES BEHIND ALUMINUM TARGETS (20 kbar Impacts)

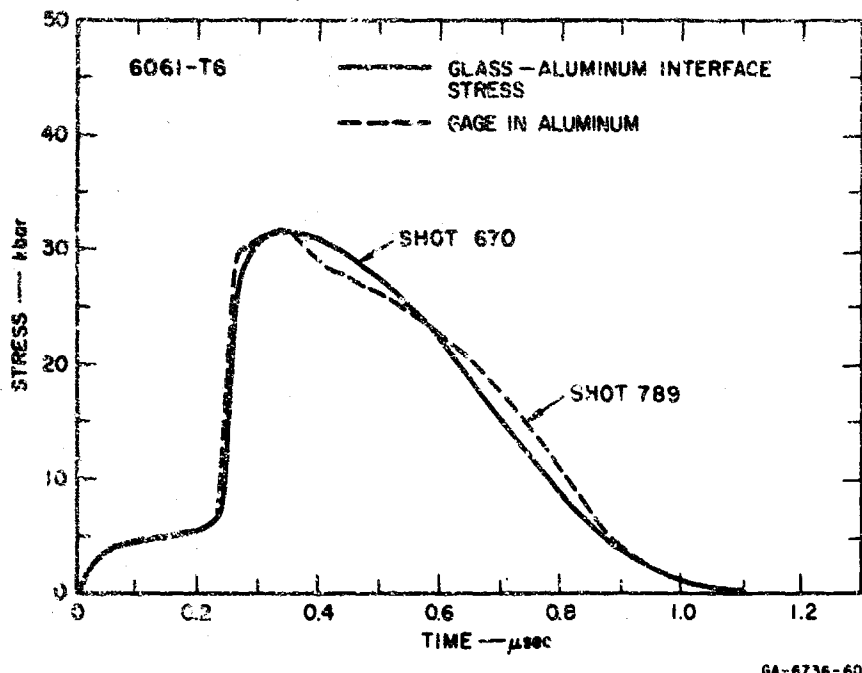


FIGURE 12 COMPARISON OF STRESS HISTORIES RECORDED AT ALUMINUM-GLASS AND ALUMINUM-ALUMINUM INTERFACES

was achieved by assuming that the steady-state portions of the wave, both elastic and plastic, were propagating at constant (but, of course different) velocities. The positioning of the profiles in time by this method gave elastic wave velocities that were in good agreement with the longitudinal sound velocity measurements.

Average values of the product  $\rho D$ , (which we shall call instantaneous impedance) as a function of stress were obtained from these profiles (as described in Section III.1) for both compressive and release waves and are plotted in Fig. 19. Averaging was accomplished by measuring  $\rho D$  as a function of stress for every combination of profiles in Figs. 16 and 17 and then weighting each  $\rho D$  value according to the initial distance between gages. This weighting procedure was used since the measurement error was a fixed time increment, and therefore the percentage error should be smaller for the larger separations. These data then provide the required information to integrate the momentum relations

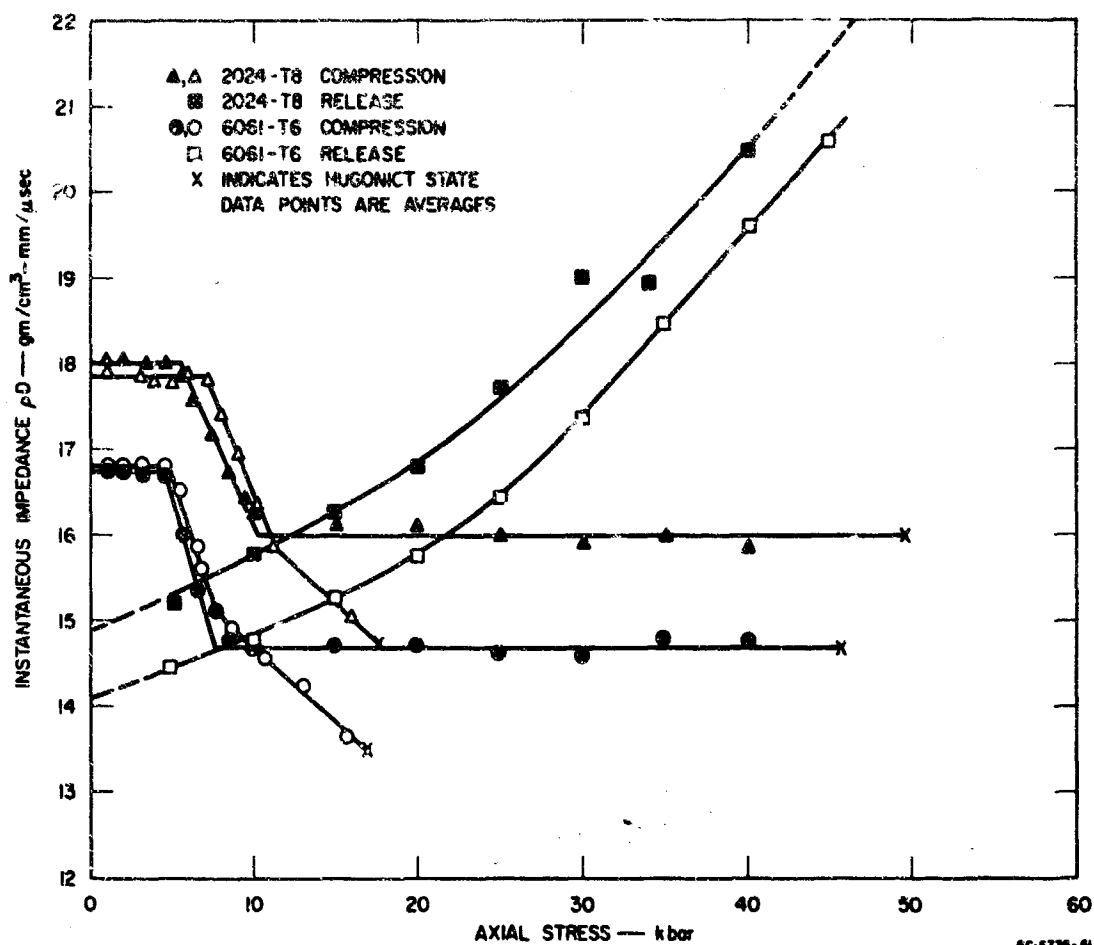


FIGURE 19 AVERAGE INSTANTANEOUS IMPEDANCE  $\rho_0 D_0$  AS A FUNCTION OF AXIAL STRESS FROM 50-kbar EXPERIMENTS IN ALUMINUM

(Eqs. 100 and 101 of Section III.1) in the stress-particle velocity and the stress-volume planes. These integrations result in the compression paths, Hugoniot points, and release adiabats shown in Figs. 20 and 21. As expected, both of these figures show a significant difference between loading and unloading paths. This hysteretic effect contributes to energy losses and attenuation.

The measured Hugoniot elastic limits (HEL) for these aluminum alloys (4.3 kbar for 6061-T6 and 5.5 kbar for 2024-T8) are in fair agreement with the static yield strength from uniaxial stress experiments. According to either von Mises or Tresca yield criteria (with a Poisson's ratio of 0.32), the HEL should be 1.9 times the static yield strength, if strain rate effects are negligible.\*

\*The relation between HEL and yield strength is given in Section V.2 as Eq. 104.

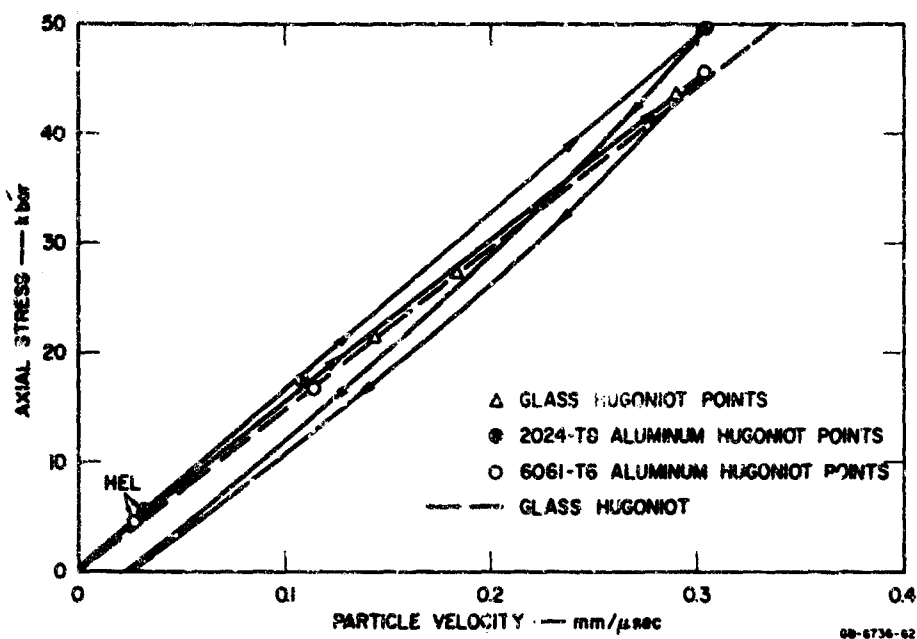


FIGURE 20 . STRESS-PARTICLE VELOCITY COMPRESSION AND RELEASE PATHS FROM 50-kbar EXPERIMENTS IN ALUMINUM

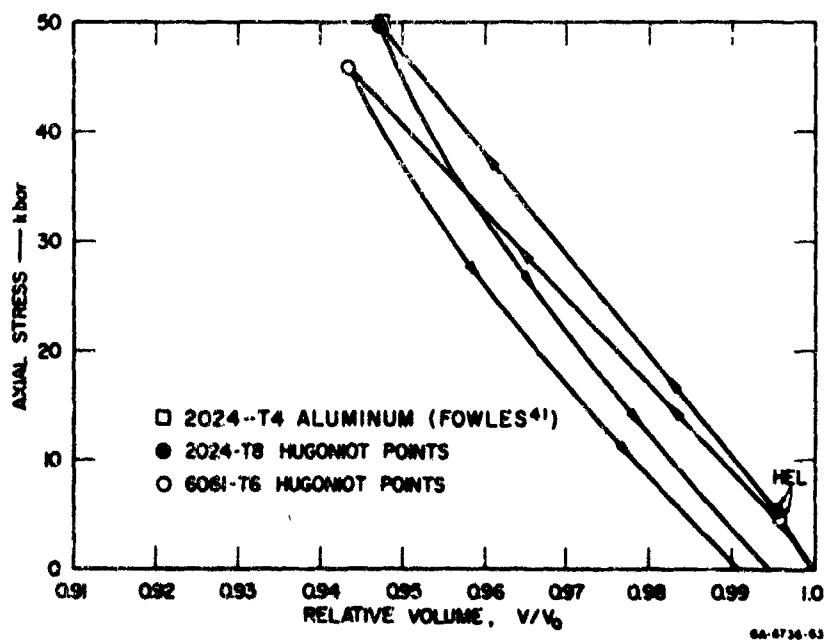


FIGURE 21 . STRESS-VOLUME COMPRESSION AND RELEASE PATHS FROM 50-kbar EXPERIMENTS IN ALUMINUM

While the HEL's do not show a strain rate effect, the stress-time profiles of Figs. 16 and 17 show a nonsteady-state yielding zone (elastic-plastic transition) that extends from the HEL to approximately 1.8 times the HEL for both aluminum alloys. The wave propagation in this yielding zone is dispersive with a time-independent, stress-dependent local disturbance velocity, a condition which generates a single distance- and time-independent compression path in the stress-particle velocity and stress-volume planes. The HEL is the stress at which dynamic yielding begins (corresponding to the proportional limit of tensile experiments) and may be measured by noting the maximum stress for which the elastic precursor is steady state. The HEL one obtains by this definition differs little from that obtained by other definitions based on the shape of the precursor profile. However, this definition provides a more rational basis for the selection of the HEL since the slope of the stress-strain curve will be a straight line up to this stress, but not beyond. The fact that yielding extends over a wide stress range for dynamic loading suggests that rate-dependent phenomena may play a role in the precursor formation. However, the HEL did not vary with propagation distance in these experiments, probably because of the relative thickness of the targets studied. The HEL would be expected to attenuate with propagation distance at very early times and over very short distances. The wave shape between the HEL and the main wave can be predicted by a rate-independent mechanism: the rounded stress-volume relation in the vicinity of the yield point.

Release adiabats measured with the above-described multiple gage technique were markedly different from those predicted by simple elastic-plastic theory. The elastic release modulus and the yield strength were both larger than predicted, and no well-defined yield point was observed during release.

Rarefaction velocities were obtained as a function of stress level from the low-stress experiments. This computation was possible because of the good impedance match between the gage material and the samples. The rarefaction velocity was obtained by observing the first reduction

in stress from a flat top in the Hugoniot experiments. The resulting rarefaction velocities are shown in Table 5 as a function of stress level. As expected these velocities are well above the zero stress sound velocities. Considerable judgment is involved in selecting the point of arrival of the rarefaction wave, and therefore it is not surprising that there is some scatter in the data.

#### b. HE Experiments on Aluminum

The HEL was overdriven in all HE experiments on aluminum alloys. The Hugoniot data from the HE experiments were obtained using techniques described in Section III.2.b and the results are presented in Figs. 13 and 14 and Tables 3 and 4. These results are in good agreement with other Hugoniot data on these materials as shown in Figs. 13 and 14. To allow measurements of the stress histories during loading and unloading, three thicknesses of each alloy (approximately 3/8 inch, 1/2 inch, and 1 inch) were impacted by 1/8-inch-thick stress-free flyer plates traveling at about 3 mm/ $\mu$ sec (HE system E). The shot configurations are shown in Fig. 9 and the instrumentation is described in Section III.2.b. Profiles for each of these thicknesses obtained from the manganin C-7 transducers are shown later in the section (Figs. 24 through 26 and 30 through 32), in combination with the corresponding calculated stress histories. The 1-inch-thick target experiments were designed to show peak stress attenuation; therefore these experiments do not yield Hugoniot data and do not appear in Tables 3 and 4.

#### 3. Calculations for 2024-T8 Aluminum

Experimental stress records used for calculational comparisons of shock attenuation were obtained at two stress levels in 2024-T8 aluminum: 50 kbar and 300 kbar. The high stress data were obtained with a manganin transducer embedded in C-7 epoxy. The impedance mismatch between C-7 and aluminum is so severe that the resulting stress records could not be readily used with the analysis procedure described in Section III.1. The tests at 50 kbar employed a manganin gage embedded in glass with an impedance very similar to that of the aluminum. Therefore, the latter data were used to develop the Bauschinger parameters. PUFF calculations



Table 5

## ALUMINUM PEAK RAREFACTION VELOCITIES

Material	Initial Velocity* (mm/ $\mu$ sec)	Peak Stress (kbar)	Stress (kbar)	Peak Rarefaction ** Velocity (mm/ $\mu$ sec)
6061-T6	6.2	45.6	45.6	7.3
6061-T6		45.6	40.0	6.8
6061-T6		45.6	30.0	6.1
6061-T6		45.6	20.0	5.6
6061-T6		45.6	10.0	5.3
6061-T6	6.2	17.0	17.0	6.8
6061-T6		17.0	10.0	6.2
6061-T6		17.0	5.0	5.6
2024-T8	6.5	49.6	49.6	7.7
2024-T8		49.6	45.0	7.4
2024-T8		49.6	40.0	7.0
2024-T8		49.6	30.0	6.4
2024-T8		49.6	20.0	5.9
2024-T8		49.6	10.0	5.6
2024-T8	6.5	17.5	17.5	6.8
2024-T8		17.5	10.0	6.1
2024-T8		17.5	5.0	5.4

\* Wave velocity of the compressional precursor at the zero stress level, (equal to the longitudinal sound velocity).

\*\* Wave velocity of leading edge of rarefaction fan measured with respect to the material at that point.

were then made to compare with the experimental records at both stress levels. The stress gage data from four low-pressure experiments on 2024-T8 aluminum are shown in Fig. 16 on a common time base, with the impact time at zero. Sets of values of  $\rho D$  were obtained from each pair of records through the use of Eq. 87. With measurements on all possible pairs of records, six curves of  $\rho D$  vs stress were obtained for the 2024-T8 aluminum. The composite  $\rho D$ -stress curves shown in Fig. 19 were the basis of a numerical integration of Eq. 101 to obtain the stress-volume relation shown in Fig. 22. To guide in the interpretation of the relation, a computed pressure-volume relation is also shown. The loading curve of Fig. 22 exhibits an elastic limit at 5 kbar, but the Rayleigh line passes between 10 kbar and the peak stress. Hence, there is a range of gradual yielding from 5 to 10 kbar. This effect is more evident in the plot of deviator stress, Fig. 7. (The deviatoric stress curves are taken from the difference between the stress and pressure curves of Fig. 22). The 5-kbar level is the magnitude of the elastic precursor. The 5 to 10 kbar yield region is associated with a gradually increasing stress between the precursor and the main wave. The unloading

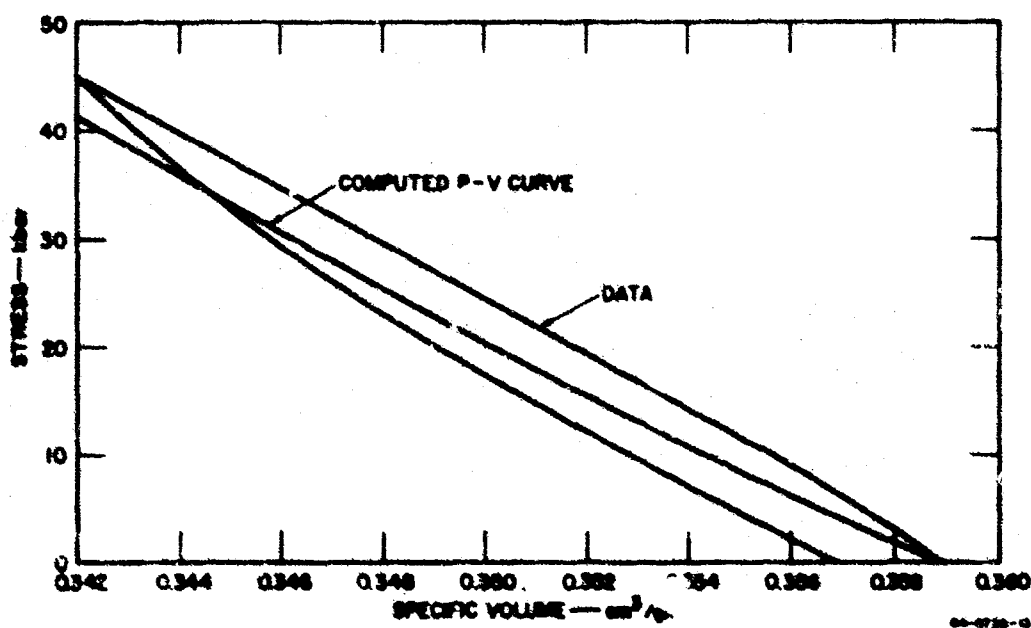


FIGURE 22. STRESS-VOLUME PATH REDUCED FROM DATA FOR 2024-T8 ALUMINUM AND A COMPUTED PRESSURE-VOLUME RELATION

curve is smooth: the sharp unloading yield point predicted by the model of ideal plasticity is not present. The slope of the unloading curve at the peak stress is noticeably steeper than the loading curve at zero stress. This increased steepness is probably associated with the larger (10 to 20 percent) bulk modulus and larger shear modulus at the higher stress. Near the point of zero stress after unloading, the deviatoric stress and hence the yield strength appears to be two or three times as large as they were during the initial loading.

The ten unknowns introduced in Eqs. 60 through 65 for the Bauschinger model --  $C$ ,  $D$ ,  $S$ ,  $M_0$ ,  $M_1$ ,  $M_2$ ,  $M_3$ ,  $V_1$ ,  $N_1$ , and  $N_2$  -- were determined by matching the experimental load-unload  $S$ - $V$  curve with the analytical curves. This required a certain amount of trial and error and the resulting set of values is by no means unique. The form of the modulus variation appeared to represent the data very well: the fit to the unloading curve is shown in Fig. 7 for  $N_2 = 1.5$ . The computed values of the parameters are shown in Table 6.

Using the Bauschinger parameters from Table 6, a PUFF calculation was made to compare with the experimental stress records shown in Fig. 16. After several tries we obtained the set of computed records shown in Fig. 23. These records were obtained using the parameter values in parentheses in Table 6. The rarefaction velocity was too small so it appeared necessary to augment the unloading shear modulus. In fact, there is still not enough attenuation in the computed records so that possibly even a higher  $M_3$  should have been used. The curvature  $N_1$  of the initial loading function was essentially eliminated by giving it a large value. With  $N_1 = 6000$ , the function has a sharp yield. The computed stress records, however, show about the right amount of rounding at the precursor front because of the artificial viscosity.

The comparison of experimental and computed stress records in Fig. 23 exhibits the following features:

- The arrival times are satisfactorily predicted by the code computations
- Peak stress is overestimated; some of the overestimate is caused by the overshooting which is characteristic of this code, some is caused by an inadequate attenuation of stress, and some by what appears to be too large values of  $C$ ,  $D$ , and  $S$ .

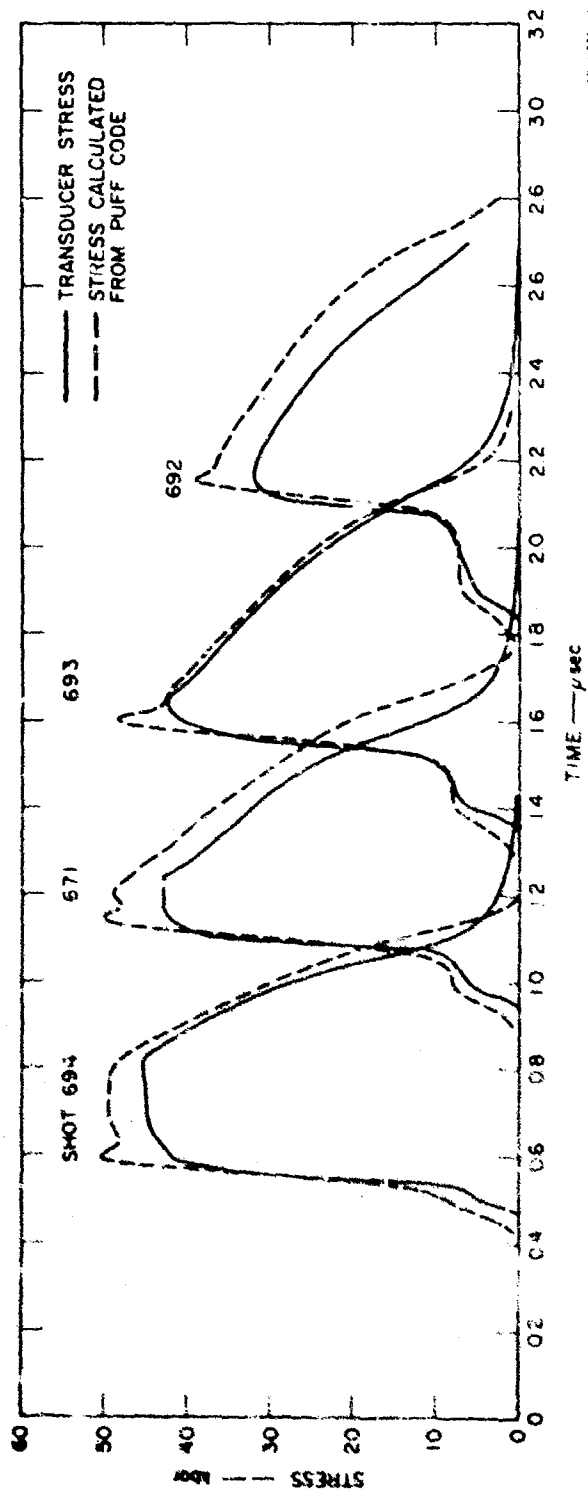


FIGURE 23. COMPARISON OF COMPUTED AND RECORDED STRESS HISTORIES  
FROM IMPACTS WITH 2024-T8 ALUMINUM AT 50-kbar

Table 6

PARAMETERS FOR THE BAUSCHINGER MODEL  
FOR 2024-T8 and 6061-T6 ALUMINUM

Parameter	2024-T8	6061-T6
EQSTC (dynes/cm <sup>2</sup> )	$7.60 \times 10^{11}$	$6.67 \times 10^{11}$
EQSTD (dynes/cm <sup>2</sup> )	$1.50 \times 10^{12}$	$(1.0 \times 10^{12})$
M <sub>1</sub> (dynes/cm <sup>2</sup> )	$3.0 \times 10^{11}$	$2.67 \times 10^{11}$
M <sub>2</sub> (dynes/cm <sup>2</sup> )	$7.63 \times 10^9$	$3.79 \times 10^{10}$
M <sub>3</sub> (dynes/cm <sup>2</sup> )	$4.45 \times 10^{11}$ $(4.82 \times 10^{11})$	$4.67 \times 10^{11}$
M <sub>4</sub> (dynes/cm <sup>2</sup> )	$2.18 \times 10^{10}$	$3.79 \times 10^{10}$
Y <sub>1</sub> (dynes/cm <sup>2</sup> )	$4.0 \times 10^9$	$3.21 \times 10^9$
N <sub>1</sub>	6.0 (6000)	6.0 (6000)
N <sub>2</sub>	1.5	1.0

Note: Parenthetical values are the final values obtained by comparing the PUFF calculations with the experimental stress records.

- The unloading arrival is fairly well predicted, and the shape of the unloading curve is well matched.

Figures 24 through 26 show the experimental data from the 300 kbar shots and the corresponding computed records. The computed predictions are very close for the thin targets (Figs. 24 and 26) but the computed stress is 20 percent low for the thickest target. These calculations were made using the same Bauschinger parameters as for the low stress computations. Hence, it is not surprising that there is some disagreement in magnitude.

We conclude then from the comparison of all the results for 2024 that the form of the Bauschinger model is well-suited to represent 2024-T8 aluminum; however, some changes in the parameters are required to quantitatively predict stress amplitudes.

#### 4. Calculations for 6061-T6 Aluminum

Impact tests used for calculational comparisons were conducted at 50 and 300 kbar, the high stress tests with a manganin C-7 gage and the low stress tests with a manganin glass gage. The series at the low stress level was used in the analysis presented in Section III.1 to obtain the Bauschinger and equation-of-state parameters. Then PUFF calculations were made to compare with the experimental records at both stress levels.

The determination of Bauschinger parameters will be sketched briefly here: it follows the same procedure as that for the 2024-T8 aluminum. The series of experimental stress records is shown in Fig. 16. The plot of  $\rho D$  versus stress derived from these records is shown in Fig. 19. The resulting stress-volume plot and stress deviator plot are shown in Figs. 27 and 28. The computed Bauschinger parameters are listed in Table 6. The PUFF computations based on these parameters are shown in Figs. 29 through 32. In general the results of comparing the computed and experimental curves are similar to the results for 2024-T8 aluminum. There is qualitative agreement between prediction and experiment but attenuation predicted is not sufficient; hence, the unloading, or rarefaction, velocity is higher than expected. The differences that

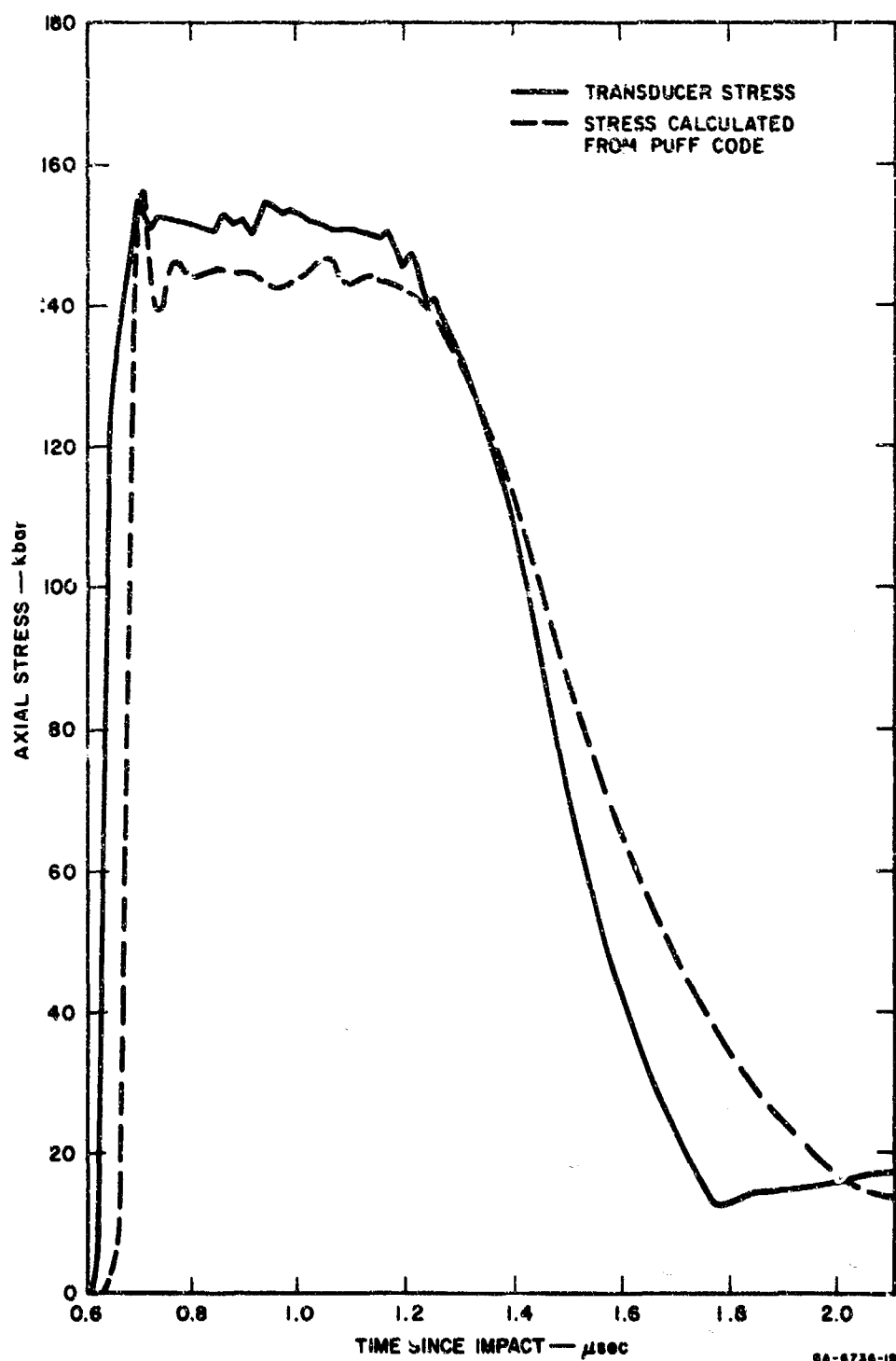


FIGURE 24. COMPARISON OF COMPUTED AND RECORDED STRESS HISTORIES FROM SHOT 13,532 IN 4.48-mm-THICK 2024-T8 ALUMINUM TARGET

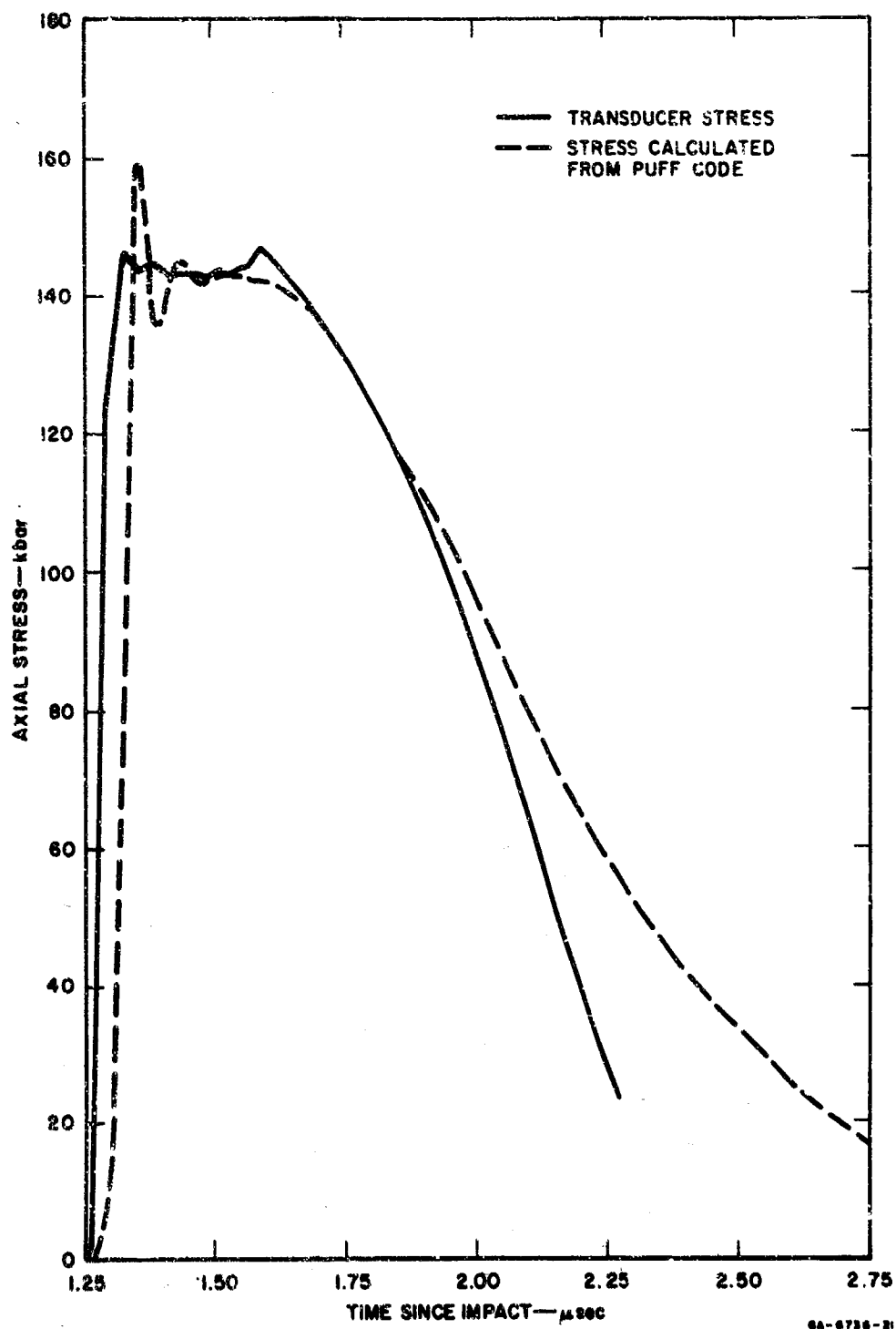


FIGURE 25. COMPARISON OF COMPUTED AND RECORDED STRESS HISTORIES FROM SHOT 13,532 IN 8.98-mm-THICK 2024-T8 ALUMINUM TARGET



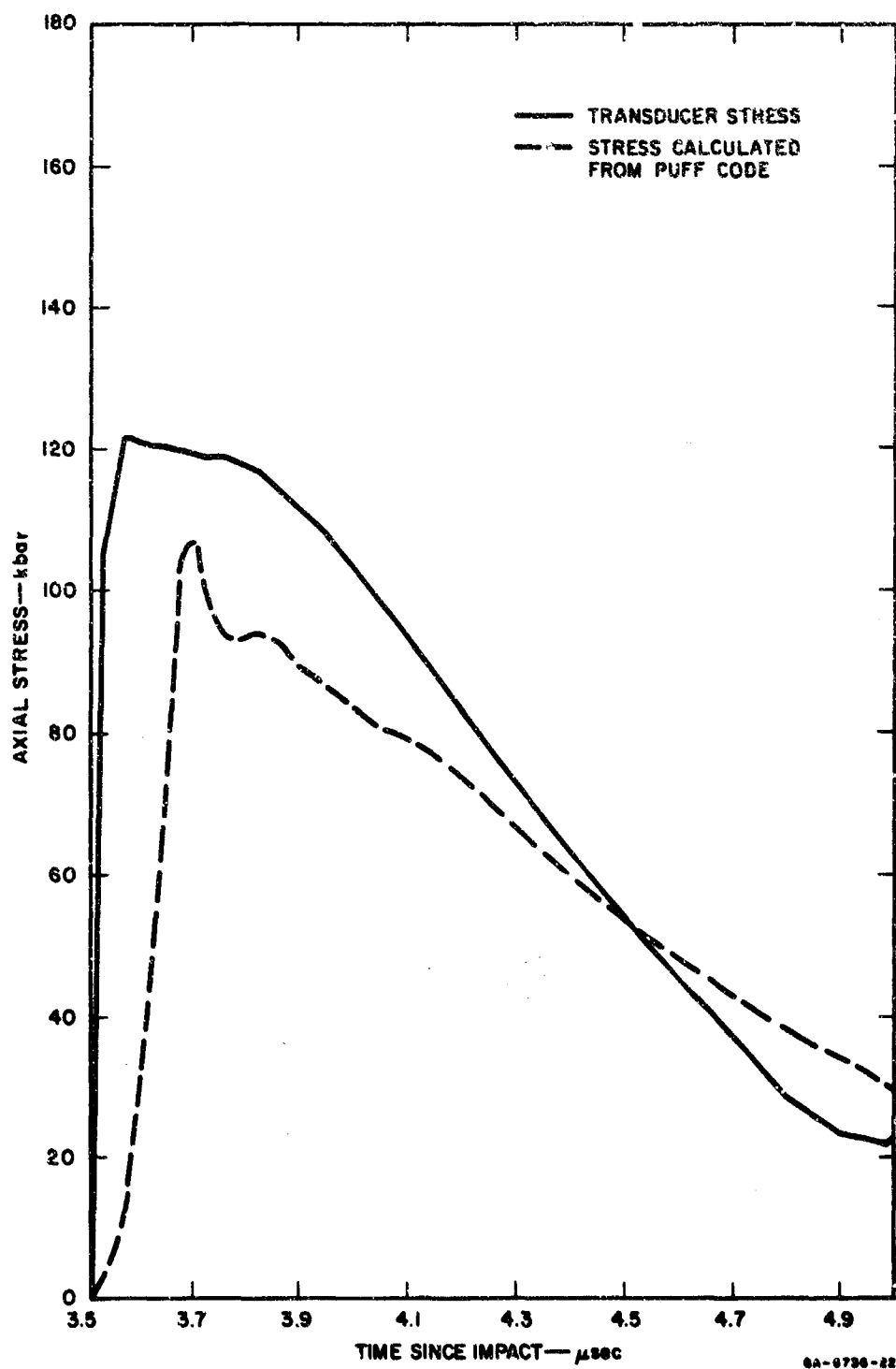


FIGURE 28. COMPARISON OF COMPUTED AND RECORDED STRESS HISTORIES FROM SHOT 13,529 IN 25.42-mm-THICK 2024-T8 ALUMINUM TARGET

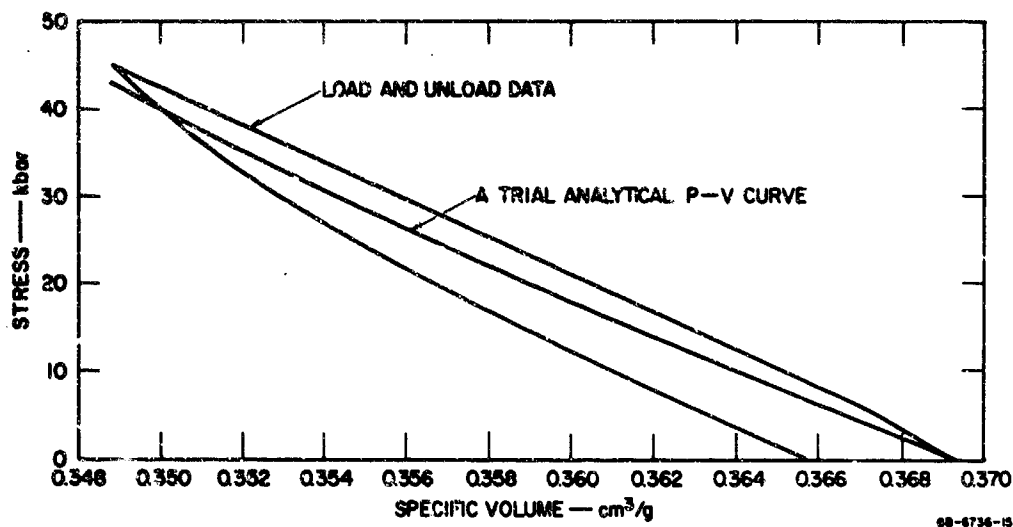


FIGURE 27 STRESS-VOLUME PATH REDUCED FROM DATA ON 6061-T6 ALUMINUM AND A COMPUTED PRESSURE-VOLUME RELATION

exist between the calculated and measured unloading portions of the waves indicate that different values of the Bauschinger parameters should permit a better quantitative match between computation and experiment.

##### 5. Summary of Results

The results of experiments and theoretical calculations with 2024-T8 and 6061-T6 aluminum fall into three main categories:

- Bauschinger effect: pronounced Bauschinger effect in both alloys governed the speed of rarefaction waves, the shape of the unloading portion of stress waves, and the stress attenuation rate. The apparent shear modulus was 60 to 70 percent larger for unloading from 50 kbar than for initial loading. No unloading yield point was observed; rather a gradual transition from elastic to plastic behavior during unloading, with a continuously decreasing shear modulus, was observed.
- No significant stress relaxation effects were observed in the dynamic experiments with either alloy for the specimen thicknesses (1/8 inch and larger) studied; this result is in accord with the experimental observation that little difference was observed between the static and dynamic yield strengths for plane strain. This result does not preclude the existence of stress relaxation effects at very early times.

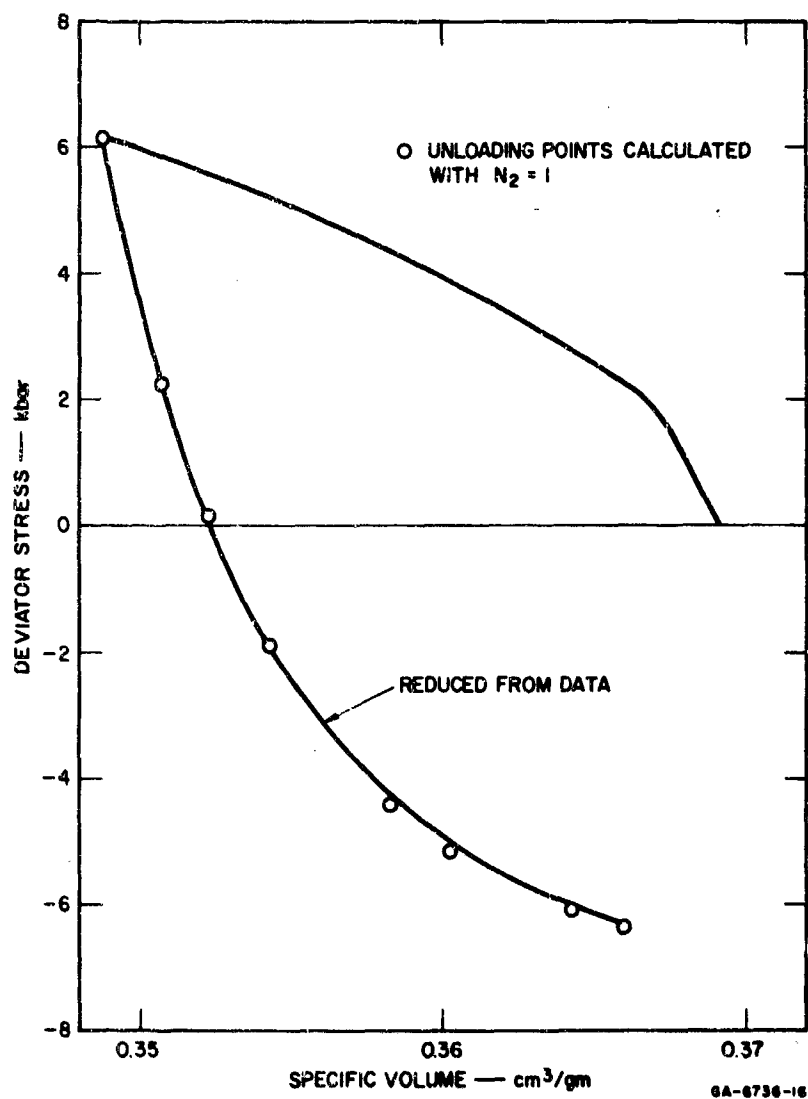


FIGURE 28. RELATIONSHIP BETWEEN DEVIATORIC STRESS AND SPECIFIC VOLUME OBTAINED FROM 50-kbar TESTS IN 6061-T6 ALUMINUM

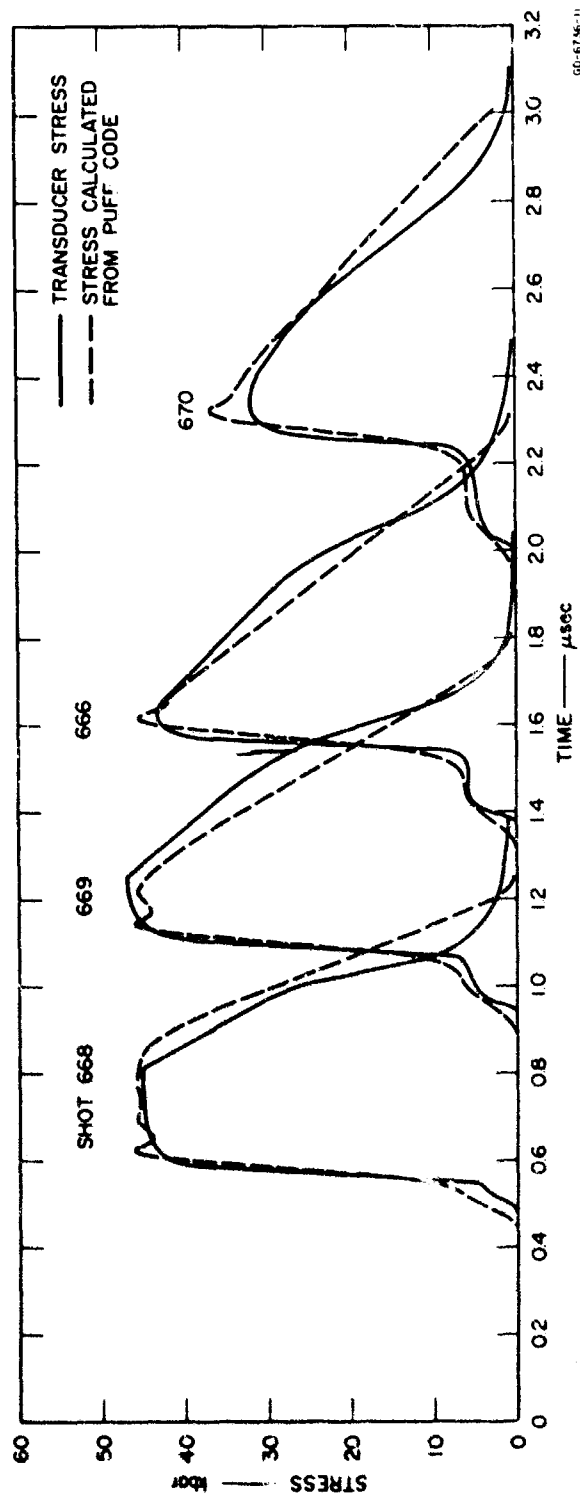


FIGURE 28. COMPARISON OF COMPUTED AND RECORDED STRESS HISTORIES  
FROM IMPACTS WITH 6061-T6 ALUMINUM AT 50-kbar

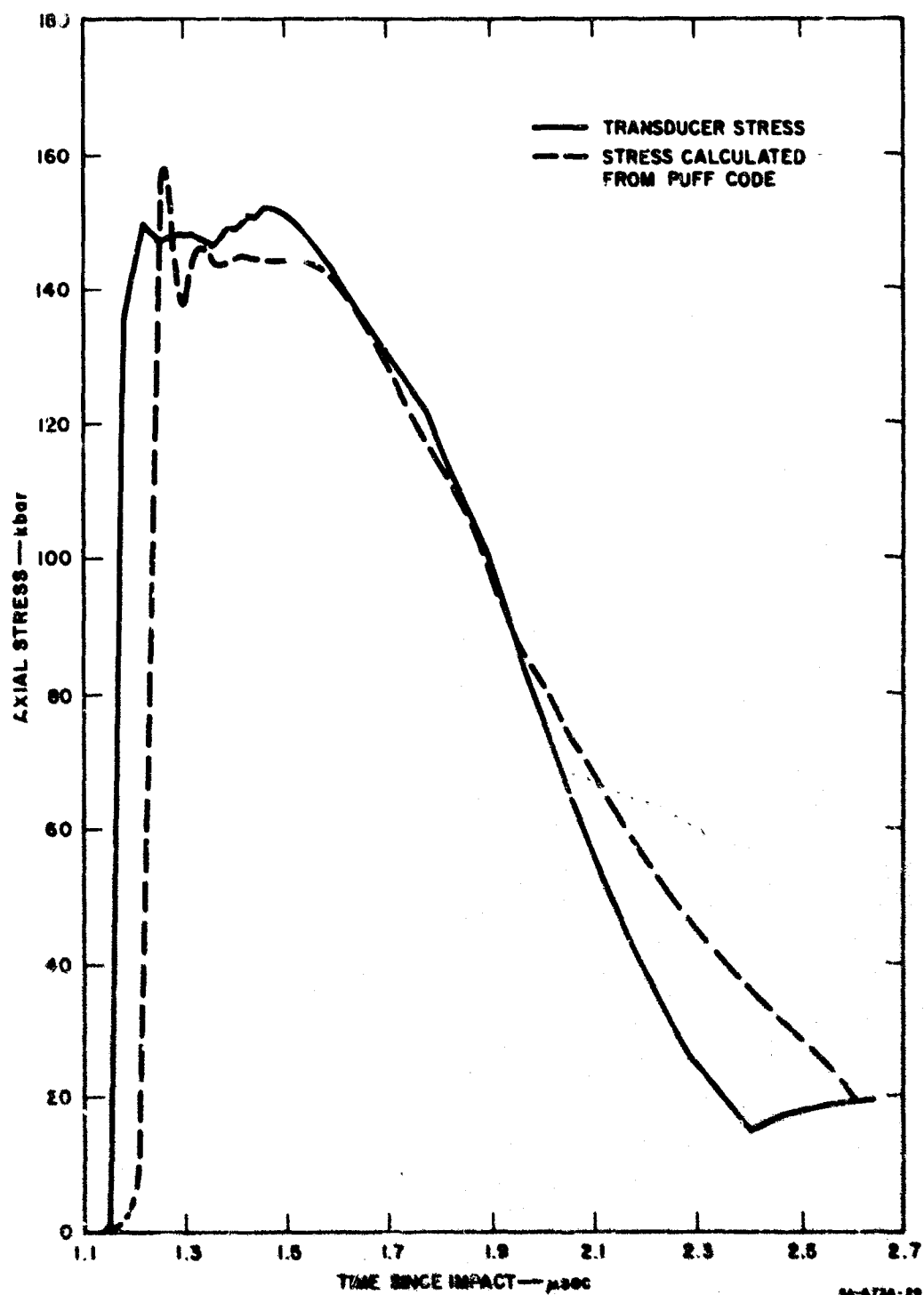


FIGURE 30. COMPARISON OF COMPUTED AND RECORDED STRESS HISTORIES FROM SHOT 13,550 IN 8.21-mm-THICK 8081-T8 ALUMINUM TARGET

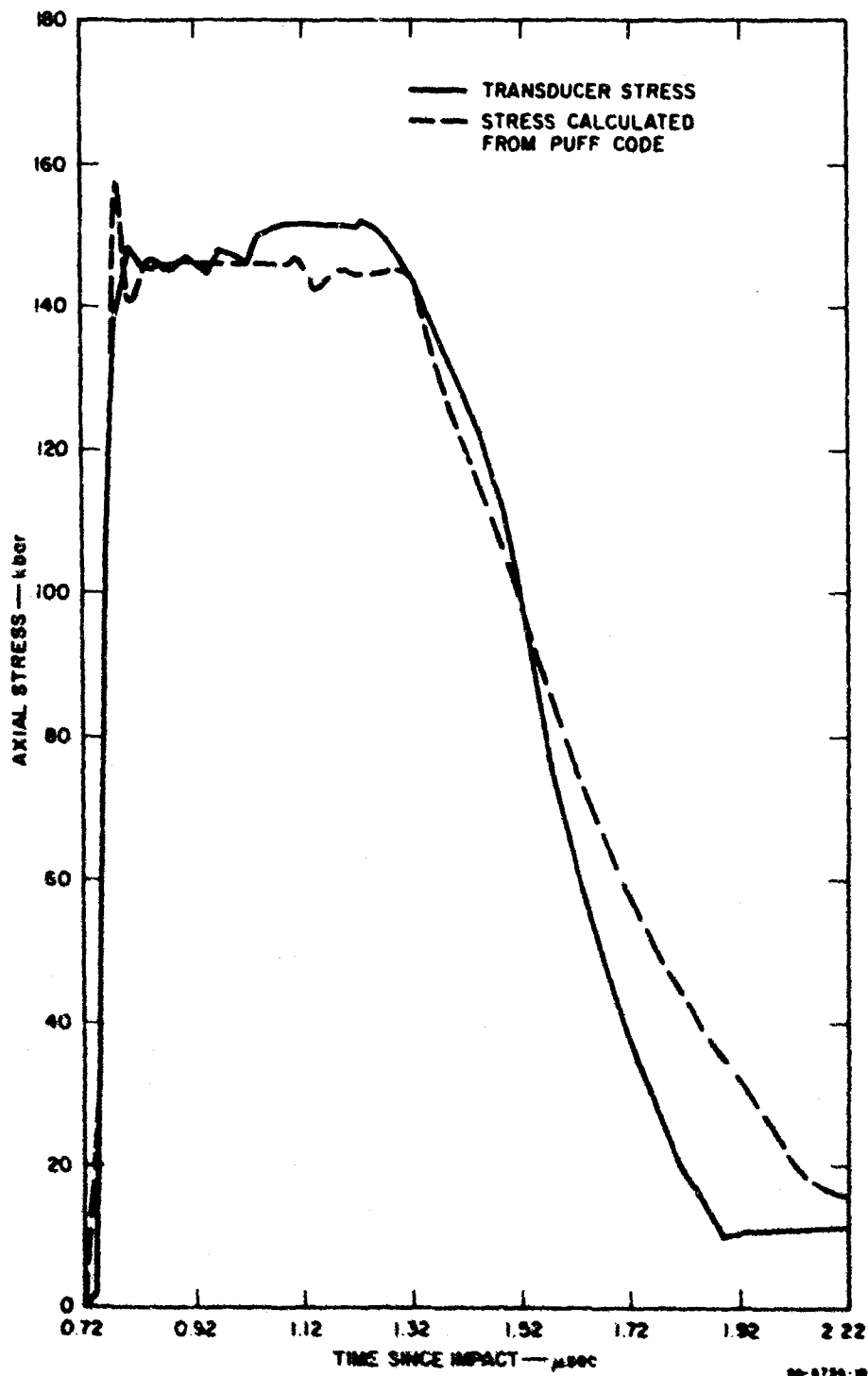


FIGURE 31. COMPARISON OF COMPUTED AND RECORDED STRESS HISTORIES FROM SHOT 13,569 IN 4.88-mm-THICK 6061-T8 ALUMINUM TARGET

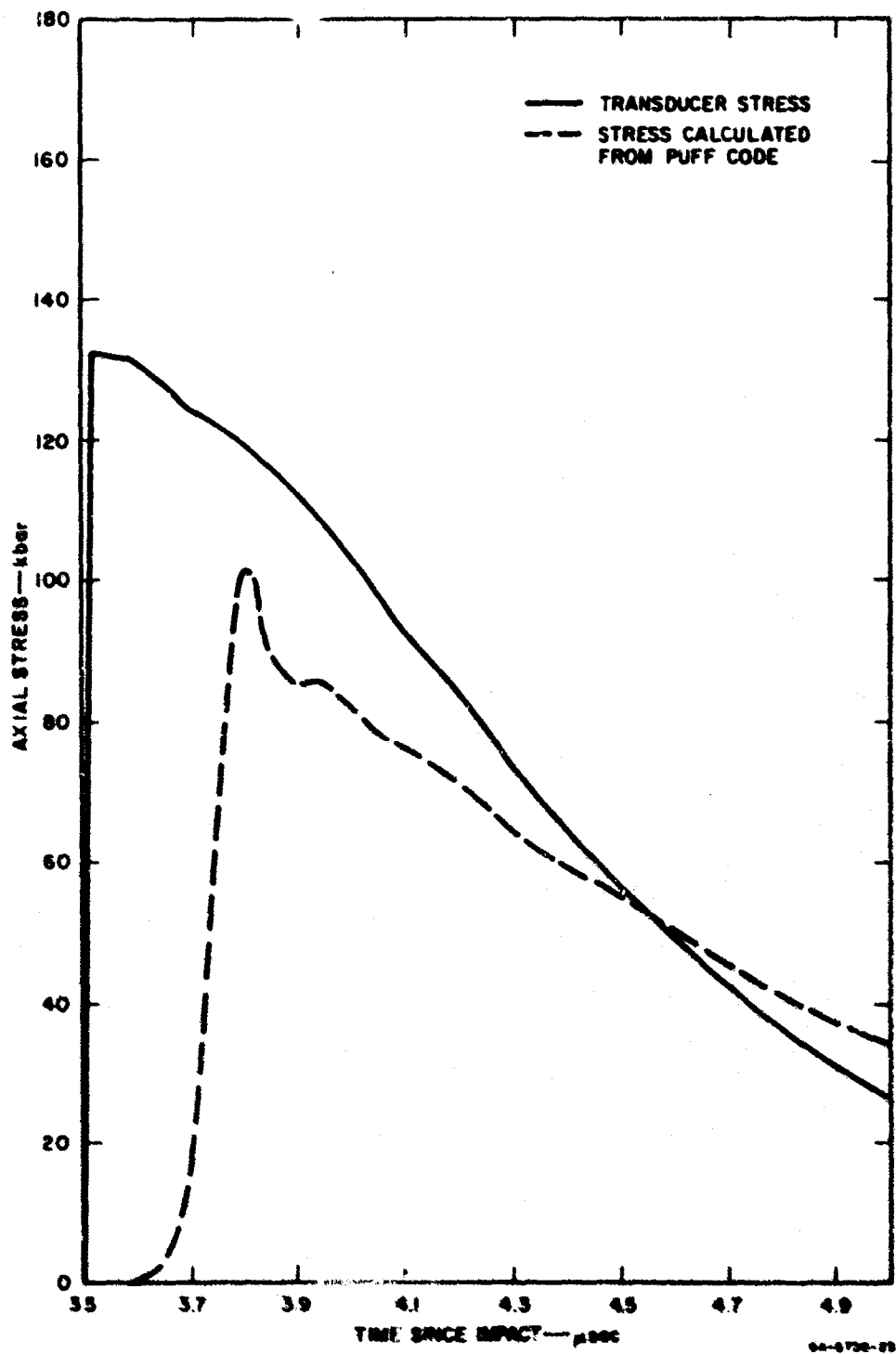


FIGURE 32. COMPARISON OF COMPUTED AND RECORDED STRESS HISTORIES FROM SHOT 13.630 IN 25-mm-THICK 6061-T8 ALUMINUM TARGET

- A large elastic-plastic transition region in the stress-volume plane was observed in the vicinity of the HEL for both alloys. This convex-upward region of negative curvature leads to a gradually rising nonsteady-state stress profile between the precursor and main wave. Errors of 5 or 10 percent may result in calculated Hugoniot points if this region is ignored and a simple one- or two-wave structure assumed instead. Fair correlation was obtained between the stress records and the stress histories calculated on the basis of the Bauschinger model in the SRI PUFF 2 code. The model appears to represent both alloys qualitatively, but the numerical values of the model parameters for each metal require further investigation.



## SECTION V

### STUDY OF TITANIUM

#### 1. Introduction

The preliminary investigation of titanium alloys was directed toward establishing Hugoniot in the low stress range, measuring shock attenuation, examining strain rate effects, looking for phase transitions, and observing the stress wave appearance.

For structural purposes, titanium is usually alloyed with other materials to improve its mechanical properties. Pure titanium is in the alpha (hcp) crystal phase at room temperature. But with the addition of certain alloying metals, the high-temperature beta (bcc) phase can be retained at room temperature.

These alloys were selected: type 50A, commercially pure (99.2 percent) titanium, that is, all alpha phase; Ti-6Al-4V (6 percent aluminum, 4 percent vanadium), an alloy with mixed alpha and beta phases; and Ti-13Cr-11V-3Al (73 percent titanium, 13 percent vanadium, 11 percent chromium, 3 percent aluminum), an alloy that is all beta phase. The Ti-6Al-4V alloy was selected because it is a material of practical importance that has been studied at intermediate strain rates, where it exhibited strain rate sensitivity (Ref. 8). The 50A titanium and Ti-13Cr-11V-3Al were chosen to study independently the behavior of each of the constituent phases of the Ti-6Al-4V alloy.

The titanium alloys were supplied by Titanium Metals Corporation of America, Los Angeles, in thicknesses of 1/16 inch to 1-1/8 inches. It did not appear to be economical nor possible within the time requirements to form all sheets of an alloy from a single billet. Therefore, the manufacturer selected sheets from billets with a nearly identical chemical composition. All sheets were supplied fully annealed, and no tempering or work hardening was performed at SRI on the sheets.

A table of quasi-static mechanical properties of these alloys is included here for reference (Table 7). Some of the information was obtained from our quasi-static and acoustic measurements listed in Appendix II, some from Molchanova (Ref. 42), from Titanium Metals Bulletin

Table 7

## PROPERTIES OF TESTED TITANIUM ALLOYS

Alloy	Density (g/cm <sup>3</sup> )	Young's Modulus (kbar)	Yield Strength (kbar)	Poisson's Ratio	Phase <sup>a</sup>
Type 50A	4.507	1070	3.5	0.328	alpha
Ti-6Al-4V	4.424	1210	9.5	0.314	alpha and beta
Ti-13V-11Cr-3Al	4.839	1040	9.3	0.332	beta

<sup>a</sup> Alpha phase is hexagonal, close packed; beta is body-centered cubic. The percentage of alpha and beta in Ti-6Al-4V depends on the heat treatment. Both Ti-6Al-4V and Ti-13Cr-11V-3Al are heat-treatable.

(Ref. 43, 44), and from Harman (Ref. 45). The Young's modulus varies from 1000 to 1200 kbar for all the heat-treatable alloys, depending on the heat treatment. It is lowest, of course, for annealed alloys (and for pure alpha, which is not sensitive to heat treatment), higher for solution treated alloys, and highest for aged and solution treated. Hence, particularly at low stresses, one would not expect a unique Hugoniot for a heat-treatable alloy. The Hugoniot for pure titanium is given by McQueen and Marsh (Ref. 46).

$$U_s = 4.779 \times 10^5 + 1.089 U \quad (102)$$

where  $U_s$  and  $U$  are shock and particle velocity in centimeter/second. The corresponding PUFF-form for the Hugoniot is

$$P = 1.028 \times 10^{12} \mu + 1.21 \times 10^{12} \mu^2 + 2.06 \times 10^{11} \mu^3 \quad (103)$$

where  $\mu$  is pressure in dyne/cm<sup>2</sup>.

## 2. Dynamic Experiments

Both gas gun and HE impact experiments were conducted on the three chosen titanium alloys. The experimental arrangement for the gas gun tests was similar to that used for the aluminum impacts (Fig. 8), except that titanium flyer plates were bonded directly to the aluminum projectile and manganin in Hi-D glass <sup>\*</sup> transducers were used. Configuration B (Fig. 9) with manganin in C-7 transducers and optical instrumentation were used for the HE experiments. The Hugoniot data obtained from these tests are summarized in Figs. 33 through 36 and Table 8.

The present data for type 50A titanium agrees closely with data from studies of Walsh et al. (Ref. 47) and McQueen and Marsh (Ref. 46). They used a gap technique that is not capable of resolving multiple shock waves associated with phase transformations. In spite of the phase transformation (described later) beginning around 50 kbar, there is good agreement between our data and theirs. This indicates that the dynamic phase transition is associated with only a small overall density change and has little effect on shock velocity.

The Hugoniot points above 100 kbar were obtained with the HE system. In all HE experiments the elastic wave was overdriven; therefore, a steady-state, single-wave analysis procedure (the impedance match method) was used to reduce the data.

In the gas gun experiments, the maximum stresses were below 100 kbar. The precursor, a second wave associated with a phase change in the case of pure titanium, and a gradually increasing stress between waves were in evidence in the stress transducer records. Two of these records are shown in Fig. 37. The upper figure shows the wave caused by the phase transformation. These complexities in the wave front necessitated the use of the integration procedure of Section III.1 to determine the stress-volume and stress-particle velocity relations. The results of these integrations are shown in Figs. 35 and 36.

The static yield strengths and Hugoniot elastic limits from the gas gun experiments on the three alloys are listed in Table 9. (Neglecting strain-rate effects, the HEL and static yield strengths of an isotropic,

<sup>\*</sup> See Section III.2.c

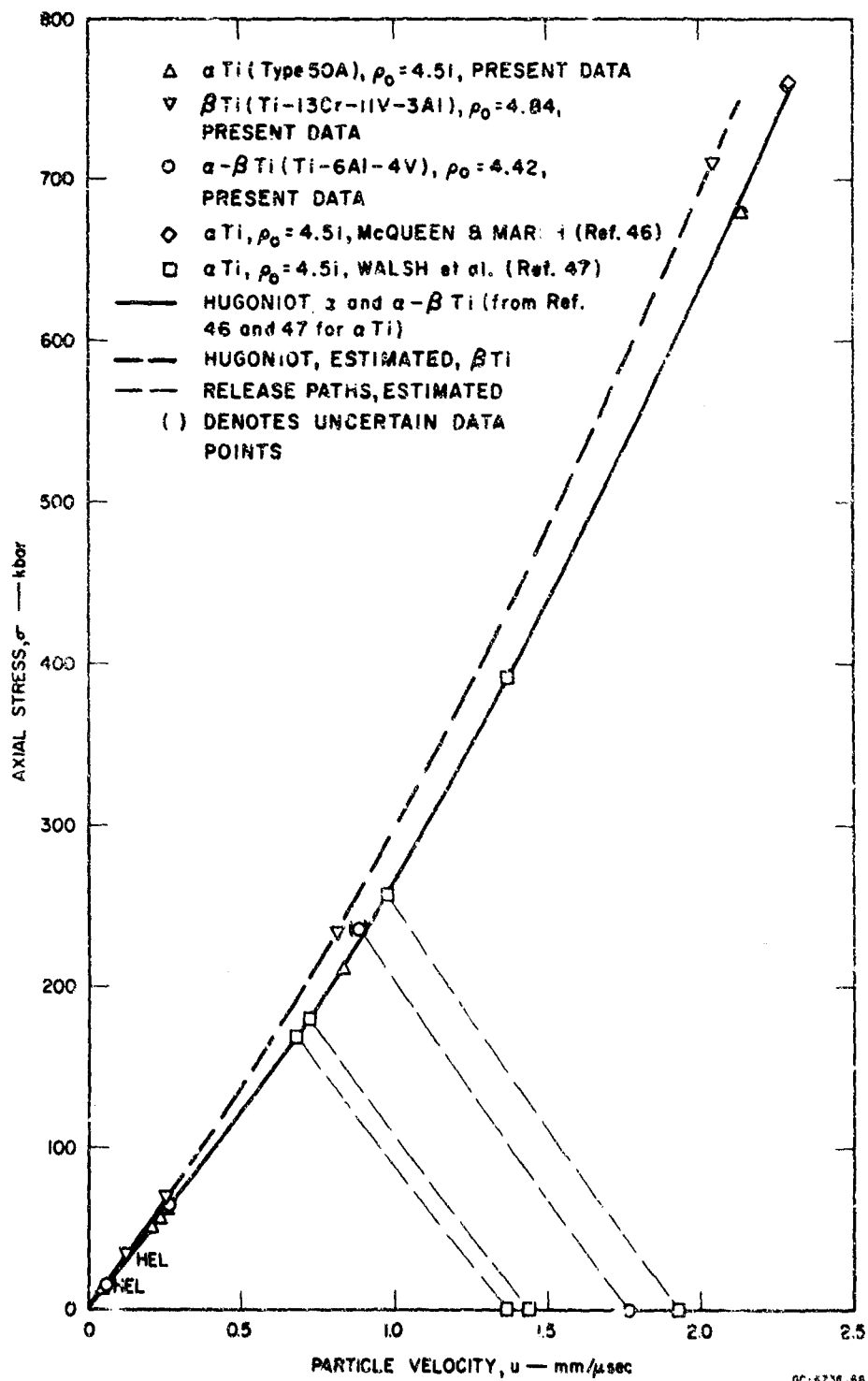


FIGURE 33 STRESS-PARTICLE VELOCITY HUGONIOT AND RELEASE DATA FOR TITANIUM ALLOYS

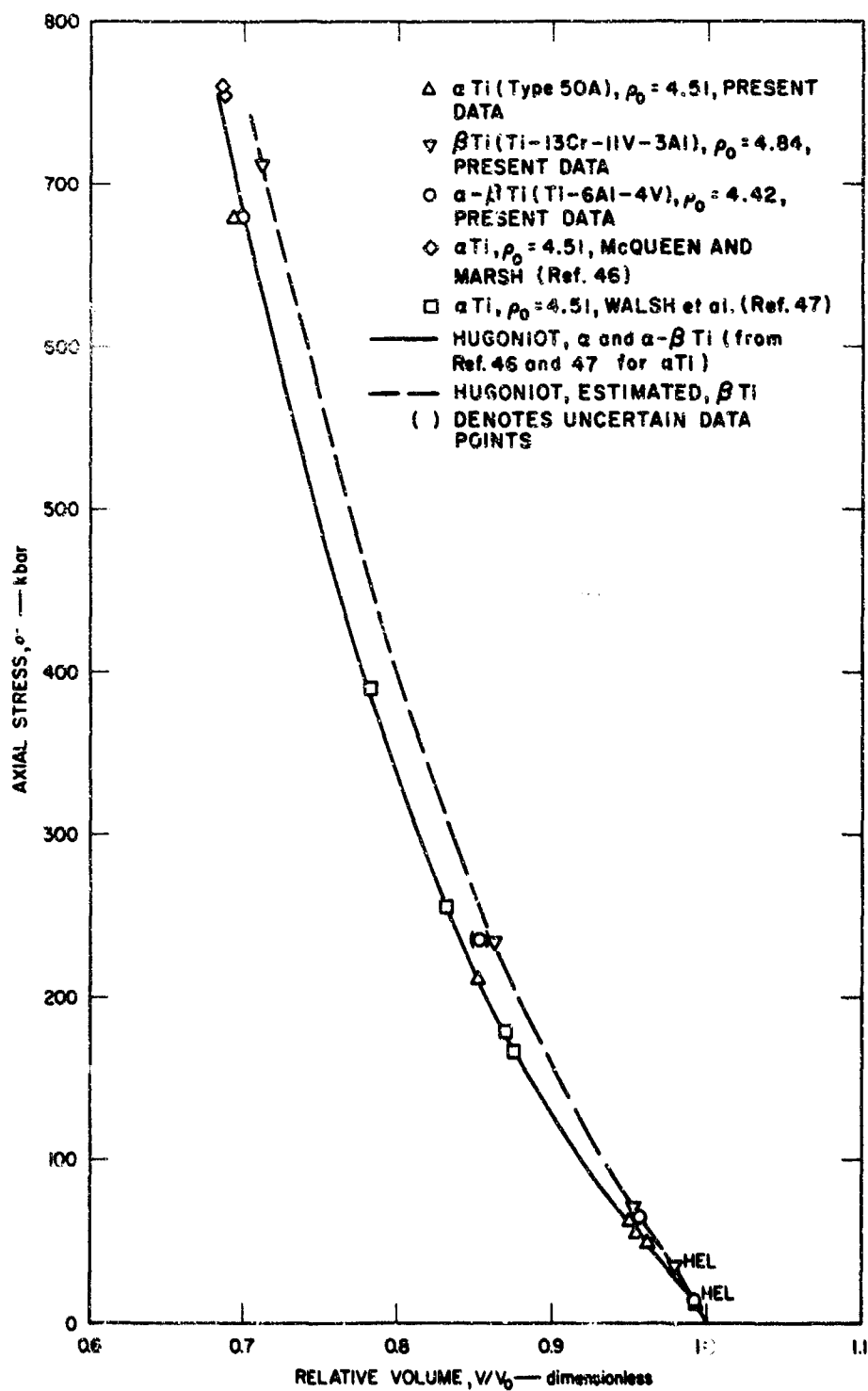


FIGURE 34 STRESS-VOLUME HUGONIOT DATA FOR TITANIUM ALLOYS

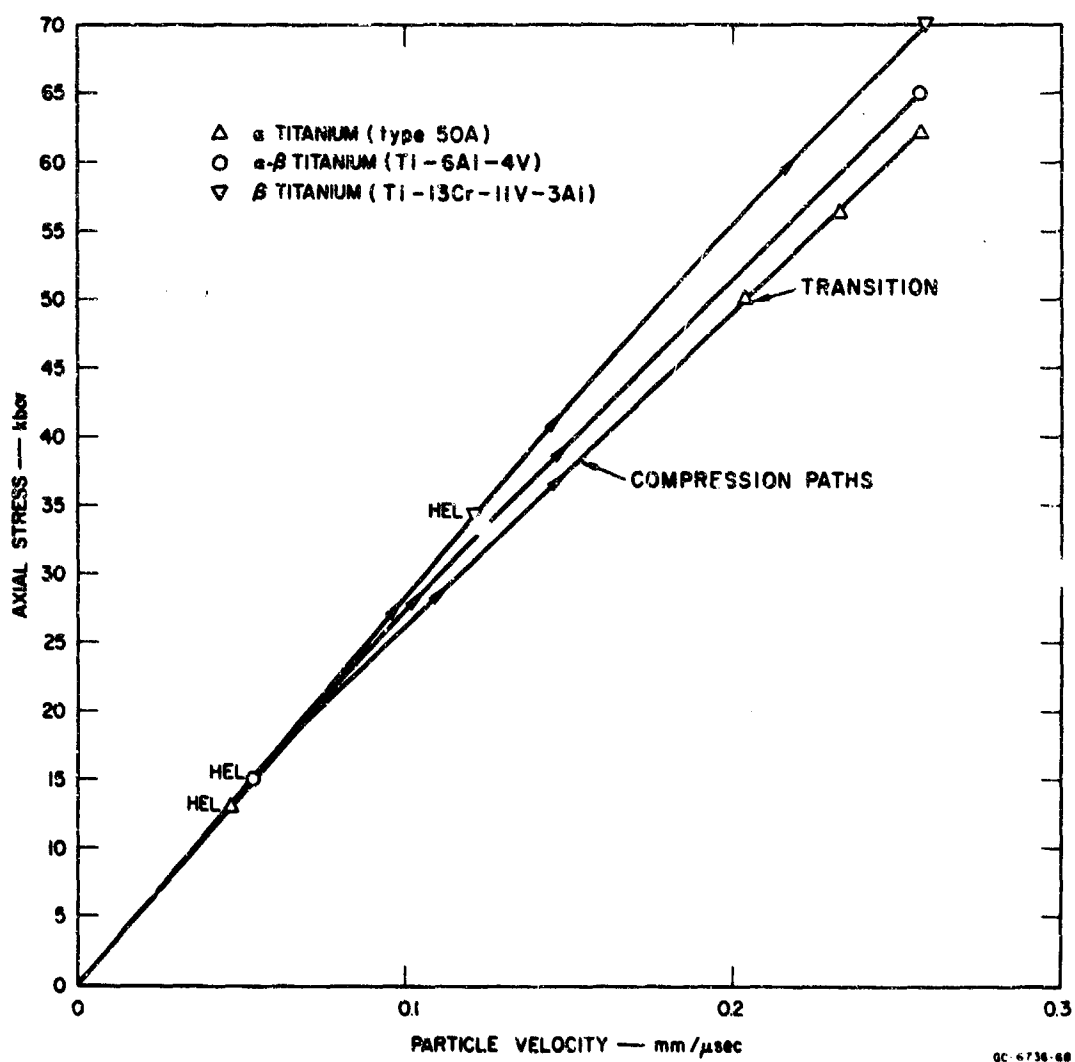


FIGURE 36 STRESS-PARTICLE VELOCITY HUGONIOT DATA AT LOW STRESSES FOR TITANIUM ALLOYS

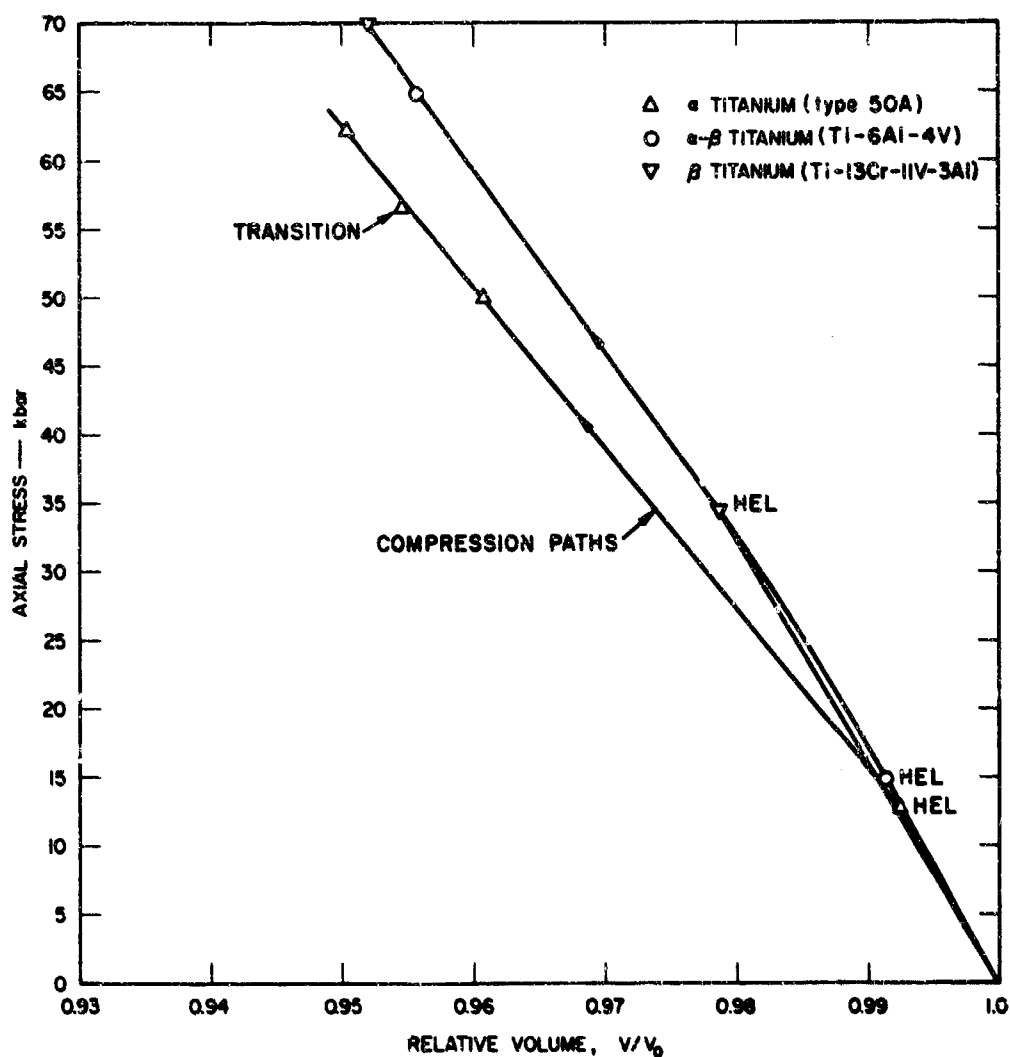


FIGURE 36 STRESS-VOLUME HUGONIOT DATA AT LOW STRESSES FOR TITANIUM ALLOYS

Table 8  
HUGONIOT DATA FOR THREE TITANIUM ALLOYS

$\alpha$  Titanium\*, Type 50A,  $\rho_0 = 4.51 \text{ g/cm}^3$

Shot No.	Driver System	Specimen Thickness (mm)	Final Hugoniot State			
			Axial Stress $\sigma$ (kbar)	Particle Velocity $u$ (mm/ $\mu$ sec)	Specific Volume $V$ ( $\text{cm}^3/\text{g}$ )	Shock Velocity $U$ (mm/ $\mu$ sec)
G 589*	Gas gun; projectile velocity = 0.466 mm/ $\mu$ sec	9.93	56.5	0.233 <sup>†</sup>	0.211	--
G 604	Gas gun; projectile velocity = 0.515 mm/ $\mu$ sec	9.95	62.2	0.258 <sup>†</sup>	0.210	--
73,526 <sup>‡</sup>	HE system D; driver free surface velocity = 1.56 mm/ $\mu$ sec	5.08	211	0.835	0.189	5.63
13,527	HE system B; driver free surface velocity = 4.85 mm/ $\mu$ sec	4.83	679	2.14	0.154	7.01
$\beta$ Titanium,** Ti-13Cr-11V-3Al, $\rho_0 = 4.84 \text{ g/cm}^3$						
G 819**	Gas gun; projectile velocity = 0.519 mm/ $\mu$ sec	6.97	70	0.259	0.197	--
13,524 <sup>††</sup>	HE system D; driver free surface velocity = 2.04 mm/ $\mu$ sec	6.76	234	0.815	0.178	3.94
13,527	HE system B; driver free surface velocity = 4.85 mm/ $\mu$ sec	6.54	712	2.05	0.147	7.13
$\alpha - \beta$ Titanium, <sup>†††</sup> Ti-6Al-4V, $\rho_0 = 4.42 \text{ g/cm}^3$						
G 791 <sup>‡‡</sup>	Gas gun shots, average	19.5	65.0 <sup>§§</sup>	0.258 <sup>†††</sup>	0.216 <sup>§§</sup>	
G 818 <sup>‡‡</sup>	Projectile velocity = 0.516 <sup>§§</sup> $\pm 0.001$ mm/ $\mu$ sec	5.72				
13,523	HE system D; driver free surface velocity = 2.10 mm/ $\mu$ sec	5.52	(237) <sup>***</sup>	(0.885) <sup>***</sup>	(0.193) <sup>***</sup>	(5.08) <sup>***</sup>
13,527	HE system B; driver free surface velocity = 4.85 mm/ $\mu$ sec	4.84	712	2.05	0.147	7.13

\* The following intermediate states were observed on Shot G589: an MEL of  $\sigma = 12.8$  kbar,  $u = 0.0404$  mm/ $\mu$ sec,  $V = 0.219 \text{ cm}^3/\text{g}$ ; and a phase transformation at  $\sigma = 30.0$  kbar,  $u = 0.204$  mm/ $\mu$ sec,  $V = 0.213 \text{ cm}^3/\text{g}$ .

<sup>†</sup> Taken to be one-half the projectile velocity.

<sup>‡</sup> In Shot 13,523 a C-7/manganin stress transducer on the Ti specimen recorded a final stress of 82 kbar. The on-Hugoniot particle velocity associated with 82 kbar is  $u = 1.45$  mm/ $\mu$ sec. This  $\sigma - u$  state represents an experimental determination of a point on the release adiabat on Ti shocked to 211 kbar.

<sup>§</sup> See Table 1 for description of HE systems.

<sup>\*\*</sup> On Shot G 819 the MEL was measured to be  $\sigma = 34.4$  kbar,  $u = 0.1215$  mm/ $\mu$ sec,  $V = 0.202 \text{ cm}^3/\text{g}$ .

<sup>††</sup> On Shot 13,524 the specimen free-surface velocity was observed to be  $1.9 \pm 0.3$  mm/ $\mu$ sec. The large experimental uncertainty is caused by a large shock tilt.

<sup>‡‡</sup> On Shots G 791 and G 818 the average MEL was determined to be  $\sigma = 18.0$  kbar,  $u = 0.0538$  mm/ $\mu$ sec,  $V = 0.224 \text{ cm}^3/\text{g}$ .

<sup>§§</sup> Averaged data from Shots G 791 and G 818.

<sup>\*\*\*</sup> Large experimental uncertainty due to poor transit time mirror cutoffs on streak camera record.



Table 9

## COMPARISON OF STATIC AND DYNAMIC YIELD STRENGTH IN TITANIUM

Alloy	Static Yield (kbar)	Hugoniot Elastic Limit (kbar)	HEL predicted from static yield and Poisson's ratio (kbar)
Type 50A	3.5	12.8	6.85
Ti-6Al-4V	9.5	15	17.5
Ti-13Cr-11V-3Al	9.3	34.4	18.4

homogeneous material obeying a von Mises or Tresca-type yield criterion are related by

$$\sigma_{HEL} = \frac{1 - \nu}{1 - 2\nu} Y \quad (104)$$

This equation was used to calculate the values in the fourth column of the table.) The HEL's for the type 50A titanium and Ti-13Cr-11V-3Al alloys are nearly double those calculated from the static data (column 4 of Table 9). By contrast, the observed HEL for Ti-6Al-4V is lower than that calculated from static data. In the stress records the Ti-6Al-4V alloy exhibited a wide yielding zone between the precursor and main wave, extending from the HEL to 2.3 times the HEL (an example of such a range is shown in Fig. 37b). The other alloys showed a smaller yielding zone (in type 50A, the yielding zone extended only to 1.3 times the HEL). The extensive yielding zone in Ti-6Al-4V is caused by a significantly rounded yield "point" in the stress-strain curve. This rounded yield point also helps to explain the occurrence of a low HEL. The experimentally measured HEL actually corresponds to the "proportional limit," the stress at which the stress-strain curve first deviates from a linear relation. Normally, the proportional limit is somewhat smaller than the so-called yield strength (0.2% offset definition used here). For a well-rounded yield point, the proportional limit could be much lower than the 0.2% offset yield point.

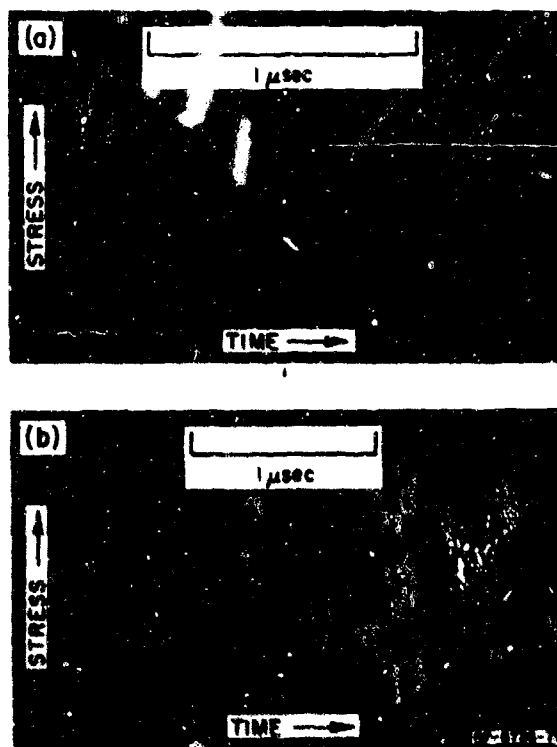


FIGURE 37 MANGANIN STRESS RECORDS  
FROM TEST G689 ON TYPE 50A  
TITANIUM AND TEST G791  
ON TI-6AL-4V

The disparity in dynamic yield behavior of the three titanium alloys indicates that low strain rate yield data are not adequate to predict dynamic yielding in these metals. The large increase in yield strength for alpha and beta titanium at high strain rates is some justification for the inclusion of a rate-dependent yield criterion in wave propagation calculations. However, attenuation of the elastic precursor (a definite sign of strain-rate effects) was not observed in any of the titanium experiments over propagation distances ranging from 5 mm to 9.5 mm. This does not imply that stress relaxation does not occur over distances less than 5 mm. The work of Isbell and Froula (Ref. 48) on very thin targets indicated that although stress relaxation was important over short distances, no further relaxation occurred after propagation distances of 7 mm; this is consistent with our results.

As mentioned above, indication of a dynamic phase transition was observed in type 50A titanium (see Fig. 37a). Shock loading to a peak stress of 56.5 kbar caused the plastic wave to split into two waves, which is the effect produced by transformation times that are comparable to or less than the wave transit time. The separation of these waves was very small even after transit through a 3/8-inch-thick sample, indicating that the overall volume change associated with this transition or partial transition is small (approximately 0.2 percent). The transition stress was 50 kbar and the transition was overdriven in subsequent experiments at a stress of 62 kbar. Our observation of such a transition was subsequently corroborated by Isbell and Froula (Ref. 48). No such transition wave was observed in either Ti-6Al-4V or Ti-13Cr-11V-3Al titanium; however, any such transition is expected to occur at different pressures in these alloys, and the ease with which the transition wave can be overdriven in 50A titanium suggests that it may take considerable investigation to discover a like transition in the other two alloys.

Rarefaction velocities were obtained as a function of stress level from the low stress experiments. These velocities are shown in Table 10 as a function of stress level. These rarefaction velocities appear to coincide with the shock velocity of the HKL (except in the case of the all

Table 10

## RAREFACTION AND SHOCK VELOCITIES IN TITANIUM ALLOYS

Shot No.	Material	Peak Stress (kbar)	Wave Velocities		
			To HEL	To Peak (mm/ $\mu$ sec)	Initial Release from Peak
G 604	Type 50A	62.0	6.1	5.05	6.1
G 791	Ti-6Al-4V	65.0	6.3	5.20	6.3
G 818	Ti-6Al-4V	65.0	6.3	--	6.3
G 819	Ti-13Cr-11V-3Al	70.0	5.8	--	6.2

beta alloy). Such a coincidence of rarefaction and initial shock velocity is actually predicted by the model of perfect plasticity. Hence, this simple plastic model might be sufficiently accurate for titanium alloys: the more complex Bauschinger model would not be required. A determination of the appropriate model should, however, be made from a comparison of computed and experimental stress records.

### 3. Initial and Terminal Observations of Shocked Titanium Specimens

Initially, the 50A titanium ("as-received") had slightly elongated grains of about 30  $\mu$  diameter. The average Vickers hardness (500 gram load) was 142. Based on the relative intensity of X-ray reflection from flat specimens, one may conclude that there is some preferred orientation of the grains. After shocking to 56 kbar, the Vickers hardness of one specimen had increased to 200. Microstructural changes are clearly evident in this specimen. Nearly all the grains appear heavily marked with parallel sets of lamellae which, for the most part, completely traverse a grain (see Fig. 33). However, some grains show additional markings that do not appear to be twins but which more closely resemble a transformation structure. X-ray diffraction examination of the shock-loaded sample disclosed no evidence of new phases; so any transformation taking place during the shock must have reverted to alpha on release of pressure.

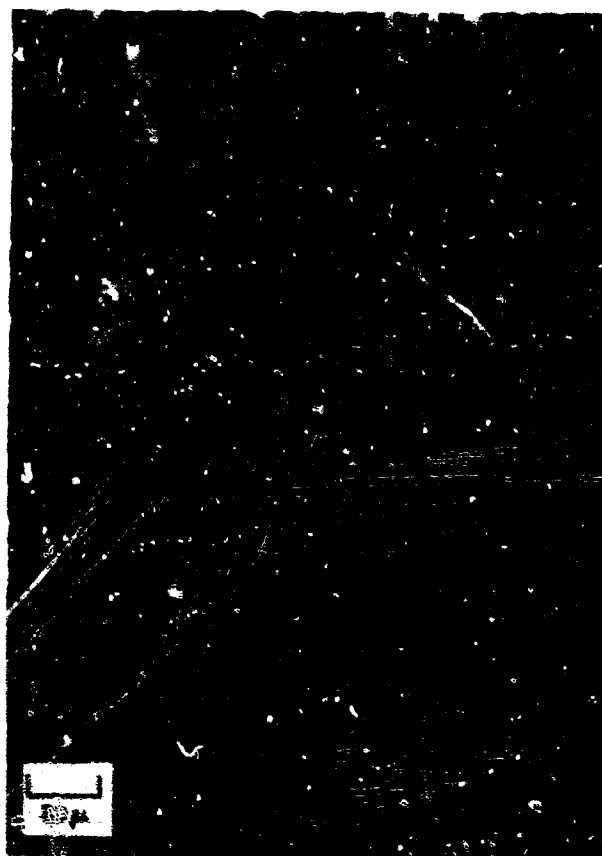


FIGURE 38 PHOTOMICROGRAPH OF TYPE 50A  
TITANIUM SAMPLE AFTER BEING  
SHOCKED TO 56 kbar

Deribas et al. (Ref. 50) have described experiments in which titanium was shock hardened to 400 Vickers. They report a microstructure characterized by "immense distortion," similar to that observed in iron shocked to pressures in excess of 100 kbar. They do not specify the pressure used to obtain this result; from their limited description of the experiments, we can estimate that pressures in the range of 150 to 400 kbar were used. While positive identification of the high-pressure phase is not possible, it is presumed to be the well-known omega (hexagonal) phase known to exist for some titanium and zirconium alloys. According to Jamieson (Ref. 49), the volume change for the alpha-omega transition in pure titanium is about 2 percent at 1 atm. He reported that the omega phase of titanium can be retained at 1 atm, but that it

reverts to the alpha structure after prolonged heating at 110°C. Deribas et al. (Ref. 50) did not report the presence of omega phase in their hardened specimens, and it appears likely that the residual temperature of the shocked titanium after release of pressure was too high to permit survival of omega in their experiments.

Our present interpretation of our experimental results is that a partial transformation of alpha titanium to the omega phase took place at a pressure of 50 kbar. (The pressure required for the static transition is not known). A volume change at the transition of at most 0.2 percent may be inferred from the transducer records. If one assumes that the volume change for the alpha-omega transition at 50 kbar is roughly the same as the 1-atm volume difference measured by Jamieson, it would appear that about 10 percent of the alpha titanium transformed in this experiment. This result is consistent with both the present metallographic results and with the increase in hardness observed. One may infer from the results of Deribas et al. (Ref. 50) that a large pressure excess is required to drive the transformation to completion in the microseconds or submicroseconds available in shock experiments. Titanium thus appears to behave in a manner similar to that of iron (Ref. 51). Although the transformation of iron to the epsilon phase has been inferred to begin at shock pressures as low as 120 kbar, complete transformation requires a shock pressure of about 160 kbar. In the case of pure iron, the high pressure phase is not retained on release of pressure. The great hardening effect observed in shock loaded iron has been attributed to the dislocation structure produced by the transformation of epsilon to alpha-iron on release of pressure. Thus, alpha titanium appears to undergo a phase transformation initiated by a shock stress of 50 kbar and completed in the range of 150 to 400 kbar. The extent of transformation depends on the stress level reached. During unloading in titanium, the high pressure phase (probably omega) is retransformed to alpha with a considerably higher hardness than the original material.

The microstructure of the shocked alpha-beta alloy (Ti-6Al-4V) was indistinguishable from the unshocked material. The virgin material had a Vickers hardness of 300 (500 gram load). The shock loaded specimen had a very marginal increase in hardness to Vickers 318.

The microstructure of the shocked beta alloy (Ti-13V-11Cr-3Al) was distinguished by the presence of parallel sets of lamellae (see Fig. 39) presumably twins, which closely resemble the twins formed by shock loading iron, molybdenum, tungsten, chromium, and other body-centered cubic metals and alloys below any transition pressure. The Vickers hardness of the unshocked material was 300 (500 gram load); the shocked specimen had the same hardness. It appears then that no transformations occurred in Ti-6Al-4V or Ti-13Cr-11V-3Al during the passage of shock waves with stresses up to 70 kbar.

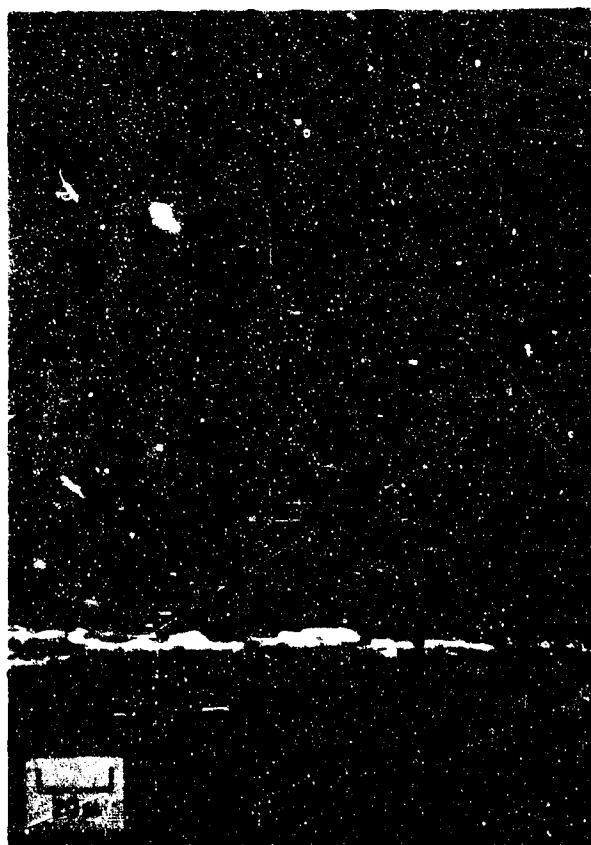


FIGURE 39 PHOTOMICROGRAPH OF Ti-13V-11Cr-3Al TITANIUM SPECIMEN AFTER BEING SHOCKED TO 70 kbar

AFWL-TR-69-96

This page intentionally left blank.



SECTION VI  
STUDY OF WOVEN QUARTZ PHENOLIC

1. Introduction

Preliminary experimental and calculational investigations have been performed to examine shock wave propagation properties between about 10 and 200 kbar for a three-dimensional (3-D) weave quartz phenolic material. The purposes of these studies were to obtain preliminary Hugoniot-type\* information for this material, to observe the character of stress waves that a highly anisotropic, heterogeneous material will support, and to determine how well present wave propagation theory, as incorporated in the SRI PUFF 2 code, is able to simulate stress wave profiles in an anisotropic, heterogeneous material.

2. Material Description

The specimen material, supplied by the Air Force Weapons Laboratory, was a composite consisting of an orthogonal 3-D weave of quartz filament potted in a phenolic resin matrix. Table II lists descriptive data supplied by AFWL with the specimens. The orthogonal weave of the quartz filaments is most easily visualized in terms of a Cartesian coordinate system with the Z axis in the direction of the axis of the right cylindrical specimen.

The weave was nearly orthogonal because all filaments lay approximately in the X, Y, or Z direction. In the Z direction the filaments were grouped together into well-contained, apparently straight bundles of square cross section with a 0.025 inch average width. These axial bundles intersected the X-Y planes (cylinder faces) in a square array with a 0.1 inch average distance center to center. According to Table II there were  $0.58 \times 10^6$  axial filaments per square inch intersecting the X-Y planes. The filaments in the X and Y directions were also arranged into bundles, but of apparently rectangular cross section. The width of a lateral bundle was approximately

---

\* A true Hugoniot point refers to an equilibrium state achieved through a steady-state shock front. In the woven material, the wave front is nonuniform and not steady state. Equilibrium between the filaments and resin requires a relatively long time and is therefore probably not established during the recording time of the experiment. The Hugoniot-type data derived from the experiments were obtained with traditional impedance match techniques, neglecting the fact that many of the conditions for valid Hugoniot data were not met.

Table 11

## DETAILED MATERIAL DESCRIPTION OF 3-D QUARTZ PHENOLIC \*

Property	Measurement
Average material density	1.69 g/cm <sup>3</sup>
Average acoustic velocity in axial direction	0.350 cm/μsec @ 1.0 MHz
Resin matrix	SC-1008 Phenolic
Resin content	33.7% by weight
Average diameter of filaments	0.00034 inch
Number of filaments in lateral (X) direction	$2.30 \times 10^8$ filaments/inch <sup>2</sup>
Number of filaments in lateral (Y) direction	$2.30 \times 10^8$ filaments/inch <sup>2</sup>
Number of filaments in axial (Z) direction	$0.58 \times 10^8$ filaments/inch <sup>2</sup>
Number of filaments per axial bundle	1920
Bundle size and spacing in the Z direction	0.025 on 0.1 inch centers

\* This information was supplied to SRI by AFWL.

0.075 inch and the thickness was about 0.025 inch. These lateral bundles were woven in a 2-D basket weave with, for example, a given X bundle passing over 1 to 8 Y bundles and under a similar number. The weave was not perfect but had an average or macroscopic rotational symmetry of  $90^\circ$  about the Z axis. The separation in the Z direction between parallel lateral bundles was about 0.05 inch center to center.

Acoustic measurements were made to determine the longitudinal velocity in the thickness direction. The velocity associated with the initial arrival averaged 4.51 mm/ $\mu$ sec. This velocity corresponds with a longitudinal modulus ( $\lambda + 2\mu$  or  $K + 4/3\mu$ ) of  $3.4 \times 10^{11}$  dynes/cm<sup>2</sup>.

### 3. Gas Gun and HE Experiments

The compression states measured in five gas gun and HE experiments performed in the 3-D weave quartz phenolic study material are summarized in Table 12 and Figs. 40 and 41; the results are discussed below. It must be pointed out that the nature of the quartz phenolic specimens, as well as direct experimental observations indicated that the flow was not steady-state. In this case the compressive "Hugoniot" states reported in Table 12 and Figs. 40 and 41 are characteristic of uniaxial flow shock wave experiments on 2 to 4-mm-thick specimens, but caution should be employed when applying them to other experimental conditions. For the purpose of describing gross average macroscopic response of material of a given thickness, we have neglected the deviations from steady-state flow.

Three gas gun shots\* were fired on the 3-D quartz phenolic discs as received. Two discs were impacted by 1/2-inch thick 2024 aluminum projectiles to obtain Hugoniot data (Shots 13,421 and 13,423) and one by a 0.0186-inch-thick annealed aluminum flyer plate (backed by 2 lb/cu ft polyurethane foam) to obtain shock attenuation information (Shot 13,422).

---

\* These experiments were performed under Contract F29601-67-C-0073.

Table 12  
"HUGONIOT" DATA FOR 3-D QUARTZ PENELOIC

Shot Number	Driver System		Specimen		Dynamic Elastic Shock Velocity (mm/sec)	Final (Hugoniot) state			Final state <sup>†</sup> in C-7 (a release state)			
	System	Flyer velocity (mm/sec)	thickness d (mm)	density $\rho$ (g/cm <sup>3</sup> )		Shock velocity, $U$ (mm/sec)	Particle velocity, $u$ (mm/sec)	axial stress, $\sigma_c$ (kbar)	Specific volume, $v$ (cm <sup>3</sup> /g)	Axial stress, $\sigma$ (kbar)	Particle velocity, $u$ (mm/sec)	Rise time: $t_r$ (microsec)
13,423	Gun	0.268	9.44	1.67	-	3.02	3.201	10.1	0.560	5.7 (4.5)	0.17 (0.14)	0.89 (0.59)
13,421	-	0.832	9.46	1.67	(1.17)	3.57	0.620	37	0.494	31 (25)	0.71 (0.60)	0.46 (0.36)
13,422	-	0.810	9.46	1.68	(4.52)	3.72	0.620	0.620	0.494	4.0 (3.3)	0.12 (0.10)	-
13,560	E (HE)	3.08	4.57	1.67	-	5.37 (5.13) <sup>††</sup>	2.07 (1.80) <sup>††</sup>	186 (210) <sup>††</sup>	0.370 (0.351) <sup>††</sup>	(1.45) <sup>††</sup>	(2.14) <sup>††</sup>	0.04 (0.04)
13,560	E (HE)	3.08	5.78	1.67	-					(1.45) <sup>††</sup>	(2.14) <sup>††</sup>	0.04

<sup>g</sup> The dynamic elastic limit was not well resolved and was not used in calculating the final state. No precursor was observed in the HE experiments.

<sup>h</sup> The release state was measured by a manganin/C-7 stress transducer. Particle velocity was calculated from the C-7 Hugoniot of Keough (1984). In the gun experiments there were two gages, one with the manganin element 0.015 inch back from the surface, the other 0.080 inch back.

<sup>i</sup> Data from the deeper element are modified by the longer travel time in C-7 and are therefore listed in parentheses.

<sup>j</sup> Projectile velocity for gun system, flyer velocity or driver free-surface velocity for HE systems.

<sup>k</sup> Rise time for 10 to 90% of the peak stress, experimental uncertainty about 25%.

<sup>l</sup> Shocks front attenuated, Hugoniot state not calculable. State at impact was probably similar to that for Shot 13,421.

<sup>m</sup> Uncertain data. There was a large variation in shock arrival time.

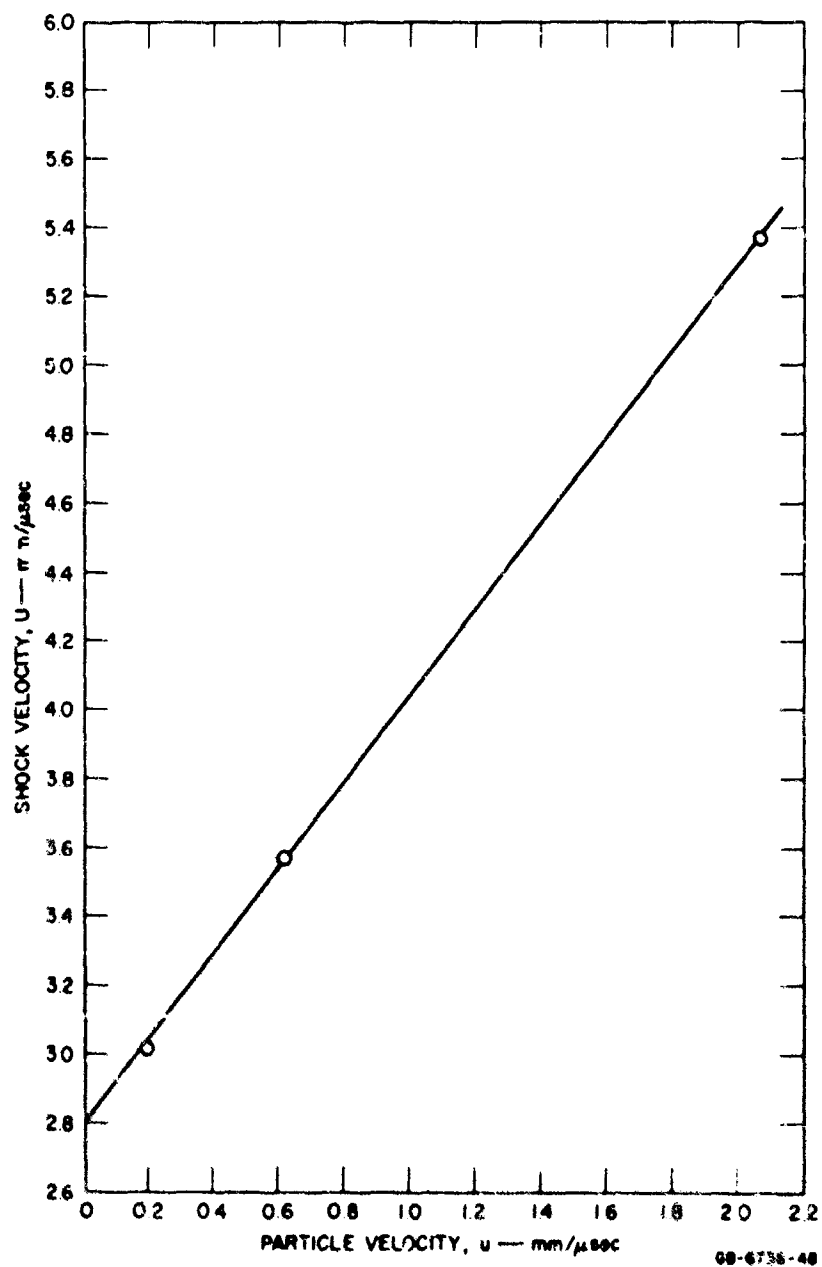


FIGURE 40 SHOCK VELOCITY-PARTICLE VELOCITY HUGONIOT DATA FOR 3-D WEAVE QUARTZ PHENOLIC

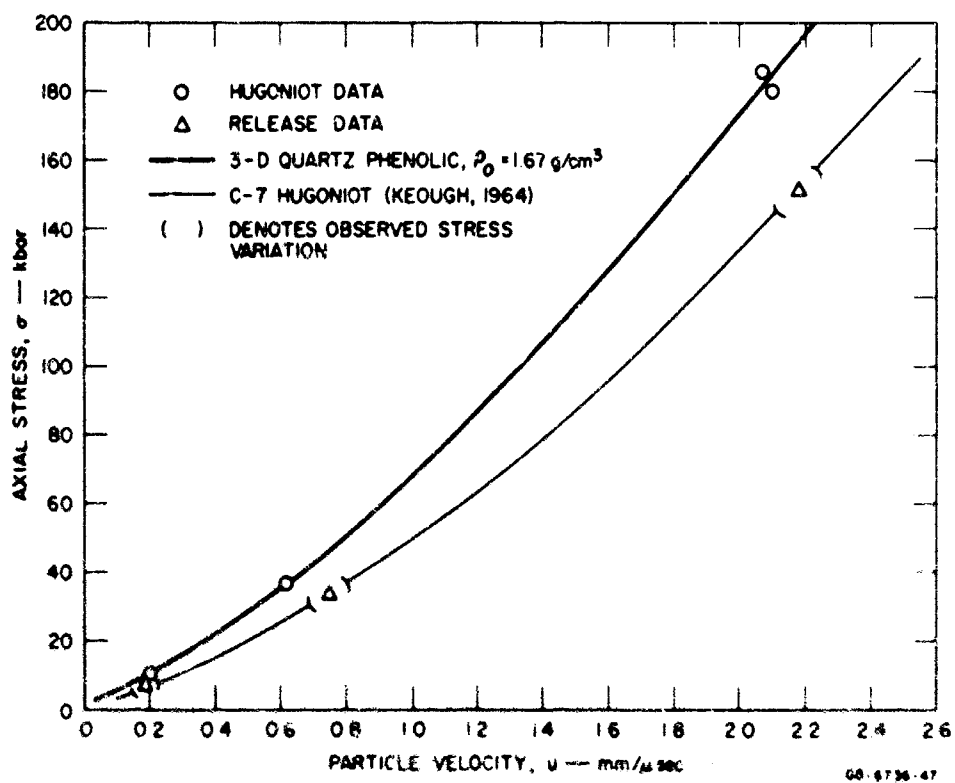


FIGURE 41 STRESS-PARTICLE VELOCITY HUGONIOT DATA FOR 3-D WEAVE QUARTZ PHENOLIC

Instrumentation on these shots consisted of two 10-ohm manganin wire gages in C-7 epoxy. (High resistance 10-ohm gages are used in low stress experiments to improve the signal-to-noise ratio.) In one gage the manganin element was positioned 0.015 inch back into the C-7 from the specimen - C-7 interface; in the other it was 0.080 inch back (the latter distance being about the same as the width of the lateral quartz fibers in the target). In all three gun shots the gage in which the element was set back 0.080 inch gave a shorter rise time and a lower stress for the main wave than the nearer gage. These changes in the wave appearance may be caused by convergence of the uneven wave front in the quartz phenolic into a planar wavefront in C7, damping of oscillations in the C-7, and tendency of the wave to shock up in the C-7. Because of the recorded evidence of nonsteady wave propagation in the C-7, the gage with the element nearer the interface was used to determine the reported loading state in the specimens. These states were calculated by the impedance match method<sup>\*</sup> using measurements of the specimen wave velocities and the projectile velocities, using the known Hugoniot for the 2024-Al projectile.

Figure 42 shows a post-shot photograph of the recovered specimen and projectile head for Shot 13,421. The lateral quartz filament bundles appear as wide, light traces in the photographs of both target and projectile, and form a nearly orthogonal grid. The small, dark squares represent the axial bundles. These axial bundles left a deeper imprint on the aluminum projectile. The noticeable variation in the imprint across the impact surface indicates the sharp differences in short impedances among the target materials. The wave in the quartz phenolic target and at the interface between the target and the C-7 epoxy will not be a smooth plane shock but will be "dimpled." As the wave propagates into the homogeneous C-7 epoxy, the faster, higher stress portions that enter the unshocked material first should gradually be dispersed

---

\* The use of the term "impedance match method" is not completely justifiable here because the wave is neither planar nor steady state.



FIGURE 42 RECOVERED 3-D WEAVE QUARTZ  
PHENOLIC TARGET AND ALUMINUM  
GAS GUN PROJECTILE HEAD WHICH  
IMPACTED IT. Impact velocity = 0.85  
mm/ $\mu$ sec, Impact stress = 37 kbar.



by nonuniaxial flow. The wave in C-7 is thus expected to become progressively smoother as it propagates, which it apparently does (as indicated by the shorter rise time measured with the 0.080 inch gage). Further confirmation of the dimpled nature of the shock front is noted in the HE experiments discussed later.

The "effective" macroscopic average Hugoniot-type data measured by the manganin gages in the C-7 transducer material are displayed along with the quartz phenolic loading data in the stress-particle velocity plane of Fig. 41. It is evident from this figure that the gage stresses do not represent a reliable measure of the release states for the quartz phenolic as they should for steady state shocks. The disagreement is attributed to stress measurement uncertainties associated with the dimpled character of the wave impinging on the manganin wire stress gage:

- Local areas of the wire sense different peak stress levels arriving at different times. Hence, the actual level recorded at the oscilloscope corresponds to some average of the local stresses in the shock wave mesh traversing the wire at a given time.
- The resistance change in the manganin due to compressive stress (causing decrease in resistance) may be masked by local strains in the manganin caused by stretching of the wire (and an increase in resistance) as it is traversed in the lateral shock by the uneven wave front.

In Shots 13,421 and 13,422 there was some evidence of the possible formation of a precursor in the quartz phenolic with a wave speed of approximately 4.5 mm/ $\mu$ sec and a peak stress estimated from manganin gage data to be about 1 kbar. The stress record from the attenuation shot, Shot 13,422, is shown in Fig. 43. In traversing 9.4 mm of quartz phenolic, the shock stress attenuated from about 30 kbar to 4 kbar. The recorded rise time was about 1  $\mu$ sec, i.e., longer than the rise time of the "Hugoniot" shots. The record shows a possible precursor at 0.6 kbar in C-7 and a reflection of the precursor off the main wave at 1.3 kbar.

Two HE experiments were performed on the quartz phenolic discs. The specimens were impacted by a high-velocity ( $\sim 3$  mm/ $\mu$ sec), 1/8-inch-thick 2024-T8 Al flyer to obtain both shock and rarefaction wave propagation information. Normal 4-ohm manganin C-7 gages (Ref. 23) - (gage element 0.010 inch into C-7 from interface) were used to monitor the

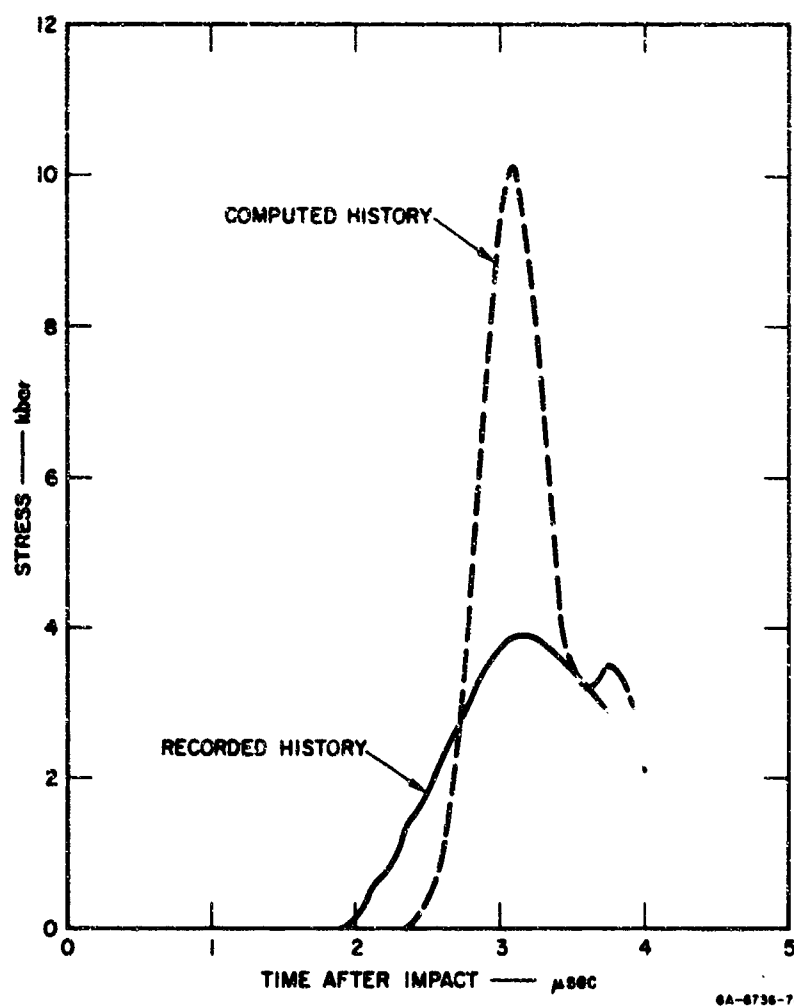


FIGURE 43 COMPARISON OF COMPUTED AND RECORDED STRESS HISTORIES FOR SHOT 13,422. 3-D quartz phenolic was impacted by a thin aluminum flyer; stress was recorded in C-7 behind target.

stress profile transmitted to C-7 by the quartz phenolic. The high-speed streak camera techniques described in Section III.2.b were used in the same experiments to record the specimen Hugoniot state and the shock planarity. The manganin gage record, after data reduction, obtained for the 2.78-mm-thick specimen is shown in Fig. 44. Note that in the HE experiment the rise time is about 50 nsec and the peak stress fluctuates by more than 10 kbar, while in the low-stress gas gun experiment the rise time is about 500 nsec and the peak stress fluctuations are negligible. Peak stress variation (with a period of approximately 0.1  $\mu$ sec) which we attribute to the dispersive nature of the 3-D specimens are apparent and support the previous observation of nonsteady flow. The rise time of  $\sim 0.02 \mu$ sec was probably caused by the nonplanarity of the impact and therefore is not necessarily associated with dissipation mechanisms in the material. The rise times observed in the HE experiments are considerably shorter than those observed in the gas gun experiments because (a) the shock tilt problem is reduced at high projectile velocities; (b) at the higher stresses the shock transit times through both the quartz and the phenolic phases of the target are considerably reduced, resulting in less variation in absolute time of arrival along the gage; and (c) differences in the shock velocities of quartz and phenolic are less at the stress levels of the HE experiments than at those of the gun shots.

No evidence of a precursor is seen in the HE experiments. This observation is consistent with the results of the gas gun experiments, since at high stresses the observed shock velocity is considerably greater than the precursor velocity measured in the gas gun experiments. The quartz phenolic release data obtained from the C-7 manganin gages in the HE experiments have a large uncertainty (similar to that discussed for the gun shots), presumably because of the dimpled nature of the wave front transmitted by the 3-D weave quartz phenolic.

#### 4. Theoretical Calculations

A limited number of calculations were made with the SRI PUFF 2 code using the usual equation of state for a solid (Eq. 29) to model the woven quartz phenolic. One computation was made to simulate a Hugoniot shot and another to model the attenuation experiment. The purpose was to compare

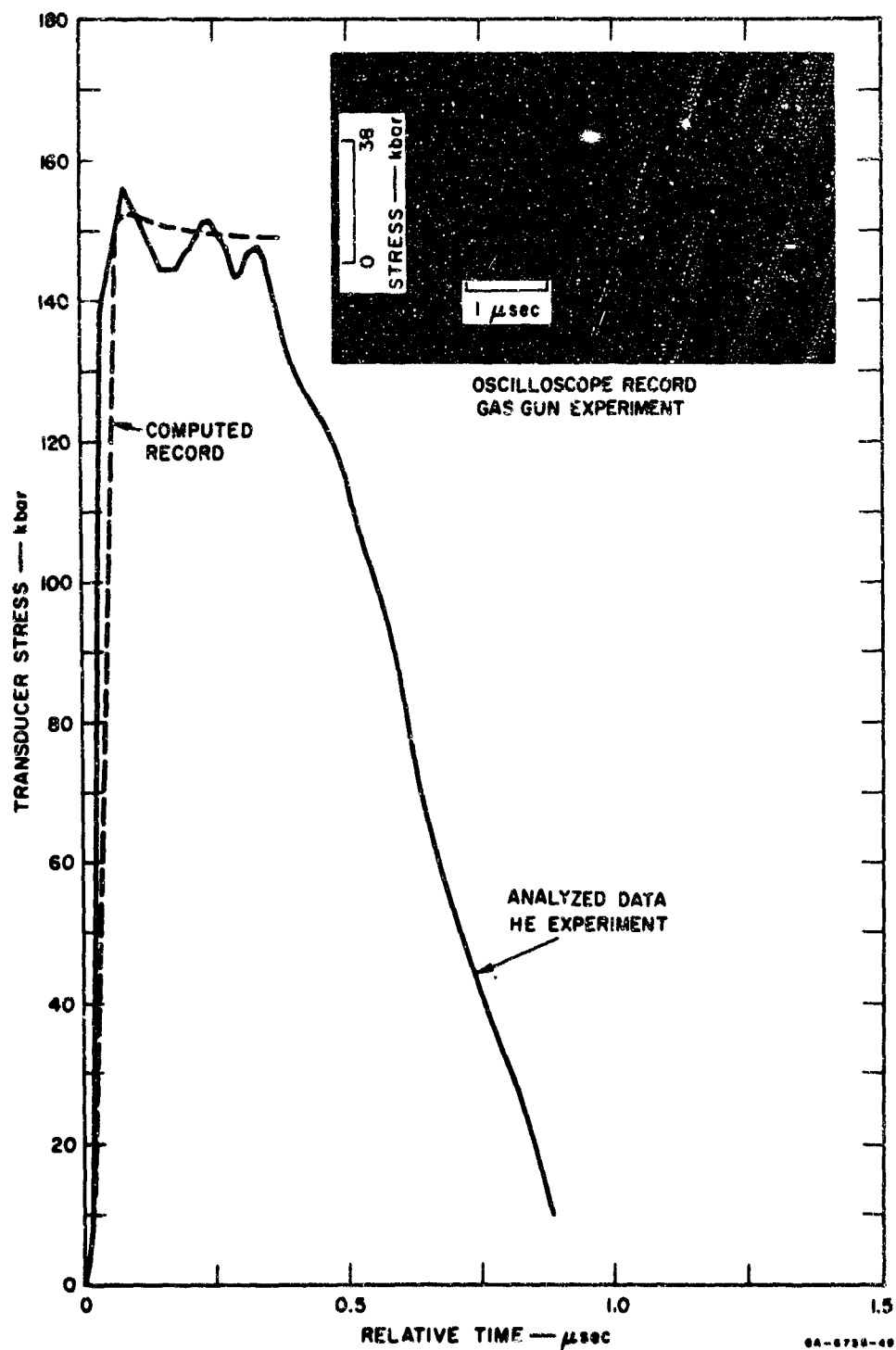


FIGURE 44 TYPICAL MANGANIN WIRE/C-7 TRANSDUCER RECORDS OF STRESS-TIME PROFILES INDUCED IN C-7 BY HIGH-STRESS (HE) AND LOW-STRESS (gas gun) SHOCK IN 3-D WEAVE QUARTZ PHENOLIC

the peak stress attained, the rise time, and the arrival time. The comparisons were intended to show whether a satisfactory prediction could be made with the usual equation-of-state formulation. If not, the computed results should indicate the types of modifications required.

The "effective" equation of state of the composite material was taken from the data of Fig. 40 to be  $U_s = 2.79 + 1.25 U_p$  (mm/ $\mu$ sec) and cast in the usual PUFF form:

$$p = 1.273 \times 10^{11} \mu + 2.157 \times 10^{11} \mu^2 + 0.837 \times 10^{11} \mu^3$$

Yield strength was taken to be zero, and only normal\* values of artificial viscosity were employed in the computations.

The first calculation simulated the attenuation shot, No. 13,422. The 2024-T8 aluminum flyer was represented by the Bauschinger model with the parameters determined in Section IV. The computed stress history at the composite/C-7 interface is shown in Fig. 43 for comparison with the experimental record. The computed history shows significant attenuation from the computed impact stress of 37 kbar. The arrival time of the computed wave crest coincides with that of the experimental record, indicating that average wave velocities are correctly represented by the analytical equation of state. The most striking differences between recorded and computed histories are the overestimate of peak stress and the underestimate of rise time.

The portion of Shot 13,560 with the thinner specimen was also modeled by a computation. The stress history at the position of the manganin wire is shown in Fig. 44 for comparison with the measured history. The computed rise (governed by cell size and artificial viscosity) is about two times as large as the measured. The peak stress is comparable to the average but is not so oscillatory.

---

\* A normal value of artificial viscosity for a computation is that which is sufficient to cause the total mechanical stress to follow a straight compression path (the Rayleigh line) during a passage of a shock. For the present computations the coefficient of nonlinear viscosity  $C_0$  was 4.0 and the linear coefficient  $C_1$  was 0.2.

The following are probable causes for the discrepancies between the computed and experimental records:

1. Computational effects:

- . Cell sizes used in the finite difference computations were 0.0001 to 0.001 inch, i.e., considerably smaller than the scale of inhomogeneity of the woven material.
- . Artificial viscosity was of normal magnitude, which usually spreads a shock front over four finite difference cells.

This combination of cell sizes and viscosity used in the calculations would normally lead to rise times longer than those observed experimentally for solids and did produce a longer rise time than that seen in the high-stress experiments.

2. Experimental effects:

- . The wavefront in quartz phenolic exhibited dispersion of the wave front associated with the variation of wave velocity between constituent materials. The oscillatory top of the stress wave at high stresses and long rise time at low stresses are indications of this dispersion phenomenon.
- . Frictional dissipation or material strength which increases with pressure is a possible dissipation mechanism.
- . Viscous damping is present in both the resin and the filaments (see Kolsky, (Ref.28) for example).
- . Concavity of the C-7 Hugoniot would lead to more rapid steepening of the shock front at high stresses than low.
- . A gage of finite dimensions has an averaging effect on a stress field with a spatial variation.

All three dissipation mechanisms--dispersive, frictional, and viscous--are present and may contribute significantly to the observed behavior. The marked difference between the comparisons at low and high pressures leads one to suspect that some of the dissipation mechanisms are highly stress dependent. A general model for composite material should probably include all three dissipation effects.

## SECTION VII

### SUMMARY AND RECOMMENDATIONS

#### 1. Summary

Four models for stress relaxation were selected and implemented in the SRI PUFF 2 wave propagation program. Their characteristics were compared with those of a general, or standard, stress relaxation model and discussed on the basis of several computer calculations. Dominant features of the computed results for all models were the attenuation with distance of the precursor and main wave and the extent to which these two waves were separated. Criteria were described for selecting a model and the model parameters.

A computational model representing the Bauschinger and related time-independent effects was constructed on the basis of previous experimental and theoretical results and the present experimental data. The model was implemented in the SRI PUFF 2 computer program, and test runs were made to indicate the nature of the results obtainable.

An experimental technique and a related data analysis method were developed for obtaining complete loading and unloading compression paths in the stress-volume and stress-particle velocity planes. The analytical method was derived and applied to the present aluminum and titanium data. The method requires data from stress and/or particle velocity gages embedded at a series of locations in the target during an impact experiment. Valid results can be obtained for both stress-relaxing and rate-independent materials during Hugoniot and attenuation experiments.

Impact experiments were conducted on 6061-T6 and 2024-T8 aluminum alloys at stress levels of 15 to 600 kbar. Hugoniot data, release adiabats, and peak rarefaction velocities were obtained. Peak rarefaction velocities were considerably higher than those predicted by the standard elastic-plastic theoretical model; and the unloading adiabat was smooth, showing no break at an unloading point as predicted by the elastic-plastic model. Records at 50 kbar and 580 kbar were compared with computations made with the Bauschinger model. Conclusions drawn from the comparisons were that the model has the correct form, although some parameters could have been chosen more felicitously. No stress relaxation effects were

observed in the aluminum, probably because the samples were all thicker than those for which time-dependent precursor decay is important.

Impact experiments were made on samples of the common structural titanium alloy Ti-6Al-4V (mixed alpha and beta phases), type 50A titanium (pure alpha phase), and Ti-13Cr-11V-3Al (pure beta phase) in the range 15 to 750 kbar. Hugoniot data, Hugoniot elastic limits (HEL), and an alpha phase transformation data were obtained. The HEL in pure alpha and pure beta was double that predicted from static yield data, but the HEL in mixed alpha-beta was about as predicted. However, in the mixed phase material there was a large elastic-plastic transition ranging from 15 to 35 kbar. The phase transformation from alpha to probably omega phase at 50 kbar in the pure alpha metal showed only a small change in shock velocity and specific volume, and was overdriven at 62 kbar, suggesting that only about 10 percent of the material transformed at this stress. No transformations were observed in the other alloys for stresses up to 70 kbar.

Five impact experiments were made with woven quartz-phenolic to obtain preliminary Hugoniot data for stresses from 10 to 200 kbar. The records show an uneven wave front, oscillation in stress at the top of the wave, questionable release adiabat data, and a very thick shock front at the lower stresses. An attenuation shot with a 0.47 mm aluminum flyer yielded a stress reduction to 15 percent of the impact stress on the 9.46 mm quartz phenolic target, and a rise time of 1  $\mu$ sec. A theoretical prediction for the attenuation shot based on a normal solid model gave much less attenuation and a steeper shock front. Evidently, highly effective dissipative mechanisms are operating in the woven material which have not yet been modeled theoretically.

## 2. Recommendations

The calculations with the Bauschinger model have led to significantly improved results for attenuation and unloading wave forms in two aluminum alloys; the model should be used whenever sufficient materials data are available for implementation.



The presently formulated Bauschinger model should undergo further development to make it more adaptable to other materials and for a wider range of stresses. Specifically,

- . more experimental data should be obtained on rarefaction velocities and unloading adiabats over a wide range of stresses in materials of structural and experimental interest, and
- . the model formulation should be expanded to include a shear modulus and yield strength that are functions of specific volume and internal energy.

Testing should be undertaken in two areas which were only considered briefly in this report:

- . impacts on preheated specimens to map the equation of state and unloading relations at higher temperatures, and
- . reverse phase transition during unloading in materials undergoing phase transitions during compression. The multiple-gage analysis should be particularly useful in such a study.

The standard impact experiments in woven materials do not yield strictly valid Hugoniot data because of the nonequilibrium states reached during the shock. The nature of the states achieved should be studied theoretically to indicate how to use the Hugoniot-like data for analytical predictions.

Experiments should be conducted to map the pseudo-equation-of-state surface for a woven material as a basis for theoretical predictions. The data could be obtained from impacts for a large range of stress levels, and with samples which have been

- . preheated to increase initial internal energy, and
- . manufactured with substantial porosity so that very large internal energies would be created during impact.

Stress levels used should include those required for vaporization.

An equation of state for woven materials should be formulated and implemented in a PUFF-type wave propagation code. The formulation should include frictional damping, viscous damping, dispersion caused by adjacency of materials with different wave velocities, and a delay mechanism such as stress relaxation.

AFWL-TR-69-96

This page intentionally left blank.

## APPENDIX I

### TEST RUNS AND LISTING OF THE SRI PUFF 2 COMPUTER CODE

#### 1. Introduction

This appendix presents test routines and results that can be used to validate the use of the SRI PUFF 2 computer code on computers other than those at SRI. The code was developed to run on the CDC 6400 at SRI. It is a modification of SRI PUFF 1 to include stress relaxation and Bauschinger effects.

Any difficulties encountered in using the code on other machines will probably arise from differences in interpretation of some FORTRAN statements or possibly in running new types of problems. Usually these differences will trigger machine diagnostic statements or they will result in catastrophic errors. In the case of diagnostics, the error is located by the machine, and it can then be corrected. For catastrophic errors, the programmer needs some assistance in locating the source of the error. We have tried to provide this assistance in two ways: inclusion of data for test runs that will exercise all major portions of the code, and insertion of prints from each subroutine. The test runs include impact and radiation deposition problems and rezoning problems for solid and porous materials. The prints in each subroutine indicate the route taken through the subroutine (i.e., which branch of each IF statement is used) and list the main input and output quantities of the subroutine. These prints are triggered by presetting the constant MAXPR to the number of prints desired from the subroutines HYDRO, JSTRESS, HAFSTEP, EQST, POREQST, and SSCAL. Similar prints are obtained from BAUSCHI, RELAX and BANDRLX by setting Serse Switch 3.

Six test problems are described in the following pages. The first problem has been run in three versions: a short test with triggering of prints from each subroutine, a short test with slightly altered data, and a full run with normal printout only. Some output from all three of these runs is given. For the other five test problems, only the full run was made. For all of the runs the major part of the output is given in the form of plots.

## 2. Input and Sample Output of Test Problems

### a. Test No. 1a

This problem, a test of the Bauschinger model implemented in the code, concerns the impact between a 6061-T6 aluminum flyer and a target of the same material. Behind the target is a manganin-glass stress transducer. The problem corresponds with shot 670 described in Section IV. This calculation is performed in three versions: a short calculation with printouts from many of the subroutines, a short calculation with printouts but using a slightly altered data deck, and a full run. The listing that follows is for the first of these computer runs. The listing includes the input data (which is essentially a reproduction of the data cards), the initial layout of the coordinate grid, test prints, the final EDIT, and the stress histories.

\*\*\* SRI PUFF 1 (6400 VERSION) \*\*\*

DATE =05/07/69

IDENT = 1 A SHORT TRIAL RUN ON BAUSCHINGER MODEL FOR 6061-T6  
COMPUTATIONS CORRESPOND TO THE 50 KBAR DATA OF ROGER WILLIAMS FOR 6061-T6  
ALUMINUM. THE BAUSCHINGER MODEL IS USED FOR BOTH THE FLYER AND TARGET.  
THE JEDITS WERE PLACED AT THE APPROXIMATE THICKNESSES OF THE THREE THINNER  
SPECIMENS SO THAT THE COMPUTATION MODELS ALL FOUR EXPERIMENTS.  
THIS COMPUTATION WAS CONTINUED FOR ONLY FIVE CYCLES WITH PRINTS FROM EACH  
SUBROUTINE.

1 NTEDT= 7 NJEDIT= 6 NREZLN= 0 NSEPRAT= 0  
2 TEDIT= 3.000E-07 1.000E-07 9.000E-07 1.200E-06 1.000E-06 2.000E-06 2.400E-06  
3 JEDITS= 56 80 128 172 232 251  
4 NEDTH= 100000 NEDIT= 10000 NPERM= 1 MAXPRN= 1  
MAXPR= 200 200 200 200 200 200 200 200 200 200 200  
7 STOPS JCYS= 5 CKS= 3.500E+00 TS= 3.000E-06  
8 NMTPL= 3 MATPL= 1 UZERO= 6.300E+04 IPLOT= 0

6061-T6 AL FLYER RHO = 2.709E+00 NSRM = 5 NYAM = 1 NPOR = 0 NCON = 0  
EQSTC = 6.670E+11 EQSTD = 1.000E+12 EQSTE = 1.220E+11 EQSTG = 2.040E+00  
EQSTH = 2.500E-01 EQSTS = 0. EQSTN = 9.493E-01 EQSTA = 8.285E-12  
COSO = 4.000E+00 C1 = 5.000E-02 -0.  
TENS(1) = -1.000E+11 TENS(2) = -1.000E+11 TENS(3) = -1.000E+11  
XPO = 6.000E+03 XP = 1.000E+00 MUUN = 6.670E+11 YADF = 1.000E+00  
YO = 3.210E+09 MU = 2.670E+11 YADD = 3.790E+10  
NZONES = 1, 25 CELLS IN 1.537E+01 CM DELX = -0. -0.

6061-T6 AL TARGET RHO = 2.709E+00 NSRM = 5 NYAM = 1 NYOR = 0 NCON = 0  
EQSTC = 6.670E+11 EQSTD = 1.000E+12 EQSTE = 1.220E+11 EQSTG = 2.040E+00  
EQSTH = 2.500E-01 EQSTS = 0. EQSTN = 9.493E-01 EQSTA = 8.285E-12  
COSO = 4.000E+00 C1 = 5.000E-02 -0.  
TENS(1) = -1.000E+11 TENS(2) = -1.000E+11 TENS(3) = -1.000E+11  
XPO = 6.000E+03 XP = 1.000E+00 MUUN = 6.670E+11 YADF = 1.000E+00  
YO = 3.210E+09 MU = 2.670E+11 YADD = 3.790E+10  
NZONES = 1, 210 CELLS IN 1.257E+00 CM DELX = -0. -0.

GLASS (MM GAGE) RHO = 2.520E+00 NSRM = 0 NYAM = 0 NPOR = 0 NCON = 0  
EQSTC = 6.780E+11 EQSTD = -6.780E+11 EQSTE = 3.000E+10 EQSTG = 2.000E+00  
EQSTH = 2.500E-01 EQSTS = 6.750E+11 EQSTN = 5.407E+00 EQSTA = 5.740E-12  
COSO = 4.000E+00 C1 = 5.000E-02 -0.  
TENS(1) = -1.000E+11 TENS(2) = -1.000E+11 TENS(3) = -1.000E+11  
NZONES = 1, 30 CELLS IN 3.150E-01 CM DELX = 6.000E-03 -0.

EQST, J= 0, N= 0, CSO= 3.776E+11, EJ= 0. , DJ= 2.709E+00, PJ= 0.  
EQST, J= 26, N= 0, CSO= 3.776E+11, EJ= 0. , DJ= 2.709E+00, PJ= 0.  
EQST, J= 237, N= 0, CSO= 3.404E+11, EJ= 0. , DJ= 2.520E+00, PJ= 0.

TEST 1a: INPUT DATA

DATE = 05/07/69 IDENT = 1 A SHORT TRIAL RUN ON BAUSCHINGER MODEL FOR 6061-T6										COND	
J	DA	X(J)	U(J)	VHL(J)	C(J)	G(J)	N(J)	T(J)	ZML(J)	MATERIAL	
		CH	CM/SEC	DYN/CM2	CM/SEC	CM/CM2	GM/CM3	DYN/CM2	GM/CM2		
1	4.149E-03	0.	6.030E+04	2.140E+09	6.147E+05	2.709E+00-1.000E+11	1.665E-02	6061-T6 AL FLYER	5	5	1
2	4.149E-03	6.148E-03	5.030E+04	2.140E+09	6.147E+05	2.709E+00-1.000E+11	1.665E-02	6061-T6 AL FLYER	5	5	2
3	4.149E-03	1.230E-02	6.030E+04	2.140E+09	6.147E+05	2.709E+00-1.000E+11	1.665E-02	6061-T6 AL FLYER	5	5	3
4	4.149E-03	1.844E-02	6.030E+04	2.140E+09	6.147E+05	2.709E+00-1.000E+11	1.665E-02	6061-T6 AL FLYER	5	5	4
5	4.149E-03	2.459E-02	6.030E+04	2.140E+09	6.147E+05	2.709E+00-1.000E+11	1.665E-02	6061-T6 AL FLYER	5	5	5
6	4.149E-03	3.074E-02	6.030E+04	2.140E+09	6.147E+05	2.709E+00-1.000E+11	1.665E-02	6061-T6 AL FLYER	5	5	6
7	4.149E-03	3.689E-02	6.030E+04	2.140E+09	6.147E+05	2.709E+00-1.000E+11	1.665E-02	6061-T6 AL FLYER	5	5	7
8	4.149E-03	4.304E-02	6.030E+04	2.140E+09	6.147E+05	2.709E+00-1.000E+11	1.665E-02	6061-T6 AL FLYER	5	5	8
9	4.149E-03	4.918E-02	6.030E+04	2.140E+09	6.147E+05	2.709E+00-1.000E+11	1.665E-02	6061-T6 AL FLYER	5	5	9
10	4.149E-03	5.533E-02	6.030E+04	2.140E+09	6.147E+05	2.709E+00-1.000E+11	1.665E-02	6061-T6 AL FLYER	5	5	10
11	4.149E-03	6.148E-02	6.030E+04	2.140E+09	6.147E+05	2.709E+00-1.000E+11	1.665E-02	6061-T6 AL FLYER	5	5	11
12	4.149E-03	6.763E-02	6.030E+04	2.140E+09	6.147E+05	2.709E+00-1.000E+11	1.665E-02	6061-T6 AL FLYER	5	5	12
13	4.149E-03	7.378E-02	6.030E+04	2.140E+09	6.147E+05	2.709E+00-1.000E+11	1.665E-02	6061-T6 AL FLYER	5	5	13
14	4.149E-03	7.993E-02	6.030E+04	2.140E+09	6.147E+05	2.709E+00-1.000E+11	1.665E-02	6061-T6 AL FLYER	5	5	14
15	4.149E-03	8.607E-02	6.030E+04	2.140E+09	6.147E+05	2.709E+00-1.000E+11	1.665E-02	6061-T6 AL FLYER	5	5	15
16	4.149E-03	9.222E-02	6.030E+04	2.140E+09	6.147E+05	2.709E+00-1.000E+11	1.665E-02	6061-T6 AL FLYER	5	5	16
17	4.149E-03	9.837E-02	6.030E+04	2.140E+09	6.147E+05	2.709E+00-1.000E+11	1.665E-02	6061-T6 AL FLYER	5	5	17
18	4.149E-03	1.045E-01	6.030E+04	2.140E+09	6.147E+05	2.709E+00-1.000E+11	1.665E-02	6061-T6 AL FLYER	5	5	18
19	4.149E-03	1.107E-01	6.030E+04	2.140E+09	6.147E+05	2.709E+00-1.000E+11	1.665E-02	6061-T6 AL FLYER	5	5	19
20	4.149E-03	1.169E-01	6.030E+04	2.140E+09	6.147E+05	2.709E+00-1.000E+11	1.665E-02	6061-T6 AL FLYER	5	5	20
21	4.149E-03	1.231E-01	6.030E+04	2.140E+09	6.147E+05	2.709E+00-1.000E+11	1.665E-02	6061-T6 AL FLYER	5	5	21
22	4.149E-03	1.293E-01	6.030E+04	2.140E+09	6.147E+05	2.709E+00-1.000E+11	1.665E-02	6061-T6 AL FLYER	5	5	22
23	4.149E-03	1.355E-01	6.030E+04	2.140E+09	6.147E+05	2.709E+00-1.000E+11	1.665E-02	6061-T6 AL FLYER	5	5	23
24	4.149E-03	1.417E-01	6.030E+04	2.140E+09	6.147E+05	2.709E+00-1.000E+11	1.665E-02	6061-T6 AL FLYER	5	5	24
25	4.149E-03	1.479E-01	6.030E+04	2.140E+09	6.147E+05	2.709E+00-1.000E+11	1.665E-02	6061-T6 AL FLYER	5	5	25
26	4.149E-03	1.541E-01	6.030E+04	2.140E+09	6.147E+05	2.709E+00-1.000E+11	1.665E-02	6061-T6 AL FLYER	5	5	26
27	5.986E-03	1.537E-01	0.	2.140E+09	6.147E+05	2.709E+00-1.000E+11	1.622E-02	6061-T6 AL TARGET	5	5	27
28	5.986E-03	1.597E-01	0.	2.140E+09	6.147E+05	2.709E+00-1.000E+11	1.622E-02	6061-T6 AL TARGET	5	5	28
29	5.986E-03	1.657E-01	0.	2.140E+09	6.147E+05	2.709E+00-1.000E+11	1.622E-02	6061-T6 AL TARGET	5	5	29
30	5.986E-03	1.717E-01	0.	2.140E+09	6.147E+05	2.709E+00-1.000E+11	1.622E-02	6061-T6 AL TARGET	5	5	30
31	5.986E-03	1.777E-01	0.	2.140E+09	6.147E+05	2.709E+00-1.000E+11	1.622E-02	6061-T6 AL TARGET	5	5	31
32	5.986E-03	1.837E-01	0.	2.140E+09	6.147E+05	2.709E+00-1.000E+11	1.622E-02	6061-T6 AL TARGET	5	5	32
33	5.986E-03	1.897E-01	0.	2.140E+09	6.147E+05	2.709E+00-1.000E+11	1.622E-02	6061-T6 AL TARGET	5	5	33
34	5.986E-03	1.957E-01	0.	2.140E+09	6.147E+05	2.709E+00-1.000E+11	1.622E-02	6061-T6 AL TARGET	5	5	34
35	5.986E-03	2.017E-01	0.	2.140E+09	6.147E+05	2.709E+00-1.000E+11	1.622E-02	6061-T6 AL TARGET	5	5	35
36	5.986E-03	2.077E-01	0.	2.140E+09	6.147E+05	2.709E+00-1.000E+11	1.622E-02	6061-T6 AL TARGET	5	5	36
37	5.986E-03	2.137E-01	0.	2.140E+09	6.147E+05	2.709E+00-1.000E+11	1.622E-02	6061-T6 AL TARGET	5	5	37
38	5.986E-03	2.197E-01	0.	2.140E+09	6.147E+05	2.709E+00-1.000E+11	1.622E-02	6061-T6 AL TARGET	5	5	38
39	5.986E-03	2.257E-01	0.	2.140E+09	6.147E+05	2.709E+00-1.000E+11	1.622E-02	6061-T6 AL TARGET	5	5	39
40	5.986E-03	2.317E-01	0.	2.140E+09	6.147E+05	2.709E+00-1.000E+11	1.622E-02	6061-T6 AL TARGET	5	5	40
41	5.986E-03	2.377E-01	0.	2.140E+09	6.147E+05	2.709E+00-1.000E+11	1.622E-02	6061-T6 AL TARGET	5	5	41
42	5.986E-03	2.437E-01	0.	2.140E+09	6.147E+05	2.709E+00-1.000E+11	1.622E-02	6061-T6 AL TARGET	5	5	42
43	5.986E-03	2.497E-01	0.	2.140E+09	6.147E+05	2.709E+00-1.000E+11	1.622E-02	6061-T6 AL TARGET	5	5	43
44	5.986E-03	2.557E-01	0.	2.140E+09	6.147E+05	2.709E+00-1.000E+11	1.622E-02	6061-T6 AL TARGET	5	5	44
45	5.986E-03	2.617E-01	0.	2.140E+09	6.147E+05	2.709E+00-1.000E+11	1.622E-02	6061-T6 AL TARGET	5	5	45
46	5.986E-03	2.677E-01	0.	2.140E+09	6.147E+05	2.709E+00-1.000E+11	1.622E-02	6061-T6 AL TARGET	5	5	46
47	5.986E-03	2.737E-01	0.	2.140E+09	6.147E+05	2.709E+00-1.000E+11	1.622E-02	6061-T6 AL TARGET	5	5	47
48	5.986E-03	2.797E-01	0.	2.140E+09	6.147E+05	2.709E+00-1.000E+11	1.622E-02	6061-T6 AL TARGET	5	5	48
49	5.986E-03	2.857E-01	0.	2.140E+09	6.147E+05	2.709E+00-1.000E+11	1.622E-02	6061-T6 AL TARGET	5	5	49
50	5.986E-03	2.917E-01	0.	2.140E+09	6.147E+05	2.709E+00-1.000E+11	1.622E-02	6061-T6 AL TARGET	5	5	50

TEST 1a: PORTION OF COORDINATE LAYOUT



MONITOR EDIT

CYCLE	TIME	DTM	JTS	ETOTAL	JFIN	JSTAR	JSMAX	SMAX	X(JSMAX)
1	1.3037E-09	4.631E-10	27	1.7839E-01	249	30	27	7.044E-09	1.5374E-01
2	1.3037E-09	4.631E-10	27	1.7839E-01	249	30	27	7.044E-09	1.5374E-01
3	1.3037E-09	4.631E-10	27	1.7839E-01	249	30	27	7.044E-09	1.5374E-01
4	1.3037E-09	4.631E-10	27	1.7839E-01	249	30	27	7.044E-09	1.5374E-01
5	1.3037E-09	4.631E-10	27	1.7839E-01	249	30	27	7.044E-09	1.5374E-01
6	1.3037E-09	4.631E-10	27	1.7839E-01	249	30	27	7.044E-09	1.5374E-01
7	1.3037E-09	4.631E-10	27	1.7839E-01	249	30	27	7.044E-09	1.5374E-01
8	1.3037E-09	4.631E-10	27	1.7839E-01	249	30	27	7.044E-09	1.5374E-01
9	1.3037E-09	4.631E-10	27	1.7839E-01	249	30	27	7.044E-09	1.5374E-01
10	1.3037E-09	4.631E-10	27	1.7839E-01	249	30	27	7.044E-09	1.5374E-01
11	1.3037E-09	4.631E-10	27	1.7839E-01	249	30	27	7.044E-09	1.5374E-01
12	1.3037E-09	4.631E-10	27	1.7839E-01	249	30	27	7.044E-09	1.5374E-01
13	1.3037E-09	4.631E-10	27	1.7839E-01	249	30	27	7.044E-09	1.5374E-01
14	1.3037E-09	4.631E-10	27	1.7839E-01	249	30	27	7.044E-09	1.5374E-01
15	1.3037E-09	4.631E-10	27	1.7839E-01	249	30	27	7.044E-09	1.5374E-01
16	1.3037E-09	4.631E-10	27	1.7839E-01	249	30	27	7.044E-09	1.5374E-01
17	1.3037E-09	4.631E-10	27	1.7839E-01	249	30	27	7.044E-09	1.5374E-01
18	1.3037E-09	4.631E-10	27	1.7839E-01	249	30	27	7.044E-09	1.5374E-01
19	1.3037E-09	4.631E-10	27	1.7839E-01	249	30	27	7.044E-09	1.5374E-01
20	1.3037E-09	4.631E-10	27	1.7839E-01	249	30	27	7.044E-09	1.5374E-01
21	1.3037E-09	4.631E-10	27	1.7839E-01	249	30	27	7.044E-09	1.5374E-01
22	1.3037E-09	4.631E-10	27	1.7839E-01	249	30	27	7.044E-09	1.5374E-01
23	1.3037E-09	4.631E-10	27	1.7839E-01	249	30	27	7.044E-09	1.5374E-01
24	1.3037E-09	4.631E-10	27	1.7839E-01	249	30	27	7.044E-09	1.5374E-01
25	1.3037E-09	4.631E-10	27	1.7839E-01	249	30	27	7.044E-09	1.5374E-01
26	1.3037E-09	4.631E-10	27	1.7839E-01	249	30	27	7.044E-09	1.5374E-01
27	1.3037E-09	4.631E-10	27	1.7839E-01	249	30	27	7.044E-09	1.5374E-01
28	1.3037E-09	4.631E-10	27	1.7839E-01	249	30	27	7.044E-09	1.5374E-01
29	1.3037E-09	4.631E-10	27	1.7839E-01	249	30	27	7.044E-09	1.5374E-01
30	1.3037E-09	4.631E-10	27	1.7839E-01	249	30	27	7.044E-09	1.5374E-01
31	1.3037E-09	4.631E-10	27	1.7839E-01	249	30	27	7.044E-09	1.5374E-01

TEST 1a: FIRST PAGE OF FIN AL TIME EDIT



TIME	S12/30J1	S23/30J2	S34/30J3	S (. 80)	S (1.28)	S (1.72)	S (2.39)	S (2.51)	JYS	DYNN	DELTIM
0.00	.005	0.000	0.000	0.000	0.000	0.000	0.000	0.000	27	.001	2.692
0.00	1.340	0.000	0.000	0.000	0.000	0.000	0.000	0.000	27	.001	.776
0.00	2.003	0.000	0.000	0.000	0.000	0.000	0.000	0.000	27	.230	.331
0.01	4.000	0.000	0.000	0.000	0.000	0.000	0.000	0.000	27	.330	.834
0.01	8.376	0.000	0.000	0.000	0.000	0.000	0.000	0.000	27	.374	1.002
0.01			0.000	0.000	0.000	0.000	0.000	0.000	27	.440	

1994

2 - 239

241 0 7

021 - 120

● ● ●

卷之四

[illegible]

TIME IN SERIES	1.02
CONVERTING TIME	0.400
PLOTTING TIME	0.000
TOTAL TIME	0.420

## TEST 1a: STRESS HISTORIES

b. Test No. 1b

This computation is identical to test 1a except that all the noninteger data are altered by 0.1 percent. The listing includes the input data initial layout of the coordinate grid, test prints, the final EDIT and the stress histories.

\*\*\* SRI PUFF 1 (6400 VERSION) \*\*\*

DATE =05/07/69

IDENT = 1 B SHORT TRIAL RUN ON BAUSCHINGER MODEL FOR 6061-T6  
COMPUTATIONS CORRESPOND TO THE 50 KBAR DATA OF ROGER WILLIAMS FOR 6061-T6  
ALUMINUM. THE BAUSCHINGER MODEL IS USED FOR BOTH THE FLYER AND TARGET.  
THE JEDITS WERE PLACED AT THE APPROXIMATE THICKNESSES OF THE THREE THINNER  
SPECIMENS SO THAT THE COMPUTATION MODELS ALL FOUR EXPERIMENTS.  
THIS COMPUTATION WAS CONTINUED FOR ONLY FIVE CYCLES WITH PRINTS FROM EACH  
SUBROUTINE. THE DATA FOR 1B ARE SLIGHTLY ALTERED FROM THOSE OF 1A.

1 NTEDT= 7 NJEDIT= 6 NREZON= 0 NSEPRAT= 0  
2 TEDIT= 3.000E-07 6.000E-07 9.000E-07 1.200E-06 1.600E-06 2.000E-06 2.400E-06  
3 JEDIT= 50 80 120 172 239 251  
6 NEDTM= 100000 NEDIT= 10000 NPERN = 1 MAXPRN = 1  
MAXPR = 100 100 100 100 100 100 100 100 100 100  
7 STOPS JCYS = 5 CKS = 3.500E+00 TS = 3.000E-06  
8 NMTRL= 3 MATFL = 1 UZERO = 6.000E+04 IPLOT = 0

6061-T6 AL FLYER RHO = 2.709E+00 NSRM = 5 NYAM = 1 NPOR = 0 NCON = 0  
EQSTC = 6.677E+11 EQSTD = 1.001E+12 EQSTE = 1.221E+11 EQSTG = 2.042E+00  
EQSTM = 2.503E-01 EQSTS = 0. EQSTN = 9.886E-01 EQSTA = 8.285E-12  
COSO = 4.004E+00 C1 = 5.005E-02 C2 = 0.  
TENS(1) = -1.001E+11 TENS(2) = -1.001E+11 TENS(3) = -1.001E+11  
XPO = 6.006E+03 XP = 1.001E+00 MUUN = 4.675E+11 YADF = 1.001E+00  
Y0 = 3.213E+09 MU = 2.673E+11 YADD = 3.794E+10  
NZONES= 1, 25 CELLS IN 1.539E-01 CM -0. -0.

6061-T6 AL TARGET RHO = 2.709E+00 NSRM = 5 NYAM = 1 NPOR = 0 NCON = 0  
EQSTC = 6.677E+11 EQSTD = 1.001E+12 EQSTE = 1.221E+11 EQSTG = 2.042E+00  
EQSTM = 2.503E-01 EQSTS = 0. EQSTN = 9.886E-01 EQSTA = 8.285E-12  
COSO = 4.004E+00 C1 = 5.005E-02 C2 = 0.  
TENS(1) = -1.001E+11 TENS(2) = -1.001E+11 TENS(3) = -1.001E+11  
XPO = 6.006E+03 XP = 1.001E+00 MUUN = 4.675E+11 YADF = 1.001E+00  
Y0 = 3.213E+09 MU = 2.673E+11 YADD = 3.794E+10  
NZONES= 1, 210 CELLS IN 1.250E+00 CM -0. -0.

GLASS (4N 6ABE) RHO = 2.520E+00 NSRM = 0 NYAM = 0 NPOR = 0 NCON = 0  
EQSTC = 8.789E+11 EQSTD = -8.789E+11 EQSTE = 3.003E+10 EQSTG = 2.002E+00  
EQSTM = 2.503E-01 EQSTS = 8.789E+11 EQSTN = 5.801E+00 EQSTA = 5.740E-12  
COSO = 4.004E+00 C1 = 5.005E-02 C2 = 0.  
TENS(1) = -1.001E+11 TENS(2) = -1.001E+11 TENS(3) = -1.001E+11  
NZONES= 1, 30 CELLS IN 3.193E-01 CM DELX = 6.006E-03 -0.

EQST, J= 0, M= 0, CSQ= 3.780E+11, EJ= 0. , DJ= 2.709E+00, PJ= 0.  
EQST, J= 26, M= 0, CSQ= 3.780E+11, EJ= 0. , DJ= 2.709E+00, PJ= 0.  
EQST, J=237, M= 0, CSQ= 3.488E+11, EJ= 0. , DJ= 2.520E+00, PJ= 0.

TEST 1b: INPUT DATA

[illegible]

J	SE	EL (J)	UT (J)	VEL (J)	C (J)	D (J)	T (J)	ZEL (J)	MATERIAL	CODE
	CM	CM	CM/SEC	GYM/CM	CM/SEC	GYM/CM	GYM/CM	CM/CM		
1	0.100E-03	0.	0.030E-04	2.142E-09	0.150E-05	2.700E-09-1.001E-11	1.000E-02	0.001-76	AL PLYER	S M 0
2	0.100E-03	0.100E-03	0.030E-04	2.142E-09	0.150E-05	2.700E-09-1.001E-11	1.000E-02	0.001-76	AL PLYER	S M 0
3	0.100E-03	1.021E-03	0.030E-04	2.142E-09	0.150E-05	2.700E-09-1.001E-11	1.000E-02	0.001-76	AL PLYER	S M 0
4	0.100E-03	1.047E-03	0.030E-04	2.142E-09	0.150E-05	2.700E-09-1.001E-11	1.000E-02	0.001-76	AL PLYER	S M 0
5	0.100E-03	1.047E-03	0.030E-04	2.142E-09	0.150E-05	2.700E-09-1.001E-11	1.000E-02	0.001-76	AL PLYER	S M 0
6	0.100E-03	2.042E-03	0.030E-04	2.142E-09	0.150E-05	2.700E-09-1.001E-11	1.000E-02	0.001-76	AL PLYER	S M 0
7	0.100E-03	3.070E-03	0.030E-04	2.142E-09	0.150E-05	2.700E-09-1.001E-11	1.000E-02	0.001-76	AL PLYER	S M 0
8	0.100E-03	3.040E-03	0.030E-04	2.142E-09	0.150E-05	2.700E-09-1.001E-11	1.000E-02	0.001-76	AL PLYER	S M 0
9	0.100E-03	3.040E-03	0.030E-04	2.142E-09	0.150E-05	2.700E-09-1.001E-11	1.000E-02	0.001-76	AL PLYER	S M 0
10	0.100E-03	5.042E-03	0.030E-04	2.142E-09	0.150E-05	2.700E-09-1.001E-11	1.000E-02	0.001-76	AL PLYER	S M 0
11	0.100E-03	5.042E-03	0.030E-04	2.142E-09	0.150E-05	2.700E-09-1.001E-11	1.000E-02	0.001-76	AL PLYER	S M 0
12	0.100E-03	6.100E-03	0.030E-04	2.142E-09	0.150E-05	2.700E-09-1.001E-11	1.000E-02	0.001-76	AL PLYER	S M 0
13	0.100E-03	7.772E-03	0.030E-04	2.142E-09	0.150E-05	2.700E-09-1.001E-11	1.000E-02	0.001-76	AL PLYER	S M 0
14	0.100E-03	7.307E-03	0.030E-04	2.142E-09	0.150E-05	2.700E-09-1.001E-11	1.000E-02	0.001-76	AL PLYER	S M 0
15	0.100E-03	8.047E-03	0.030E-04	2.142E-09	0.150E-05	2.700E-09-1.001E-11	1.000E-02	0.001-76	AL PLYER	S M 0
16	0.100E-03	8.047E-03	0.030E-04	2.142E-09	0.150E-05	2.700E-09-1.001E-11	1.000E-02	0.001-76	AL PLYER	S M 0
17	0.100E-03	9.012E-03	0.030E-04	2.142E-09	0.150E-05	2.700E-09-1.001E-11	1.000E-02	0.001-76	AL PLYER	S M 0
18	0.100E-03	9.012E-03	0.030E-04	2.142E-09	0.150E-05	2.700E-09-1.001E-11	1.000E-02	0.001-76	AL PLYER	S M 0
19	0.100E-03	1.160E-01	0.030E-04	2.142E-09	0.150E-05	2.700E-09-1.001E-11	1.000E-02	0.001-76	AL PLYER	S M 0
20	0.100E-03	1.170E-01	0.030E-04	2.142E-09	0.150E-05	2.700E-09-1.001E-11	1.000E-02	0.001-76	AL PLYER	S M 0
21	0.100E-03	1.231E-01	0.030E-04	2.142E-09	0.150E-05	2.700E-09-1.001E-11	1.000E-02	0.001-76	AL PLYER	S M 0
22	0.100E-03	1.292E-01	0.030E-04	2.142E-09	0.150E-05	2.700E-09-1.001E-11	1.000E-02	0.001-76	AL PLYER	S M 0
23	0.100E-03	1.304E-01	0.030E-04	2.142E-09	0.150E-05	2.700E-09-1.001E-11	1.000E-02	0.001-76	AL PLYER	S M 0
24	0.100E-03	1.304E-01	0.030E-04	2.142E-09	0.150E-05	2.700E-09-1.001E-11	1.000E-02	0.001-76	AL PLYER	S M 0
25	0.100E-03	1.304E-01	0.030E-04	2.142E-09	0.150E-05	2.700E-09-1.001E-11	1.000E-02	0.001-76	AL PLYER	S M 0
26	0.100E-03	1.304E-01	0.030E-04	2.142E-09	0.150E-05	2.700E-09-1.001E-11	1.000E-02	0.001-76	AL PLYER	S M 0
27	0.000E-03	1.304E-01	0.	2.142E-09	0.150E-05	2.700E-09-1.001E-11	1.023E-02	0.001-76	AL TARGT	S M 0
28	0.000E-03	1.304E-01	0.	2.142E-09	0.150E-05	2.700E-09-1.001E-11	1.023E-02	0.001-76	AL TARGT	S M 0
29	0.000E-03	1.304E-01	0.	2.142E-09	0.150E-05	2.700E-09-1.001E-11	1.023E-02	0.001-76	AL TARGT	S M 0
30	0.000E-03	1.710E-01	0.	2.142E-09	0.150E-05	2.700E-09-1.001E-11	1.023E-02	0.001-76	AL TARGT	S M 0
31	0.000E-03	1.770E-01	0.	2.142E-09	0.150E-05	2.700E-09-1.001E-11	1.023E-02	0.001-76	AL TARGT	S M 0
32	0.000E-03	1.770E-01	0.	2.142E-09	0.150E-05	2.700E-09-1.001E-11	1.023E-02	0.001-76	AL TARGT	S M 0
33	0.000E-03	1.900E-01	0.	2.142E-09	0.150E-05	2.700E-09-1.001E-11	1.023E-02	0.001-76	AL TARGT	S M 0
34	0.000E-03	1.900E-01	0.	2.142E-09	0.150E-05	2.700E-09-1.001E-11	1.023E-02	0.001-76	AL TARGT	S M 0
35	0.000E-03	2.010E-01	0.	2.142E-09	0.150E-05	2.700E-09-1.001E-11	1.023E-02	0.001-76	AL TARGT	S M 0
36	0.000E-03	2.130E-01	0.	2.142E-09	0.150E-05	2.700E-09-1.001E-11	1.023E-02	0.001-76	AL TARGT	S M 0
37	0.000E-03	2.130E-01	0.	2.142E-09	0.150E-05	2.700E-09-1.001E-11	1.023E-02	0.001-76	AL TARGT	S M 0
38	0.000E-03	2.190E-01	0.	2.142E-09	0.150E-05	2.700E-09-1.001E-11	1.023E-02	0.001-76	AL TARGT	S M 0
39	0.000E-03	2.290E-01	0.	2.142E-09	0.150E-05	2.700E-09-1.001E-11	1.023E-02	0.001-76	AL TARGT	S M 0
40	0.000E-03	2.290E-01	0.	2.142E-09	0.150E-05	2.700E-09-1.001E-11	1.023E-02	0.001-76	AL TARGT	S M 0
41	0.000E-03	2.310E-01	0.	2.142E-09	0.150E-05	2.700E-09-1.001E-11	1.023E-02	0.001-76	AL TARGT	S M 0
42	0.000E-03	2.370E-01	0.	2.142E-09	0.150E-05	2.700E-09-1.001E-11	1.023E-02	0.001-76	AL TARGT	S M 0
43	0.000E-03	2.300E-01	0.	2.142E-09	0.150E-05	2.700E-09-1.001E-11	1.023E-02	0.001-76	AL TARGT	S M 0
44	0.000E-03	2.077E-01	0.	2.142E-09	0.150E-05	2.700E-09-1.001E-11	1.023E-02	0.001-76	AL TARGT	S M 0
45	0.000E-03	2.177E-01	0.	2.142E-09	0.150E-05	2.700E-09-1.001E-11	1.023E-02	0.001-76	AL TARGT	S M 0
46	0.000E-03	2.077E-01	0.	2.142E-09	0.150E-05	2.700E-09-1.001E-11	1.023E-02	0.001-76	AL TARGT	S M 0
47	0.000E-03	2.777E-01	0.	2.142E-09	0.150E-05	2.700E-09-1.001E-11	1.023E-02	0.001-76	AL TARGT	S M 0
48	0.000E-03	2.777E-01	0.	2.142E-09	0.150E-05	2.700E-09-1.001E-11	1.023E-02	0.001-76	AL TARGT	S M 0
49	0.000E-03	2.907E-01	0.	2.142E-09	0.150E-05	2.700E-09-1.001E-11	1.023E-02	0.001-76	AL TARGT	S M 0
50	0.000E-03	2.917E-01	0.	2.142E-09	0.150E-05	2.700E-09-1.001E-11	1.023E-02	0.001-76	AL TARGT	S M 0

**TEST 1b: PORTION OF COORDINATE LAYOUT**

DATE = 08/07/69 IDENT = 1 B SHORT TRIAL RUN ON BAUSCHINGER MODEL FOR 6051-T6

J	DX CM	X(J) CM	U(J) CM/SEC	VWL(J) DYN/CM2	C(J) CM/SEC	O(J) CM/CH3	T(J) DYN/CM2	ZWL(J) CM/CH2	MATERIAL	COMO	J
1	6.156E-03	0.	6.030E-04	2.142E-09	6.150E-05	2.709E-00-1.001E-11	1.623E-02	6051-T6	AL FLYER	S	1
2	6.156E-03	6.156E-03	6.030E-04	2.142E-09	6.150E-05	2.709E-00-1.001E-11	1.623E-02	6051-T6	AL FLYER	S	2
3	6.156E-03	1.231E-02	6.030E-04	2.142E-09	6.150E-05	2.709E-00-1.001E-11	1.623E-02	6051-T6	AL FLYER	S	3
4	6.156E-03	1.947E-02	6.030E-04	2.142E-09	6.150E-05	2.709E-00-1.001E-11	1.623E-02	6051-T6	AL FLYER	S	4
5	6.156E-03	2.462E-02	6.030E-04	2.142E-09	6.150E-05	2.709E-00-1.001E-11	1.623E-02	6051-T6	AL FLYER	S	5
6	6.156E-03	3.078E-02	6.030E-04	2.142E-09	6.150E-05	2.709E-00-1.001E-11	1.623E-02	6051-T6	AL FLYER	S	6
7	6.156E-03	3.694E-02	6.030E-04	2.142E-09	6.150E-05	2.709E-00-1.001E-11	1.623E-02	6051-T6	AL FLYER	S	7
8	6.156E-03	4.309E-02	6.030E-04	2.142E-09	6.150E-05	2.709E-00-1.001E-11	1.623E-02	6051-T6	AL FLYER	S	8
9	6.156E-03	4.925E-02	6.030E-04	2.142E-09	6.150E-05	2.709E-00-1.001E-11	1.623E-02	6051-T6	AL FLYER	S	9
10	6.156E-03	5.540E-02	6.030E-04	2.142E-09	6.150E-05	2.709E-00-1.001E-11	1.623E-02	6051-T6	AL FLYER	S	10
11	6.156E-03	6.156E-02	6.030E-04	2.142E-09	6.150E-05	2.709E-00-1.001E-11	1.623E-02	6051-T6	AL FLYER	S	11
12	6.156E-03	6.772E-02	6.030E-04	2.142E-09	6.150E-05	2.709E-00-1.001E-11	1.623E-02	6051-T6	AL FLYER	S	12
13	6.156E-03	7.387E-02	6.030E-04	2.142E-09	6.150E-05	2.709E-00-1.001E-11	1.623E-02	6051-T6	AL FLYER	S	13
14	6.156E-03	8.003E-02	6.030E-04	2.142E-09	6.150E-05	2.709E-00-1.001E-11	1.623E-02	6051-T6	AL FLYER	S	14
15	6.156E-03	8.618E-02	6.030E-04	2.142E-09	6.150E-05	2.709E-00-1.001E-11	1.623E-02	6051-T6	AL FLYER	S	15
16	6.156E-03	9.234E-02	6.030E-04	2.142E-09	6.150E-05	2.709E-00-1.001E-11	1.623E-02	6051-T6	AL FLYER	S	16
17	6.156E-03	9.850E-02	6.030E-04	2.142E-09	6.150E-05	2.709E-00-1.001E-11	1.623E-02	6051-T6	AL FLYER	S	17
18	6.156E-03	1.047E-01	6.030E-04	2.142E-09	6.150E-05	2.709E-00-1.001E-11	1.623E-02	6051-T6	AL FLYER	S	18
19	6.156E-03	1.108E-01	6.030E-04	2.142E-09	6.150E-05	2.709E-00-1.001E-11	1.623E-02	6051-T6	AL FLYER	S	19
20	6.156E-03	1.170E-01	6.030E-04	2.142E-09	6.150E-05	2.709E-00-1.001E-11	1.623E-02	6051-T6	AL FLYER	S	20
21	6.156E-03	1.231E-01	6.030E-04	2.142E-09	6.150E-05	2.709E-00-1.001E-11	1.623E-02	6051-T6	AL FLYER	S	21
22	6.156E-03	1.293E-01	6.030E-04	2.142E-09	6.150E-05	2.709E-00-1.001E-11	1.623E-02	6051-T6	AL FLYER	S	22
23	6.156E-03	1.354E-01	6.030E-04	2.142E-09	6.150E-05	2.709E-00-1.001E-11	1.623E-02	6051-T6	AL FLYER	S	23
24	6.156E-03	1.416E-01	6.030E-04	2.142E-09	6.150E-05	2.709E-00-1.001E-11	1.623E-02	6051-T6	AL FLYER	S	24
25	6.156E-03	1.477E-01	6.030E-04	2.142E-09	6.150E-05	2.709E-00-1.001E-11	1.623E-02	6051-T6	AL FLYER	S	25
26	6.156E-03	1.539E-01	6.030E-04	2.142E-09	6.150E-05	2.709E-00-1.001E-11	1.623E-02	6051-T6	AL FLYER	S	26
27	5.990E-03	1.339E-01	0.	2.142E-09	6.150E-05	2.709E-00-1.001E-11	1.623E-02	6051-T6	AL TARGET	S	27
28	5.990E-03	1.599E-01	0.	2.142E-09	6.150E-05	2.709E-00-1.001E-11	1.623E-02	6051-T6	AL TARGET	S	28
29	5.990E-03	1.599E-01	0.	2.142E-09	6.150E-05	2.709E-00-1.001E-11	1.623E-02	6051-T6	AL TARGET	S	29
30	5.990E-03	1.719E-01	0.	2.142E-09	6.150E-05	2.709E-00-1.001E-11	1.623E-02	6051-T6	AL TARGET	S	30
31	5.990E-03	1.719E-01	0.	2.142E-09	6.150E-05	2.709E-00-1.001E-11	1.623E-02	6051-T6	AL TARGET	S	31
32	5.990E-03	1.839E-01	0.	2.142E-09	6.150E-05	2.709E-00-1.001E-11	1.623E-02	6051-T6	AL TARGET	S	32
33	5.990E-03	1.839E-01	0.	2.142E-09	6.150E-05	2.709E-00-1.001E-11	1.623E-02	6051-T6	AL TARGET	S	33
34	5.990E-03	1.959E-01	0.	2.142E-09	6.150E-05	2.709E-00-1.001E-11	1.623E-02	6051-T6	AL TARGET	S	34
35	5.990E-03	2.018E-01	0.	2.142E-09	6.150E-05	2.709E-00-1.001E-11	1.623E-02	6051-T6	AL TARGET	S	35
36	5.990E-03	2.078E-01	0.	2.142E-09	6.150E-05	2.709E-00-1.001E-11	1.623E-02	6051-T6	AL TARGET	S	36
37	5.990E-03	2.138E-01	0.	2.142E-09	6.150E-05	2.709E-00-1.001E-11	1.623E-02	6051-T6	AL TARGET	S	37
38	5.990E-03	2.198E-01	0.	2.142E-09	6.150E-05	2.709E-00-1.001E-11	1.623E-02	6051-T6	AL TARGET	S	38
39	5.990E-03	2.258E-01	0.	2.142E-09	6.150E-05	2.709E-00-1.001E-11	1.623E-02	6051-T6	AL TARGET	S	39
40	5.990E-03	2.318E-01	0.	2.142E-09	6.150E-05	2.709E-00-1.001E-11	1.623E-02	6051-T6	AL TARGET	S	40
41	5.990E-03	2.378E-01	0.	2.142E-09	6.150E-05	2.709E-00-1.001E-11	1.623E-02	6051-T6	AL TARGET	S	41
42	5.990E-03	2.438E-01	0.	2.142E-09	6.150E-05	2.709E-00-1.001E-11	1.623E-02	6051-T6	AL TARGET	S	42
43	5.990E-03	2.497E-01	0.	2.142E-09	6.150E-05	2.709E-00-1.001E-11	1.623E-02	6051-T6	AL TARGET	S	43
44	5.990E-03	2.557E-01	0.	2.142E-09	6.150E-05	2.709E-00-1.001E-11	1.623E-02	6051-T6	AL TARGET	S	44
45	5.990E-03	2.617E-01	0.	2.142E-09	6.150E-05	2.709E-00-1.001E-11	1.623E-02	6051-T6	AL TARGET	S	45
46	5.990E-03	2.677E-01	0.	2.142E-09	6.150E-05	2.709E-00-1.001E-11	1.623E-02	6051-T6	AL TARGET	S	46
47	5.990E-03	2.737E-01	0.	2.142E-09	6.150E-05	2.709E-00-1.001E-11	1.623E-02	6051-T6	AL TARGET	S	47
48	5.990E-03	2.797E-01	0.	2.142E-09	6.150E-05	2.709E-00-1.001E-11	1.623E-02	6051-T6	AL TARGET	S	48
49	5.990E-03	2.857E-01	0.	2.142E-09	6.150E-05	2.709E-00-1.001E-11	1.623E-02	6051-T6	AL TARGET	S	49
50	5.990E-03	2.917E-01	0.	2.142E-09	6.150E-05	2.709E-00-1.001E-11	1.623E-02	6051-T6	AL TARGET	S	50

TEST 1b: PORTION OF COORDINATE LAYOUT

[illegible]

**TEST 1b: PORTION OF TEST PRINTS**

MOMENTUM EDIT

CYCLE 5 1.3945E-09 4.4840E-10 27 1.7462E+01 269 30 27 7.0505E+09 1.5394E-01  
 0.5657E-06 3.5637E-06 0. 2.5133E+04 2.5140E+04 3.5189E-08 2.5140E+04 0. 0. 0.  
 0.4455E-05 1.5394E-01 1.4119E+00 1.7272E+00 1.7272E+00 1.7272E+00 26 1.8232E+10 1.5394E-01

TIME EDIT NO. 1 AT N = 5, TIME = 1.39395E-09 SECS, JSTAR = 30, CALC TIME IS 5.468 SECS

J	X	U	R	P	S	EH	D	C	J	COND	Y, NM, MU	SD OR NT
CELL	CM	CH/SEC	DYN/CH2	YIN/CH2	DYN/CH2	EROS	GM/CH3	CM/SEC	CELL		( DYN/CM2 OR 1/CM)	
1	000084	60300	0.	0.	0.	0.	2.7090	6.1498E+05	1	S R	6091-T6 AL	FLYER
2	006240	60300	0.	0.	0.	0.	2.7090	6.1498E+05	2	S M R	6091-T6 AL	FLYER
3	012396	60300	0.	0.	0.	0.	2.7090	6.1498E+05	3	S M R	6091-T6 AL	FLYER
4	018552	60300	0.	0.	0.	0.	2.7090	6.1498E+05	4	S M R	6091-T6 AL	FLYER
5	024708	60300	0.	0.	0.	0.	2.7090	6.1498E+05	5	S M R	6091-T6 AL	FLYER
6	030864	60300	0.	0.	0.	0.	2.7090	6.1498E+05	6	S M R	6091-T6 AL	FLYER
7	037026	60300	0.	0.	0.	0.	2.7090	6.1498E+05	7	S M R	6091-T6 AL	FLYER
8	043176	60300	0.	0.	0.	0.	2.7090	6.1498E+05	8	S M R	6091-T6 AL	FLYER
9	049332	60300	0.	0.	0.	0.	2.7090	6.1498E+05	9	S M R	6091-T6 AL	FLYER
10	055488	60300	0.	0.	0.	0.	2.7090	6.1498E+05	10	S M R	6091-T6 AL	FLYER
11	061644	60300	0.	0.	0.	0.	2.7090	6.1498E+05	11	S M R	6091-T6 AL	FLYER
12	067800	60300	0.	0.	0.	0.	2.7090	6.1498E+05	12	S M R	6091-T6 AL	FLYER
13	073956	60300	0.	0.	0.	0.	2.7090	6.1498E+05	13	S M R	6091-T6 AL	FLYER
14	080112	60300	0.	0.	0.	0.	2.7090	6.1498E+05	14	S M R	6091-T6 AL	FLYER
15	086268	60300	0.	0.	0.	0.	2.7090	6.1498E+05	15	S M R	6091-T6 AL	FLYER
16	092424	60300	0.	0.	0.	0.	2.7090	6.1498E+05	16	S M R	6091-T6 AL	FLYER
17	098580	60300	0.	0.	0.	0.	2.7090	6.1498E+05	17	S M R	6091-T6 AL	FLYER
18	104736	60300	0.	0.	0.	0.	2.7090	6.1498E+05	18	S M R	6091-T6 AL	FLYER
19	110892	60300	0.	0.	0.	0.	2.7090	6.1498E+05	19	S M R	6091-T6 AL	FLYER
20	117048	60300	0.	0.	0.	0.	2.7090	6.1498E+05	20	S M R	6091-T6 AL	FLYER
21	123204	60300	0.	0.	0.	0.	2.7090	6.1498E+05	21	S M R	6091-T6 AL	FLYER
22	129360	60300	7.488E+01	1.602E+01	2.580E+01	1.409E-07	2.7090	6.1485E+05	22	S M R	6091-T6 AL	FLYER
23	135516	60300	1.492E+05	4.368E+04	6.699E+04	4.747E-01	2.7090	6.1485E+05	23	S M R	6091-T6 AL	FLYER
24	141672	60296	7.438E+07	2.868E+07	4.389E+07	6.903E+04	2.7091	6.1487E+05	24	S M R	6091-T6 AL	FLYER
25	0147827	99236	7.530E+09	2.373E+09	3.594E+09	2.427E+07	2.7183	6.1661E+05	25	S M R	6091-T6 AL	FLYER
26	0153942	30143	1.823E+10	4.691E+09	6.908E+09	0.	2.7273	6.1829E+05	26	S L R	6091-T6 AL	FLYER
27	0153942	30143	1.823E+10	4.616E+09	7.050E+09	2.494E+07	2.7278	6.1838E+05	27	S R A	6091-T6 AL	TARGET
28	0159801	1100	7.630E+09	2.437E+09	3.691E+09	7.385E+04	2.7186	6.1665E+05	28	S M R	6091-T6 AL	TARGET
29	0165801	5	7.812E+07	3.039E+07	4.650E+07	5.450E-01	2.7091	6.1487E+05	29	S M R	6091-T6 AL	TARGET
30	0171071	0	1.617E+05	4.797E+04	7.357E+04	1.700E-07	2.7090	6.1485E+05	30	S M R	6091-T6 AL	TARGET
31	0177862	0	8.206E+01	1.896E+01	2.908E+01	0.	2.7090	6.1485E+05	31	S M R	6091-T6 AL	TARGET

TEST 1b: FIRST PAGE OF FINAL TIME EDIT





c. Test No. 1c

This computation represents the normal production run of Test 1. The results are a sample of those obtainable with the Bauschinger model. The listing included in the following pages contains the input data, one page of the initial layout, the final momentum EDIT, time EDIT, and two pages of the stress histories. In addition, there are computer-generated plots of deviatoric stress versus specific volume, of stress-distance curves, and stress histories.

\*\*\* SRI PUFF 1 (S400 VERSION) \*\*\*

DATE =05/06/69

IDENT = 1 C NORMAL RUN. TEST OF BAUSCHINGER MODEL ON 6061-T6  
COMPUTATIONS CORRESPOND TO THE 50 KSI DATA OF ROGER WILLIAMS FOR 6061-T6  
ALUMINUM. THE BAUSCHINGER MODEL IS USED FOR BOTH THE FLYER AND TARGET.  
THE JEDITS WERE PLACED AT THE APPROXIMATE THICKNESSES OF THE THREE THINNER  
SPECIMENS SO THAT THE COMPUTATION MODELS ALL FOUR EXPERIMENTS.

1 NTENT= 7 NJEDIT= 6 NREZON= 0 NSEPRAT= C  
2 TENDITS= 3.000E-07 6.000E-07 9.000E-07 1.200E-06 1.600E-06 2.000E-06 2.400E-06  
3 JEDITS= 50 80 120 172 229 251  
6 NEDTH= 100000 NEDIT= 10000 NPERN = 1 -0  
7 STOPS JCYCS = 1250 CKS = 3.500E+00 TS = 3.000E-06  
8 NMTHLS= 3 MATFL = 1 UZERO = 6.036E+04 IPLOT = 0

6061-T6 AL FLYER RHO = 2.709E+00 NSRM = 5 NYAM = 1 NPOR = 0 NCON = 0  
EQSTC = 6.670E+11 EQSTD = 1.000E+12 EQSTE = 1.220E+11 EQSTG = 2.040E+00  
EQSTH = 2.500E-01 EQSTS = 0. EQSTN = 9.893E-01 EQSTA = 6.285E-12  
COSQ = 4.000E+00 C1 = 5.000E-02 -0.  
TENS(1)= -1.000E+11 TENS(2)= -1.000E+11 TENS(3)= -1.000E+11  
XPO = 6.000E+03 XP = 1.000E+00 MUUM = 4.670E+11 YADF = 1.000E+00  
YO = 3.210E+09 MU = 2.670E+11 YADD = 3.790E+10  
NZONES= 1, 25 CELLS IN 1.537E-01 CM DELX= -0. -0.

6061-T6 AL TARGET RHO = 2.709E+00 NSRM = 5 NYAM = 1 NYOR = 0 NCON = 0  
EQSTC = 6.670E+11 EQSTD = 1.000E+12 EQSTE = 1.220E+11 EQSTG = 2.040E+00  
EQSTH = 2.500E-01 EQSTS = 0. EQSTN = 9.893E-01 EQSTA = 6.285E-12  
COSQ = 4.000E+00 C1 = 5.000E-02 -0.  
TENS(1)= -1.000E+11 TENS(2)= -1.000E+11 TENS(3)= -1.000E+11  
XPO = 6.000E+03 XP = 1.000E+00 MUUM = 4.670E+11 YADF = 1.000E+00  
YO = 3.210E+09 MU = 2.670E+11 YADD = 3.790E+10  
NZONES= 1, 210 CELLS IN 1.257E+00 CM DELX= -0. -0.

GLASS (MN GAGE) RHO = 2.520E+00 NSRM = 0 NYAM = 0 NPOR = 0 NCON = 0  
EQSTC = 6.780E+11 EQSTD = -8.780E+11 EQSTE = 3.000E+10 EQSTG = 2.000E+00  
EQSTH = 2.500E-01 EQSTS = 8.780E+11 EQSTN = 5.807E+00 EQSTA = 5.740E-12  
COSQ = 4.000E+00 C1 = 5.000E-02 -0.  
TENS(1)= -1.000E+11 TENS(2)= -1.000E+11 TENS(3)= -1.000E+11  
NZONES= 1, 30 CELLS IN 3.150E-01 CM DELX = 6.069E-03 -0.

TEST 1c: INPUT DATA



061-196

MATERIAL	COND	J
6001-T6 AL	TARGET	51
6001-T6 AL	TARGET	52
6001-T6 AL	TARGET	53
6001-T6 AL	TARGET	54
6001-T6 AL	TARGET	55
6001-T6 AL	TARGET	56
6001-T6 AL	TARGET	57
6001-T6 AL	TARGET	58
6001-T6 AL	TARGET	59
6001-T6 AL	TARGET	60
6001-T6 AL	TARGET	61
6001-T6 AL	TARGET	62
6001-T6 AL	TARGET	63
6001-T6 AL	TARGET	64
6001-T6 AL	TARGET	65
6001-T6 AL	TARGET	66
6001-T6 AL	TARGET	67
6001-T6 AL	TARGET	68
6001-T6 AL	TARGET	69
6001-T6 AL	TARGET	70
6001-T6 AL	TARGET	71
6001-T6 AL	TARGET	72
6001-T6 AL	TARGET	73
6001-T6 AL	TARGET	74
6001-T6 AL	TARGET	75
6001-T6 AL	TARGET	76
6001-T6 AL	TARGET	77
6001-T6 AL	TARGET	78
6001-T6 AL	TARGET	79
6001-T6 AL	TARGET	80
6001-T6 AL	TARGET	81
6001-T6 AL	TARGET	82
6001-T6 AL	TARGET	83
6001-T6 AL	TARGET	84
6001-T6 AL	TARGET	85
6001-T6 AL	TARGET	86
6001-T6 AL	TARGET	87
6001-T6 AL	TARGET	88
6001-T6 AL	TARGET	89
6001-T6 AL	TARGET	90
6001-T6 AL	TARGET	91
6001-T6 AL	TARGET	92
6001-T6 AL	TARGET	93
6001-T6 AL	TARGET	94
6001-T6 AL	TARGET	95
6001-T6 AL	TARGET	96
6001-T6 AL	TARGET	97
6001-T6 AL	TARGET	98
6001-T6 AL	TARGET	99
6001-T6 AL	TARGET	100





DATE = 05/06/69 IDENT = 1 C NORMAL RUN. TEST OF BAUSCHINGER MODEL ON 0001-76

J	DX	X(J)	U(J)	YHL(J)	G(J)	D(J)	T(J)	ZHL(J)	MATERIAL	COND	J
	CM	CM	CM/SEC	DYN/CM2	CM/SEC	SM/CM3	DYN/CM2	GM/CM2			
151	5.986E-03	8.959E-01	0.	2.140E+09	6.147E+05	2.709E+00	1.000E+11	1.622E-02	0001-76 AL TARGET	S M 0	151
152	5.986E-03	9.019E-01	0.	2.140E+09	6.147E+05	2.709E+00	1.000E+11	1.622E-02	0001-76 AL TARGET	S M 0	152
153	5.986E-03	9.079E-01	0.	2.140E+09	6.147E+05	2.709E+00	1.000E+11	1.622E-02	0001-76 AL TARGET	S M 0	153
154	5.986E-03	9.139E-01	0.	2.140E+09	6.147E+05	2.709E+00	1.000E+11	1.622E-02	0001-76 AL TARGET	S M 0	154
155	5.986E-03	9.199E-01	0.	2.140E+09	6.147E+05	2.709E+00	1.000E+11	1.622E-02	0001-76 AL TARGET	S M 0	155
156	5.986E-03	9.259E-01	0.	2.140E+09	6.147E+05	2.709E+00	1.000E+11	1.622E-02	0001-76 AL TARGET	S M 0	156
157	5.986E-03	9.318E-01	0.	2.140E+09	6.147E+05	2.709E+00	1.000E+11	1.622E-02	0001-76 AL TARGET	S M 0	157
158	5.986E-03	9.378E-01	0.	2.140E+09	6.147E+05	2.709E+00	1.000E+11	1.622E-02	0001-76 AL TARGET	S M 0	158
159	5.986E-03	9.438E-01	0.	2.140E+09	6.147E+05	2.709E+00	1.000E+11	1.622E-02	0001-76 AL TARGET	S M 0	159
160	5.986E-03	9.498E-01	0.	2.140E+09	6.147E+05	2.709E+00	1.000E+11	1.622E-02	0001-76 AL TARGET	S M 0	160
161	5.986E-03	9.558E-01	0.	2.140E+09	6.147E+05	2.709E+00	1.000E+11	1.622E-02	0001-76 AL TARGET	S M 0	161
162	5.986E-03	9.618E-01	0.	2.140E+09	6.147E+05	2.709E+00	1.000E+11	1.622E-02	0001-76 AL TARGET	S M 0	162
163	5.986E-03	9.678E-01	0.	2.140E+09	6.147E+05	2.709E+00	1.000E+11	1.622E-02	0001-76 AL TARGET	S M 0	163
164	5.986E-03	9.737E-01	0.	2.140E+09	6.147E+05	2.709E+00	1.000E+11	1.622E-02	0001-76 AL TARGET	S M 0	164
165	5.986E-03	9.797E-01	0.	2.140E+09	6.147E+05	2.709E+00	1.000E+11	1.622E-02	0001-76 AL TARGET	S M 0	165
166	5.986E-03	9.857E-01	0.	2.140E+09	6.147E+05	2.709E+00	1.000E+11	1.622E-02	0001-76 AL TARGET	S M 0	166
167	5.986E-03	9.917E-01	0.	2.140E+09	6.147E+05	2.709E+00	1.000E+11	1.622E-02	0001-76 AL TARGET	S M 0	167
168	5.986E-03	9.977E-01	0.	2.140E+09	6.147E+05	2.709E+00	1.000E+11	1.622E-02	0001-76 AL TARGET	S M 0	168
169	5.986E-03	1.004E+00	0.	2.140E+09	6.147E+05	2.709E+00	1.000E+11	1.622E-02	0001-76 AL TARGET	S M 0	169
170	5.986E-03	1.010E+00	0.	2.140E+09	6.147E+05	2.709E+00	1.000E+11	1.622E-02	0001-76 AL TARGET	S M 0	170
171	5.986E-03	1.016E+00	0.	2.140E+09	6.147E+05	2.709E+00	1.000E+11	1.622E-02	0001-76 AL TARGET	S M 0	171
172	5.986E-03	1.022E+00	0.	2.140E+09	6.147E+05	2.709E+00	1.000E+11	1.622E-02	0001-76 AL TARGET	S M 0	172
173	5.986E-03	1.028E+00	0.	2.140E+09	6.147E+05	2.709E+00	1.000E+11	1.622E-02	0001-76 AL TARGET	S M 0	173
174	5.986E-03	1.034E+00	0.	2.140E+09	6.147E+05	2.709E+00	1.000E+11	1.622E-02	0001-76 AL TARGET	S M 0	174
175	5.986E-03	1.040E+00	0.	2.140E+09	6.147E+05	2.709E+00	1.000E+11	1.622E-02	0001-76 AL TARGET	S M 0	175
176	5.986E-03	1.046E+00	0.	2.140E+09	6.147E+05	2.709E+00	1.000E+11	1.622E-02	0001-76 AL TARGET	S M 0	176
177	5.986E-03	1.052E+00	0.	2.140E+09	6.147E+05	2.709E+00	1.000E+11	1.622E-02	0001-76 AL TARGET	S M 0	177
178	5.986E-03	1.058E+00	0.	2.140E+09	6.147E+05	2.709E+00	1.000E+11	1.622E-02	0001-76 AL TARGET	S M 0	178
179	5.986E-03	1.064E+00	0.	2.140E+09	6.147E+05	2.709E+00	1.000E+11	1.622E-02	0001-76 AL TARGET	S M 0	179
180	5.986E-03	1.070E+00	0.	2.140E+09	6.147E+05	2.709E+00	1.000E+11	1.622E-02	0001-76 AL TARGET	S M 0	180
181	5.986E-03	1.075E+00	0.	2.140E+09	6.147E+05	2.709E+00	1.000E+11	1.622E-02	0001-76 AL TARGET	S M 0	181
182	5.986E-03	1.081E+00	0.	2.140E+09	6.147E+05	2.709E+00	1.000E+11	1.622E-02	0001-76 AL TARGET	S M 0	182
183	5.986E-03	1.087E+00	0.	2.140E+09	6.147E+05	2.709E+00	1.000E+11	1.622E-02	0001-76 AL TARGET	S M 0	183
184	5.986E-03	1.093E+00	0.	2.140E+09	6.147E+05	2.709E+00	1.000E+11	1.622E-02	0001-76 AL TARGET	S M 0	184
185	5.986E-03	1.099E+00	0.	2.140E+09	6.147E+05	2.709E+00	1.000E+11	1.622E-02	0001-76 AL TARGET	S M 0	185
186	5.986E-03	1.105E+00	0.	2.140E+09	6.147E+05	2.709E+00	1.000E+11	1.622E-02	0001-76 AL TARGET	S M 0	186
187	5.986E-03	1.111E+00	0.	2.140E+09	6.147E+05	2.709E+00	1.000E+11	1.622E-02	0001-76 AL TARGET	S M 0	187
188	5.986E-03	1.117E+00	0.	2.140E+09	6.147E+05	2.709E+00	1.000E+11	1.622E-02	0001-76 AL TARGET	S M 0	188
189	5.986E-03	1.123E+00	0.	2.140E+09	6.147E+05	2.709E+00	1.000E+11	1.622E-02	0001-76 AL TARGET	S M 0	189
190	5.986E-03	1.129E+00	0.	2.140E+09	6.147E+05	2.709E+00	1.000E+11	1.622E-02	0001-76 AL TARGET	S M 0	190
191	5.986E-03	1.135E+00	0.	2.140E+09	6.147E+05	2.709E+00	1.000E+11	1.622E-02	0001-76 AL TARGET	S M 0	191
192	5.986E-03	1.141E+00	0.	2.140E+09	6.147E+05	2.709E+00	1.000E+11	1.622E-02	0001-76 AL TARGET	S M 0	192
193	5.986E-03	1.147E+00	0.	2.140E+09	6.147E+05	2.709E+00	1.000E+11	1.622E-02	0001-76 AL TARGET	S M 0	193
194	5.986E-03	1.153E+00	0.	2.140E+09	6.147E+05	2.709E+00	1.000E+11	1.622E-02	0001-76 AL TARGET	S M 0	194
195	5.986E-03	1.159E+00	0.	2.140E+09	6.147E+05	2.709E+00	1.000E+11	1.622E-02	0001-76 AL TARGET	S M 0	195
196	5.986E-03	1.165E+00	0.	2.140E+09	6.147E+05	2.709E+00	1.000E+11	1.622E-02	0001-76 AL TARGET	S M 0	196
197	5.986E-03	1.171E+00	0.	2.140E+09	6.147E+05	2.709E+00	1.000E+11	1.622E-02	0001-76 AL TARGET	S M 0	197
198	5.986E-03	1.177E+00	0.	2.140E+09	6.147E+05	2.709E+00	1.000E+11	1.622E-02	0001-76 AL TARGET	S M 0	198
199	5.986E-03	1.183E+00	0.	2.140E+09	6.147E+05	2.709E+00	1.000E+11	1.622E-02	0001-76 AL TARGET	S M 0	199
200	5.986E-03	1.189E+00	0.	2.140E+09	6.147E+05	2.709E+00	1.000E+11	1.622E-02	0001-76 AL TARGET	S M 0	200

TEST 1c: COORDINATE LAYOUT (continued)

DATE = 05/06/69 IDENT = 1 C NORMAL RUN. TEST OF RAUSCHINGER MODEL ON 6061-T6

J	DA CM	X(J) CM	U(J) CM/SEC	YML(J) DYN/CM2	C(J) CM/SEC	O(J) CM/CM3	T(J) DYN/CM2	ZML(J) GM/CM2	MATERIAL	COMM	J
201	5.986E-03	1.195E+00	0.	2.140E+09	6.147E+05	2.709E+00	1.000E+11	1.622E-02	6061-T6 AL TARGET	S N B	201
202	5.986E-03	1.201E+00	0.	2.140E+09	6.147E+05	2.709E+00	1.000E+11	1.622E-02	6061-T6 AL TARGET	S N B	202
203	5.986E-03	1.207E+00	0.	2.140E+09	6.147E+05	2.709E+00	1.000E+11	1.622E-02	6061-T6 AL TARGET	S N B	203
204	5.986E-03	1.213E+00	0.	2.140E+09	6.147E+05	2.709E+00	1.000E+11	1.622E-02	6061-T6 AL TARGET	S N B	204
205	5.986E-03	1.219E+00	0.	2.140E+09	6.147E+05	2.709E+00	1.000E+11	1.622E-02	6061-T6 AL TARGET	S N B	205
206	5.986E-03	1.225E+00	0.	2.140E+09	6.147E+05	2.709E+00	1.000E+11	1.622E-02	6061-T6 AL TARGET	S N B	206
207	5.986E-03	1.231E+00	0.	2.140E+09	6.147E+05	2.709E+00	1.000E+11	1.622E-02	6061-T6 AL TARGET	S N B	207
208	5.986E-03	1.237E+00	0.	2.140E+09	6.147E+05	2.709E+00	1.000E+11	1.622E-02	6061-T6 AL TARGET	S N B	208
209	5.986E-03	1.243E+00	0.	2.140E+09	6.147E+05	2.709E+00	1.000E+11	1.622E-02	6061-T6 AL TARGET	S N B	209
210	5.986E-03	1.249E+00	0.	2.140E+09	6.147E+05	2.709E+00	1.000E+11	1.622E-02	6061-T6 AL TARGET	S N B	210
211	5.986E-03	1.255E+00	0.	2.140E+09	6.147E+05	2.709E+00	1.000E+11	1.622E-02	6061-T6 AL TARGET	S N B	211
212	5.986E-03	1.261E+00	0.	2.140E+09	6.147E+05	2.709E+00	1.000E+11	1.622E-02	6061-T6 AL TARGET	S N B	212
213	5.986E-03	1.267E+00	0.	2.140E+09	6.147E+05	2.709E+00	1.000E+11	1.622E-02	6061-T6 AL TARGET	S N B	213
214	5.986E-03	1.273E+00	0.	2.140E+09	6.147E+05	2.709E+00	1.000E+11	1.622E-02	6061-T6 AL TARGET	S N B	214
215	5.986E-03	1.279E+00	0.	2.140E+09	6.147E+05	2.709E+00	1.000E+11	1.622E-02	6061-T6 AL TARGET	S N B	215
216	5.986E-03	1.285E+00	0.	2.140E+09	6.147E+05	2.709E+00	1.000E+11	1.622E-02	6061-T6 AL TARGET	S N B	216
217	5.986E-03	1.291E+00	0.	2.140E+09	6.147E+05	2.709E+00	1.000E+11	1.622E-02	6061-T6 AL TARGET	S N B	217
218	5.986E-03	1.297E+00	0.	2.140E+09	6.147E+05	2.709E+00	1.000E+11	1.622E-02	6061-T6 AL TARGET	S N B	218
219	5.986E-03	1.303E+00	0.	2.140E+09	6.147E+05	2.709E+00	1.000E+11	1.622E-02	6061-T6 AL TARGET	S N B	219
220	5.986E-03	1.309E+00	0.	2.140E+09	6.147E+05	2.709E+00	1.000E+11	1.622E-02	6061-T6 AL TARGET	S N B	220
221	5.986E-03	1.315E+00	0.	2.140E+09	6.147E+05	2.709E+00	1.000E+11	1.622E-02	6061-T6 AL TARGET	S N B	221
222	5.986E-03	1.321E+00	0.	2.140E+09	6.147E+05	2.709E+00	1.000E+11	1.622E-02	6061-T6 AL TARGET	S N B	222
223	5.986E-03	1.327E+00	0.	2.140E+09	6.147E+05	2.709E+00	1.000E+11	1.622E-02	6061-T6 AL TARGET	S N B	223
224	5.986E-03	1.333E+00	0.	2.140E+09	6.147E+05	2.709E+00	1.000E+11	1.622E-02	6061-T6 AL TARGET	S N B	224
225	5.986E-03	1.339E+00	0.	2.140E+09	6.147E+05	2.709E+00	1.000E+11	1.622E-02	6061-T6 AL TARGET	S N B	225
226	5.986E-03	1.345E+00	0.	2.140E+09	6.147E+05	2.709E+00	1.000E+11	1.622E-02	6061-T6 AL TARGET	S N B	226
227	5.986E-03	1.351E+00	0.	2.140E+09	6.147E+05	2.709E+00	1.000E+11	1.622E-02	6061-T6 AL TARGET	S N B	227
228	5.986E-03	1.357E+00	0.	2.140E+09	6.147E+05	2.709E+00	1.000E+11	1.622E-02	6061-T6 AL TARGET	S N B	228
229	5.986E-03	1.363E+00	0.	2.140E+09	6.147E+05	2.709E+00	1.000E+11	1.622E-02	6061-T6 AL TARGET	S N B	229
230	5.986E-03	1.369E+00	0.	2.140E+09	6.147E+05	2.709E+00	1.000E+11	1.622E-02	6061-T6 AL TARGET	S N B	230
231	5.986E-03	1.375E+00	0.	2.140E+09	6.147E+05	2.709E+00	1.000E+11	1.622E-02	6061-T6 AL TARGET	S N B	231
232	5.986E-03	1.381E+00	0.	2.140E+09	6.147E+05	2.709E+00	1.000E+11	1.622E-02	6061-T6 AL TARGET	S N B	232
233	5.986E-03	1.387E+00	0.	2.140E+09	6.147E+05	2.709E+00	1.000E+11	1.622E-02	6061-T6 AL TARGET	S N B	233
234	5.986E-03	1.393E+00	0.	2.140E+09	6.147E+05	2.709E+00	1.000E+11	1.622E-02	6061-T6 AL TARGET	S N B	234
235	5.986E-03	1.399E+00	0.	2.140E+09	6.147E+05	2.709E+00	1.000E+11	1.622E-02	6061-T6 AL TARGET	S N B	235
236	5.986E-03	1.405E+00	0.	2.140E+09	6.147E+05	2.709E+00	1.000E+11	1.622E-02	6061-T6 AL TARGET	S N B	236
237	0.	1.411E+00	0.	2.140E+09	6.147E+05	2.709E+00	1.000E+11	0.	6061-T6 AL TARGET	S L B	237
238	6.000E-03	1.411E+00	0.	0.	5.903E+05	2.520E+00	1.000E+11	1.512E-02	GLASS (MA GAGE)	S R B	238
239	6.310E-03	1.417E+00	0.	0.	5.903E+05	2.520E+00	1.000E+11	1.590E-02	GLASS (MA GAGE)	S N B	239
240	6.621E-03	1.423E+00	0.	0.	5.903E+05	2.520E+00	1.000E+11	1.668E-02	GLASS (MA GAGE)	S N B	240
241	6.931E-03	1.430E+00	0.	0.	5.903E+05	2.520E+00	1.000E+11	1.747E-02	GLASS (MA GAGE)	S N B	241
242	7.241E-03	1.437E+00	0.	0.	5.903E+05	2.520E+00	1.000E+11	1.825E-02	GLASS (MA GAGE)	S N B	242
243	7.552E-03	1.444E+00	0.	0.	5.903E+05	2.520E+00	1.000E+11	1.903E-02	GLASS (MA GAGE)	S N B	243
244	7.862E-03	1.451E+00	0.	0.	5.903E+05	2.520E+00	1.000E+11	1.981E-02	GLASS (MA GAGE)	S N B	244
245	8.172E-03	1.459E+00	0.	0.	5.903E+05	2.520E+00	1.000E+11	2.059E-02	GLASS (MA GAGE)	S N B	245
246	8.483E-03	1.467E+00	0.	0.	5.903E+05	2.520E+00	1.000E+11	2.138E-02	GLASS (MA GAGE)	S N B	246
247	8.793E-03	1.476E+00	0.	0.	5.903E+05	2.520E+00	1.000E+11	2.216E-02	GLASS (MA GAGE)	S N B	247
248	9.103E-03	1.485E+00	0.	0.	5.903E+05	2.520E+00	1.000E+11	2.294E-02	GLASS (MA GAGE)	S N B	248
249	9.414E-03	1.494E+00	0.	0.	5.903E+05	2.520E+00	1.000E+11	2.372E-02	GLASS (MA GAGE)	S N B	249
250	9.724E-03	1.503E+00	0.	0.	5.903E+05	2.520E+00	1.000E+11	2.450E-02	GLASS (MA GAGE)	S N B	250

TEST 1c: COORDINATE LAYOUT (continued)



DATE = 05/06/69 IDENT = I C NORMAL RUN. TEST OF BAUSCHINGER MODEL ON 6061-T6

J	DA	X(J)	U(J)	YML(J)	C(J)	D(J)	T(J)	ZML(J)	MATERIAL	COND	J
	CM	CM	CM/SEC	DYN/CM2	CM/SEC	GM/CM3	DYN/CM2	GM/CM2			
251	1.903E-02	1.513E+00	0.	0.	5.903E+05	2.520E+00-1.000E+11	2.529E-02	GLASS	(MM GAGE)	S M B	251
252	1.034E-02	1.523E+00	0.	0.	5.903E+05	2.520E+00-1.000E+11	2.607E-02	GLASS	(MM GAGE)	S M B	252
253	1.068E-02	1.533E+00	0.	0.	5.903E+05	2.520E+00-1.000E+11	2.645E-02	GLASS	(MM GAGE)	S M B	253
254	1.097E-02	1.542E+00	0.	0.	5.903E+05	2.520F+00-1.000E+11	2.743E-02	GLASS	(MM GAGE)	S M B	254
255	1.128E-02	1.552E+00	0.	0.	5.903E+05	2.520F+00-1.000E+11	2.842E-02	GLASS	(MM GAGE)	S M B	255
256	1.159E-02	1.562E+00	0.	0.	5.903E+05	2.520F+00-1.000E+11	2.920E-02	GLASS	(MM GAGE)	S M B	256
257	1.190E-02	1.572E+00	0.	0.	5.903E+05	2.520E+00-1.000E+11	2.998E-02	GLASS	(MM GAGE)	S M B	257
258	1.221E-02	1.590E+00	0.	0.	5.903E+05	2.520E+00-1.000E+11	3.076E-02	GLASS	(MM GAGE)	S M B	258
259	1.252E-02	1.602E+00	0.	0.	5.903E+05	2.520E+00-1.000E+11	3.154E-02	GLASS	(MM GAGE)	S M B	259
260	1.283E-02	1.614E+00	0.	0.	5.903E+05	2.520E+00-1.000E+11	3.232E-02	GLASS	(MM GAGE)	S M B	260
261	1.314E-02	1.627E+00	0.	0.	5.903E+05	2.520E+00-1.000E+11	3.311E-02	GLASS	(MM GAGE)	S M B	261
262	1.345E-02	1.640E+00	0.	0.	5.903E+05	2.520E+00-1.000E+11	3.389E-02	GLASS	(MM GAGE)	S M B	262
263	1.376E-02	1.654E+00	0.	0.	5.903E+05	2.520E+00-1.000E+11	3.467E-02	GLASS	(MM GAGE)	S M B	263
264	1.407E-02	1.668E+00	0.	0.	5.903E+05	2.520E+00-1.000E+11	3.545E-02	GLASS	(MM GAGE)	S M B	264
265	1.438E-02	1.682E+00	0.	0.	5.903E+05	2.520F+00-1.000E+11	3.624E-02	GLASS	(MM GAGE)	S M B	265
266	1.469E-02	1.696E+00	0.	0.	5.903E+05	2.520F+00-1.000E+11	3.702E-02	GLASS	(MM GAGE)	S M B	266
267	1.500E-02	1.711E+00	0.	0.	5.903E+05	2.520E+00-1.000E+11	3.780E-02	GLASS	(MM GAGE)	S M B	267
268	1.531E-02	1.726E+00	0.	0.	5.907E+05	2.520F+00-1.000E+11	0.	GLASS	(MM GAGE)	S L	268
1.942 SECONDS.											
THE TO COMPLETE GENRAT IS											

TIME TO COMPLETE GENRAT IS 1.942 SECONDS.

TEST 1c: COORDINATE LAYOUT (concluded)

# MOMENTUM EDIT

CELL	TIME	DTM	JTS	ETOTAL	JFIN	JSTAR	JSMAX	SMAX	X(JSMAX)
1	3.0012E-06	7.2449E-09	232	1.7450E+01	269	268	239	3.7510E+09	1.4270E+00
2	3.0012E-06	7.2449E-09	232	1.7450E+01	269	268	239	3.7510E+09	1.4270E+00
3	3.0012E-06	7.2449E-09	232	1.7450E+01	269	268	239	3.7510E+09	1.4270E+00
4	3.0012E-06	7.2449E-09	232	1.7450E+01	269	268	239	3.7510E+09	1.4270E+00
5	3.0012E-06	7.2449E-09	232	1.7450E+01	269	268	239	3.7510E+09	1.4270E+00
6	3.0012E-06	7.2449E-09	232	1.7450E+01	269	268	239	3.7510E+09	1.4270E+00
7	3.0012E-06	7.2449E-09	232	1.7450E+01	269	268	239	3.7510E+09	1.4270E+00
8	3.0012E-06	7.2449E-09	232	1.7450E+01	269	268	239	3.7510E+09	1.4270E+00
9	3.0012E-06	7.2449E-09	232	1.7450E+01	269	268	239	3.7510E+09	1.4270E+00
10	3.0012E-06	7.2449E-09	232	1.7450E+01	269	268	239	3.7510E+09	1.4270E+00
11	3.0012E-06	7.2449E-09	232	1.7450E+01	269	268	239	3.7510E+09	1.4270E+00
12	3.0012E-06	7.2449E-09	232	1.7450E+01	269	268	239	3.7510E+09	1.4270E+00
13	3.0012E-06	7.2449E-09	232	1.7450E+01	269	268	239	3.7510E+09	1.4270E+00
14	3.0012E-06	7.2449E-09	232	1.7450E+01	269	268	239	3.7510E+09	1.4270E+00
15	3.0012E-06	7.2449E-09	232	1.7450E+01	269	268	239	3.7510E+09	1.4270E+00
16	3.0012E-06	7.2449E-09	232	1.7450E+01	269	268	239	3.7510E+09	1.4270E+00
17	3.0012E-06	7.2449E-09	232	1.7450E+01	269	268	239	3.7510E+09	1.4270E+00
18	3.0012E-06	7.2449E-09	232	1.7450E+01	269	268	239	3.7510E+09	1.4270E+00
19	3.0012E-06	7.2449E-09	232	1.7450E+01	269	268	239	3.7510E+09	1.4270E+00
20	3.0012E-06	7.2449E-09	232	1.7450E+01	269	268	239	3.7510E+09	1.4270E+00
21	3.0012E-06	7.2449E-09	232	1.7450E+01	269	268	239	3.7510E+09	1.4270E+00
22	3.0012E-06	7.2449E-09	232	1.7450E+01	269	268	239	3.7510E+09	1.4270E+00
23	3.0012E-06	7.2449E-09	232	1.7450E+01	269	268	239	3.7510E+09	1.4270E+00
24	3.0012E-06	7.2449E-09	232	1.7450E+01	269	268	239	3.7510E+09	1.4270E+00
25	3.0012E-06	7.2449E-09	232	1.7450E+01	269	268	239	3.7510E+09	1.4270E+00
26	3.0012E-06	7.2449E-09	232	1.7450E+01	269	268	239	3.7510E+09	1.4270E+00

TEST 1C: FINAL MOMENTUM EDIT AND PORTION OF TIME EDIT

J	K	U	R	P	S	CHL	D	C	J	COND	AL	TARGET	V.	MU	SD	OR	MT
27	175401	2449	1.2892E+00	6.0932E+00	1.2992E+00	1.376E+00	2.7300	0.1804E+05	27	S R N	0001-T6	AL	TARGET	9.585E+09	-5.904E+09		
28	161399	2450	1.4700E+00	6.1890E+00	1.4000E+00	1.900E+00	2.7303	0.1807E+05	28	S M F	0001-T6	AL	TARGET	7.335E+09	-6.066E+09		
29	101239	2440	1.7000E+00	6.1700E+00	1.7000E+00	1.700E+00	2.7298	0.1807E+05	29	S M F	0001-T6	AL	TARGET	7.287E+09	-5.935E+09		
30	101239	2416	2.297E+00	6.172E+00	2.297E+00	1.753E+00	2.7300	0.1807E+05	30	S M F	0001-T6	AL	TARGET	7.216E+09	-5.972E+09		
31	101239	2403	2.614E+00	6.243E+00	2.7300E+00	1.716E+00	2.7304	0.1803E+05	31	S M F	0001-T6	AL	TARGET	7.216E+09	-5.970E+09		
32	211017	2353	3.341E+00	6.279E+00	3.339E+00	1.652E+00	2.7304	0.1805E+05	32	S M F	0001-T6	AL	TARGET	7.143E+09	-5.935E+09		
33	211009	2331	3.700E+00	6.273E+00	3.730E+00	1.612E+00	2.7307	0.1805E+05	33	S M F	0001-T6	AL	TARGET	7.079E+09	-5.874E+09		
34	211033	2317	3.700E+00	6.244E+00	3.948E+00	1.608E+00	2.7307	0.1803E+05	34	S M F	0001-T6	AL	TARGET	7.072E+09	-5.830E+09		
35	222971	2313	4.010E+00	6.213E+00	4.015E+00	1.577E+00	2.7306	0.1801E+05	35	S M F	0001-T6	AL	TARGET	7.054E+09	-5.797E+09		
36	222971	2311	4.038E+00	6.231E+00	4.032E+00	1.537E+00	2.7307	0.1803E+05	36	S M F	0001-T6	AL	TARGET	7.021E+09	-5.759E+09		
37	234147	2311	4.038E+00	6.228E+00	4.054E+00	1.520E+00	2.7304	0.1802E+05	37	S M F	0001-T6	AL	TARGET	6.994E+09	-5.775E+09		
38	240700	2311	4.050E+00	6.102E+00	4.059E+00	1.501E+00	2.7306	0.1808E+05	38	S M F	0001-T6	AL	TARGET	6.994E+09	-5.782E+09		
39	240700	2311	4.044E+00	6.103E+00	4.046E+00	1.474E+00	2.7306	0.1808E+05	39	S M F	0001-T6	AL	TARGET	6.970E+09	-5.747E+09		
40	240700	2311	4.044E+00	6.103E+00	4.046E+00	1.469E+00	2.7307	0.1809E+05	40	S M F	0001-T6	AL	TARGET	6.955E+09	-5.752E+09		
41	240401	2312	4.023E+00	6.101E+00	4.027E+00	1.459E+00	2.7306	0.1808E+05	41	S M F	0001-T6	AL	TARGET	6.968E+09	-5.772E+09		
42	240401	2311	3.994E+00	6.101E+00	3.994E+00	1.434E+00	2.7307	0.1808E+05	42	S M F	0001-T6	AL	TARGET	6.947E+09	-5.663E+09		
43	270477	2314	3.994E+00	6.117E+00	3.994E+00	1.415E+00	2.7306	0.1805E+05	43	S M F	0001-T6	AL	TARGET	6.947E+09	-5.672E+09		
44	270416	2310	4.010E+00	6.069E+00	4.010E+00	1.392E+00	2.7304	0.1802E+05	44	S M F	0001-T6	AL	TARGET	6.957E+09	-5.718E+09		
45	240200	2312	4.037E+00	6.069E+00	4.037E+00	1.373E+00	2.7306	0.1804E+05	45	S M F	0001-T6	AL	TARGET	6.955E+09	-5.665E+09		
46	240200	2312	3.947E+00	6.069E+00	3.947E+00	1.364E+00	2.7306	0.1804E+05	46	S M F	0001-T6	AL	TARGET	6.945E+09	-5.648E+09		
47	240200	2301	3.860E+00	6.044E+00	3.860E+00	1.345E+00	2.7304	0.1801E+05	47	S M F	0001-T6	AL	TARGET	6.947E+09	-5.652E+09		
48	240200	2302	3.860E+00	6.044E+00	3.860E+00	1.345E+00	2.7304	0.1801E+05	48	S M F	0001-T6	AL	TARGET	6.950E+09	-5.751E+09		
49	240200	2302	3.860E+00	6.044E+00	3.860E+00	1.345E+00	2.7304	0.1801E+05	49	S M F	0001-T6	AL	TARGET	6.950E+09	-5.751E+09		
50	240200	2302	3.860E+00	6.044E+00	3.860E+00	1.345E+00	2.7304	0.1801E+05	50	S M F	0001-T6	AL	TARGET	6.936E+09	-5.643E+09		
51	240200	2401	3.860E+00	6.044E+00	3.860E+00	1.345E+00	2.7304	0.1801E+05	51	S M F	0001-T6	AL	TARGET	6.936E+09	-5.643E+09		
52	240200	2401	3.860E+00	6.044E+00	3.860E+00	1.345E+00	2.7304	0.1801E+05	52	S M F	0001-T6	AL	TARGET	6.936E+09	-5.643E+09		
53	240200	2401	3.860E+00	6.044E+00	3.860E+00	1.345E+00	2.7304	0.1801E+05	53	S M F	0001-T6	AL	TARGET	6.936E+09	-5.643E+09		
54	240200	2401	3.860E+00	6.044E+00	3.860E+00	1.345E+00	2.7304	0.1801E+05	54	S M F	0001-T6	AL	TARGET	6.936E+09	-5.643E+09		
55	240200	2401	3.860E+00	6.044E+00	3.860E+00	1.345E+00	2.7304	0.1801E+05	55	S M F	0001-T6	AL	TARGET	6.936E+09	-5.643E+09		
56	240200	2401	3.860E+00	6.044E+00	3.860E+00	1.345E+00	2.7304	0.1801E+05	56	S M F	0001-T6	AL	TARGET	6.936E+09	-5.643E+09		
57	240200	2401	3.860E+00	6.044E+00	3.860E+00	1.345E+00	2.7304	0.1801E+05	57	S M F	0001-T6	AL	TARGET	6.936E+09	-5.643E+09		
58	240200	2401	3.860E+00	6.044E+00	3.860E+00	1.345E+00	2.7304	0.1801E+05	58	S M F	0001-T6	AL	TARGET	6.936E+09	-5.643E+09		
59	240200	2401	3.860E+00	6.044E+00	3.860E+00	1.345E+00	2.7304	0.1801E+05	59	S M F	0001-T6	AL	TARGET	6.936E+09	-5.643E+09		
60	240200	2401	3.860E+00	6.044E+00	3.860E+00	1.345E+00	2.7304	0.1801E+05	60	S M F	0001-T6	AL	TARGET	6.936E+09	-5.643E+09		
61	240200	2401	3.860E+00	6.044E+00	3.860E+00	1.345E+00	2.7304	0.1801E+05	61	S M F	0001-T6	AL	TARGET	6.936E+09	-5.643E+09		
62	240200	2401	3.860E+00	6.044E+00	3.860E+00	1.345E+00	2.7304	0.1801E+05	62	S M F	0001-T6	AL	TARGET	6.936E+09	-5.643E+09		
63	240200	2401	3.860E+00	6.044E+00	3.860E+00	1.345E+00	2.7304	0.1801E+05	63	S M F	0001-T6	AL	TARGET	6.936E+09	-5.643E+09		
64	240200	2401	3.860E+00	6.044E+00	3.860E+00	1.345E+00	2.7304	0.1801E+05	64	S M F	0001-T6	AL	TARGET	6.936E+09	-5.643E+09		
65	240200	2401	3.860E+00	6.044E+00	3.860E+00	1.345E+00	2.7304	0.1801E+05	65	S M F	0001-T6	AL	TARGET	6.936E+09	-5.643E+09		
66	240200	2401	3.860E+00	6.044E+00	3.860E+00	1.345E+00	2.7304	0.1801E+05	66	S M F	0001-T6	AL	TARGET	6.936E+09	-5.643E+09		
67	240200	2401	3.860E+00	6.044E+00	3.860E+00	1.345E+00	2.7304	0.1801E+05	67	S M F	0001-T6	AL	TARGET	6.936E+09	-5.643E+09		
68	240200	2401	3.860E+00	6.044E+00	3.860E+00	1.345E+00	2.7304	0.1801E+05	68	S M F	0001-T6	AL	TARGET	6.936E+09	-5.643E+09		
69	240200	2401	3.860E+00	6.044E+00	3.860E+00	1.345E+00	2.7304	0.1801E+05	69	S M F	0001-T6	AL	TARGET	6.936E+09	-5.643E+09		

TEST 1C: FINAL TIME EDIT (continued)



SCRTIME OUTPUT, TIME IN MICROSECS, S IN KBARS, DTAM IN NANOSECS, DELTIM IN SECS											
N	TIME	512/50J	523/50J	534/50J	S ( 50 )	S (128)	S (172)	S (256)	JTS	DTNH	DELTIM
51	.237	46.368	0.000	3.791	19.1914	0.0000	0.0000	0.0000	48	6.496	.260
52	.244	46.337	0.000	4.778	27.2134	0.0000	0.0000	0.0000	49	6.481	.258
53	.250	46.297	0.000	5.726	35.0794	0.0000	0.0000	0.0000	49	6.507	.258
54	.257	46.379	0.000	6.434	41.8474	0.0000	0.0000	0.0000	50	6.494	.266
55	.263	46.447	0.000	6.833	44.4544	0.0000	0.0000	0.0000	50	6.453	.270
56	.278	46.293	0.000	0.971	45.6424	0.0000	0.0000	0.0000	51	6.516	.278
57	.276	46.616	0.000	4.647	45.5334	0.0000	0.0000	0.0000	52	6.497	.278
58	.283	46.442	0.000	4.641	45.2444	0.0000	0.0000	0.0000	52	6.512	.286
59	.290	46.494	0.000	6.822	45.2940	0.0000	0.0000	0.0000	53	6.511	.294
60	.296	46.489	0.000	6.584	45.6147	0.0000	0.0000	0.0000	53	6.504	.296
61	.300	46.486	0.000	6.893	45.6127	0.0000	0.0000	0.0000	54	6.052	.294
62	.308	46.497	0.000	6.784	45.6287	0.0000	0.0000	0.0000	54	6.459	.304
63	.311	46.584	0.000	6.774	45.6560	0.0000	0.0000	0.0000	55	5.831	.304
64	.317	46.534	0.000	6.749	45.7040	0.0000	0.0000	0.0000	55	6.552	.310
65	.324	46.515	0.000	6.761	45.8457	0.0000	0.0000	0.0000	56	6.550	.312
66	.330	46.498	0.000	6.714	45.9447	0.0000	0.0000	0.0000	57	6.514	.314
67	.337	46.446	0.000	6.726	45.9247	0.0000	0.0000	0.0000	57	6.521	.316
68	.343	46.837	0.000	6.731	46.0450	0.0000	0.0000	0.0000	58	6.529	.320
69	.359	46.867	0.000	6.741	46.1847	0.0000	0.0000	0.0000	59	6.519	.324
70	.366	46.808	0.000	6.698	46.1287	0.0000	0.0000	0.0000	59	6.539	.332
71	.363	46.504	0.000	6.693	46.1120	0.0000	0.0000	0.0000	60	6.526	.336
72	.369	46.602	0.000	6.674	46.1130	0.0000	0.0000	0.0000	60	6.527	.338
73	.374	46.633	0.000	6.632	46.2137	0.0000	0.0000	0.0000	61	6.543	.338
74	.383	46.644	0.000	6.637	46.1827	0.0000	0.0000	0.0000	62	6.527	.348
75	.389	46.620	0.000	6.636	46.2240	0.0000	0.0000	0.0000	62	6.539	.348
76	.394	46.614	0.000	6.644	46.3340	0.0000	0.0000	0.0000	63	6.539	.354
77	.402	46.647	0.000	6.633	46.3377	0.0000	0.0000	0.0000	64	6.532	.354
78	.409	46.647	0.000	6.608	46.3357	0.0000	0.0000	0.0000	64	6.535	.362
79	.418	46.651	0.000	6.598	46.3410	0.0000	0.0000	0.0000	65	6.537	.362
80	.422	46.691	0.000	6.600	46.4160	0.0000	0.0000	0.0000	66	6.546	.368
81	.429	46.649	0.000	6.587	46.4297	0.0000	0.0000	0.0000	66	6.550	.368
82	.436	46.684	0.000	6.594	46.3837	0.0000	0.0000	0.0000	67	6.551	.376
83	.441	46.714	0.000	6.584	46.3310	0.0000	0.0000	0.0000	67	6.551	.380
84	.448	46.726	0.000	6.598	46.6730	0.0000	0.0000	0.0000	68	6.547	.384
85	.456	46.893	0.000	6.551	46.4977	0.0000	0.0000	0.0000	68	6.543	.392
86	.461	46.922	0.000	6.526	46.4747	0.0000	0.0000	0.0000	69	6.546	.394
87	.466	46.911	0.000	6.525	46.4820	0.0000	0.0000	0.0000	70	6.550	.402
88	.474	46.914	0.000	6.536	46.5517	0.0000	0.0000	0.0000	70	6.550	.408
89	.471	46.991	0.000	6.526	46.5747	0.0000	0.0000	0.0000	71	6.537	.408
90	.477	46.949	0.000	6.526	46.5690	0.0000	0.0000	0.0000	72	6.547	.412
91	.484	46.918	0.000	6.516	46.6167	0.0000	0.0000	0.0000	72	6.541	.410
92	.487	46.914	0.000	6.504	46.6110	0.0000	0.0000	0.0000	73	6.554	.414
93	.494	46.914	0.000	6.499	46.6440	0.0000	0.0000	0.0000	73	6.551	.420
94	.499	46.9571	0.000	6.492	46.6747	0.0000	0.0000	0.0000	74	6.568	.426
95	.506	46.992	0.000	6.479	46.6777	0.0000	0.0000	0.0000	75	6.583	.432
96	.514	46.992	0.000	6.475	46.6840	0.0000	0.0000	0.0000	75	6.584	.436
97	.523	46.992	0.000	6.475	46.6840	0.0000	0.0000	0.0000	76	6.593	.436
98	.534	46.992	0.000	6.475	46.6840	0.0000	0.0000	0.0000	77	6.598	.440
99	.544	46.992	0.000	6.475	46.6840	0.0000	0.0000	0.0000	77	6.598	.446
100	.554	46.992	0.000	6.475	46.6840	0.0000	0.0000	0.0000	78	6.598	.452

TEST 1c: STRESS HISTORIES (continued)

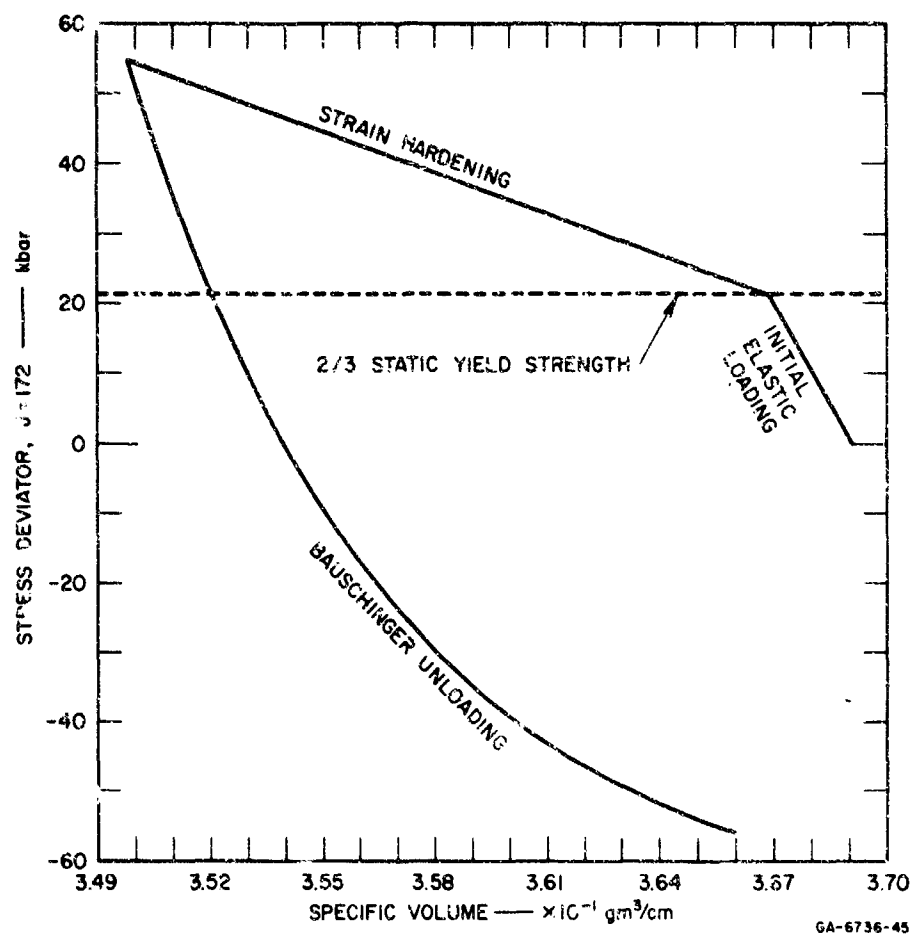


FIGURE 45 TEST 1c: SAMPLE PLOT OF STRESS DEVIATOR  
(Curves plotted by computer from calculated results)

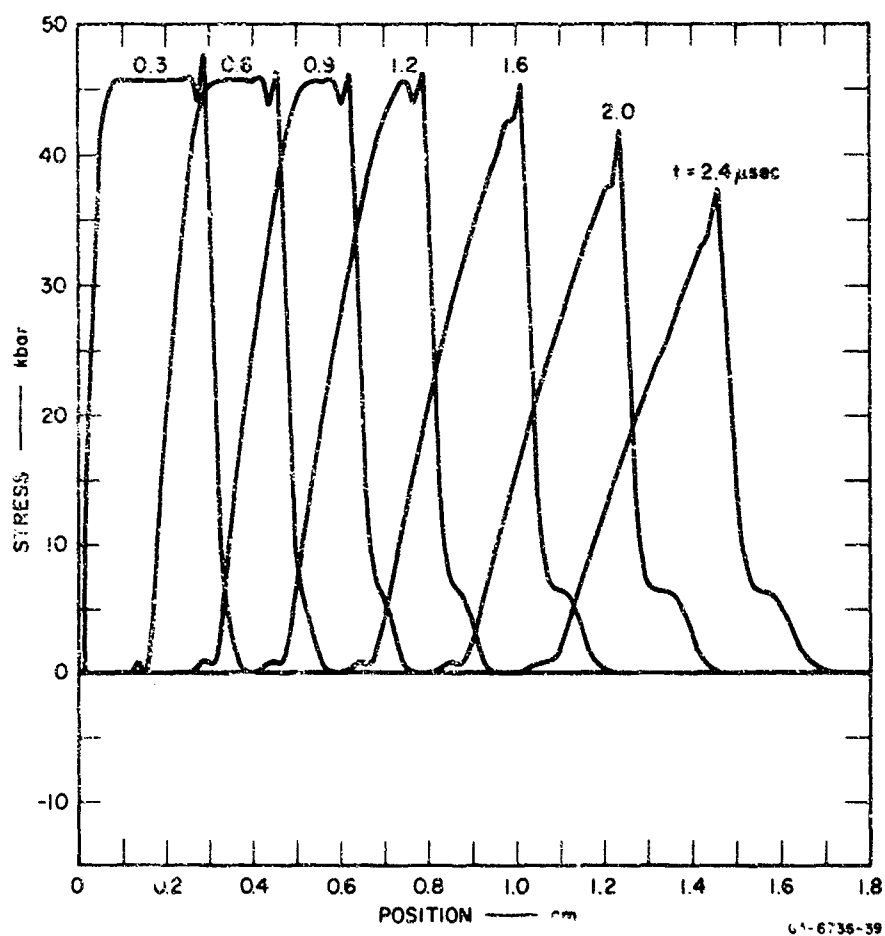


FIGURE 46 TEST 1c: SUMMARY PLOT OF ALL TIME EDITS

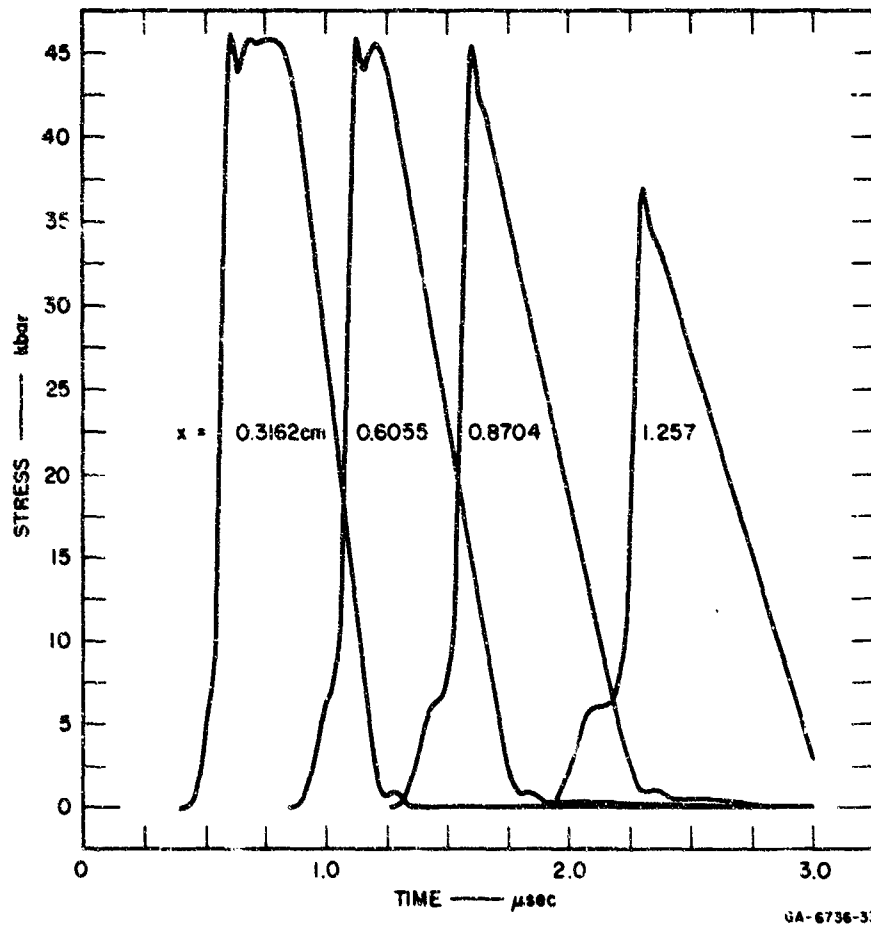


FIGURE 47 TEST 1c: SUMMARY OF STRESS HISTORIES  
AT FOUR JEDIT LOCATIONS



d. Test No. 2

A simple impact between a solid aluminum flyer and an aluminum target is given as Test 2. Neither stress relaxation nor Bauschinger effect is included, so the problem could be run with any one-dimensional wave propagation code containing an elasto-plastic equation of state. The listing in the next pages includes the input data, a page of the initial layout, and samples of the final EDIT and stress histories. The EDITs , stress histories, and a deviatoric stress-volume path are shown in the figures.

\*\*\* SRI PLT F 1 (6400 VERSION) \*\*\*

DATE 04/22/69

IDENT = 2 MODEL 0: AL/AL IMPACT, NO RELAXATION OR BAUSCHINGER

FLYER AND TARGET ARE BOTH OF 2024-T8 ALUMINUM

1 NTEUT= 5 NJEDIT= 6 NREZON= 0 NSEPRAT= 0

2 TENITS= 5.000E-07 1.000E-06 1.500E-06 2.000E-06 2.500E-06

3 JEDITS= 38 75 112 147 224 261

6 NEDTH= 100000 NEDIT= 10000 NPERN = 1 -0

7 STOPS JCYCS = 1250 CKS = 4.000E+00 TS = 2.800E-06

8 NMTRLS= 2 MATFL = 1 UZERO = 2.000E+04 IPIOT = 1

AL FLYER RMO = 2.785E+00 NSRM = 0 NYAM 1 NPOR 0 NCON = 0

EQSTC = 7.550E+11 EQSTD = 1.290E+12 EQSTE = 1.220E+11 EQSTG = 2.040E+00

EQSTM = 2.500E+01 EQSTS = 1.197E+12 1.089E+00 7.525E-12

COSQ = 4.000E+00 C1 = 1.500E-01 C2 = 0.

TENS(1)= -1.000E+11 TENS(2)= -1.000E+11 TENS(3)= -1.000E+11

YQ = 2.500E+09 MU = 2.870E+11 YADD = 0.

NZONES= 1, 148 CELLS IN 2.000E+00 CM -0.

AL TARGET RMO = 2.785E+00 NSRM = 0 NYAM 1 NPOR 0 NCON = 0

EQSTC = 7.550E+11 EQSTD = 1.290E+12 EQSTE = 1.220E+11 EQSTG = 2.040E+00

EQSTM = 2.500E+01 EQSTS = 1.197E+12 1.089E+00 7.525E-12

COSQ = 4.000E+00 C1 = 1.500E-01 C2 = 0.

TENS(1)= -1.000E+11 TENS(2)= -1.000E+11 TENS(3)= -1.000E+11

YQ = 2.500E+09 MU = 2.870E+11 YADD = 0.

NZONES= 1, 148 CELLS IN 2.000E+00 CM -0.

TEST 2: INPUT DATA

DATE = 04/22/69 IDENT = 2 MODEL 0: AL/AL IMPACT: NO RELAXATION OR BAUSCHINGER

J	DA	X(J)	U(J)	YML(J)	C(J)	D(J)	T(J)	ZML(J)	MATERIAL	CONO	J
CM	CM	CM/SEC	CM/CM2	CM/CM2	CM/CM2	CM/CM2	CM/CM2	CM/CM2			
1	1.351E-02	0.	2.000E-04	1.667E-09	6.394E-05	2.785E-00-1.000E-11	3.764E-02	3.764E-02	AL FLYER	S M 0	1
2	1.351E-02	1.731E-02	2.000E-04	1.667E-09	6.394E-05	2.785E-00-1.000E-11	3.764E-02	3.764E-02	AL FLYER	S M 0	2
3	1.351E-02	2.731E-02	2.000E-04	1.667E-09	6.394E-05	2.785E-00-1.000E-11	3.764E-02	3.764E-02	AL FLYER	S M 0	3
4	1.351E-02	4.054E-02	2.000E-04	1.667E-09	6.394E-05	2.785E-00-1.000E-11	3.764E-02	3.764E-02	AL FLYER	S M 0	4
5	1.351E-02	5.405E-02	2.000E-04	1.667E-09	6.394E-05	2.785E-00-1.000E-11	3.764E-02	3.764E-02	AL FLYER	S M 0	5
6	1.351E-02	6.757E-02	2.000E-04	1.667E-09	6.394E-05	2.785E-00-1.000E-11	3.764E-02	3.764E-02	AL FLYER	S M 0	6
7	1.351E-02	8.109E-02	2.000E-04	1.667E-09	6.394E-05	2.785E-00-1.000E-11	3.764E-02	3.764E-02	AL FLYER	S M 0	7
8	1.351E-02	9.459E-02	2.000E-04	1.667E-09	6.394E-05	2.785E-00-1.000E-11	3.764E-02	3.764E-02	AL FLYER	S M 0	8
9	1.351E-02	1.081E-01	2.000E-04	1.667E-09	6.394E-05	2.785E-00-1.000E-11	3.764E-02	3.764E-02	AL FLYER	S M 0	9
10	1.351E-02	1.216E-01	2.000E-04	1.667E-09	6.394E-05	2.785E-00-1.000E-11	3.764E-02	3.764E-02	AL FLYER	S M 0	10
11	1.351E-02	1.351E-01	2.000E-04	1.667E-09	6.394E-05	2.785E-00-1.000E-11	3.764E-02	3.764E-02	AL FLYER	S M 0	11
12	1.351E-02	1.486E-01	2.000E-04	1.667E-09	6.394E-05	2.785E-00-1.000E-11	3.764E-02	3.764E-02	AL FLYER	S M 0	12
13	1.351E-02	1.622E-01	2.000E-04	1.667E-09	6.394E-05	2.785E-00-1.000E-11	3.764E-02	3.764E-02	AL FLYER	S M 0	13
14	1.351E-02	1.757E-01	2.000E-04	1.667E-09	6.394E-05	2.785E-00-1.000E-11	3.764E-02	3.764E-02	AL FLYER	S M 0	14
15	1.351E-02	1.892E-01	2.000E-04	1.667E-09	6.394E-05	2.785E-00-1.000E-11	3.764E-02	3.764E-02	AL FLYER	S M 0	15
16	1.351E-02	2.027E-01	2.000E-04	1.667E-09	6.394E-05	2.785E-00-1.000E-11	3.764E-02	3.764E-02	AL FLYER	S M 0	16
17	1.351E-02	2.162E-01	2.000E-04	1.667E-09	6.394E-05	2.785E-00-1.000E-11	3.764E-02	3.764E-02	AL FLYER	S M 0	17
18	1.351E-02	2.297E-01	2.000E-04	1.667E-09	6.394E-05	2.785E-00-1.000E-11	3.764E-02	3.764E-02	AL FLYER	S M 0	18
19	1.351E-02	2.432E-01	2.000E-04	1.667E-09	6.394E-05	2.785E-00-1.000E-11	3.764E-02	3.764E-02	AL FLYER	S M 0	19
20	1.351E-02	2.567E-01	2.000E-04	1.667E-09	6.394E-05	2.785E-00-1.000E-11	3.764E-02	3.764E-02	AL FLYER	S M 0	20
21	1.351E-02	2.703E-01	2.000E-04	1.667E-09	6.394E-05	2.785E-00-1.000E-11	3.764E-02	3.764E-02	AL FLYER	S M 0	21
22	1.351E-02	2.838E-01	2.000E-04	1.667E-09	6.394E-05	2.785E-00-1.000E-11	3.764E-02	3.764E-02	AL FLYER	S M 0	22
23	1.351E-02	2.973E-01	2.000E-04	1.667E-09	6.394E-05	2.785E-00-1.000E-11	3.764E-02	3.764E-02	AL FLYER	S M 0	23
24	1.351E-02	3.108E-01	2.000E-04	1.667E-09	6.394E-05	2.785E-00-1.000E-11	3.764E-02	3.764E-02	AL FLYER	S M 0	24
25	1.351E-02	3.243E-01	2.000E-04	1.667E-09	6.394E-05	2.785E-00-1.000E-11	3.764E-02	3.764E-02	AL FLYER	S M 0	25
26	1.351E-02	3.378E-01	2.000E-04	1.667E-09	6.394E-05	2.785E-00-1.000E-11	3.764E-02	3.764E-02	AL FLYER	S M 0	26
27	1.351E-02	3.513E-01	2.000E-04	1.667E-09	6.394E-05	2.785E-00-1.000E-11	3.764E-02	3.764E-02	AL FLYER	S M 0	27
28	1.351E-02	3.648E-01	2.000E-04	1.667E-09	6.394E-05	2.785E-00-1.000E-11	3.764E-02	3.764E-02	AL FLYER	S M 0	28
29	1.351E-02	3.783E-01	2.000E-04	1.667E-09	6.394E-05	2.785E-00-1.000E-11	3.764E-02	3.764E-02	AL FLYER	S M 0	29
30	1.351E-02	3.918E-01	2.000E-04	1.667E-09	6.394E-05	2.785E-00-1.000E-11	3.764E-02	3.764E-02	AL FLYER	S M 0	30
31	1.351E-02	4.053E-01	2.000E-04	1.667E-09	6.394E-05	2.785E-00-1.000E-11	3.764E-02	3.764E-02	AL FLYER	S M 0	31
32	1.351E-02	4.188E-01	2.000E-04	1.667E-09	6.394E-05	2.785E-00-1.000E-11	3.764E-02	3.764E-02	AL FLYER	S M 0	32
33	1.351E-02	4.323E-01	2.000E-04	1.667E-09	6.394E-05	2.785E-00-1.000E-11	3.764E-02	3.764E-02	AL FLYER	S M 0	33
34	1.351E-02	4.458E-01	2.000E-04	1.667E-09	6.394E-05	2.785E-00-1.000E-11	3.764E-02	3.764E-02	AL FLYER	S M 0	34
35	1.351E-02	4.593E-01	2.000E-04	1.667E-09	6.394E-05	2.785E-00-1.000E-11	3.764E-02	3.764E-02	AL FLYER	S M 0	35
36	1.351E-02	4.728E-01	2.000E-04	1.667E-09	6.394E-05	2.785E-00-1.000E-11	3.764E-02	3.764E-02	AL FLYER	S M 0	36
37	1.351E-02	4.863E-01	2.000E-04	1.667E-09	6.394E-05	2.785E-00-1.000E-11	3.764E-02	3.764E-02	AL FLYER	S M 0	37
38	1.351E-02	4.998E-01	2.000E-04	1.667E-09	6.394E-05	2.785E-00-1.000E-11	3.764E-02	3.764E-02	AL FLYER	S M 0	38
39	1.351E-02	5.133E-01	2.000E-04	1.667E-09	6.394E-05	2.785E-00-1.000E-11	3.764E-02	3.764E-02	AL FLYER	S M 0	39
40	1.351E-02	5.268E-01	2.000E-04	1.667E-09	6.394E-05	2.785E-00-1.000E-11	3.764E-02	3.764E-02	AL FLYER	S M 0	40
41	1.351E-02	5.403E-01	2.000E-04	1.667E-09	6.394E-05	2.785E-00-1.000E-11	3.764E-02	3.764E-02	AL FLYER	S M 0	41
42	1.351E-02	5.538E-01	2.000E-04	1.667E-09	6.394E-05	2.785E-00-1.000E-11	3.764E-02	3.764E-02	AL FLYER	S M 0	42
43	1.351E-02	5.673E-01	2.000E-04	1.667E-09	6.394E-05	2.785E-00-1.000E-11	3.764E-02	3.764E-02	AL FLYER	S M 0	43
44	1.351E-02	5.808E-01	2.000E-04	1.667E-09	6.394E-05	2.785E-00-1.000E-11	3.764E-02	3.764E-02	AL FLYER	S M 0	44
45	1.351E-02	5.943E-01	2.000E-04	1.667E-09	6.394E-05	2.785E-00-1.000E-11	3.764E-02	3.764E-02	AL FLYER	S M 0	45
46	1.351E-02	6.078E-01	2.000E-04	1.667E-09	6.394E-05	2.785E-00-1.000E-11	3.764E-02	3.764E-02	AL FLYER	S M 0	46
47	1.351E-02	6.213E-01	2.000E-04	1.667E-09	6.394E-05	2.785E-00-1.000E-11	3.764E-02	3.764E-02	AL FLYER	S M 0	47
48	1.351E-02	6.348E-01	2.000E-04	1.667E-09	6.394E-05	2.785E-00-1.000E-11	3.764E-02	3.764E-02	AL FLYER	S M 0	48
49	1.351E-02	6.483E-01	2.000E-04	1.667E-09	6.394E-05	2.785E-00-1.000E-11	3.764E-02	3.764E-02	AL FLYER	S M 0	49
50	1.351E-02	6.618E-01	2.000E-04	1.667E-09	6.394E-05	2.785E-00-1.000E-11	3.764E-02	3.764E-02	AL FLYER	S M 0	50

TEST 2: PORTION OF COORDINATE LAYOUT

MOMENTUM EDIT

CYCLE	TIME	DTM	JTS	ETOTAL	JFIN	JSTAR	JSMAX	SMAX	X(JSMAX)							
228	2.0026E-06	1.4054E-08	254	2.6528E-01	297	298	61	1.5794E+18	8.5994E-01							
OTPP	DTMPLS	EMVPS	EMVPS	EMVPL	EMVPR	EMVPP	EMVPM	POTPOS	POTNEG							
7.1523E-06	2.3331E-06	0.	1.1100E-05	3.4447E-04	7.6113E-04	1.1204E-05	0.	0.	0.							
X(1)	X(JMAX)	X(JMAX)	X(JMAX)	X(JFIN)	JMAX	RMAX	X(JMAX)									
5.6051E-02	2.0200E-06	4.0000E-06	9.	4.0000E-06	61	1.5794E+18	8.5994E-01									
TIME EDIT NO. 6 AT M = . TIME = 2.80250E-06 SECS. JSTAR = 298. CALC TIME IS 107.836 SECS																
CELL	J	A	U	M	P	S	CHI	D	C	J	COND	CM/SEC	CM/CM3	Y, MM, MU	SD OR NT	
1	056051	19994	7.534E-06	4.508E-06	6.914E-06	0.	1.170E+00	2.7850	6.3942E+05	1	S	R	AL	FLYER	1.667E+09	
2	060945	19994	7.534E-06	4.508E-06	6.914E-06	0.	1.419E+01	2.7850	6.3942E+05	2	S	M	A	AL	FLYER	1.667E+09
3	063878	19994	1.443E-07	1.125E-07	1.060E-07	6.58E-01	6.58E-01	2.7850	6.3942E+05	3	S	M	A	AL	FLYER	1.667E+09
4	064591	19994	3.686E-07	2.250E-07	3.403E-07	2.520E+02	2.520E+02	2.7850	6.3942E+05	4	S	M	A	AL	FLYER	1.667E+09
5	1.1100	19994	6.853E-07	4.217E-07	4.353E-07	8.537E+02	8.537E+02	2.7850	6.3942E+05	5	S	M	A	AL	FLYER	1.667E+09
6	1.2347	19994	1.214E-06	7.699E-07	1.130E-06	2.642E+03	2.642E+03	2.7850	6.3942E+05	6	S	M	A	AL	FLYER	1.667E+09
7	1.37129	19994	2.056E-06	1.276E-06	1.923E-06	7.699E+03	7.699E+03	2.7850	6.3942E+05	7	S	M	A	AL	FLYER	1.667E+09
8	1.50639	19994	3.336E-06	2.001E-06	3.135E-06	1.953E+04	1.953E+04	2.7850	6.3942E+05	8	S	M	A	AL	FLYER	1.667E+09
9	1.64146	19994	5.145E-06	3.250E-06	4.896E-06	4.866E+04	4.866E+04	2.7850	6.3942E+05	9	S	M	A	AL	FLYER	1.667E+09
10	1.77656	19994	7.715E-06	4.861E-06	7.321E-06	1.021E+05	1.021E+05	2.7850	6.3942E+05	10	S	M	A	AL	FLYER	1.667E+09
11	1.91157	19994	1.099E-05	6.943E-06	1.048E-05	2.050E+05	2.050E+05	2.7850	6.3942E+05	11	S	M	A	AL	FLYER	1.667E+09
12	2.04656	19994	1.499E-05	9.552E-06	1.438E-05	3.775E+05	3.775E+05	2.7850	6.3942E+05	12	S	M	A	AL	FLYER	1.667E+09
13	2.18159	19994	1.960E-05	1.256E-05	1.889E-05	6.944E+05	6.944E+05	2.7850	6.3942E+05	13	S	M	A	AL	FLYER	1.667E+09
14	2.31638	19994	2.450E-05	1.594E-05	2.382E-05	9.944E+05	9.944E+05	2.7850	6.3942E+05	14	S	M	A	AL	FLYER	1.667E+09
15	2.45129	19994	2.962E-05	1.920E-05	2.846E-05	1.433E+06	1.433E+06	2.7850	6.3942E+05	15	S	M	A	AL	FLYER	1.667E+09
16	2.58597	19994	3.442E-05	2.243E-05	3.370E-05	1.920E+06	1.920E+06	2.7850	6.3942E+05	16	S	M	A	AL	FLYER	1.667E+09
17	2.72068	19994	3.868E-05	2.533E-05	3.805E-05	2.410E+06	2.410E+06	2.7850	6.3942E+05	17	S	M	A	AL	FLYER	1.667E+09
18	2.85535	19994	4.223E-05	2.777E-05	4.171E-05	2.859E+06	2.859E+06	2.7850	6.3942E+05	18	S	M	A	AL	FLYER	1.667E+09
19	2.98997	19994	4.608E-05	3.049E-05	4.450E-05	3.233E+06	3.233E+06	2.7850	6.3942E+05	19	S	M	A	AL	FLYER	1.667E+09
20	3.12457	19994	4.997E-05	3.310E-05	4.648E-05	3.510E+06	3.510E+06	2.7850	6.3942E+05	20	S	M	A	AL	FLYER	1.667E+09
21	3.25915	19994	5.381E-05	3.560E-05	4.812E-05	3.710E+06	3.710E+06	2.7850	6.3942E+05	21	S	M	A	AL	FLYER	1.667E+09
22	3.39371	19994	5.761E-05	3.801E-05	4.954E-05	3.916E+06	3.916E+06	2.7850	6.3942E+05	22	S	M	A	AL	FLYER	1.667E+09
23	3.52827	19994	6.141E-05	4.041E-05	5.096E-05	4.122E+06	4.122E+06	2.7850	6.3942E+05	23	S	M	A	AL	FLYER	1.667E+09
24	3.66282	19994	6.521E-05	4.281E-05	5.238E-05	4.328E+06	4.328E+06	2.7850	6.3942E+05	24	S	M	A	AL	FLYER	1.667E+09
25	3.79737	19994	6.901E-05	4.521E-05	5.380E-05	4.534E+06	4.534E+06	2.7850	6.3942E+05	25	S	M	A	AL	FLYER	1.667E+09
26	3.93192	19994	7.281E-05	4.761E-05	5.522E-05	4.740E+06	4.740E+06	2.7850	6.3942E+05	26	S	M	A	AL	FLYER	1.667E+09
27	4.06646	19994	7.661E-05	5.001E-05	5.664E-05	4.946E+06	4.946E+06	2.7850	6.3942E+05	27	S	M	A	AL	FLYER	1.667E+09
28	4.20101	19994	8.041E-05	5.241E-05	5.806E-05	5.152E+06	5.152E+06	2.7850	6.3942E+05	28	S	M	A	AL	FLYER	1.667E+09
29	4.33554	19994	8.421E-05	5.481E-05	5.948E-05	5.358E+06	5.358E+06	2.7850	6.3942E+05	29	S	M	A	AL	FLYER	1.667E+09
30	4.47007	19994	8.801E-05	5.721E-05	6.090E-05	5.564E+06	5.564E+06	2.7850	6.3942E+05	30	S	M	A	AL	FLYER	1.667E+09
31	4.60458	19994	9.181E-05	5.961E-05	6.232E-05	5.770E+06	5.770E+06	2.7850	6.3942E+05	31	S	M	A	AL	FLYER	1.667E+09
32	4.73907	19994	9.561E-05	6.201E-05	6.374E-05	5.976E+06	5.976E+06	2.7850	6.3942E+05	32	S	M	A	AL	FLYER	1.667E+09
33	4.87357	19994	9.941E-05	6.441E-05	6.516E-05	6.182E+06	6.182E+06	2.7850	6.3942E+05	33	S	M	A	AL	FLYER	1.667E+09
34	5.00807	19994	1.032E-04	6.681E-05	6.658E-05	6.388E+06	6.388E+06	2.7850	6.3942E+05	34	S	M	A	AL	FLYER	1.667E+09
35	5.14257	19994	1.070E-04	6.921E-05	6.800E-05	6.594E+06	6.594E+06	2.7850	6.3942E+05	35	S	M	A	AL	FLYER	1.667E+09
36	5.27707	19994	1.108E-04	7.161E-05	6.942E-05	6.800E+06	6.800E+06	2.7850	6.3942E+05	36	S	M	A	AL	FLYER	1.667E+09
37	5.41157	19994	1.146E-04	7.401E-05	7.084E-05	7.006E+06	7.006E+06	2.7850	6.3942E+05	37	S	M	A	AL	FLYER	1.667E+09
38	5.54607	19994	1.184E-04	7.641E-05	7.226E-05	7.212E+06	7.212E+06	2.7850	6.3942E+05	38	S	M	A	AL	FLYER	1.667E+09
39	5.68057	19994	1.222E-04	7.881E-05	7.368E-05	7.418E+06	7.418E+06	2.7850	6.3942E+05	39	S	M	A	AL	FLYER	1.667E+09
40	5.81507	19994	1.260E-04	8.121E-05	7.510E-05	7.624E+06	7.624E+06	2.7850	6.3942E+05	40	S	M	A	AL	FLYER	1.667E+09
41	5.94957	19994	1.298E-04	8.361E-05	7.652E-05	7.830E+06	7.830E+06	2.7850	6.3942E+05	41	S	M	A	AL	FLYER	1.667E+09
42	6.08407	19994	1.336E-04	8.601E-05	7.794E-05	8.036E+06	8.036E+06	2.7850	6.3942E+05	42	S	M	A	AL	FLYER	1.667E+09
43	6.21857	19994	1.374E-04	8.841E-05	7.936E-05	8.242E+06	8.242E+06	2.7850	6.3942E+05	43	S	M	A	AL	FLYER	1.667E+09

TEST 2: FINAL MOMENTUM EDIT AND PORTION OF TIME EDIT



SCRIPE OUTPUT, TIME IN MICROSECS, S IN HOURS, DTW IN MILLISECONDS, DELTIM IN SECS													
N	TIME	512/50J1	523/50J2	534/50J3	S ( 36)	S ( 75)	S (112)	S (187)	S (224)	S (261)	J75	DTW	DELTIM
1	.320	.001	0.000	0.000	0.0000	0.0000	0.0000	0.0000	0.0000	0.0000	150	.001	2.106
2	.320	.001	0.000	0.000	0.0000	0.0000	0.0000	0.0000	0.0000	0.0000	150	.001	.048
3	.320	.001	0.000	0.000	0.0000	0.0000	0.0000	0.0000	0.0000	0.0000	148	.012	.050
4	.320	.001	0.000	0.000	0.0000	0.0000	0.0000	0.0000	0.0000	0.0000	150	.034	.054
5	.320	.001	0.000	0.000	0.0000	0.0000	0.0000	0.0000	0.0000	0.0000	150	.001	.000
6	.320	.001	0.000	0.000	0.0000	0.0000	0.0000	0.0000	0.0000	0.0000	150	1.057	.000
7	.320	.001	0.000	0.000	0.0000	0.0000	0.0000	0.0000	0.0000	0.0000	150	1.269	.002
8	.320	.001	0.000	0.000	0.0000	0.0000	0.0000	0.0000	0.0000	0.0000	150	1.322	.004
9	.320	.001	0.000	0.000	0.0000	0.0000	0.0000	0.0000	0.0000	0.0000	150	1.027	.070
10	.320	.001	0.000	0.000	0.0000	0.0000	0.0000	0.0000	0.0000	0.0000	150	2.192	.072
11	.320	.001	0.000	0.000	0.0000	0.0000	0.0000	0.0000	0.0000	0.0000	150	2.430	.072
12	.320	.001	0.000	0.000	0.0000	0.0000	0.0000	0.0000	0.0000	0.0000	150	3.157	.074
13	.320	.001	0.000	0.000	0.0000	0.0000	0.0000	0.0000	0.0000	0.0000	150	3.700	.074
14	.320	.001	0.000	0.000	0.0000	0.0000	0.0000	0.0000	0.0000	0.0000	150	4.545	.078
15	.320	.001	0.000	0.000	0.0000	0.0000	0.0000	0.0000	0.0000	0.0000	150	5.455	.080
16	.320	.001	0.000	0.000	0.0000	0.0000	0.0000	0.0000	0.0000	0.0000	150	6.546	.082
17	.320	.001	0.000	0.000	0.0000	0.0000	0.0000	0.0000	0.0000	0.0000	151	7.895	.086
18	.320	.001	0.000	0.000	0.0000	0.0000	0.0000	0.0000	0.0000	0.0000	151	9.426	.088
19	.320	.001	0.000	0.000	0.0000	0.0000	0.0000	0.0000	0.0000	0.0000	151	11.311	.092
20	.320	.001	0.000	0.000	0.0000	0.0000	0.0000	0.0000	0.0000	0.0000	152	13.573	.096
21	.320	.001	0.000	0.000	0.0000	0.0000	0.0000	0.0000	0.0000	0.0000	152	13.844	.096
22	.320	.001	0.000	0.000	0.0000	0.0000	0.0000	0.0000	0.0000	0.0000	153	13.751	.104
23	.320	.001	0.000	0.000	0.0000	0.0000	0.0000	0.0000	0.0000	0.0000	153	13.032	.110
24	.320	.001	0.000	0.000	0.0000	0.0000	0.0000	0.0000	0.0000	0.0000	154	13.061	.112
25	.320	.001	0.000	0.000	0.0000	0.0000	0.0000	0.0000	0.0000	0.0000	154	13.847	.116
26	.320	.001	0.000	0.000	0.0000	0.0000	0.0000	0.0000	0.0000	0.0000	155	13.043	.130
27	.320	.001	0.000	0.000	0.0000	0.0000	0.0000	0.0000	0.0000	0.0000	155	13.066	.124
28	.320	.001	0.000	0.000	0.0000	0.0000	0.0000	0.0000	0.0000	0.0000	156	13.073	.120
29	.320	.001	0.000	0.000	0.0000	0.0000	0.0000	0.0000	0.0000	0.0000	156	13.809	.134
30	.320	.001	0.000	0.000	0.0000	0.0000	0.0000	0.0000	0.0000	0.0000	157	13.902	.136
31	.320	.001	0.000	0.000	0.0000	0.0000	0.0000	0.0000	0.0000	0.0000	157	13.906	.142
32	.320	.001	0.000	0.000	0.0000	0.0000	0.0000	0.0000	0.0000	0.0000	158	13.920	.142
33	.320	.001	0.000	0.000	0.0000	0.0000	0.0000	0.0000	0.0000	0.0000	158	13.923	.150
34	.320	.001	0.000	0.000	0.0000	0.0000	0.0000	0.0000	0.0000	0.0000	159	13.935	.152
35	.320	.001	0.000	0.000	0.0000	0.0000	0.0000	0.0000	0.0000	0.0000	159	13.937	.156
36	.320	.001	0.000	0.000	0.0000	0.0000	0.0000	0.0000	0.0000	0.0000	160	13.949	.162
37	.320	.001	0.000	0.000	0.0000	0.0000	0.0000	0.0000	0.0000	0.0000	160	13.947	.166
38	.320	.001	0.000	0.000	0.0000	0.0000	0.0000	0.0000	0.0000	0.0000	161	13.959	.170
39	.320	.001	0.000	0.000	0.0000	0.0000	0.0000	0.0000	0.0000	0.0000	161	13.956	.172
40	.320	.001	0.000	0.000	0.0000	0.0000	0.0000	0.0000	0.0000	0.0000	162	13.948	.184
41	.320	.001	0.000	0.000	0.0000	0.0000	0.0000	0.0000	0.0000	0.0000	162	13.945	.180
42	.320	.001	0.000	0.000	0.0000	0.0000	0.0000	0.0000	0.0000	0.0000	162	13.976	.184
43	.320	.001	0.000	0.000	0.0000	0.0000	0.0000	0.0000	0.0000	0.0000	163	13.971	.190
44	.320	.001	0.000	0.000	0.0000	0.0000	0.0000	0.0000	0.0000	0.0000	164	13.984	.194
45	.320	.001	0.000	0.000	0.0000	0.0000	0.0000	0.0000	0.0000	0.0000	165	13.978	.198
46	.320	.001	0.000	0.000	0.0000	0.0000	0.0000	0.0000	0.0000	0.0000	165	13.988	.204
47	.320	.001	0.000	0.000	0.0000	0.0000	0.0000	0.0000	0.0000	0.0000	166	13.984	.204
48	.320	.001	0.000	0.000	0.0000	0.0000	0.0000	0.0000	0.0000	0.0000	167	13.991	.210
49	.320	.001	0.000	0.000	0.0000	0.0000	0.0000	0.0000	0.0000	0.0000	167	13.989	.214
50	.320	.001	0.000	0.000	0.0000	0.0000	0.0000	0.0000	0.0000	0.0000	167	13.995	.218

TEST 2: FIRST PAGE OF STRESS HISTORIES



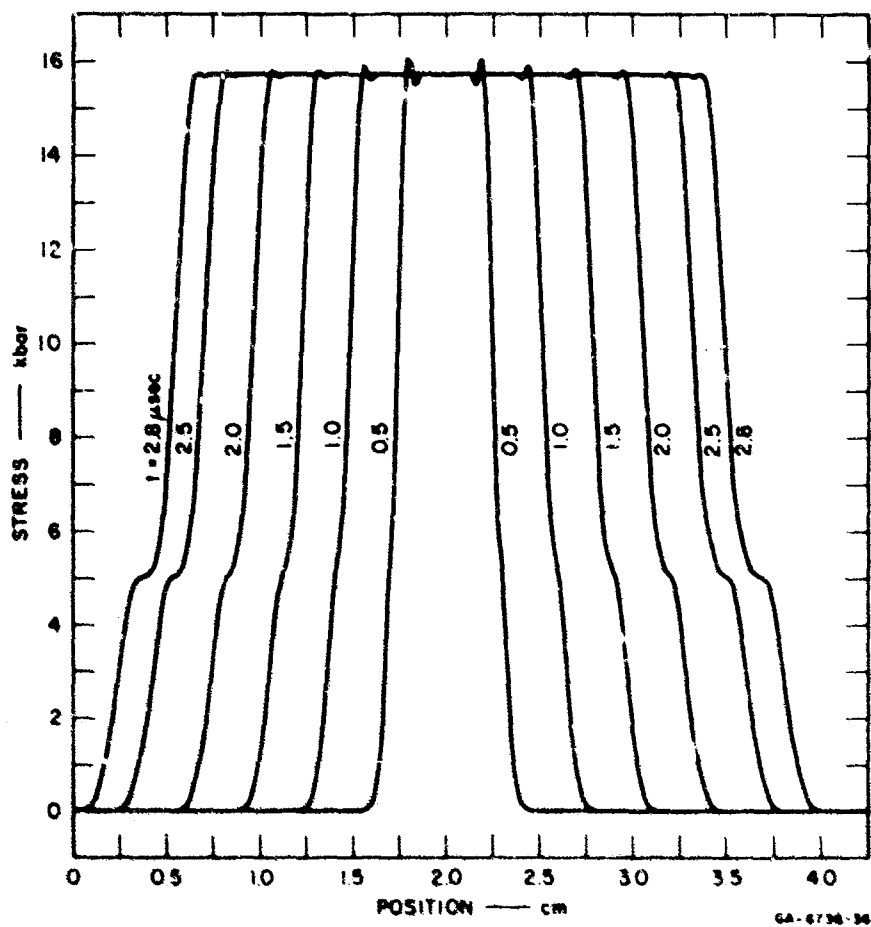


FIGURE 48 TEST 2: SUMMARY PLOT OF TIME EDITS



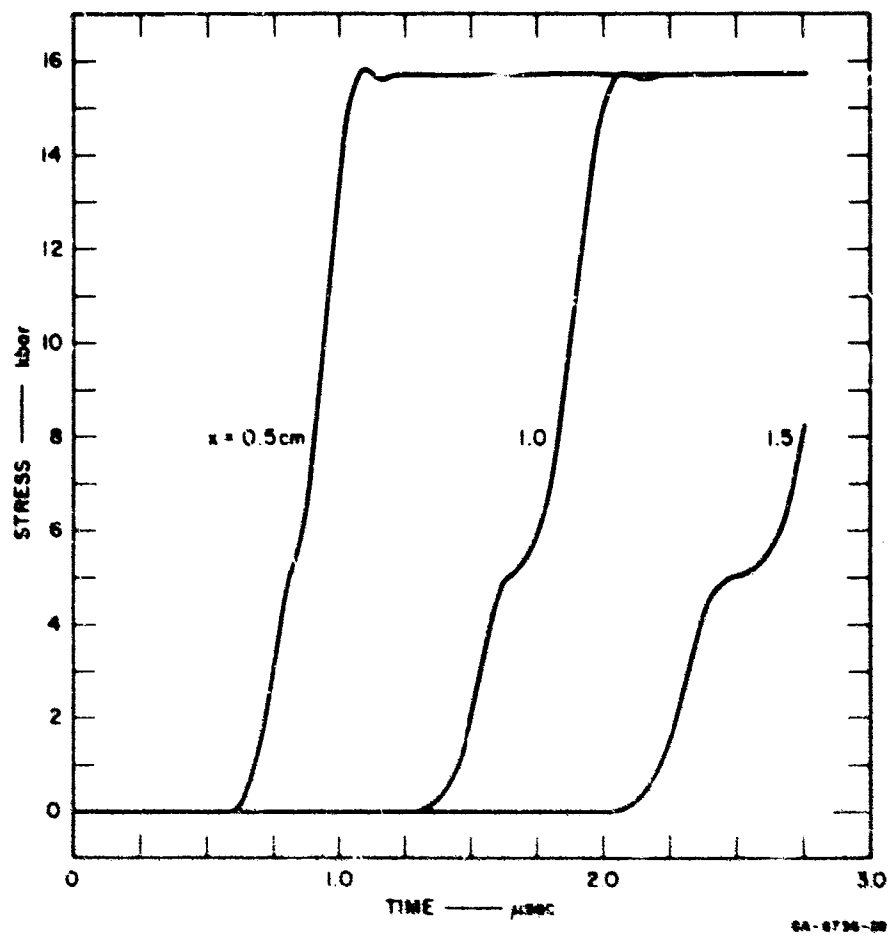


FIGURE 49 TEST 2: SUMMARY OF STRESS HISTORIES  
AT THREE JEDIT LOCATIONS

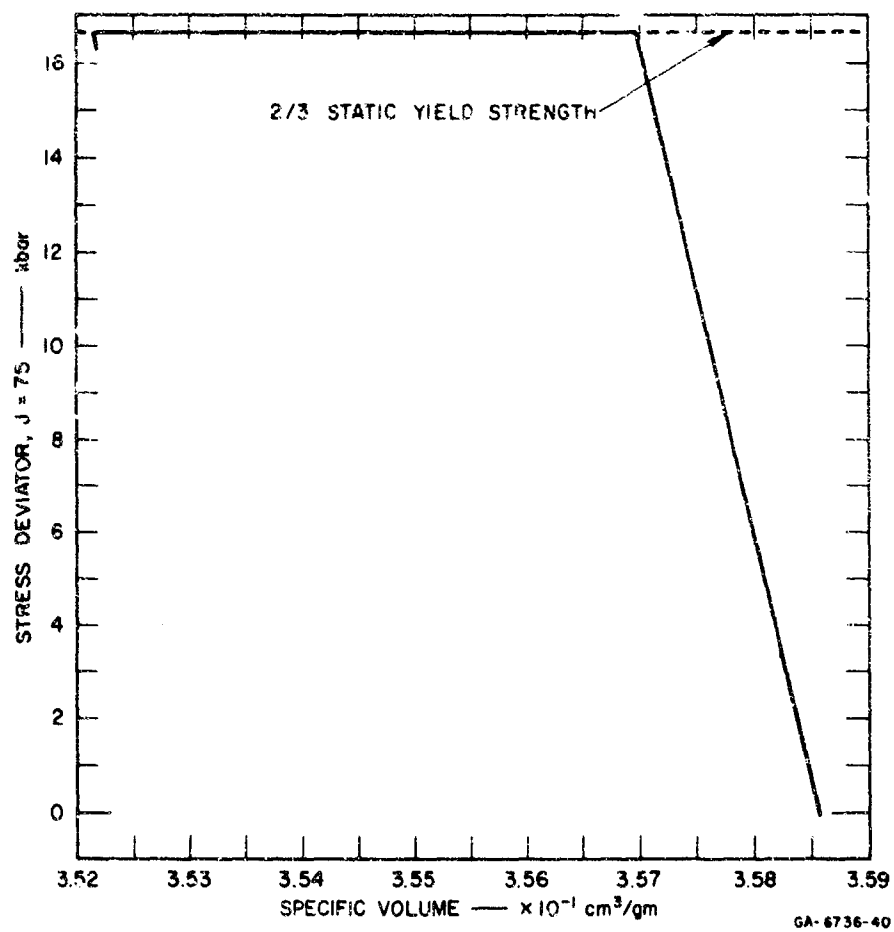


FIGURE 50 TEST 2: SAMPLE PLOT OF STRESS DEVIATOR

e. Test No. 3

The stress relaxation mechanism of Model 1 (simple anelastic model) is tested in Test 3. The configuration is a symmetric impact between two plates of 2024-T3 aluminum. The plates have different relaxation parameters but are otherwise identical. The listing included on the following pages contains the input data, and portions of the initial layout, and final EDIT and stress histories. The EDITS, stress histories, and a deviatoric stress-volume path are shown in the figures.

\*\*\* SMI PUFF 1 (6400 VERSION) \*\*\*

DATE =06/25/69

IDENT = 3 MODEL 1: AL/AL IMPACT, STANDARD ANELASTIC RELAXATION  
BOTH FLYER AND TARGET ARE OF 2024-T3 AND THE STANDARD ANELASTIC SOLID  
STRESS RELAXATION MODEL IS USED FOR BOTH. HOWEVER, THE ONE PARAMETER, TRLX,  
IS DIFFERENT IN THE FLYER AND TARGET.

1 NTEST= 5 NJEDIT= 6 NREZON= 0 NSEPRAT= 0  
2 TEDIT= 5.000E-07 1.000E-06 1.500E-06 2.000E-06 2.500E-06  
3 JEDIT= 38 75 112 187 224 261  
6 NEDTN= 10000 NEDIT= 10000 NPERN = 1 -0  
7 STOPS JCYCS = 1250 CKS = 4.000E+00 TS = 2.800E-06  
8 NMTLS= 2 MATFL = 1 UZERO = 2.000E+04 IPLOT = 1

AL FLYER RHOS = 2.785E+00 NSRM = 1 NYAM = 1 NPOR = 0 NCON = 0  
EQSTC = 7.550E+11 EQSTD = 1.290E+12 EQSTL = 1.220E+11 EQSTG = 2.040E+00  
EQSTM = 2.500E-01 EQSTS = 1.197E+12 1.089E+00 7.525E-12  
COSO = 4.000E+00 C1 = 1.500E-01 C2 = 0.  
TENS(1) = -1.000E+11 TENS(2) = -1.000E+11 TENS(3) = -1.000E+11  
TRLX = 1.500E-07 -0. -0. -0.  
VO = 2.500E+09 MU = 2.870E+11 YADD = 0.  
NZONES= 1, 148 CELLS IN 2.000E+00 CM -0. -0.

AL TARGET RHOS = 2.785E+00 NSRM = 1 NYAM = 1 NPOR = 0 NCON = 0  
EQSTC = 7.550E+11 EQSTD = 1.290E+12 EQSTE = 1.220E+11 EQSTG = 2.040E+00  
EQSTM = 2.500E-01 EQSTS = 1.197E+12 1.089E+00 7.525E-12  
COSO = 4.000E+00 C1 = 1.500E-01 C2 = 0.  
TENS(1) = -1.000E+11 TENS(2) = -1.000E+11 TENS(3) = -1.000E+11  
TRLX = 3.000E-07 -0. -0. -0.  
VO = 2.500E+09 MU = 2.870E+11 YADD = 0.  
NZONES= 1, 148 CELLS IN 2.000E+00 CM -0. -0.

TEST 3: INPUT DATA

DATE = 04/25/69 IDENT = 3 MODEL 1.0 AL/AL IMPACT. STANDARD ANELASTIC RELATION

J	DA	X(J)	U(J)	YHL(J)	C(J)	D(J)	T(J)	ZHL(J)	MATERIAL	COND	J
1	1.351E-02	0.	2.000E+04	1.667E+09	6.394E+05	2.785E+00	1.000E+11	3.764E-02	AL FLYER	3.5 M	1
2	1.351E-02	1.351E-02	2.000E+04	1.667E+09	6.394E+05	2.785E+00	1.000E+11	3.764E-02	AL FLYER	3.5 M	2
3	1.351E-02	2.703E-02	2.000E+04	1.667E+09	6.394E+05	2.785E+00	1.000E+11	3.764E-02	AL FLYER	3.5 M	3
4	1.351E-02	4.054E-02	2.000E+04	1.667E+09	6.394E+05	2.785E+00	1.000E+11	3.764E-02	AL FLYER	3.5 M	4
5	1.351E-02	5.405E-02	2.000E+04	1.667E+09	6.394E+05	2.785E+00	1.000E+11	3.764E-02	AL FLYER	3.5 M	5
6	1.351E-02	6.757E-02	2.000E+04	1.667E+09	6.394E+05	2.785E+00	1.000E+11	3.764E-02	AL FLYER	3.5 M	6
7	1.351E-02	8.108E-02	2.000E+04	1.667E+09	6.394E+05	2.785E+00	1.000E+11	3.764E-02	AL FLYER	3.5 M	7
8	1.351E-02	9.459E-02	2.000E+04	1.667E+09	6.394E+05	2.785E+00	1.000E+11	3.764E-02	AL FLYER	3.5 M	8
9	1.351E-02	1.081E-01	2.000E+04	1.667E+09	6.394E+05	2.785E+00	1.000E+11	3.764E-02	AL FLYER	3.5 M	9
10	1.351E-02	1.216E-01	2.000E+04	1.667E+09	6.394E+05	2.785E+00	1.000E+11	3.764E-02	AL FLYER	3.5 M	10
11	1.351E-02	1.351E-01	2.000E+04	1.667E+09	6.394E+05	2.785E+00	1.000E+11	3.764E-02	AL FLYER	3.5 M	11
12	1.351E-02	1.486E-01	2.000E+04	1.667E+09	6.394E+05	2.785E+00	1.000E+11	3.764E-02	AL FLYER	3.5 M	12
13	1.351E-02	1.622E-01	2.000E+04	1.667E+09	6.394E+05	2.785E+00	1.000E+11	3.764E-02	AL FLYER	3.5 M	13
14	1.351E-02	1.757E-01	2.000E+04	1.667E+09	6.394E+05	2.785E+00	1.000E+11	3.764E-02	AL FLYER	3.5 M	14
15	1.351E-02	1.892E-01	2.000E+04	1.667E+09	6.394E+05	2.785E+00	1.000E+11	3.764E-02	AL FLYER	3.5 M	15
16	1.351E-02	2.027E-01	2.000E+04	1.667E+09	6.394E+05	2.785E+00	1.000E+11	3.764E-02	AL FLYER	3.5 M	16
17	1.351E-02	2.162E-01	2.000E+04	1.667E+09	6.394E+05	2.785E+00	1.000E+11	3.764E-02	AL FLYER	3.5 M	17
18	1.351E-02	2.297E-01	2.000E+04	1.667E+09	6.394E+05	2.785E+00	1.000E+11	3.764E-02	AL FLYER	3.5 M	18
19	1.351E-02	2.432E-01	2.000E+04	1.667E+09	6.394E+05	2.785E+00	1.000E+11	3.764E-02	AL FLYER	3.5 M	19
20	1.351E-02	2.568E-01	2.000E+04	1.667E+09	6.394E+05	2.785E+00	1.000E+11	3.764E-02	AL FLYER	3.5 M	20
21	1.351E-02	2.703E-01	2.000E+04	1.667E+09	6.394E+05	2.785E+00	1.000E+11	3.764E-02	AL FLYER	3.5 M	21
22	1.351E-02	2.838E-01	2.000E+04	1.667E+09	6.394E+05	2.785E+00	1.000E+11	3.764E-02	AL FLYER	3.5 M	22
23	1.351E-02	2.973E-01	2.000E+04	1.667E+09	6.394E+05	2.785E+00	1.000E+11	3.764E-02	AL FLYER	3.5 M	23
24	1.351E-02	3.108E-01	2.000E+04	1.667E+09	6.394E+05	2.785E+00	1.000E+11	3.764E-02	AL FLYER	3.5 M	24
25	1.351E-02	3.243E-01	2.000E+04	1.667E+09	6.394E+05	2.785E+00	1.000E+11	3.764E-02	AL FLYER	3.5 M	25
26	1.351E-02	3.378E-01	2.000E+04	1.667E+09	6.394E+05	2.785E+00	1.000E+11	3.764E-02	AL FLYER	3.5 M	26
27	1.351E-02	3.514E-01	2.000E+04	1.667E+09	6.394E+05	2.785E+00	1.000E+11	3.764E-02	AL FLYER	3.5 M	27
28	1.351E-02	3.649E-01	2.000E+04	1.667E+09	6.394E+05	2.785E+00	1.000E+11	3.764E-02	AL FLYER	3.5 M	28
29	1.351E-02	3.784E-01	2.000E+04	1.667E+09	6.394E+05	2.785E+00	1.000E+11	3.764E-02	AL FLYER	3.5 M	29
30	1.351E-02	3.919E-01	2.000E+04	1.667E+09	6.394E+05	2.785E+00	1.000E+11	3.764E-02	AL FLYER	3.5 M	30
31	1.351E-02	4.054E-01	2.000E+04	1.667E+09	6.394E+05	2.785E+00	1.000E+11	3.764E-02	AL FLYER	3.5 M	31
32	1.351E-02	4.189E-01	2.000E+04	1.667E+09	6.394E+05	2.785E+00	1.000E+11	3.764E-02	AL FLYER	3.5 M	32
33	1.351E-02	4.324E-01	2.000E+04	1.667E+09	6.394E+05	2.785E+00	1.000E+11	3.764E-02	AL FLYER	3.5 M	33
34	1.351E-02	4.459E-01	2.000E+04	1.667E+09	6.394E+05	2.785E+00	1.000E+11	3.764E-02	AL FLYER	3.5 M	34
35	1.351E-02	4.594E-01	2.000E+04	1.667E+09	6.394E+05	2.785E+00	1.000E+11	3.764E-02	AL FLYER	3.5 M	35
36	1.351E-02	4.730E-01	2.000E+04	1.667E+09	6.394E+05	2.785E+00	1.000E+11	3.764E-02	AL FLYER	3.5 M	36
37	1.351E-02	4.865E-01	2.000E+04	1.667E+09	6.394E+05	2.785E+00	1.000E+11	3.764E-02	AL FLYER	3.5 M	37
38	1.351E-02	5.000E-01	2.000E+04	1.667E+09	6.394E+05	2.785E+00	1.000E+11	3.764E-02	AL FLYER	3.5 M	38
39	1.351E-02	5.135E-01	2.000E+04	1.667E+09	6.394E+05	2.785E+00	1.000E+11	3.764E-02	AL FLYER	3.5 M	39
40	1.351E-02	5.270E-01	2.000E+04	1.667E+09	6.394E+05	2.785E+00	1.000E+11	3.764E-02	AL FLYER	3.5 M	40
41	1.351E-02	5.405E-01	2.000E+04	1.667E+09	6.394E+05	2.785E+00	1.000E+11	3.764E-02	AL FLYER	3.5 M	41
42	1.351E-02	5.541E-01	2.000E+04	1.667E+09	6.394E+05	2.785E+00	1.000E+11	3.764E-02	AL FLYER	3.5 M	42
43	1.351E-02	5.676E-01	2.000E+04	1.667E+09	6.394E+05	2.785E+00	1.000E+11	3.764E-02	AL FLYER	3.5 M	43
44	1.351E-02	5.811E-01	2.000E+04	1.667E+09	6.394E+05	2.785E+00	1.000E+11	3.764E-02	AL FLYER	3.5 M	44
45	1.351E-02	5.946E-01	2.000E+04	1.667E+09	6.394E+05	2.785E+00	1.000E+11	3.764E-02	AL FLYER	3.5 M	45
46	1.351E-02	6.081E-01	2.000E+04	1.667E+09	6.394E+05	2.785E+00	1.000E+11	3.764E-02	AL FLYER	3.5 M	46
47	1.351E-02	6.216E-01	2.000E+04	1.667E+09	6.394E+05	2.785E+00	1.000E+11	3.764E-02	AL FLYER	3.5 M	47
48	1.351E-02	6.351E-01	2.000E+04	1.667E+09	6.394E+05	2.785E+00	1.000E+11	3.764E-02	AL FLYER	3.5 M	48
49	1.351E-02	6.486E-01	2.000E+04	1.667E+09	6.394E+05	2.785E+00	1.000E+11	3.764E-02	AL FLYER	3.5 M	49
50	1.351E-02	6.622E-01	2.000E+04	1.667E+09	6.394E+05	2.785E+00	1.000E+11	3.764E-02	AL FLYER	3.5 M	50

TEST 3: PORTION OF COORDINATE LAYOUT

MOMENTUM EDIT

CELL	J	A	CM	CH/SEC	DTN/CM2	U/FIN	JTS	ETOTAL	JFIN	JSTAR	JSMAX	SMAX	X(JSMAX)
1	0.00145	19989	0.	0.	0.	0.	0.	0.	0.	0.	0.	0.	0.
2	0.00145	19989	0.	0.	0.	0.	0.	0.	0.	0.	0.	0.	0.
3	0.00145	19989	0.	0.	0.	0.	0.	0.	0.	0.	0.	0.	0.
4	0.00145	19989	0.	0.	0.	0.	0.	0.	0.	0.	0.	0.	0.
5	0.00145	19989	0.	0.	0.	0.	0.	0.	0.	0.	0.	0.	0.
6	0.00145	19989	0.	0.	0.	0.	0.	0.	0.	0.	0.	0.	0.
7	0.00145	19989	0.	0.	0.	0.	0.	0.	0.	0.	0.	0.	0.
8	0.00145	19989	0.	0.	0.	0.	0.	0.	0.	0.	0.	0.	0.
9	0.00145	19989	0.	0.	0.	0.	0.	0.	0.	0.	0.	0.	0.
10	0.00145	19989	0.	0.	0.	0.	0.	0.	0.	0.	0.	0.	0.
11	0.00145	19989	0.	0.	0.	0.	0.	0.	0.	0.	0.	0.	0.
12	0.00145	19989	0.	0.	0.	0.	0.	0.	0.	0.	0.	0.	0.
13	0.00145	19989	0.	0.	0.	0.	0.	0.	0.	0.	0.	0.	0.
14	0.00145	19989	0.	0.	0.	0.	0.	0.	0.	0.	0.	0.	0.
15	0.00145	19989	0.	0.	0.	0.	0.	0.	0.	0.	0.	0.	0.
16	0.00145	19989	0.	0.	0.	0.	0.	0.	0.	0.	0.	0.	0.
17	0.00145	19989	0.	0.	0.	0.	0.	0.	0.	0.	0.	0.	0.
18	0.00145	19989	0.	0.	0.	0.	0.	0.	0.	0.	0.	0.	0.
19	0.00145	19989	0.	0.	0.	0.	0.	0.	0.	0.	0.	0.	0.
20	0.00145	19989	0.	0.	0.	0.	0.	0.	0.	0.	0.	0.	0.
21	0.00145	19989	0.	0.	0.	0.	0.	0.	0.	0.	0.	0.	0.
22	0.00145	19989	0.	0.	0.	0.	0.	0.	0.	0.	0.	0.	0.
23	0.00145	19989	0.	0.	0.	0.	0.	0.	0.	0.	0.	0.	0.
24	0.00145	19989	0.	0.	0.	0.	0.	0.	0.	0.	0.	0.	0.
25	0.00145	19989	0.	0.	0.	0.	0.	0.	0.	0.	0.	0.	0.
26	0.00145	19989	0.	0.	0.	0.	0.	0.	0.	0.	0.	0.	0.
27	0.00145	19989	0.	0.	0.	0.	0.	0.	0.	0.	0.	0.	0.
28	0.00145	19989	0.	0.	0.	0.	0.	0.	0.	0.	0.	0.	0.
29	0.00145	19989	0.	0.	0.	0.	0.	0.	0.	0.	0.	0.	0.
30	0.00145	19989	0.	0.	0.	0.	0.	0.	0.	0.	0.	0.	0.
31	0.00145	19989	0.	0.	0.	0.	0.	0.	0.	0.	0.	0.	0.
32	0.00145	19989	0.	0.	0.	0.	0.	0.	0.	0.	0.	0.	0.
33	0.00145	19989	0.	0.	0.	0.	0.	0.	0.	0.	0.	0.	0.
34	0.00145	19989	0.	0.	0.	0.	0.	0.	0.	0.	0.	0.	0.
35	0.00145	19989	0.	0.	0.	0.	0.	0.	0.	0.	0.	0.	0.
36	0.00145	19989	0.	0.	0.	0.	0.	0.	0.	0.	0.	0.	0.
37	0.00145	19989	0.	0.	0.	0.	0.	0.	0.	0.	0.	0.	0.
38	0.00145	19989	0.	0.	0.	0.	0.	0.	0.	0.	0.	0.	0.
39	0.00145	19989	0.	0.	0.	0.	0.	0.	0.	0.	0.	0.	0.
40	0.00145	19989	0.	0.	0.	0.	0.	0.	0.	0.	0.	0.	0.
41	0.00145	19989	0.	0.	0.	0.	0.	0.	0.	0.	0.	0.	0.
42	0.00145	19989	0.	0.	0.	0.	0.	0.	0.	0.	0.	0.	0.
43	0.00145	19989	0.	0.	0.	0.	0.	0.	0.	0.	0.	0.	0.

TIME EDIT NO. 6 AT N = 237, TIME = 2.0726E-06 SECS, JSTAR = 248, CALC TIME IS 149.922 SECS

TEST 3: FINAL MOMENTUM: EDIT AND PORTION OF TIME EDIT

44	0.3348	12016	1.309E+10	1.070E+10	1.305E+10	3.544E+07	2.8234	6.4772E+05	44	S	N	A	AL	FLYER	1.667E+09	2.349E+09
45	0.39777	11869	1.327E+10	1.090E+10	1.323E+10	3.662E+07	2.8241	6.4787E+05	45	S	N	A	AL	FLYER	1.667E+09	2.329E+09
46	0.50102	11768	1.344E+10	1.110E+10	1.341E+10	3.777E+07	2.8247	6.4803E+05	46	S	N	A	AL	FLYER	1.667E+09	2.309E+09
47	0.613423	11652	1.361E+10	1.126E+10	1.357E+10	3.888E+07	2.8254	6.4817E+05	47	S	N	A	AL	FLYER	1.667E+09	2.288E+09
48	0.66742	11542	1.376E+10	1.146E+10	1.373E+10	3.996E+07	2.8260	6.4831E+05	48	S	N	A	AL	FLYER	1.667E+09	2.266E+09
49	0.70858	11437	1.391E+10	1.164E+10	1.388E+10	4.100E+07	2.8266	6.4845E+05	49	S	N	A	AL	FLYER	1.667E+09	2.244E+09
50	0.73371	11337	1.405E+10	1.174E+10	1.402E+10	4.200E+07	2.8272	6.4857E+05	50	S	N	A	AL	FLYER	1.667E+09	2.222E+09
51	0.74682	11243	1.418E+10	1.195E+10	1.419E+10	4.296E+07	2.8277	6.4869E+05	51	S	N	A	AL	FLYER	1.667E+09	2.199E+09
52	0.751246	11153	1.430E+10	1.210E+10	1.436E+10	4.389E+07	2.8282	6.4881E+05	52	S	N	A	AL	FLYER	1.667E+09	2.177E+09
53	0.75250	11069	1.442E+10	1.224E+10	1.449E+10	4.477E+07	2.8287	6.4892E+05	53	S	N	A	AL	FLYER	1.667E+09	2.154E+09
54	0.75690	10990	1.453E+10	1.237E+10	1.451E+10	4.562E+07	2.8292	6.4902E+05	54	S	N	A	AL	FLYER	1.667E+09	2.132E+09
55	0.75990	10915	1.463E+10	1.244E+10	1.461E+10	4.643E+07	2.8296	6.4912E+05	55	S	N	A	AL	FLYER	1.667E+09	2.110E+09
56	0.76260	10844	1.472E+10	1.261E+10	1.472E+10	4.720E+07	2.8300	6.4921E+05	56	S	N	A	AL	FLYER	1.667E+09	2.088E+09
57	0.76498	10778	1.481E+10	1.272E+10	1.480E+10	4.793E+07	2.8304	6.4930E+05	57	S	N	A	AL	FLYER	1.667E+09	2.066E+09
58	0.76794	10716	1.490E+10	1.283E+10	1.489E+10	4.862E+07	2.8308	6.4938E+05	58	S	N	A	AL	FLYER	1.667E+09	2.045E+09
59	0.77088	10650	1.498E+10	1.293E+10	1.496E+10	4.928E+07	2.8311	6.4946E+05	59	S	N	A	AL	FLYER	1.667E+09	2.025E+09
60	0.77381	10583	1.506E+10	1.302E+10	1.503E+10	4.990E+07	2.8315	6.4953E+05	60	S	N	A	AL	FLYER	1.667E+09	2.005E+09
61	0.77672	10515	1.512E+10	1.311E+10	1.510E+10	5.049E+07	2.8318	6.4960E+05	61	S	N	A	AL	FLYER	1.667E+09	1.984E+09
62	0.77961	10449	1.518E+10	1.319E+10	1.516E+10	5.105E+07	2.8320	6.4966E+05	62	S	N	A	AL	FLYER	1.667E+09	1.967E+09
63	0.78250	10381	1.524E+10	1.327E+10	1.522E+10	5.157E+07	2.8323	6.4972E+05	63	S	N	A	AL	FLYER	1.667E+09	1.949E+09
64	0.78537	10315	1.529E+10	1.334E+10	1.528E+10	5.206E+07	2.8326	6.4978E+05	64	S	N	A	AL	FLYER	1.667E+09	1.932E+09
65	0.78823	10247	1.534E+10	1.341E+10	1.533E+10	5.252E+07	2.8328	6.4983E+05	65	S	N	A	AL	FLYER	1.667E+09	1.915E+09
66	0.79108	10179	1.538E+10	1.347E+10	1.537E+10	5.296E+07	2.8330	6.4988E+05	66	S	N	A	AL	FLYER	1.667E+09	1.899E+09
67	0.79392	10115	1.542E+10	1.353E+10	1.542E+10	5.336E+07	2.8332	6.4993E+05	67	S	N	A	AL	FLYER	1.667E+09	1.884E+09
68	0.79675	10047	1.546E+10	1.358E+10	1.546E+10	5.374E+07	2.8334	6.4997E+05	68	S	N	A	AL	FLYER	1.667E+09	1.869E+09
69	0.79958	10079	1.550E+10	1.363E+10	1.549E+10	5.410E+07	2.8336	6.5001E+05	69	S	N	A	AL	FLYER	1.667E+09	1.855E+09
70	0.80239	10011	1.553E+10	1.368E+10	1.552E+10	5.443E+07	2.8337	6.5004E+05	70	S	N	A	AL	FLYER	1.667E+09	1.842E+09
71	0.80520	9943	1.556E+10	1.372E+10	1.555E+10	5.475E+07	2.8339	6.5008E+05	71	S	N	A	AL	FLYER	1.667E+09	1.830E+09
72	0.80800	9875	1.559E+10	1.376E+10	1.558E+10	5.506E+07	2.8340	6.5011E+05	72	S	N	A	AL	FLYER	1.667E+09	1.818E+09
73	0.81080	9807	1.561E+10	1.380E+10	1.561E+10	5.531E+07	2.8341	6.5014E+05	73	S	N	A	AL	FLYER	1.667E+09	1.806E+09
74	0.81359	9739	1.563E+10	1.383E+10	1.563E+10	5.556E+07	2.8342	6.5016E+05	74	S	N	A	AL	FLYER	1.667E+09	1.794E+09
75	0.81637	9671	1.566E+10	1.386E+10	1.565E+10	5.580E+07	2.8344	6.5019E+05	75	S	N	A	AL	FLYER	1.667E+09	1.782E+09
76	0.81915	9603	1.568E+10	1.389E+10	1.567E+10	5.601E+07	2.8346	6.5021E+05	76	S	N	A	AL	FLYER	1.667E+09	1.770E+09
77	0.82193	9535	1.569E+10	1.392E+10	1.568E+10	5.622E+07	2.8348	6.5023E+05	77	S	N	A	AL	FLYER	1.667E+09	1.759E+09
78	0.82470	9467	1.571E+10	1.394E+10	1.570E+10	5.641E+07	2.8349	6.5025E+05	78	S	N	A	AL	FLYER	1.667E+09	1.752E+09
79	0.82747	9399	1.572E+10	1.396E+10	1.572E+10	5.659E+07	2.8347	6.5026E+05	79	S	N	A	AL	FLYER	1.667E+09	1.744E+09
80	0.83023	9331	1.573E+10	1.398E+10	1.573E+10	5.675E+07	2.8348	6.5028E+05	80	S	N	A	AL	FLYER	1.667E+09	1.738E+09
81	0.83299	9263	1.574E+10	1.400E+10	1.574E+10	5.691E+07	2.8349	6.5029E+05	81	S	N	A	AL	FLYER	1.667E+09	1.731E+09
82	0.83575	9195	1.575E+10	1.402E+10	1.575E+10	5.705E+07	2.8349	6.5030E+05	82	S	N	A	AL	FLYER	1.667E+09	1.726E+09
83	0.83851	9127	1.576E+10	1.403E+10	1.576E+10	5.719E+07	2.8349	6.5032E+05	83	S	N	A	AL	FLYER	1.667E+09	1.720E+09
84	0.84126	9059	1.577E+10	1.404E+10	1.577E+10	5.732E+07	2.8350	6.5033E+05	84	S	N	A	AL	FLYER	1.667E+09	1.715E+09
85	0.84401	9091	1.577E+10	1.404E+10	1.577E+10	5.744E+07	2.8350	6.5034E+05	85	S	N	A	AL	FLYER	1.667E+09	1.711E+09
86	0.84676	9023	1.578E+10	1.405E+10	1.578E+10	5.755E+07	2.8351	6.5034E+05	86	S	N	A	AL	FLYER	1.667E+09	1.706E+09
87	0.84951	8955	1.579E+10	1.406E+10	1.579E+10	5.766E+07	2.8351	6.5035E+05	87	S	N	A	AL	FLYER	1.667E+09	1.702E+09
88	0.85225	8887	1.579E+10	1.406E+10	1.579E+10	5.776E+07	2.8351	6.5036E+05	88	S	N	A	AL	FLYER	1.667E+09	1.699E+09
89	0.85500	8819	1.579E+10	1.406E+10	1.579E+10	5.785E+07	2.8351	6.5036E+05	89	S	N	A	AL	FLYER	1.667E+09	1.695E+09
90	0.85775	8751	1.580E+10	1.407E+10	1.580E+10	5.794E+07	2.8352	6.5037E+05	90	S	N	A	AL	FLYER	1.667E+09	1.692E+09
91	0.86049	8683	1.580E+10	1.407E+10	1.580E+10	5.803E+07	2.8352	6.5037E+05	91	S	N	A	AL	FLYER	1.667E+09	1.689E+09
92	0.86324	8615	1.580E+10	1.407E+10	1.580E+10	5.811E+07	2.8352	6.5038E+05	92	S	N	A	AL	FLYER	1.667E+09	1.687E+09
93	0.86598	8547	1.580E+10	1.407E+10	1.580E+10	5.819E+07	2.8352	6.5038E+05	93	S	N	A	AL	FLYER	1.667E+09	1.684E+09
94	0.86872	8479	1.580E+10	1.407E+10	1.580E+10	5.828E+07	2.8352	6.5038E+05	94	S	N	A	AL	FLYER	1.667E+09	1.682E+09
95	0.87146	8411	1.580E+10	1.407E+10	1.580E+10	5.836E+07	2.8352	6.5039E+05	95	S	N	A	AL	FLYER	1.667E+09	1.680E+09
96	0.87420	8343	1.580E+10	1.407E+10	1.580E+10	5.845E+07	2.8353	6.5039E+05	96	S	N	A	AL	FLYER	1.667E+09	1.679E+09
97	0.87694	8275	1.580E+10	1.407E+10	1.580E+10	5.852E+07	2.8353	6.5039E+05	97	S	N	A	AL	FLYER	1.667E+09	1.677E+09
98	0.87968	8207	1.580E+10	1.407E+10	1.580E+10	5.859E+07	2.8353	6.5040E+05	98	S	N	A	AL	FLYER	1.667E+09	1.676E+09
99	0.88242	8139	1.580E+10	1.407E+10	1.580E+10	5.866E+07	2.8353	6.5040E+05	99	S	N	A	AL	FLYER	1.667E+09	1.674E+09
100	0.88516	8071	1.580E+10	1.407E+10	1.580E+10	5.874E+07	2.8353	6.5040E+05	100	S	N	A	AL	FLYER	1.667E+09	1.673E+09
101	0.88790	8003	1.580E+10	1.407E+10	1.580E+10	5.882E+07	2.8353	6.5040E+05	101	S	N	A	AL	FLYER	1.667E+09	1.673E+09

TES 3: FINAL TIME EDIT (continued)

SCHEMATIC OUTPUT, TIME IN MICROSECS, S IN ROARS, DTIM IN NANOSECS, DELTIM IN SECS

N	TIME	S12/SOJ1	S23/SOJ2	S34/SOJ3	S ( 38)	S ( 75)	S (112)	S (187)	S (226)	S (261)	JTS	DTIM	DELYIM
1	.000	.000	.000	.000	.0000	.0000	.0000	.0000	.0000	.0000	150	.001	2.132
2	.001	.000	.000	.000	.0000	.0000	.0000	.0000	.0000	.0000	150	.010	.050
3	.001	.000	.000	.000	.0000	.0000	.0000	.0000	.0000	.0000	150	.012	.054
4	.002	.000	.000	.000	.0000	.0000	.0000	.0000	.0000	.0000	150	.734	.054
5	.003	.000	.000	.000	.0000	.0000	.0000	.0000	.0000	.0000	150	.001	.064
6	.004	.000	.000	.000	.0000	.0000	.0000	.0000	.0000	.0000	150	1.037	.066
7	.005	.000	.000	.000	.0000	.0000	.0000	.0000	.0000	.0000	150	1.269	.066
8	.007	.000	.000	.000	.0000	.0000	.0000	.0000	.0000	.0000	150	1.522	.072
9	.008	.000	.000	.000	.0000	.0000	.0000	.0000	.0000	.0000	150	1.827	.076
10	.011	.000	.000	.000	.0000	.0000	.0000	.0000	.0000	.0000	150	2.192	.078
11	.013	.000	.000	.000	.0000	.0000	.0000	.0000	.0000	.0000	150	2.630	.082
12	.016	.000	.000	.000	.0000	.0000	.0000	.0000	.0000	.0000	150	3.157	.082
13	.020	.000	.000	.000	.0000	.0000	.0000	.0000	.0000	.0000	150	3.708	.082
14	.025	.000	.000	.000	.0000	.0000	.0000	.0000	.0000	.0000	150	4.545	.086
15	.030	.000	.000	.000	.0000	.0000	.0000	.0000	.0000	.0000	140	5.455	.090
16	.037	.000	.000	.000	.0000	.0000	.0000	.0000	.0000	.0000	151	6.546	.096
17	.045	.000	.000	.000	.0000	.0000	.0000	.0000	.0000	.0000	151	7.855	.096
18	.054	.000	.000	.000	.0000	.0000	.0000	.0000	.0000	.0000	151	9.426	.100
19	.065	.000	.000	.000	.0000	.0000	.0000	.0000	.0000	.0000	152	11.311	.108
20	.079	.000	.000	.000	.0000	.0000	.0000	.0000	.0000	.0000	152	13.573	.112
21	.093	.000	.000	.000	.0000	.0000	.0000	.0000	.0000	.0000	153	13.787	.114
22	.106	.000	.000	.000	.0000	.0000	.0000	.0000	.0000	.0000	153	13.782	.122
23	.120	.000	.000	.000	.0000	.0000	.0000	.0000	.0000	.0000	154	13.865	.126
24	.134	.000	.000	.000	.0000	.0000	.0000	.0000	.0000	.0000	155	13.842	.134
25	.148	.000	.000	.000	.0000	.0000	.0000	.0000	.0000	.0000	155	13.845	.138
26	.162	.000	.000	.000	.0000	.0000	.0000	.0000	.0000	.0000	156	13.916	.152
27	.176	.000	.000	.000	.0000	.0000	.0000	.0000	.0000	.0000	157	13.985	.166
28	.190	.000	.000	.000	.0000	.0000	.0000	.0000	.0000	.0000	157	13.923	.184
29	.204	.000	.000	.000	.0000	.0000	.0000	.0000	.0000	.0000	158	13.955	.160
30	.218	.000	.000	.000	.0000	.0000	.0000	.0000	.0000	.0000	159	13.950	.168
31	.232	.000	.000	.000	.0000	.0000	.0000	.0000	.0000	.0000	159	13.969	.176
32	.246	.000	.000	.000	.0000	.0000	.0000	.0000	.0000	.0000	160	13.986	.176
33	.260	.000	.000	.000	.0000	.0000	.0000	.0000	.0000	.0000	161	13.986	.184
34	.274	.000	.000	.000	.0000	.0000	.0000	.0000	.0000	.0000	161	14.003	.186
35	.288	.000	.000	.000	.0000	.0000	.0000	.0000	.0000	.0000	162	14.012	.196
36	.302	.000	.000	.000	.0000	.0000	.0000	.0000	.0000	.0000	163	14.014	.202
37	.316	.000	.000	.000	.0000	.0000	.0000	.0000	.0000	.0000	163	14.031	.208
38	.330	.000	.000	.000	.0000	.0000	.0000	.0000	.0000	.0000	164	14.034	.208
39	.344	.000	.000	.000	.0000	.0000	.0000	.0000	.0000	.0000	165	14.036	.216
40	.358	.000	.000	.000	.0000	.0000	.0000	.0000	.0000	.0000	165	14.054	.222
41	.372	.000	.000	.000	.0000	.0000	.0000	.0000	.0000	.0000	166	14.053	.230
42	.386	.000	.000	.000	.0000	.0000	.0000	.0000	.0000	.0000	166	14.058	.234
43	.400	.000	.000	.000	.0000	.0000	.0000	.0000	.0000	.0000	168	14.068	.240
44	.414	.000	.000	.000	.0000	.0000	.0000	.0000	.0000	.0000	168	14.068	.242
45	.428	.000	.000	.000	.0000	.0000	.0000	.0000	.0000	.0000	168	14.068	.250
46	.442	.000	.000	.000	.0000	.0000	.0000	.0000	.0000	.0000	168	14.059	.256
47	.456	.000	.000	.000	.0000	.0000	.0000	.0000	.0000	.0000	168	14.059	.262
48	.470	.000	.000	.000	.0000	.0000	.0000	.0000	.0000	.0000	168	14.059	.266
49	.484	.000	.000	.000	.0000	.0000	.0000	.0000	.0000	.0000	168	14.058	.274
50	.498	.000	.000	.000	.0000	.0000	.0000	.0000	.0000	.0000	168	14.058	.274

TEST 3: FIRST PAGE OF STRESS HISTORIES



SCHEME OUTPUT. TIME IN MICROSECS. S IN KBARS, DTMM IN NANOSECS. DELTIM IN SECS												
N	TIME	S12/SOJ1	S27/SOJ2	S36/SOJ3	S( 75)	S(112)	S(187)	S(224)	S(261)	JTS	DTMM	DELTIM
51	.598	16.164	0.000	0.000	0.0000	.0003	0.0000	0.0000	0.0000	173	1.009	.206
52	.592	16.161	0.000	0.000	0.0000	.0000	0.0000	0.0000	0.0000	148	1.931	1.638
53	.584	16.156	0.000	0.000	0.0000	.0000	0.0000	0.0000	0.0000	148	2.317	.206
54	.577	16.154	0.000	0.000	0.0000	.0000	0.0000	0.0000	0.0000	148	2.701	.208
55	.571	16.150	0.000	0.000	0.0000	.0000	0.0000	0.0000	0.0000	148	3.085	.208
56	.564	16.145	0.000	0.000	0.0000	.0000	0.0000	0.0000	0.0000	148	3.469	.200
57	.559	16.139	0.000	0.000	0.0000	.0000	0.0000	0.0000	0.0000	148	3.853	.200
58	.552	16.131	0.000	0.000	0.0000	.0000	0.0000	0.0000	0.0000	148	4.237	.204
59	.546	16.123	0.000	0.000	0.0000	.0000	0.0000	0.0000	0.0000	148	4.621	.204
60	.540	16.113	0.000	0.000	0.0000	.0000	0.0000	0.0000	0.0000	148	5.005	.206
61	.534	16.102	0.000	0.000	0.0000	.0000	0.0000	0.0000	0.0000	148	5.389	.204
62	.528	16.090	0.000	0.000	0.0000	.0000	0.0000	0.0000	0.0000	148	5.773	.204
63	.522	16.073	0.000	0.000	0.0000	.0000	0.0000	0.0000	0.0000	148	6.157	.206
64	.516	16.064	0.000	0.000	0.0000	.0000	0.0000	0.0000	0.0000	148	6.541	.206
65	.510	16.053	0.000	0.000	0.0000	.0000	0.0000	0.0000	0.0000	148	6.925	.206
66	.504	16.042	0.000	0.000	0.0000	.0000	0.0000	0.0000	0.0000	148	7.309	.206
67	.498	16.032	0.000	0.000	0.0000	.0000	0.0000	0.0000	0.0000	148	7.693	.206
68	.492	16.023	0.000	0.000	0.0000	.0000	0.0000	0.0000	0.0000	148	8.077	.206
69	.486	16.014	0.000	0.000	0.0000	.0000	0.0000	0.0000	0.0000	148	8.461	.206
70	.480	16.006	0.000	0.000	0.0000	.0000	0.0000	0.0000	0.0000	148	8.845	.206
71	.474	15.991	0.000	0.000	0.0000	.0000	0.0000	0.0000	0.0000	148	9.229	.206
72	.468	15.980	0.000	0.000	0.0000	.0000	0.0000	0.0000	0.0000	148	9.613	.206
73	.462	15.963	0.000	0.000	0.0000	.0000	0.0000	0.0000	0.0000	148	10.000	.206
74	.456	15.976	0.000	0.000	0.0000	.0000	0.0000	0.0000	0.0000	148	10.384	.206
75	.450	15.969	0.000	0.000	0.0000	.0000	0.0000	0.0000	0.0000	148	10.768	.206
76	.444	15.963	0.000	0.000	0.0000	.0000	0.0000	0.0000	0.0000	148	11.152	.206
77	.438	15.957	0.000	0.000	0.0000	.0000	0.0000	0.0000	0.0000	148	11.536	.206
78	.432	15.951	0.000	0.000	0.0000	.0000	0.0000	0.0000	0.0000	148	11.920	.206
79	.426	15.945	0.000	0.000	0.0000	.0000	0.0000	0.0000	0.0000	148	12.304	.206
80	.420	15.940	0.000	0.000	0.0000	.0000	0.0000	0.0000	0.0000	148	12.688	.206
81	.414	15.935	0.000	0.000	0.0000	.0000	0.0000	0.0000	0.0000	148	13.072	.206
82	.408	15.929	0.000	0.000	0.0000	.0000	0.0000	0.0000	0.0000	148	13.456	.206
83	.402	15.924	0.000	0.000	0.0000	.0000	0.0000	0.0000	0.0000	148	13.840	.206
84	.396	15.918	0.000	0.000	0.0000	.0000	0.0000	0.0000	0.0000	148	14.224	.206
85	.390	15.912	0.000	0.000	0.0000	.0000	0.0000	0.0000	0.0000	148	14.608	.206
86	.384	15.906	0.000	0.000	0.0000	.0000	0.0000	0.0000	0.0000	148	14.992	.206
87	.378	15.900	0.000	0.000	0.0000	.0000	0.0000	0.0000	0.0000	148	15.376	.206
88	.372	15.893	0.000	0.000	0.0000	.0000	0.0000	0.0000	0.0000	148	15.760	.206
89	.366	15.887	0.000	0.000	0.0000	.0000	0.0000	0.0000	0.0000	148	16.144	.206
90	.360	15.881	0.000	0.000	0.0000	.0000	0.0000	0.0000	0.0000	148	16.528	.206
91	.354	15.875	0.000	0.000	0.0000	.0000	0.0000	0.0000	0.0000	148	16.912	.206
92	.348	15.869	0.000	0.000	0.0000	.0000	0.0000	0.0000	0.0000	148	17.296	.206
93	.342	15.863	0.000	0.000	0.0000	.0000	0.0000	0.0000	0.0000	148	17.680	.206
94	.336	15.857	0.000	0.000	0.0000	.0000	0.0000	0.0000	0.0000	148	18.064	.206
95	.330	15.851	0.000	0.000	0.0000	.0000	0.0000	0.0000	0.0000	148	18.448	.206
96	.324	15.845	0.000	0.000	0.0000	.0000	0.0000	0.0000	0.0000	148	18.832	.206
97	.318	15.839	0.000	0.000	0.0000	.0000	0.0000	0.0000	0.0000	148	19.216	.206
98	.312	15.833	0.000	0.000	0.0000	.0000	0.0000	0.0000	0.0000	148	19.600	.206
99	.306	15.827	0.000	0.000	0.0000	.0000	0.0000	0.0000	0.0000	148	19.984	.206
100	.300	15.821	0.000	0.000	0.0000	.0000	0.0000	0.0000	0.0000	148	20.368	.206

TEST 3: STRESS HISTORIES (continued)

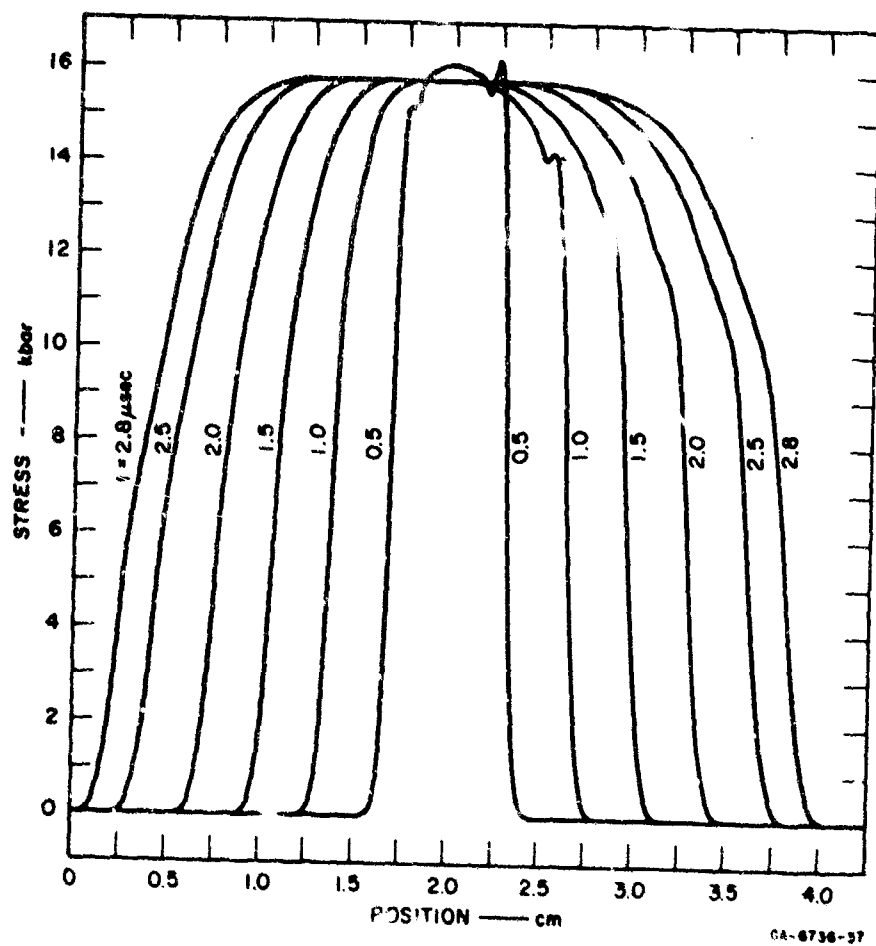


FIGURE 51 TEST 3: SUMMARY PLOT OF TIME EDITS

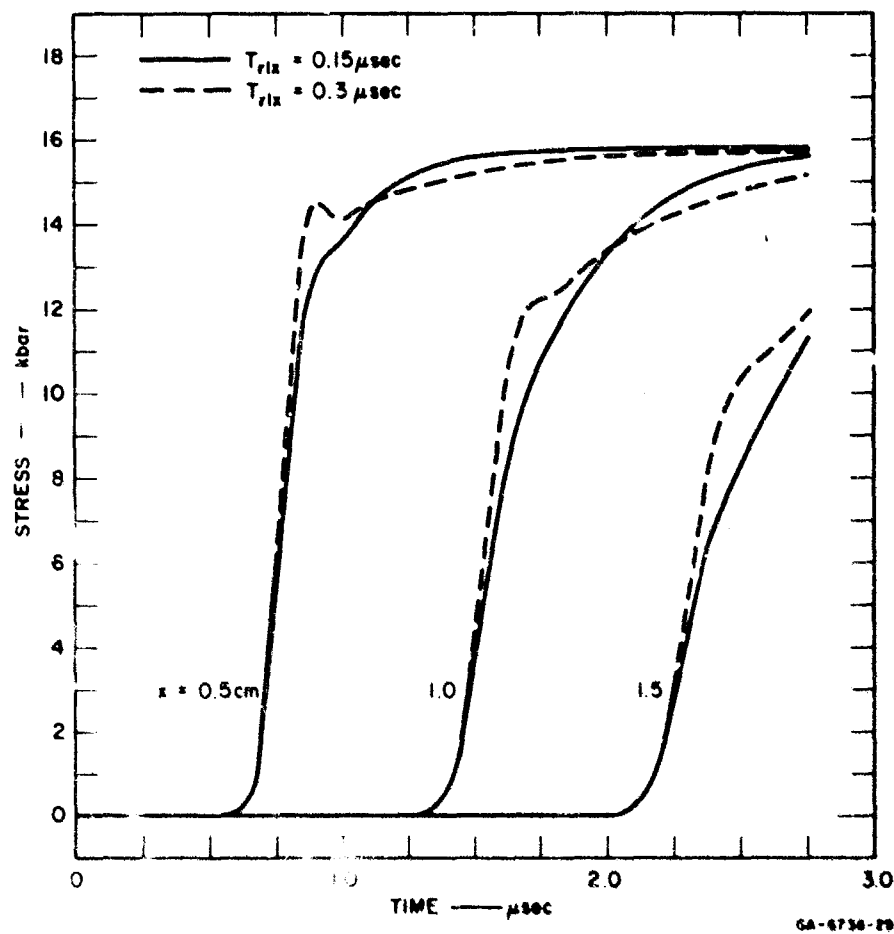


FIGURE 52 TEST 3: SUMMARY OF STRESS HISTORIES AT SIX JET LOCATIONS

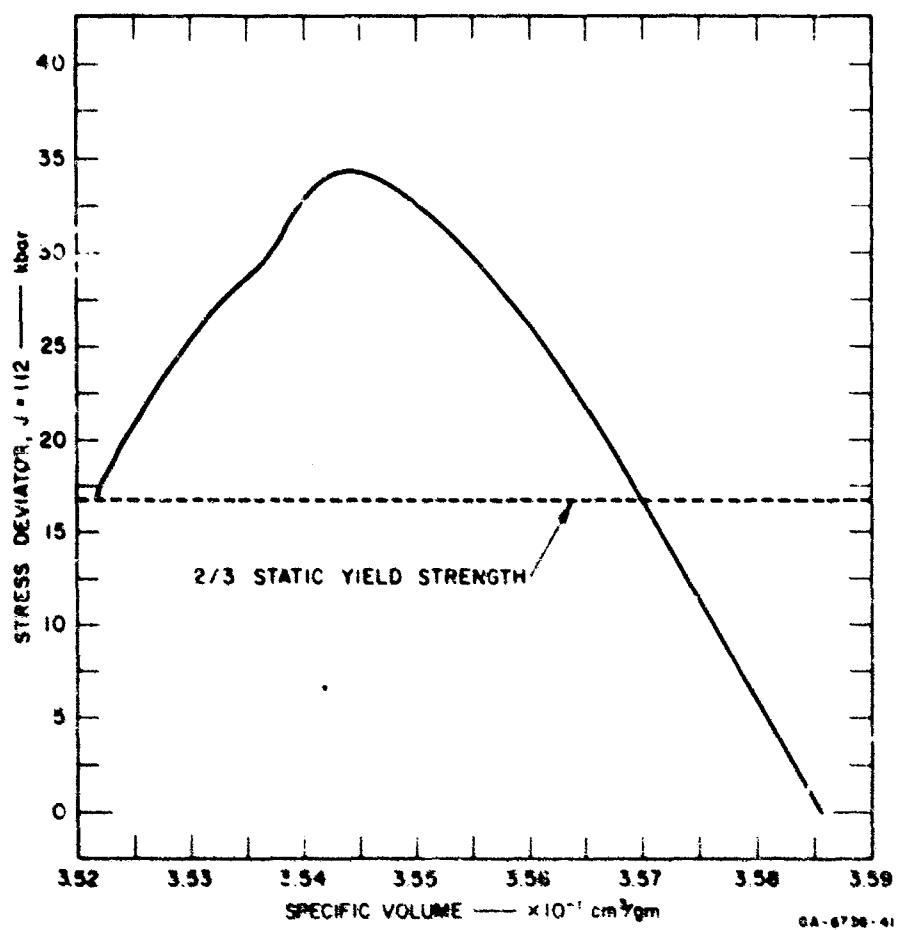


FIGURE 63 TEST 3: SAMPLE PLOT OF STRESS DEVIATOR

f. Test No. 4

The stress relaxation mechanism of Model 2 (Band's model) is tested in Test 4. The configuration is a symmetric impact between two plates of 2024-T8 aluminum. The plates have different relaxation parameters but are otherwise identical. The listing included on the following pages contains the input data, and portions of the initial layout, and final EDIT and stress histories. The EDITs, stress histories, and a deviatoric stress-volume path are shown in the figures.

\*\*\* SHI PUFF 1 (6400 VERSION) \*\*\*

DATE #05/13/69

IDENT # 4 MODEL 2, BAND RELAXATION MODEL, IRON/IRON IMPACT  
 THE DISLOCATION MULTIPLICATION PARAMETER, GEE, IS DIFFERENT IN THE FLYER  
 AND THE TARGET. ALL OTHER PARAMETERS ARE IDENTICAL.

1 NTEIT# 5 NJEIT# 6 NREZON# 0 NSEPHAT# 0  
 2 TEN115# 1.333E-07 2.667E-07 4.000E-07 5.333E-07 6.667E-07  
 3 JEIITS# 53 85 117 182 214 246  
 6 NEOTM# 100000 NEDIT# 10000 NPEHN# 1 MAXPHN# 0  
 7 STOPS JCYCS# 1210 CKS# 4.000E+00 TS# 8.000E-07  
 8 NMTHLS# 2 MATFL# 1 UZEMO# 2.500E+04 IPLU1# 1

IRON FLYER RHOS# 7.850E+00 NSRM# 2 NYAM# 1 NPOR# 0 NCON# 0  
 EQSTC# 1.741E+12 EQSTD# 0. EQSTE# 8.400E+10 EQSTG# 1.600E+00  
 EQSTM# 2.500E-01 EQSTS# 0. EQSTH# 1.650E+00 EQSTI# 7.214E-12  
 COSQ# 4.000E+00 C1# 1.500E-01 C2# 0.  
 TENS(1)# -1.000E+11 TENS(2)# -1.000E+11 TENS(3)# -1.000E+11  
 T1# 1.000E-06 T2# 4.000E-06 BEE# 1.980E+10 VM# 3.220E+05  
 GEE# 5.000E-02 EPS# 9.000E-01 NMO# 5.000E+00 NTO# 2.000E+01  
 YO# 5.000E+09 MU# 8.140E+11 YADD# 0.  
 NZONES# 1, 148 CELLS IN 6.000E-01 CM -0. -0.

IRON TARGET RHOS# 7.850E+00 NSRM# 2 NYAM# 1 NPOR# 0 NCON# 0  
 EQSTC# 1.741E+12 EQSTD# 0. EQSTE# 8.400E+10 EQSTG# 1.600E+00  
 EQSTM# 2.500E-01 EQSTS# 0. EQSTH# 1.650E+00 EQSTI# 7.214E-12  
 COSQ# 4.000E+00 C1# 1.500E-01 C2# 0.  
 TENS(1)# -1.000E+11 TENS(2)# -1.000E+11 TENS(3)# -1.000E+11  
 T1# 1.000E-06 T2# 4.000E-06 HFE# 1.980E+10 VM# 3.220E+05  
 GEE# 0. EPS# 9.000E-01 NMO# 5.000E+00 NTO# 2.000E+01  
 YO# 5.000E+09 MU# 8.140E+11 YADD# 0.  
 NZONES# 1, 148 CELLS IN 6.000E-01 CM -0. -0.

#### TEST 4: INPUT DATA



[illegible]

TEST 4: FINAL MOMENTUM EDIT AND PORTION OF TIME EDIT



44	1.3392	20787	1.949E+10	1.473E+10	1.433E+10	9.702E+06	7.9072	5.9921E+05	44	S	N	A	ON	FLYER	1.385E+02	1.401E+02
45	1.98016	20586	2.022E+10	1.366E+10	2.008E+10	1.064E+07	7.9100	5.9917E+05	45	S	N	A	IRON	FLYER	1.412E+02	1.426E+02
46	2.22039	20370	2.108E+10	1.411E+10	2.092E+10	1.194E+07	7.9134	5.9910E+05	46	S	N	A	IRON	FLYER	1.436E+02	1.447E+02
47	2.26059	20114	2.209E+10	1.501E+10	2.195E+10	1.324E+07	7.9174	5.9908E+05	47	S	N	A	IRON	FLYER	1.456E+02	1.466E+02
48	2.10078	19813	2.324E+10	1.609E+10	2.305E+10	1.511E+07	7.9222	5.9899E+05	48	S	N	A	IRON	FLYER	1.473E+02	1.481E+02
49	2.24043	19651	2.465E+10	1.735E+10	2.439E+10	1.771E+07	7.9274	5.9897E+05	49	S	N	A	IRON	FLYER	1.487E+02	1.494E+02
50	2.24106	19405	2.623E+10	1.881E+10	2.653E+10	2.016E+07	7.9344	5.9882E+05	50	S	N	A	IRON	FLYER	1.499E+02	1.504E+02
51	2.26110	19598	2.800E+10	2.048E+10	2.766E+10	2.342E+07	7.9419	5.9871E+05	51	S	N	A	IRON	FLYER	1.509E+02	1.513E+02
52	2.26110	19598	2.800E+10	2.048E+10	2.766E+10	2.342E+07	7.9419	5.9871E+05	52	S	N	A	IRON	FLYER	1.517E+02	1.521E+02
53	2.26111	19552	3.200E+10	2.42E+10	3.160E+10	2.200E+07	7.9591	5.9846E+05	53	S	N	A	IRON	FLYER	1.524E+02	1.527E+02
54	2.24117	19492	3.624E+10	2.82E+10	3.571E+10	2.706E+07	7.9585	5.9833E+05	54	S	N	A	IRON	FLYER	1.529E+02	1.532E+02
55	2.24108	19431	3.624E+10	2.82E+10	3.571E+10	2.706E+07	7.9585	5.9833E+05	55	S	N	A	IRON	FLYER	1.534E+02	1.537E+02
56	2.24109	19381	3.627E+10	3.060E+10	3.747E+10	2.774E+07	7.9872	5.9805E+05	56	S	N	A	IRON	FLYER	1.537E+02	1.540E+02
57	2.26077	19381	3.627E+10	3.060E+10	3.747E+10	2.774E+07	7.9872	5.9805E+05	57	S	N	A	IRON	FLYER	1.540E+02	1.543E+02
58	2.26055	19223	4.143E+10	3.331E+10	4.151E+10	3.609E+07	8.0034	5.9781E+05	58	S	N	A	IRON	FLYER	1.543E+02	1.546E+02
59	2.26030	14521	4.330E+10	3.544E+10	4.302E+10	4.248E+07	8.0104	5.9770E+05	59	S	N	A	IRON	FLYER	1.545E+02	1.548E+02
60	2.26031	14177	4.451E+10	3.725E+10	4.431E+10	4.675E+07	8.0170	5.9761E+05	60	S	N	A	IRON	FLYER	1.546E+02	1.549E+02
61	2.26194	13847	4.559E+10	3.741E+10	4.519E+10	7.028E+07	8.0222	5.9753E+05	61	S	N	A	IRON	FLYER	1.547E+02	1.549E+02
62	2.26935	13846	4.655E+10	3.734E+10	4.628E+10	7.329E+07	8.0266	5.9747E+05	62	S	N	A	IRON	FLYER	1.548E+02	1.549E+02
63	2.26949	13444	4.714E+10	4.019E+10	4.701E+10	7.583E+07	8.0302	5.9741E+05	63	S	N	A	IRON	FLYER	1.549E+02	1.550E+02
64	2.27361	13286	4.771E+10	4.085E+10	4.760E+10	7.748E+07	8.0332	5.9733E+05	64	S	N	A	IRON	FLYER	1.550E+02	1.551E+02
65	2.27822	13153	4.817E+10	4.141E+10	4.808E+10	7.972E+07	8.0356	5.9733E+05	65	S	N	A	IRON	FLYER	1.551E+02	1.551E+02
66	2.26182	13043	4.854E+10	4.186E+10	4.846E+10	8.121E+07	8.037	5.9730E+05	66	S	N	A	IRON	FLYER	1.551E+02	1.551E+02
67	2.26374	12953	4.884E+10	4.24E+10	4.878E+10	8.245E+07	8.0394	5.9727E+05	67	S	N	A	IRON	FLYER	1.551E+02	1.551E+02
68	2.26367	12874	4.909E+10	4.256E+10	4.93E+10	8.350E+07	8.0408	5.9725E+05	68	S	N	A	IRON	FLYER	1.552E+02	1.552E+02
69	2.26367	12816	4.929E+10	4.282E+10	4.925E+10	8.440E+07	8.0420	5.9724E+05	69	S	N	A	IRON	FLYER	1.552E+02	1.552E+02
70	2.26367	12764	4.946E+10	4.305E+10	4.942E+10	8.516E+07	8.0430	5.9722E+05	70	S	N	A	IRON	FLYER	1.552E+02	1.552E+02
71	3.01570	12720	4.960E+10	4.325E+10	4.957E+10	8.542E+07	8.0439	5.9721E+05	71	S	N	A	IRON	FLYER	1.553E+02	1.553E+02
72	3.05526	12683	4.972E+10	4.341E+10	4.969E+10	8.630E+07	8.0448	5.9720E+05	72	S	N	A	IRON	FLYER	1.553E+02	1.553E+02
73	3.04662	12651	4.982E+10	4.356E+10	4.940E+10	8.690E+07	8.0453	5.9719E+05	73	S	N	A	IRON	FLYER	1.553E+02	1.553E+02
74	3.14338	12623	4.990E+10	4.364E+10	4.946E+10	8.734E+07	8.0458	5.9718E+05	74	S	N	A	IRON	FLYER	1.553E+02	1.553E+02
75	3.14338	12594	4.994E+10	4.364E+10	4.946E+10	8.734E+07	8.0463	5.9717E+05	75	S	N	A	IRON	FLYER	1.553E+02	1.553E+02
76	3.21344	12578	5.004E+10	4.374E+10	5.003E+10	8.809E+07	8.0468	5.9714E+05	76	S	N	A	IRON	FLYER	1.553E+02	1.553E+02
77	3.25303	12560	5.010E+10	4.398E+10	5.008E+10	8.840E+07	8.0472	5.9716E+05	77	S	N	A	IRON	FLYER	1.553E+02	1.553E+02
78	3.29258	12544	5.014E+10	4.406E+10	5.013E+10	8.869E+07	8.0475	5.9715E+05	78	S	N	A	IRON	FLYER	1.553E+02	1.553E+02
79	3.33212	12524	5.014E+10	4.413E+10	5.017E+10	8.894E+07	8.0478	5.9715E+05	79	S	N	A	IRON	FLYER	1.553E+02	1.553E+02
80	3.37166	12517	5.022E+10	4.419E+10	5.021E+10	8.918E+07	8.0481	5.9715E+05	80	S	N	A	IRON	FLYER	1.554E+02	1.554E+02
81	3.41121	12506	5.025E+10	4.425E+10	5.024E+10	8.940E+07	8.0484	5.9714E+05	81	S	N	A	IRON	FLYER	1.554E+02	1.554E+02
82	3.45024	12496	5.027E+10	4.430E+10	5.027E+10	8.964E+07	8.0486	5.9714E+05	82	S	N	A	IRON	FLYER	1.554E+02	1.554E+02
83	3.49024	12487	5.030E+10	4.435E+10	5.029E+10	8.978E+07	8.0488	5.9713E+05	83	S	N	A	IRON	FLYER	1.554E+02	1.554E+02
84	3.52982	12474	5.032E+10	4.439E+10	5.031E+10	8.996E+07	8.0490	5.9713E+05	84	S	N	A	IRON	FLYER	1.554E+02	1.554E+02
85	3.56936	12472	5.034E+10	4.443E+10	5.033E+10	9.012E+07	8.0492	5.9713E+05	85	S	N	A	IRON	FLYER	1.554E+02	1.554E+02
86	3.60890	12460	5.036E+10	4.446E+10	5.035E+10	9.026E+07	8.0493	5.9713E+05	86	S	N	A	IRON	FLYER	1.554E+02	1.554E+02
87	3.64844	12450	5.037E+10	4.450E+10	5.037E+10	9.039E+07	8.0495	5.9713E+05	87	S	N	A	IRON	FLYER	1.554E+02	1.554E+02
88	3.68747	12440	5.039E+10	4.453E+10	5.038E+10	9.052E+07	8.0496	5.9713E+05	88	S	N	A	IRON	FLYER	1.554E+02	1.554E+02
89	3.72751	12430	5.040E+10	4.456E+10	5.039E+10	9.065E+07	8.0497	5.9713E+05	89	S	N	A	IRON	FLYER	1.554E+02	1.554E+02
90	3.76704	12424	5.041E+10	4.458E+10	5.040E+10	9.077E+07	8.0498	5.9713E+05	90	S	N	A	IRON	FLYER	1.554E+02	1.554E+02
91	3.80657	12415	5.042E+10	4.461E+10	5.041E+10	9.089E+07	8.0500	5.9713E+05	91	S	N	A	IRON	FLYER	1.554E+02	1.554E+02
92	3.84611	12408	5.042E+10	4.463E+10	5.042E+10	9.100E+07	8.0501	5.9713E+05	92	S	N	A	IRON	FLYER	1.554E+02	1.554E+02
93	3.88564	12404	5.043E+10	4.465E+10	5.043E+10	9.110E+07	8.0501	5.9713E+05	93	S	N	A	IRON	FLYER	1.554E+02	1.554E+02
94	3.92517	12431	5.044E+10	4.467E+10	5.043E+10	9.121E+07	8.0502	5.9713E+05	94	S	N	A	IRON	FLYER	1.554E+02	1.554E+02
95	3.96471	12428	5.044E+10	4.469E+10	5.044E+10	9.131E+07	8.0503	5.9713E+05	95	S	N	A	IRON	FLYER	1.554E+02	1.554E+02
96	4.00424	12426	5.045E+10	4.470E+10	5.044E+10	9.140E+07	8.0504	5.9713E+05	96	S	N	A	IRON	FLYER	1.554E+02	1.554E+02
97	4.04377	12423	5.045E+10	4.472E+10	5.045E+10	9.150E+07	8.0505	5.9713E+05	97	S	N	A	IRON	FLYER	1.554E+02	1.554E+02
98	4.08333	12421	5.045E+10	4.473E+10	5.045E+10	9.159E+07	8.0505	5.9713E+05	98	S	N	A	IRON	FLYER	1.554E+02	1.554E+02
99	4.12283	12419	5.046E+10	4.475E+10	5.045E+10	9.169E+07	8.0506	5.9713E+05	99	S	N	A	IRON	FLYER	1.554E+02	1.554E+02
100	4.16236	12417	5.046E+10	4.476E+10	5.046E+10	9.177E+07	8.0507	5.9713E+05	100	S	N	A	IRON	FLYER	1.554E+02	1.554E+02
101	4.20189	12415	5.046E+10	4.478E+10	5.046E+10	9.185E+07	8.0507	5.9713E+05	101	S	N	A	IRON	FLYER	1.554E+02	1.554E+02

TEST 4: FINAL TIME EDIT (continued)

SCREEN OUTPUT. TIME IN MICROSECS. S IN KBARS. DTW IN MICROSECS. DELTIM IN SECS													
N	TIME	S12/SQJ1	S23/SQJ2	S34/SQJ3	S1 S33	S1 S53	S1 S17	S1 S182	S1 S214	S1 S246	JTS	DTW	DELTIM
1	.000	.000	.000	.000	.0000	.0000	.0000	.0000	.0000	.0000	150	.001	2.168
2	.000	1.428	.000	.000	.0000	.0000	.0000	.0000	.0000	.0000	148	.163	.052
3	.000	3.131	.000	.000	.0000	.0000	.0000	.0000	.0000	.0000	150	.195	.054
4	.001	5.165	.000	.000	.0000	.0000	.0000	.0000	.0000	.0000	150	.235	.058
5	.001	7.577	.000	.000	.0000	.0000	.0000	.0000	.0000	.0000	150	.267	.064
6	.001	10.433	.000	.000	.0000	.0000	.0000	.0000	.0000	.0000	150	.338	.076
7	.002	13.795	.000	.000	.0000	.0000	.0000	.0000	.0000	.0000	150	.405	.084
8	.002	17.726	.000	.000	.0000	.0000	.0000	.0000	.0000	.0000	150	.486	.086
9	.003	22.259	.000	.000	.0000	.0000	.0000	.0000	.0000	.0000	150	.584	.092
10	.003	27.377	.000	.000	.0000	.0000	.0000	.0000	.0000	.0000	150	.700	.094
11	.004	32.916	.000	.000	.0000	.0000	.0000	.0000	.0000	.0000	150	.841	.094
12	.005	38.497	.000	.000	.0000	.0000	.0000	.0000	.0000	.0000	148	1.009	.114
13	.006	43.434	.000	.000	.0000	.0000	.0000	.0000	.0000	.0000	148	1.453	.116
14	.006	47.438	.000	.000	.0000	.0000	.0000	.0000	.0000	.0000	151	1.743	.126
15	.010	50.453	.000	.000	.0000	.0000	.0000	.0000	.0000	.0000	151	2.092	.132
16	.012	52.386	.000	.000	.0000	.0000	.0000	.0000	.0000	.0000	151	2.510	.146
17	.014	53.221	.000	.000	.0000	.0000	.0000	.0000	.0000	.0000	151	3.012	.154
18	.017	53.165	.000	.000	.0000	.0000	.0000	.0000	.0000	.0000	152	3.614	.154
19	.021	52.788	.000	.000	.0000	.0000	.0000	.0000	.0000	.0000	152	4.317	.150
20	.025	52.565	.000	.000	.0000	.0000	.0000	.0000	.0000	.0000	153	4.447	.174
21	.030	52.621	.000	.000	.0000	.0000	.0000	.0000	.0000	.0000	154	4.434	.170
22	.034	52.407	.000	.000	.0000	.0000	.0000	.0000	.0000	.0000	145	4.449	.198
23	.039	52.148	.000	.000	.0000	.0000	.0000	.0000	.0000	.0000	144	4.474	.208
24	.043	51.999	.000	.000	.0000	.0000	.0000	.0000	.0000	.0000	143	4.476	.226
25	.047	51.866	.000	.000	.0000	.0000	.0000	.0000	.0000	.0000	143	4.494	.228
26	.052	51.770	.000	.000	.0000	.0000	.0000	.0000	.0000	.0000	142	4.488	.242
27	.056	51.709	.000	.000	.0000	.0000	.0000	.0000	.0000	.0000	142	4.499	.254
28	.061	51.646	.000	.000	.0000	.0000	.0000	.0000	.0000	.0000	141	4.498	.266
29	.065	51.564	.000	.000	.0000	.0000	.0000	.0000	.0000	.0000	140	4.505	.278
30	.070	51.514	.000	.000	.0000	.0000	.0000	.0000	.0000	.0000	140	4.506	.288
31	.074	51.477	.000	.000	.0000	.0000	.0000	.0000	.0000	.0000	140	4.511	.300
32	.079	51.431	.000	.000	.0000	.0000	.0000	.0000	.0000	.0000	139	4.511	.312
33	.083	51.380	.000	.000	.0000	.0000	.0000	.0000	.0000	.0000	139	4.516	.320
34	.088	51.342	.000	.000	.0000	.0000	.0000	.0000	.0000	.0000	138	4.515	.336
35	.092	51.312	.000	.000	.0000	.0000	.0000	.0000	.0000	.0000	138	4.520	.346
36	.097	51.280	.000	.000	.0000	.0000	.0000	.0000	.0000	.0000	137	4.519	.360
37	.102	51.248	.000	.000	.0000	.0000	.0000	.0000	.0000	.0000	137	4.523	.368
38	.106	51.221	.000	.000	.0000	.0000	.0000	.0000	.0000	.0000	136	4.523	.382
39	.111	51.198	.000	.000	.0000	.0000	.0000	.0000	.0000	.0000	135	4.526	.394
40	.115	51.173	.000	.000	.0000	.0000	.0000	.0000	.0000	.0000	135	4.528	.404
41	.120	51.149	.000	.000	.0000	.0000	.0000	.0000	.0000	.0000	135	4.528	.422
42	.124	51.127	.000	.000	.0000	.0000	.0000	.0000	.0000	.0000	134	4.528	.438
43	.129	51.109	.000	.000	.0000	.0000	.0000	.0000	.0000	.0000	134	4.528	.440
44	.133	51.091	.000	.000	.0000	.0000	.0000	.0000	.0000	.0000	134	4.528	.440
45	.133	51.111	.000	.000	.0000	.0000	.0000	.0000	.0000	.0000	134	4.528	.440
46	.133	51.110	.000	.000	.0000	.0000	.0000	.0000	.0000	.0000	134	4.528	.440
47	.134	51.109	.000	.000	.0000	.0000	.0000	.0000	.0000	.0000	134	4.528	.440
48	.134	51.108	.000	.000	.0000	.0000	.0000	.0000	.0000	.0000	134	4.528	.440
49	.134	51.107	.000	.000	.0000	.0000	.0000	.0000	.0000	.0000	134	4.528	.440
50	.134	51.106	.000	.000	.0000	.0000	.0000	.0000	.0000	.0000	134	4.528	.440

TEST 4: FIRST PAGE OF STRESS HISTORIES



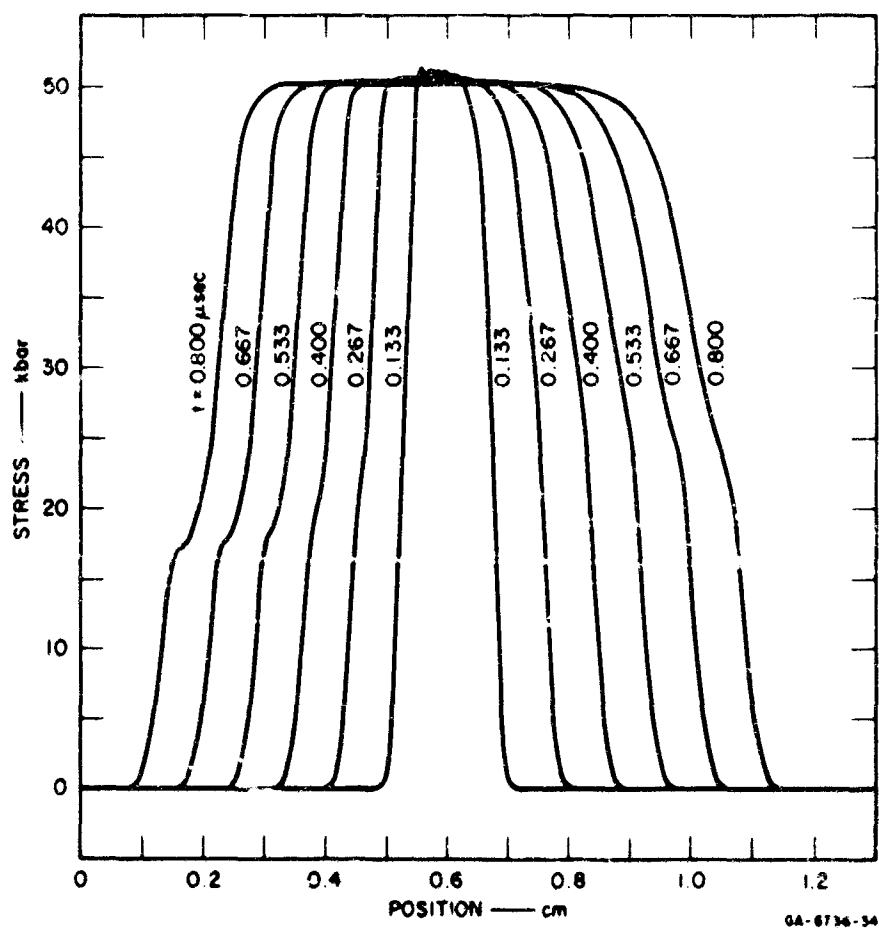


FIGURE 64 TEST 4: SUMMARY PLOT OF TIME EDITS

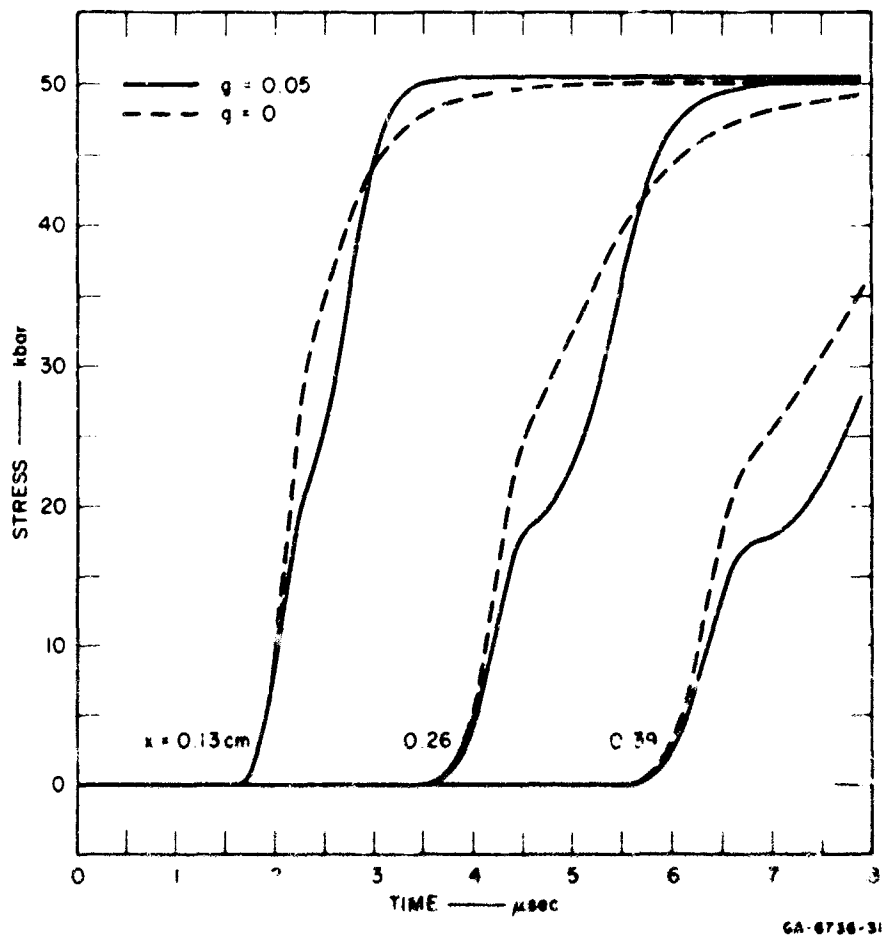


FIGURE 55 TEST 4: SUMMARY OF STRESS HISTORIES AT SIX JET LOCATIONS

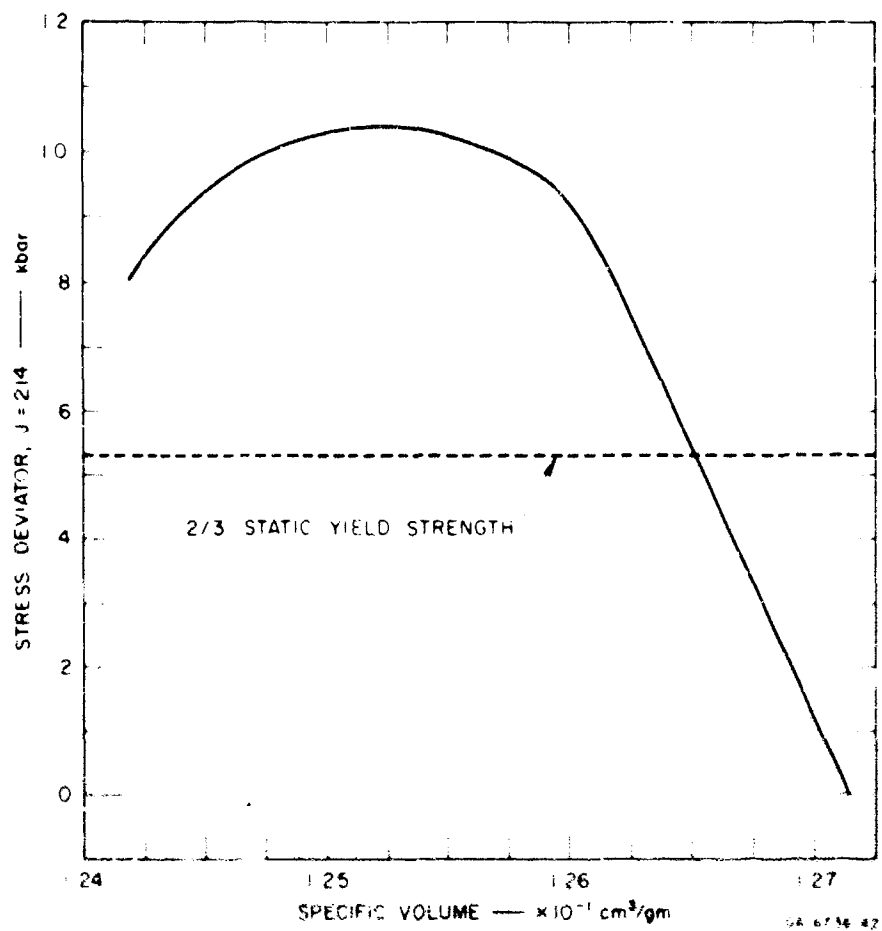


FIGURE 56 TEST 4: SAMPLE PLOT OF STRESS DEVIATOR

g. Test No. 5

The stress relaxation mechanism of Model 3 (Gilman's model) is tested in Test 5. The configuration is a symmetric impact between two plates of 2024-T8 aluminum. The plates have different relaxation parameters but are otherwise identical. The listing included on the following pages contains the input data, and portions of the initial layout, and final EDIT and stress histories. The EDITs, stress histories, and a deviatoric stress-volume path are shown in the figures.

\*\*\* SHI PUFF 1 (6400 VERSION) \*\*\*

DATE =05/13/69

IDENT = 5 MODEL 3: GILMAN RELAXATION MODEL, IRON/IRON MODEL  
 THE DISLOCATION MULTIPLICATION PARAMETER, PHI, IS DIFFERENT IN THE FLYER  
 AND IN THE TARGET. ALL OTHER PARAMETERS ARE IDENTICAL.

1 NTEST= 5 NJEDIT= 6 NREZON= 0 NSEPHAT= 0  
 2 TEDIT= 1.333E-07 2.667E-07 4.000E-07 5.333E-07 6.667E-07  
 3 JEDIT= 53 85 117 182 214 246  
 6 NEDTM= 10000 NEDIT= 10000 NPERN = 1 -0  
 7 STOPS JCYS = 1000 CKS = 4.000E+00 TS = 8.000E-07  
 8 NMTHLS= 2 MAYFL = 1 UZERO = 2.500E+04 -0

IRON FLYER RHOS = 7.850E+00 NSRM = 3 NYAM = 1 NPOR = 0 NCON = 0  
 EQSTC = 1.741E+12 EUSTD = 0. EUSTE = 8.400E+10 EUSTG = 1.600E+00  
 ERSTM = 2.500E+01 EUSTS = 0. 1.650E+00 7.214E-12  
 C9SQ = 4.000E+00 C1 = 1.500E-01 C2 = 0.  
 TENS(1)= -1.000E+11 TENS(2)= -1.000E+11 TENS(3)= -1.000E+11  
 CEE = 2.000E+03 PHI = 1.000E+03 HEE = 1.940E+10 VM = 3.220E+05  
 BNMO = 5.000E+00 -0. -0. -0.  
 YO = 5.000E+09 MU = 8.140E+11 YADD = 0.  
 NZONES= 1. 148 CELLS IN 6.000E-01 CM -0. -0.

IRON TARGET RHOS = 7.850E+00 NSRM = 3 NYAM = 1 NPOR = 0 NCON = 0  
 EQSTC = 1.741E+12 EUSTD = 0. EUSTE = 8.400E+10 EUSTG = 1.600E+00  
 ERSTM = 2.500E+01 EUSTS = 0. 1.650E+00 7.214E-12  
 C9SQ = 4.000E+00 C1 = 1.500E-01 C2 = 0.  
 TENS(1)= -1.000E+11 TENS(2)= -1.000E+11 TENS(3)= -1.000E+11  
 CEE = 2.000E+03 PHI = 0. HEE = 1.940E+10 VM = 3.220E+05  
 BNMO = 5.000E+00 -0. -0. -0.  
 YO = 5.000E+09 MU = 8.140E+11 YADD = 0.  
 NZONES= 1. 148 CELLS IN 6.000E-01 CM -0. -0.

TEST 5: INPUT DATA



DATE = 05/13/69 IDENT = 5 MODEL 3, GILMAN RELAXATION MODEL, IRON/IRON MODEL

J	DA	CM	X(J)	U(J)	YML(J)	CM/SEC	D(J)	T(J)	ZML(J)	MATERIAL	COM	J
1	4.054E-03	0.		2.500E+04	3.333E+09	6.001E+05	7.850E+00-1.000E+11	3.182E-02	IRON FLYER	5 N 8	1	
2	4.054E-03	4.054E-03		2.500E+04	3.333E+09	6.001E+05	7.850E+00-1.000E+11	3.182E-02	IRON FLYER	5 N 8	2	
3	4.054E-03	8.108E-03		2.500E+04	3.333E+09	6.001E+05	7.850E+00-1.000E+11	3.182E-02	IRON FLYER	5 N 8	3	
4	4.054E-03	1.216E-02		2.500E+04	3.333E+09	6.001E+05	7.850E+00-1.000E+11	3.182E-02	IRON FLYER	5 N 8	4	
5	4.054E-03	1.622E-02		2.500E+04	3.333E+09	6.001E+05	7.850E+00-1.000E+11	3.182E-02	IRON FLYER	5 N 8	5	
6	4.054E-03	2.027E-02		2.500E+04	3.333E+09	6.001E+05	7.850E+00-1.000E+11	3.182E-02	IRON FLYER	5 N 8	6	
7	4.054E-03	2.432E-02		2.500E+04	3.333E+09	6.001E+05	7.850E+00-1.000E+11	3.182E-02	IRON FLYER	5 N 8	7	
8	4.054E-03	2.838E-02		2.500E+04	3.333E+09	6.001E+05	7.850E+00-1.000E+11	3.182E-02	IRON FLYER	5 N 8	8	
9	4.054E-03	3.243E-02		2.500E+04	3.333E+09	6.001E+05	7.850E+00-1.000E+11	3.182E-02	IRON FLYER	5 N 8	9	
10	4.054E-03	3.649E-02		2.500E+04	3.333E+09	6.001E+05	7.850E+00-1.000E+11	3.182E-02	IRON FLYER	5 N 8	10	
11	4.054E-03	4.054E-02		2.500E+04	3.333E+09	6.001E+05	7.850E+00-1.000E+11	3.182E-02	IRON FLYER	5 N 8	11	
12	4.054E-03	4.459E-02		2.500E+04	3.333E+09	6.001E+05	7.850E+00-1.000E+11	3.182E-02	IRON FLYER	5 N 8	12	
13	4.054E-03	4.865E-02		2.500E+04	3.333E+09	6.001E+05	7.850E+00-1.000E+11	3.182E-02	IRON FLYER	5 N 8	13	
14	4.054E-03	5.270E-02		2.500E+04	3.333E+09	6.001E+05	7.850E+00-1.000E+11	3.182E-02	IRON FLYER	5 N 8	14	
15	4.054E-03	5.674E-02		2.500E+04	3.333E+09	6.001E+05	7.850E+00-1.000E+11	3.182E-02	IRON FLYER	5 N 8	15	
16	4.054E-03	6.081E-02		2.500E+04	3.333E+09	6.001E+05	7.850E+00-1.000E+11	3.182E-02	IRON FLYER	5 N 8	16	
17	4.054E-03	6.486E-02		2.500E+04	3.333E+09	6.001E+05	7.850E+00-1.000E+11	3.182E-02	IRON FLYER	5 N 8	17	
18	4.054E-03	6.892E-02		2.500E+04	3.333E+09	6.001E+05	7.850E+00-1.000E+11	3.182E-02	IRON FLYER	5 N 8	18	
19	4.054E-03	7.297E-02		2.500E+04	3.333E+09	6.001E+05	7.850E+00-1.000E+11	3.182E-02	IRON FLYER	5 N 8	19	
20	4.054E-03	7.703E-02		2.500E+04	3.333E+09	6.001E+05	7.850E+00-1.000E+11	3.182E-02	IRON FLYER	5 N 8	20	
21	4.054E-03	8.108E-02		2.500E+04	3.333E+09	6.001E+05	7.850E+00-1.000E+11	3.182E-02	IRON FLYER	5 N 8	21	
22	4.054E-03	8.514E-02		2.500E+04	3.333E+09	6.001E+05	7.850E+00-1.000E+11	3.182E-02	IRON FLYER	5 N 8	22	
23	4.054E-03	8.919E-02		2.500E+04	3.333E+09	6.001E+05	7.850E+00-1.000E+11	3.182E-02	IRON FLYER	5 N 8	23	
24	4.054E-03	9.325E-02		2.500E+04	3.333E+09	6.001E+05	7.850E+00-1.000E+11	3.182E-02	IRON FLYER	5 N 8	24	
25	4.054E-03	9.730E-02		2.500E+04	3.333E+09	6.001E+05	7.850E+00-1.000E+11	3.182E-02	IRON FLYER	5 N 8	25	
26	4.054E-03	1.014E-01		2.500E+04	3.333E+09	6.001E+05	7.850E+00-1.000E+11	3.182E-02	IRON FLYER	5 N 8	26	
27	4.054E-03	1.054E-01		2.500E+04	3.333E+09	6.001E+05	7.850E+00-1.000E+11	3.182E-02	IRON FLYER	5 N 8	27	
28	4.054E-03	1.095E-01		2.500E+04	3.333E+09	6.001E+05	7.850E+00-1.000E+11	3.182E-02	IRON FLYER	5 N 8	28	
29	4.054E-03	1.135E-01		2.500E+04	3.333E+09	6.001E+05	7.850E+00-1.000E+11	3.182E-02	IRON FLYER	5 N 8	29	
30	4.054E-03	1.176E-01		2.500E+04	3.333E+09	6.001E+05	7.850E+00-1.000E+11	3.182E-02	IRON FLYER	5 N 8	30	
31	4.054E-03	1.216E-01		2.500E+04	3.333E+09	6.001E+05	7.850E+00-1.000E+11	3.182E-02	IRON FLYER	5 N 8	31	
32	4.054E-03	1.257E-01		2.500E+04	3.333E+09	6.001E+05	7.850E+00-1.000E+11	3.182E-02	IRON FLYER	5 N 8	32	
33	4.054E-03	1.297E-01		2.500E+04	3.333E+09	6.001E+05	7.850E+00-1.000E+11	3.182E-02	IRON FLYER	5 N 8	33	
34	4.054E-03	1.338E-01		2.500E+04	3.333E+09	6.001E+05	7.850E+00-1.000E+11	3.182E-02	IRON FLYER	5 N 8	34	
35	4.054E-03	1.378E-01		2.500E+04	3.333E+09	6.001E+05	7.850E+00-1.000E+11	3.182E-02	IRON FLYER	5 N 8	35	
36	4.054E-03	1.419E-01		2.500E+04	3.333E+09	6.001E+05	7.850E+00-1.000E+11	3.182E-02	IRON FLYER	5 N 8	36	
37	4.054E-03	1.459E-01		2.500E+04	3.333E+09	6.001E+05	7.850E+00-1.000E+11	3.182E-02	IRON FLYER	5 N 8	37	
38	4.054E-03	1.500E-01		2.500E+04	3.333E+09	6.001E+05	7.850E+00-1.000E+11	3.182E-02	IRON FLYER	5 N 8	38	
39	4.054E-03	1.541E-01		2.500E+04	3.333E+09	6.001E+05	7.850E+00-1.000E+11	3.182E-02	IRON FLYER	5 N 8	39	
40	4.054E-03	1.581E-01		2.500E+04	3.333E+09	6.001E+05	7.850E+00-1.000E+11	3.182E-02	IRON FLYER	5 N 8	40	
41	4.054E-03	1.622E-01		2.500E+04	3.333E+09	6.001E+05	7.850E+00-1.000E+11	3.182E-02	IRON FLYER	5 N 8	41	
42	4.054E-03	1.662E-01		2.500E+04	3.333E+09	6.001E+05	7.850E+00-1.000E+11	3.182E-02	IRON FLYER	5 N 8	42	
43	4.054E-03	1.703E-01		2.500E+04	3.333E+09	6.001E+05	7.850E+00-1.000E+11	3.182E-02	IRON FLYER	5 N 8	43	
44	4.054E-03	1.743E-01		2.500E+04	3.333E+09	6.001E+05	7.850E+00-1.000E+11	3.182E-02	IRON FLYER	5 N 8	44	
45	4.054E-03	1.784E-01		2.500E+04	3.333E+09	6.001E+05	7.850E+00-1.000E+11	3.182E-02	IRON FLYER	5 N 8	45	
46	4.054E-03	1.824E-01		2.500E+04	3.333E+09	6.001E+05	7.850E+00-1.000E+11	3.182E-02	IRON FLYER	5 N 8	46	
47	4.054E-03	1.865E-01		2.500E+04	3.333E+09	6.001E+05	7.850E+00-1.000E+11	3.182E-02	IRON FLYER	5 N 8	47	
48	4.054E-03	1.905E-01		2.500E+04	3.333E+09	6.001E+05	7.850E+00-1.000E+11	3.182E-02	IRON FLYER	5 N 8	48	
49	4.054E-03	1.946E-01		2.500E+04	3.333E+09	6.001E+05	7.850E+00-1.000E+11	3.182E-02	IRON FLYER	5 N 8	49	
50	4.054E-03	1.986E-01		2.500E+04	3.333E+09	6.001E+05	7.850E+00-1.000E+11	3.182E-02	IRON FLYER	5 N 8	50	

TEST 5: PORTION OF COORDINATE LAYOUT

MOMENTUM EDIT

CYCLE	TIME	UTM	JTS	ETOTAL	JFM	JSTAR	JSMAX	SMAX	X(JSMAX)								
211	8.0337E-07	4.5557E-09	150	3.5049E-01	299	291	194	5.2674E-10	7.6639E-01								
DIPP	OTPLS	ENWEO	ENWPO	ENWPL	ENWPR	ENWPP	ENWOM	POTPOS	POTHEG								
2.2778E-06	1.8424E-06	0.	1.1775E-05	9.7051E-04	2.2671E-04	1.1972E-05	0.	0.	0.								
X(JRND1)	X(JRND2)	X(JRND3)	X(JRND4)	X(JRND5)	JRND6	RMAX	X(JRMAX)										
2.0084E-02	6.1066E-01	1.2000E+00	0.	1.2000E+00	193	5.2676E-10	7.6639E-01										
TIME EDIT NO. 6 AT M = 211, TIME = 8.0337E-07 SECS, JSTAR = 291, CALC TIME IS 222.558 SECS																	
J	CELL	A	U	K	P	S	EHL	D	C	J	COMP	Y	MM	MU	SD	OR	NT
1	0.02084	25000	0.	0.	0.	0.	7.468E-14	7.8516	6.0012E-05	1	S	A	IRON	FLYER	5.000E+00	2.874E-03	1
2	0.04138	25000	7.794E+00	4.800E+00	7.794E+00	0.	2.049E-12	7.8500	6.0004E-05	2	S	N	IRON	FLYER	5.000E+00	2.874E-03	2
3	0.08192	25000	2.959E+01	1.603E+01	2.959E+01	9.585E-01	3.671E-10	7.8500	6.0004E-05	3	S	N	IRON	FLYER	5.000E+00	2.874E-03	3
4	0.02246	25000	1.096E+02	2.193E+02	3.568E+02	5.061E-09	5.061E-09	7.8500	6.0004E-05	4	S	N	IRON	FLYER	5.000E+00	2.874E-03	4
5	0.06398	25000	4.864E+02	7.844E+02	1.273E+03	6.365E-08	6.365E-08	7.8500	6.0004E-05	5	S	N	IRON	FLYER	5.000E+00	2.874E-03	5
6	0.04355	25000	1.456E+03	2.402E+03	4.353E+03	7.320E-07	7.320E-07	7.8500	6.0004E-05	6	S	N	IRON	FLYER	5.000E+00	2.874E-03	6
7	0.04409	25000	4.942E+03	8.764E+03	1.423E+04	7.365E-06	7.365E-06	7.8500	6.0004E-05	7	S	N	IRON	FLYER	5.000E+00	2.874E-03	7
8	0.08463	25000	1.610E+04	2.737E+04	4.435E+04	7.365E-05	7.365E-05	7.8500	6.0004E-05	8	S	N	IRON	FLYER	5.000E+00	2.874E-03	8
9	0.02517	25000	5.012E+04	8.164E+04	1.325E+05	6.839E-04	6.839E-04	7.8500	6.0004E-05	9	S	N	IRON	FLYER	5.000E+00	2.874E-03	9
10	0.05657	25000	1.690E+05	2.327E+05	3.777E+05	5.136E-03	5.136E-03	7.8500	6.0004E-05	10	S	N	IRON	FLYER	5.000E+00	2.874E-03	10
11	0.06679	25000	4.232E+05	6.335E+05	1.020E+06	3.730E-02	3.730E-02	7.8500	6.0004E-05	11	S	N	IRON	FLYER	5.000E+00	2.874E-03	11
12	0.04625	25000	1.168E+06	1.647E+06	2.674E+06	2.401E-01	2.401E-01	7.8500	6.0004E-05	12	S	N	IRON	FLYER	5.000E+00	2.874E-03	12
13	0.08733	24999	2.975E+06	4.092E+06	6.643E+06	1.502E+00	1.502E+00	7.8500	6.0003E-05	13	S	N	IRON	FLYER	5.000E+00	2.874E-03	13
14	0.07287	24998	7.363E+06	1.047E+07	1.576E+07	4.173E+01	4.173E+01	7.8501	6.0003E-05	14	S	N	IRON	FLYER	5.000E+00	2.874E-03	14
15	0.07681	24996	1.740E+07	2.400E+07	3.725E+07	1.917E+02	1.917E+02	7.8502	6.0003E-05	15	S	N	IRON	FLYER	5.000E+00	2.874E-03	15
16	0.08495	24992	3.926E+07	4.759E+07	7.725E+07	1.917E+02	1.917E+02	7.8504	6.0003E-05	16	S	N	IRON	FLYER	5.000E+00	2.874E-03	16
17	0.04949	24984	1.739E+08	9.627E+07	1.595E+08	1.074E+03	1.074E+03	7.8509	6.0002E-05	17	S	N	IRON	FLYER	5.000E+00	2.874E-03	17
18	0.09305	24930	3.412E+08	1.937E+08	3.144E+08	1.074E+03	1.074E+03	7.8516	6.0002E-05	18	S	N	IRON	FLYER	5.000E+00	2.874E-03	18
19	0.07110	24868	6.387E+08	3.642E+08	5.912E+08	1.060E+09	1.060E+09	7.8529	6.0001E-05	19	S	N	IRON	FLYER	5.000E+00	2.874E-03	19
20	0.11163	24765	1.139E+09	6.530E+08	1.060E+09	3.313E+04	3.313E+04	7.8529	6.0001E-05	20	S	N	IRON	FLYER	5.000E+00	2.874E-03	20
21	0.10215	24600	1.937E+09	1.116E+09	1.819E+09	9.452E+04	9.452E+04	7.8550	5.9997E-05	21	S	N	IRON	FLYER	5.000E+00	2.874E-03	21
22	0.10266	24352	3.133E+09	1.814E+09	2.944E+09	2.442E+05	2.442E+05	7.8626	5.9992E-05	22	S	N	IRON	FLYER	5.000E+00	2.874E-03	22
23	0.13314	24042	4.819E+09	2.807E+09	4.553E+09	5.704E+05	5.704E+05	7.8686	5.9986E-05	23	S	N	IRON	FLYER	5.000E+00	2.874E-03	23
24	0.13360	23539	7.043E+09	4.127E+09	6.694E+09	1.203E+06	1.203E+06	7.8760	5.9978E-05	24	S	N	IRON	FLYER	5.000E+00	2.874E-03	24
25	0.12441	22969	9.778E+09	5.760E+09	9.350E+09	2.290E+06	2.290E+06	7.8845	5.9955E-05	25	S	N	IRON	FLYER	5.000E+00	2.874E-03	25
26	0.12441	22316	1.290E+10	7.661E+09	1.243E+10	3.938E+06	3.938E+06	7.8935	5.9942E-05	26	S	N	IRON	FLYER	5.000E+00	2.874E-03	26
27	0.12441	21626	1.619E+10	9.681E+09	1.568E+10	6.135E+06	6.135E+06	7.9024	5.9924E-05	27	S	N	IRON	FLYER	5.000E+00	2.874E-03	27
28	0.13305	20955	1.937E+10	1.167E+10	1.888E+10	8.707E+06	8.707E+06	7.9105	5.9917E-05	28	S	N	IRON	FLYER	5.000E+00	2.874E-03	28
29	0.17530	20351	2.221E+10	1.348E+10	2.176E+10	1.406E+07	1.406E+07	7.9177	5.9907E-05	29	S	N	IRON	FLYER	5.000E+00	2.874E-03	29
30	0.17530	19821	2.467E+10	1.508E+10	2.429E+10	1.681E+07	1.681E+07	7.9243	5.9897E-05	30	S	N	IRON	FLYER	5.000E+00	2.874E-03	30
31	0.15569	19339	2.680E+10	1.655E+10	2.653E+10	1.972E+07	1.972E+07	7.9300	5.9888E-05	31	S	N	IRON	FLYER	5.000E+00	2.874E-03	31
32	0.15569	18873	2.959E+10	1.798E+10	2.865E+10	2.289E+07	2.289E+07	7.9371	5.9878E-05	32	S	N	IRON	FLYER	5.000E+00	2.874E-03	32
33	0.15395	18404	3.111E+10	1.944E+10	3.077E+10	2.637E+07	2.637E+07	7.9438	5.9869E-05	33	S	N	IRON	FLYER	5.000E+00	2.874E-03	33
34	0.15395	17928	3.325E+10	2.093E+10	3.290E+10	2.637E+07	2.637E+07	7.9506	5.9859E-05	34	S	N	IRON	FLYER	5.000E+00	2.874E-03	34
35	0.17607	17451	3.538E+10	2.244E+10	3.503E+10	3.346E+07	3.346E+07	7.9571	5.9850E-05	35	S	N	IRON	FLYER	5.000E+00	2.874E-03	35
36	0.19608	16941	3.742E+10	2.392E+10	3.708E+10	3.759E+07	3.759E+07	7.9633	5.9840E-05	36	S	N	IRON	FLYER	5.000E+00	2.874E-03	36
37	0.19608	16562	3.931E+10	2.530E+10	3.901E+10	4.110E+07	4.110E+07	7.9689	5.9833E-05	37	S	N	IRON	FLYER	5.000E+00	2.874E-03	37
38	0.13601	16175	4.100E+10	2.656E+10	4.073E+10	4.431E+07	4.431E+07	7.9739	5.9825E-05	38	S	N	IRON	FLYER	5.000E+00	2.874E-03	38
39	0.17593	15836	4.247E+10	2.768E+10	4.224E+10	4.717E+07	4.717E+07	7.9782	5.9819E-05	39	S	N	IRON	FLYER	5.000E+00	2.874E-03	39
40	0.191583	15544	4.373E+10	2.864E+10	4.352E+10	4.968E+07	4.968E+07	7.9818	5.9814E-05	40	S	N	IRON	FLYER	5.000E+00	2.874E-03	40
41	0.19571	15296	4.478E+10	2.947E+10	4.461E+10	5.188E+07	5.188E+07	7.9818	5.9814E-05	41	S	N	IRON	FLYER	5.000E+00	2.874E-03	41
42	0.19571	15086	4.567E+10	3.018E+10	4.553E+10	5.188E+07	5.188E+07	7.9850	5.9809E-05	42	S	N	IRON	FLYER	5.000E+00	2.874E-03	42
43	0.19554	15086	4.567E+10	3.018E+10	4.553E+10	5.188E+07	5.188E+07	7.9850	5.9809E-05	43	S	N	IRON	FLYER	5.000E+00	2.874E-03	43

TEST 5: FINAL MOMENTUM EDIT AND PORTION OF TIME EDIT

44	193542	14907	4.642E+10	3.079E+10	4.629E+10	5.380E+07	7.9877	5.980E+05	44	S	N	A	IRON	FLYER	3.278E-01	5.172E-03
45	197526	14754	4.703E+10	3.131E+10	4.755E+10	5.540E+07	7.9900	5.9801E+05	45	S	N	A	IRON	FLYER	2.949E-01	5.383E-03
46	201508	14623	4.759E+10	3.177E+10	4.750E+10	5.695E+07	7.9920	5.9799E+05	46	S	N	A	IRON	FLYER	2.673E-01	5.419E-03
47	205499	14509	4.805E+10	3.216E+10	4.797E+10	5.826E+07	7.9938	5.9799E+05	47	S	N	A	IRON	FLYER	2.441E-01	5.527E-03
48	209471	14410	4.845E+10	3.251E+10	4.834E+10	5.942E+07	7.9954	5.9799E+05	48	S	N	A	IRON	FLYER	2.242E-01	5.627E-03
49	213451	14322	4.880E+10	3.282E+10	4.874E+10	6.046E+07	7.9967	5.9799E+05	49	S	N	A	IRON	FLYER	2.072E-01	5.720E-03
50	217430	14245	4.911E+10	3.311E+10	4.906E+10	6.140E+07	7.9980	5.9799E+05	50	S	N	A	IRON	FLYER	1.924E-01	5.807E-03
51	221409	14176	4.938E+10	3.335E+10	4.933E+10	6.225E+07	7.9991	5.9788E+05	51	S	N	A	IRON	FLYER	1.794E-01	5.889E-03
52	225387	14114	4.962E+10	3.357E+10	4.958E+10	6.302E+07	8.0001	5.9788E+05	52	S	N	A	IRON	FLYER	1.681E-01	5.965E-03
53	229365	14058	4.984E+10	3.378E+10	4.980E+10	6.373E+07	8.0010	5.9788E+05	53	S	N	A	IRON	FLYER	1.580E-01	6.038E-03
54	233342	14007	5.003E+10	3.396E+10	5.000E+10	6.438E+07	8.0018	5.9788E+05	54	S	N	A	IRON	FLYER	1.490E-01	6.104E-03
55	237319	13961	5.021E+10	3.413E+10	5.017E+10	6.498E+07	8.0026	5.9788E+05	55	S	N	A	IRON	FLYER	1.409E-01	6.171E-03
56	241296	13919	5.037E+10	3.429E+10	5.034E+10	6.554E+07	8.0033	5.9788E+05	56	S	N	A	IRON	FLYER	1.337E-01	6.232E-03
57	245272	13880	5.051E+10	3.444E+10	5.048E+10	6.606E+07	8.0039	5.9788E+05	57	S	N	A	IRON	FLYER	1.271E-01	6.291E-03
58	249248	13844	5.064E+10	3.457E+10	5.062E+10	6.654E+07	8.0045	5.9788E+05	58	S	N	A	IRON	FLYER	1.211E-01	6.347E-03
59	253224	13812	5.076E+10	3.470E+10	5.074E+10	6.699E+07	8.0051	5.9788E+05	59	S	N	A	IRON	FLYER	1.157E-01	6.400E-03
60	257199	13782	5.087E+10	3.481E+10	5.085E+10	6.742E+07	8.0056	5.9779E+05	60	S	N	A	IRON	FLYER	1.107E-01	6.451E-03
61	261174	13754	5.097E+10	3.492E+10	5.095E+10	6.781E+07	8.0060	5.9779E+05	61	S	N	A	IRON	FLYER	1.061E-01	6.500E-03
62	265149	13729	5.106E+10	3.502E+10	5.104E+10	6.818E+07	8.0065	5.9779E+05	62	S	N	A	IRON	FLYER	1.019E-01	6.547E-03
63	269124	13705	5.114E+10	3.511E+10	5.112E+10	6.853E+07	8.0068	5.9779E+05	63	S	N	A	IRON	FLYER	9.804E-02	6.592E-03
64	273098	13684	5.121E+10	3.520E+10	5.120E+10	6.885E+07	8.0073	5.9779E+05	64	S	N	A	IRON	FLYER	9.443E-02	6.635E-03
65	277073	13663	5.128E+10	3.528E+10	5.126E+10	6.916E+07	8.0076	5.9779E+05	65	S	N	A	IRON	FLYER	9.108E-02	6.677E-03
66	281047	13644	5.134E+10	3.536E+10	5.133E+10	6.945E+07	8.0080	5.9779E+05	66	S	N	A	IRON	FLYER	8.796E-02	6.717E-03
67	285021	13626	5.140E+10	3.543E+10	5.139E+10	6.972E+07	8.0083	5.9779E+05	67	S	N	A	IRON	FLYER	8.505E-02	6.755E-03
68	288995	13608	5.146E+10	3.551E+10	5.145E+10	6.998E+07	8.0086	5.9779E+05	68	S	N	A	IRON	FLYER	8.235E-02	6.793E-03
69	292968	13591	5.152E+10	3.558E+10	5.151E+10	7.025E+07	8.0090	5.9779E+05	69	S	N	A	IRON	FLYER	7.983E-02	6.829E-03
70	296942	13575	5.157E+10	3.565E+10	5.156E+10	7.052E+07	8.0093	5.9779E+05	70	S	N	A	IRON	FLYER	7.745E-02	6.863E-03
71	300915	13559	5.162E+10	3.571E+10	5.161E+10	7.077E+07	8.0096	5.9779E+05	71	S	N	A	IRON	FLYER	7.518E-02	6.897E-03
72	304888	13544	5.167E+10	3.577E+10	5.166E+10	7.101E+07	8.0098	5.9779E+05	72	S	N	A	IRON	FLYER	7.302E-02	6.931E-03
73	308862	13530	5.172E+10	3.583E+10	5.171E+10	7.123E+07	8.0101	5.9779E+05	73	S	N	A	IRON	FLYER	7.090E-02	6.963E-03
74	312835	13517	5.176E+10	3.588E+10	5.175E+10	7.145E+07	8.0103	5.9779E+05	74	S	N	A	IRON	FLYER	6.906E-02	6.995E-03
75	316807	13504	5.180E+10	3.593E+10	5.179E+10	7.165E+07	8.0105	5.9779E+05	75	S	N	A	IRON	FLYER	6.724E-02	7.026E-03
76	320780	13492	5.184E+10	3.598E+10	5.183E+10	7.185E+07	8.0108	5.9779E+05	76	S	N	A	IRON	FLYER	6.553E-02	7.055E-03
77	324753	13481	5.187E+10	3.603E+10	5.187E+10	7.205E+07	8.0110	5.9779E+05	77	S	N	A	IRON	FLYER	6.391E-02	7.084E-03
78	328725	13470	5.191E+10	3.608E+10	5.190E+10	7.224E+07	8.0112	5.9779E+05	78	S	N	A	IRON	FLYER	6.236E-02	7.112E-03
79	332698	13460	5.194E+10	3.612E+10	5.193E+10	7.242E+07	8.0114	5.9779E+05	79	S	N	A	IRON	FLYER	6.090E-02	7.139E-03
80	336670	13450	5.197E+10	3.616E+10	5.196E+10	7.260E+07	8.0116	5.9779E+05	80	S	N	A	IRON	FLYER	5.950E-02	7.166E-03
81	340642	13441	5.199E+10	3.621E+10	5.199E+10	7.277E+07	8.0117	5.9779E+05	81	S	N	A	IRON	FLYER	5.816E-02	7.192E-03
82	344615	13431	5.202E+10	3.625E+10	5.201E+10	7.294E+07	8.0119	5.9779E+05	82	S	N	A	IRON	FLYER	5.689E-02	7.217E-03
83	348587	13423	5.205E+10	3.629E+10	5.204E+10	7.311E+07	8.0121	5.9779E+05	83	S	N	A	IRON	FLYER	5.567E-02	7.242E-03
84	352559	13414	5.207E+10	3.632E+10	5.206E+10	7.327E+07	8.0123	5.9779E+05	84	S	N	A	IRON	FLYER	5.450E-02	7.266E-03
85	356531	13406	5.209E+10	3.636E+10	5.209E+10	7.343E+07	8.0124	5.9779E+05	85	S	N	A	IRON	FLYER	5.338E-02	7.289E-03
86	360502	13398	5.212E+10	3.640E+10	5.211E+10	7.359E+07	8.0126	5.9779E+05	86	S	N	A	IRON	FLYER	5.231E-02	7.313E-03
87	364474	13390	5.214E+10	3.643E+10	5.213E+10	7.374E+07	8.0127	5.9779E+05	87	S	N	A	IRON	FLYER	5.128E-02	7.336E-03
88	368446	13383	5.216E+10	3.647E+10	5.215E+10	7.389E+07	8.0129	5.9779E+05	88	S	N	A	IRON	FLYER	5.029E-02	7.358E-03
89	372417	13376	5.218E+10	3.650E+10	5.217E+10	7.403E+07	8.0130	5.9779E+05	89	S	N	A	IRON	FLYER	4.934E-02	7.380E-03
90	376389	13369	5.219E+10	3.653E+10	5.219E+10	7.417E+07	8.0132	5.9779E+05	90	S	N	A	IRON	FLYER	4.843E-02	7.401E-03
91	380360	13363	5.221E+10	3.656E+10	5.221E+10	7.431E+07	8.0133	5.9779E+05	91	S	N	A	IRON	FLYER	4.755E-02	7.422E-03
92	384332	13356	5.223E+10	3.659E+10	5.222E+10	7.445E+07	8.0134	5.9779E+05	92	S	N	A	IRON	FLYER	4.670E-02	7.442E-03
93	388303	13350	5.224E+10	3.662E+10	5.224E+10	7.458E+07	8.0136	5.9779E+05	93	S	N	A	IRON	FLYER	4.586E-02	7.462E-03
94	392274	13344	5.226E+10	3.665E+10	5.225E+10	7.471E+07	8.0137	5.9779E+05	94	S	N	A	IRON	FLYER	4.509E-02	7.482E-03
95	396246	13338	5.227E+10	3.667E+10	5.227E+10	7.484E+07	8.0138	5.9779E+05	95	S	N	A	IRON	FLYER	4.433E-02	7.502E-03
96	400217	13333	5.229E+10	3.670E+10	5.228E+10	7.497E+07	8.0139	5.9779E+05	96	S	N	A	IRON	FLYER	4.360E-02	7.521E-03
97	404188	13327	5.230E+10	3.673E+10	5.230E+10	7.510E+07	8.0140	5.9779E+05	97	S	N	A	IRON	FLYER	4.289E-02	7.539E-03
98	408159	13322	5.231E+10	3.675E+10	5.231E+10	7.522E+07	8.0141	5.9779E+05	98	S	N	A	IRON	FLYER	4.220E-02	7.558E-03
99	412130	13317	5.232E+10	3.677E+10	5.232E+10	7.534E+07	8.0142	5.9779E+05	99	S	N	A	IRON	FLYER	4.154E-02	7.576E-03
100	416101	13312	5.233E+10	3.680E+10	5.233E+10	7.547E+07	8.0143	5.9779E+05	100	S	N	A	IRON	FLYER	4.090E-02	7.593E-03
101	420072	13307	5.234E+10	3.682E+10	5.234E+10	7.559E+07	8.0144	5.9779E+05	101	S	N	A	IRON	FLYER	4.027E-02	7.611E-03

TEST 5: FINAL TIME EDIT (continued)



SCRIBE OUTPUT: TIME IN MICROSECS. S IF KRAVS. DTIM IN NANSECS. DELTIM IN SECS									
N	TIME	S12/SOJ1	S23/SOJ2	S34/SOJ3	S ( 53 )	S ( 65 )	S (117)	S (162)	S (244)
51	.135	53.284	0.000	0.000	0.000	0.000	0.000	0.000	0.000
52	.135	53.283	0.000	0.000	0.000	0.000	0.000	0.000	0.000
53	.136	53.282	0.000	0.000	0.000	0.000	0.000	0.000	0.000
54	.136	53.281	0.000	0.000	0.000	0.000	0.000	0.000	0.000
55	.137	53.194	0.000	0.000	0.000	0.000	0.000	0.000	0.000
56	.138	53.194	0.000	0.000	0.000	0.000	0.000	0.000	0.000
57	.139	53.196	0.000	0.000	0.000	0.000	0.000	0.000	0.000
58	.140	53.194	0.000	0.000	0.000	0.000	0.000	0.000	0.000
59	.142	53.191	0.000	0.000	0.000	0.000	0.000	0.000	0.000
60	.144	53.188	0.000	0.000	0.000	0.000	0.000	0.000	0.000
61	.144	53.185	0.000	0.000	0.000	0.000	0.000	0.000	0.000
62	.148	53.181	0.000	0.000	0.000	0.000	0.000	0.000	0.000
63	.151	53.176	0.000	0.000	0.000	0.000	0.000	0.000	0.000
64	.155	53.170	0.000	0.000	0.000	0.000	0.000	0.000	0.000
65	.159	53.163	0.000	0.000	0.000	0.000	0.000	0.000	0.000
66	.164	53.159	0.000	0.000	0.000	0.000	0.000	0.000	0.000
67	.169	53.155	0.000	0.000	0.000	0.000	0.000	0.000	0.000
68	.173	53.151	0.000	0.000	0.000	0.000	0.000	0.000	0.000
69	.178	53.144	0.000	0.000	0.000	0.000	0.000	0.000	0.000
70	.182	53.141	0.000	0.000	0.000	0.000	0.000	0.000	0.000
71	.187	53.140	0.000	0.000	0.000	0.000	0.000	0.000	0.000
72	.192	53.140	0.000	0.000	0.000	0.000	0.000	0.000	0.000
73	.196	53.139	0.000	0.000	0.000	0.000	0.000	0.000	0.000
74	.201	53.141	0.000	0.000	0.000	0.000	0.000	0.000	0.000
75	.205	53.144	0.000	0.000	0.000	0.000	0.000	0.000	0.000
76	.210	53.149	0.000	0.000	0.000	0.000	0.000	0.000	0.000
77	.214	53.152	0.000	0.000	0.000	0.000	0.000	0.000	0.000
78	.219	53.154	0.000	0.000	0.000	0.000	0.000	0.000	0.000
79	.223	53.152	0.000	0.000	0.000	0.000	0.000	0.000	0.000
80	.228	53.146	0.000	0.000	0.000	0.000	0.000	0.000	0.000
81	.232	53.137	0.000	0.000	0.000	0.000	0.000	0.000	0.000
82	.237	53.125	0.000	0.000	0.000	0.000	0.000	0.000	0.000
83	.241	53.111	0.000	0.000	0.000	0.000	0.000	0.000	0.000
84	.246	53.094	0.000	0.000	0.000	0.000	0.000	0.000	0.000
85	.251	53.075	0.000	0.000	0.000	0.000	0.000	0.000	0.000
86	.255	53.051	0.000	0.000	0.000	0.000	0.000	0.000	0.000
87	.260	53.020	0.000	0.000	0.000	0.000	0.000	0.000	0.000
88	.264	52.991	0.000	0.000	0.000	0.000	0.000	0.000	0.000
89	.267	52.961	0.000	0.000	0.000	0.000	0.000	0.000	0.000
90	.270	52.939	0.000	0.000	0.000	0.000	0.000	0.000	0.000
91	.273	52.921	0.000	0.000	0.000	0.000	0.000	0.000	0.000
92	.276	52.914	0.000	0.000	0.000	0.000	0.000	0.000	0.000
93	.282	52.922	0.000	0.000	0.000	0.000	0.000	0.000	0.000
94	.287	52.934	0.000	0.000	0.000	0.000	0.000	0.000	0.000
95	.292	52.947	0.000	0.000	0.000	0.000	0.000	0.000	0.000
96	.296	52.954	0.000	0.000	0.000	0.000	0.000	0.000	0.000
97	.301	52.964	0.000	0.000	0.000	0.000	0.000	0.000	0.000
98	.305	52.963	0.000	0.000	0.000	0.000	0.000	0.000	0.000
99	.310	52.959	0.000	0.000	0.000	0.000	0.000	0.000	0.000
100	.314	52.952	0.000	0.000	0.000	0.000	0.000	0.000	0.000

TEST 5: STRESS HISTORIES (continued)

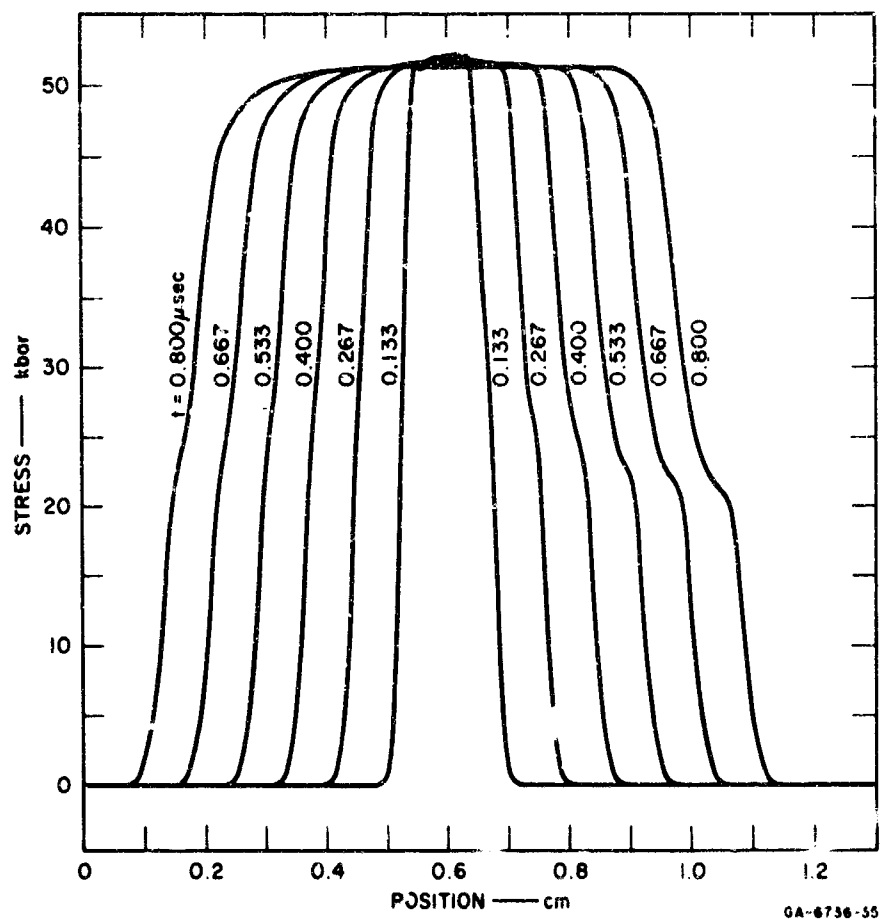


FIGURE 57 TEST 5: SUMMARY PLOT OF TIME EDITS

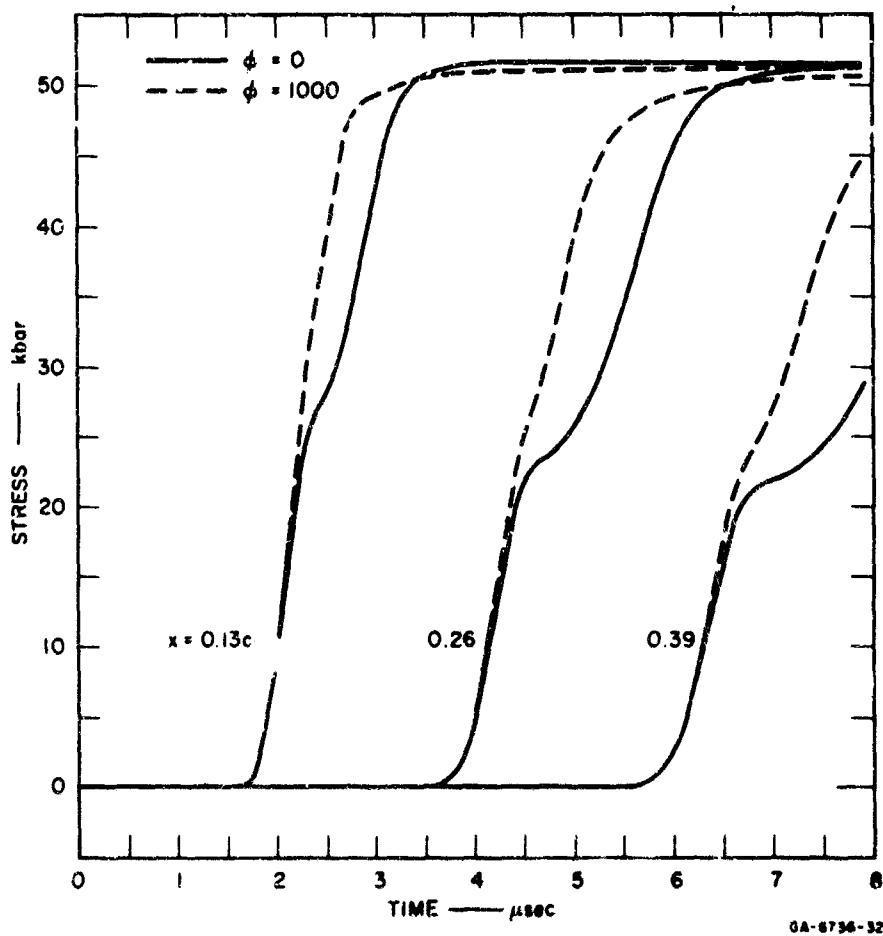


FIGURE 68 TEST 5: SUMMARY OF STRESS HISTORIES AT SIX JET LOCATIONS

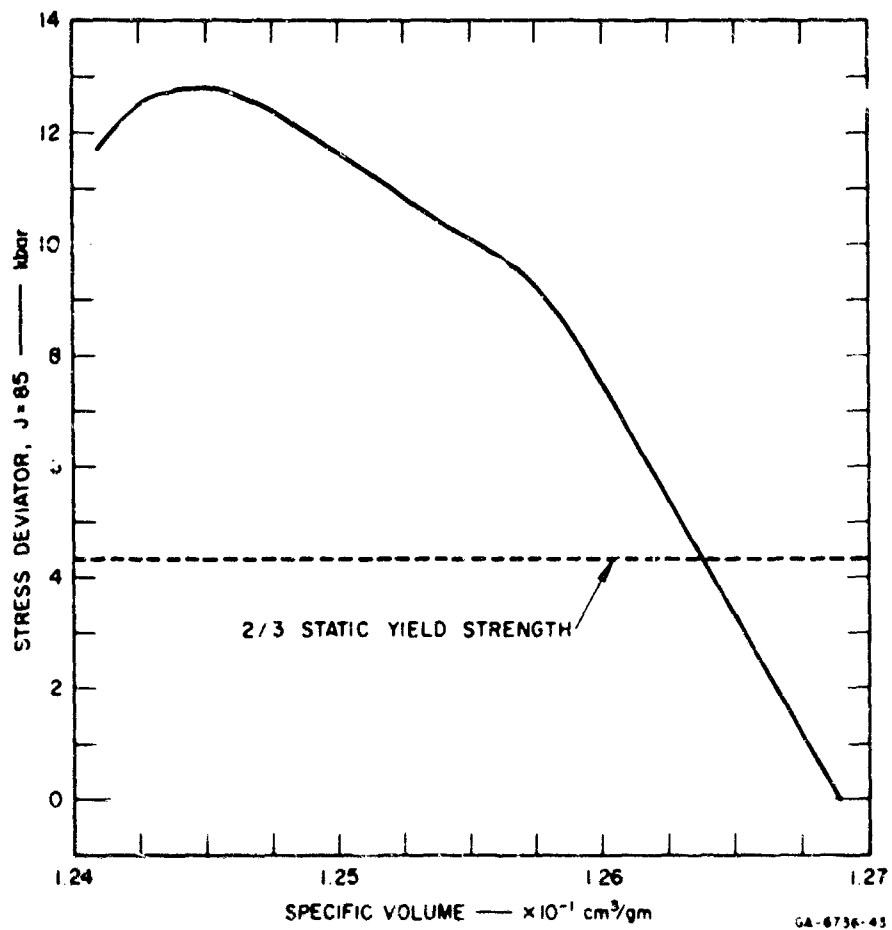


FIGURE 59 TEST 5: SAMPLE PLOT OF STRESS DEVIATOR



h. Test No. 6

The stress relaxation mechanism of Model 4 (two parameters, variable yield model) is tested in Test 6. The configuration is a symmetric impact between two plates of 2024-T8 aluminum. The plates have different relaxation parameters but are otherwise identical. The listing included on the following pages contains the input data, and portions of the initial layout, and final EDIT and stress histories. The EDITs, stress histories, and a deviatoric stress-volume path are shown in the figures.

\*\*\* SRI PUFF 1 (6400 VERSION) \*\*\*

DATE =04/28/69

IDENT = 6 MODEL 4: TWO-PARAMETER, VARIABLE YIELD RELAXATION MODEL  
IMPACT OF TWO 2024-T3 ALUMINUM PLATES, EACH DESCRIBED BY THE TWO-PARAMETER  
YIELD MODEL. THE TWO PLATES HAVE DIFFERENT VALUES OF THE YIELD RELAXATION  
TIME,  $\tau$ , BUT ALL OTHER PARAMETERS ARE THE SAME.

1 NTEDT= 5 NJEDIT= 6 NREZON= 0 NSEPRAT= 0  
2 TEDIT= 5.000E-07 1.000E-06 1.500E-06 2.000E-06 2.500E-06  
3 JEDIT= 30 75 112 187 224 261  
6 NEDTM= 100000 NEDIT= 10000 NPERM = 1 -0  
7 STOPS JCYS = 1250 CKS = 4.000E+00 TS = 2.000E-06  
8 NMYRL= 2 NATFL = 1 UZERO = 2.000E+04 IPLOT = 1

AL FLYER RMOS = 2.705E+00 NSRM = 4 NYAM = 1 NPOR = 0 NCON = 0  
EOSTC = 7.550E+11 EOSTD = 1.290E+12 EOSTE = 1.220E+11 EOSTG = 2.040E+00  
EOSTH = 2.500E-01 EOSTS = 1.197E+12 1.000E+00 7.929E-12  
C0S0 = 4.000E+00 C1 = 1.500E-01 C2 = 0.  
TENS(1) = -1.000E+11 TENS(2) = -1.000E+11 TENS(3) = -1.000E+11  
PALK = 1.000E-07 TY = 1.000E-07 -0.  
Y0 = 2.500E+09 MU = 2.870E+11 YADD = 0.  
NZONE= 1, 148 CELLS IN 2.000E+00 CM -0.

AL TARGE! RMOS = 2.705E+00 NSRM = 4 NYAM = 1 NPOR = 0 NCON = 0  
EOSTC = 7.550E+11 EOSTD = 1.290E+12 EOSTE = 1.220E+11 EOSTG = 2.040E+00  
EOSTH = 2.500E-01 EOSTS = 1.197E+12 1.000E+00 7.929E-12  
C0S0 = 4.000E+00 C1 = 1.500E-01 C2 = 0.  
TENS(1) = -1.000E+11 TENS(2) = -1.000E+11 TENS(3) = -1.000E+11  
PALK = 1.000E-07 TY = 5.000E-08 -0.  
Y0 = 2.500E+09 MU = 2.870E+11 YADD = 0.  
NZONE= 1, 148 CELLS IN 2.000E+00 CM -0.

TEST 6: INPUT DATA

J	GA	RT(J)	U(J)	VM(J)	C(J)	OT(J)	T(J)	ZML(J)	MATERIAL	CONV	J
1	1.26E-02	9.	2.000E-04	1.007E-09	0.304E-05	2.705E-08-1.000E-11	3.704E-02	3.704E-02	AL FLYER	5	5
2	1.26E-02	1.201E-02	2.000E-04	1.007E-09	0.304E-05	2.705E-08-1.000E-11	3.704E-02	3.704E-02	AL FLYER	5	5
3	1.26E-02	2.702E-02	2.000E-04	1.007E-09	0.304E-05	2.705E-08-1.000E-11	3.704E-02	3.704E-02	AL FLYER	5	5
4	1.26E-02	4.004E-02	2.000E-04	1.007E-09	0.304E-05	2.705E-08-1.000E-11	3.704E-02	3.704E-02	AL FLYER	5	5
5	1.26E-02	5.406E-02	2.000E-04	1.007E-09	0.304E-05	2.705E-08-1.000E-11	3.704E-02	3.704E-02	AL FLYER	5	5
6	1.26E-02	6.707E-02	2.000E-04	1.007E-09	0.304E-05	2.705E-08-1.000E-11	3.704E-02	3.704E-02	AL FLYER	5	5
7	1.26E-02	8.008E-02	2.000E-04	1.007E-09	0.304E-05	2.705E-08-1.000E-11	3.704E-02	3.704E-02	AL FLYER	5	5
8	1.26E-02	9.309E-02	2.000E-04	1.007E-09	0.304E-05	2.705E-08-1.000E-11	3.704E-02	3.704E-02	AL FLYER	5	5
9	1.26E-02	1.061E-01	2.000E-04	1.007E-09	0.304E-05	2.705E-08-1.000E-11	3.704E-02	3.704E-02	AL FLYER	5	5
10	1.26E-02	1.213E-01	2.000E-04	1.007E-09	0.304E-05	2.705E-08-1.000E-11	3.704E-02	3.704E-02	AL FLYER	5	5
11	1.26E-02	1.371E-01	2.000E-04	1.007E-09	0.304E-05	2.705E-08-1.000E-11	3.704E-02	3.704E-02	AL FLYER	5	5
12	1.26E-02	1.400E-01	2.000E-04	1.007E-09	0.304E-05	2.705E-08-1.000E-11	3.704E-02	3.704E-02	AL FLYER	5	5
13	1.26E-02	1.423E-01	2.000E-04	1.007E-09	0.304E-05	2.705E-08-1.000E-11	3.704E-02	3.704E-02	AL FLYER	5	5
14	1.26E-02	1.437E-01	2.000E-04	1.007E-09	0.304E-05	2.705E-08-1.000E-11	3.704E-02	3.704E-02	AL FLYER	5	5
15	1.26E-02	1.442E-01	2.000E-04	1.007E-09	0.304E-05	2.705E-08-1.000E-11	3.704E-02	3.704E-02	AL FLYER	5	5
16	1.26E-02	1.447E-01	2.000E-04	1.007E-09	0.304E-05	2.705E-08-1.000E-11	3.704E-02	3.704E-02	AL FLYER	5	5
17	1.26E-02	1.452E-01	2.000E-04	1.007E-09	0.304E-05	2.705E-08-1.000E-11	3.704E-02	3.704E-02	AL FLYER	5	5
18	1.26E-02	1.457E-01	2.000E-04	1.007E-09	0.304E-05	2.705E-08-1.000E-11	3.704E-02	3.704E-02	AL FLYER	5	5
19	1.26E-02	1.462E-01	2.000E-04	1.007E-09	0.304E-05	2.705E-08-1.000E-11	3.704E-02	3.704E-02	AL FLYER	5	5
20	1.26E-02	1.467E-01	2.000E-04	1.007E-09	0.304E-05	2.705E-08-1.000E-11	3.704E-02	3.704E-02	AL FLYER	5	5
21	1.26E-02	1.472E-01	2.000E-04	1.007E-09	0.304E-05	2.705E-08-1.000E-11	3.704E-02	3.704E-02	AL FLYER	5	5
22	1.26E-02	1.477E-01	2.000E-04	1.007E-09	0.304E-05	2.705E-08-1.000E-11	3.704E-02	3.704E-02	AL FLYER	5	5
23	1.26E-02	1.482E-01	2.000E-04	1.007E-09	0.304E-05	2.705E-08-1.000E-11	3.704E-02	3.704E-02	AL FLYER	5	5
24	1.26E-02	1.487E-01	2.000E-04	1.007E-09	0.304E-05	2.705E-08-1.000E-11	3.704E-02	3.704E-02	AL FLYER	5	5
25	1.26E-02	1.492E-01	2.000E-04	1.007E-09	0.304E-05	2.705E-08-1.000E-11	3.704E-02	3.704E-02	AL FLYER	5	5
26	1.26E-02	1.497E-01	2.000E-04	1.007E-09	0.304E-05	2.705E-08-1.000E-11	3.704E-02	3.704E-02	AL FLYER	5	5
27											

203

MOMENTUM EDIT

CYCLE	TIME	UTMM	JTS	ETOTAL	JFIN	JSTAR	JSHAX	SMAX	X(JSHAX)	Y	MU	SD OR NT
236	2.88043E+06	1.4060E+08	103	2.6492E+01	299	298	176	1.5010E+10	2.3733E+08	0.	0.	0.
DIP	DIPULS	EMVPE	EMVPS	EMVPL	EMVPR	EMVPP	EMVPH	POTPOS	POTNEG			
7.1451E+06	5.0053E+06	0.	1.110E+05	7.9137E+04	3.3826E+04	1.1296E+05	0.					
X(1)	X(JSHOX1)	X(JSHOX2)	X(JSHOX3)	X(JFIN)	JMAX	JMAX	X(JSHAX)					
5.615E+06	2.0201E+06	4.0000E+00	0.	4.0000E+00	176	15010E+10	2.3733E+08					
TIME EDIT NO. 6 AT M = 236. TIME = 2.60327E+06 SECS, JS AR = 298. CALC TIME IS 161.16 SECS												

TIME EDIT NO. 6 AT M = 230. TIME = 2.6027E+06 SECS. JS AR = 290. CALC TIME IS 161.146 SECS

TEST 6: FINAL MOMENTUM EDIT AND PORTION OF TIME EDIT

44	6.33321	1.270E+10	1.028E+10	1.267E+10	3.297E+07	2.8216	6.4732E+05	44	S	N	A	AL	FLYER	2.048E+09	2.444E+09
45	6.66657	1.287E+10	1.039E+10	1.284E+10	3.399E+07	2.8223	6.4747E+05	45	S	N	A	AL	FLYER	2.038E+09	2.446E+09
46	6.59991	1.303E+10	1.057E+10	1.300E+10	3.508E+07	2.8229	6.4761E+05	46	S	N	A	AL	FLYER	2.029E+09	2.430E+09
47	6.73322	1.314E+10	1.074E+10	1.316E+10	3.607E+07	2.8235	6.4775E+05	47	S	N	A	AL	FLYER	2.019E+09	2.411E+09
48	6.86653	1.334E+10	1.091E+10	1.331E+10	3.711E+07	2.8241	6.4789E+05	48	S	N	A	AL	FLYER	2.009E+09	2.392E+09
49	6.99984	1.344E+10	1.108E+10	1.345E+10	3.807E+07	2.8247	6.4803E+05	49	S	N	A	AL	FLYER	1.999E+09	2.372E+09
50	7.13315	1.362E+10	1.124E+10	1.352E+10	3.901E+07	2.8252	6.4817E+05	50	S	N	A	AL	FLYER	1.987E+09	2.351E+09
51	7.26646	1.375E+10	1.139E+10	1.359E+10	3.993E+07	2.8258	6.4831E+05	51	S	N	A	AL	FLYER	1.976E+09	2.330E+09
52	7.39977	1.388E+10	1.154E+10	1.365E+10	4.093E+07	2.8263	6.4845E+05	52	S	N	A	AL	FLYER	1.965E+09	2.308E+09
53	7.53308	1.399E+10	1.168E+10	1.372E+10	4.174E+07	2.8268	6.4859E+05	53	S	N	A	AL	FLYER	1.954E+09	2.287E+09
54	7.66639	1.411E+10	1.182E+10	1.408E+10	4.257E+07	2.8272	6.4873E+05	54	S	N	A	AL	FLYER	1.942E+09	2.265E+09
55	7.79970	1.422E+10	1.195E+10	1.419E+10	4.345E+07	2.8277	6.4887E+05	55	S	N	A	AL	FLYER	1.932E+09	2.243E+09
56	7.93301	1.432E+10	1.207E+10	1.430E+10	4.420E+07	2.8281	6.4899E+05	56	S	N	A	AL	FLYER	1.922E+09	2.221E+09
57	8.06632	1.442E+10	1.219E+10	1.440E+10	4.502E+07	2.8286	6.4908E+05	57	S	N	A	AL	FLYER	1.910E+09	2.199E+09
58	8.19963	1.451E+10	1.231E+10	1.449E+10	4.571E+07	2.8290	6.4917E+05	58	S	N	A	AL	FLYER	1.899E+09	2.177E+09
59	8.33294	1.460E+10	1.242E+10	1.458E+10	4.639E+07	2.8293	6.4926E+05	59	S	N	A	AL	FLYER	1.887E+09	2.156E+09
60	8.46625	1.468E+10	1.253E+10	1.466E+10	4.712E+07	2.8297	6.4935E+05	60	S	N	A	AL	FLYER	1.878E+09	2.134E+09
61	8.59956	1.476E+10	1.263E+10	1.474E+10	4.784E+07	2.8301	6.4942E+05	61	S	N	A	AL	FLYER	1.869E+09	2.112E+09
62	8.73287	1.483E+10	1.273E+10	1.482E+10	4.842E+07	2.8304	6.4950E+05	62	S	N	A	AL	FLYER	1.859E+09	2.093E+09
63	8.86618	1.491E+10	1.281E+10	1.489E+10	4.909E+07	2.8307	6.4957E+05	63	S	N	A	AL	FLYER	1.849E+09	2.074E+09
64	8.99949	1.499E+10	1.290E+10	1.496E+10	4.962E+07	2.8310	6.4964E+05	64	S	N	A	AL	FLYER	1.839E+09	2.054E+09
65	9.13280	1.503E+10	1.298E+10	1.502E+10	5.024E+07	2.8313	6.4970E+05	65	S	N	A	AL	FLYER	1.828E+09	2.035E+09
66	9.26611	1.509E+10	1.306E+10	1.508E+10	5.070E+07	2.8316	6.4975E+05	66	S	N	A	AL	FLYER	1.818E+09	2.016E+09
67	9.39942	1.515E+10	1.313E+10	1.514E+10	5.128E+07	2.8318	6.4980E+05	67	S	N	A	AL	FLYER	1.807E+09	1.998E+09
68	9.53273	1.520E+10	1.320E+10	1.519E+10	5.186E+07	2.8321	6.4985E+05	68	S	N	A	AL	FLYER	1.798E+09	1.979E+09
69	9.66604	1.525E+10	1.327E+10	1.524E+10	5.221E+07	2.8323	6.4990E+05	69	S	N	A	AL	FLYER	1.789E+09	1.960E+09
70	9.79935	1.529E+10	1.333E+10	1.528E+10	5.269E+07	2.8325	6.4995E+05	70	S	N	A	AL	FLYER	1.780E+09	1.941E+09
71	9.93266	1.533E+10	1.339E+10	1.532E+10	5.306E+07	2.8327	6.4999E+05	71	S	N	A	AL	FLYER	1.772E+09	1.923E+09
72	1.00589	1.537E+10	1.344E+10	1.536E+10	5.351E+07	2.8329	6.5003E+05	72	S	N	A	AL	FLYER	1.765E+09	1.905E+09
73	1.01910	1.541E+10	1.349E+10	1.540E+10	5.383E+07	2.8331	6.5007E+05	73	S	N	A	AL	FLYER	1.758E+09	1.886E+09
74	1.03231	1.544E+10	1.354E+10	1.543E+10	5.423E+07	2.8332	6.5011E+05	74	S	N	A	AL	FLYER	1.751E+09	1.873E+09
75	1.04552	1.547E+10	1.359E+10	1.546E+10	5.444E+07	2.8334	6.5015E+05	75	S	N	A	AL	FLYER	1.745E+09	1.854E+09
76	1.05873	1.550E+10	1.363E+10	1.549E+10	5.485E+07	2.8335	6.5019E+05	76	S	N	A	AL	FLYER	1.740E+09	1.836E+09
77	1.07194	1.553E+10	1.367E+10	1.552E+10	5.508E+07	2.8337	6.5023E+05	77	S	N	A	AL	FLYER	1.735E+09	1.824E+09
78	1.08515	1.555E+10	1.371E+10	1.555E+10	5.543E+07	2.8338	6.5026E+05	78	S	N	A	AL	FLYER	1.730E+09	1.814E+09
79	1.09836	1.557E+10	1.374E+10	1.557E+10	5.563E+07	2.8339	6.5029E+05	79	S	N	A	AL	FLYER	1.725E+09	1.804E+09
80	1.11157	1.559E+10	1.377E+10	1.559E+10	5.596E+07	2.8340	6.5031E+05	80	S	N	A	AL	FLYER	1.721E+09	1.794E+09
81	1.12478	1.561E+10	1.380E+10	1.561E+10	5.612E+07	2.8342	6.5031E+05	81	S	N	A	AL	FLYER	1.717E+09	1.785E+09
82	1.13799	1.563E+10	1.383E+10	1.563E+10	5.642E+07	2.8343	6.5031E+05	82	S	N	A	AL	FLYER	1.714E+09	1.777E+09
83	1.15120	1.565E+10	1.386E+10	1.565E+10	5.655E+07	2.8344	6.5031E+05	83	S	N	A	AL	FLYER	1.711E+09	1.770E+09
84	1.16441	1.566E+10	1.388E+10	1.566E+10	5.695E+07	2.8345	6.5032E+05	84	S	N	A	AL	FLYER	1.708E+09	1.762E+09
85	1.17762	1.568E+10	1.390E+10	1.568E+10	5.723E+07	2.8346	6.5032E+05	85	S	N	A	AL	FLYER	1.705E+09	1.755E+09
86	1.19083	1.569E+10	1.393E+10	1.569E+10	5.749E+07	2.8347	6.5032E+05	86	S	N	A	AL	FLYER	1.701E+09	1.748E+09
87	1.20404	1.571E+10	1.395E+10	1.571E+10	5.754E+07	2.8347	6.5032E+05	87	S	N	A	AL	FLYER	1.698E+09	1.741E+09
88	1.21725	1.572E+10	1.396E+10	1.572E+10	5.759E+07	2.8347	6.5032E+05	88	S	N	A	AL	FLYER	1.695E+09	1.734E+09
89	1.23046	1.573E+10	1.398E+10	1.573E+10	5.785E+07	2.8348	6.5032E+05	89	S	N	A	AL	FLYER	1.692E+09	1.728E+09
90	1.24367	1.574E+10	1.399E+10	1.574E+10	5.805E+07	2.8348	6.5032E+05	90	S	N	A	AL	FLYER	1.690E+09	1.723E+09
91	1.25688	1.574E+10	1.400E+10	1.574E+10	5.811E+07	2.8349	6.5032E+05	91	S	N	A	AL	FLYER	1.688E+09	1.718E+09
92	1.27009	1.574E+10	1.401E+10	1.574E+10	5.811E+07	2.8349	6.5032E+05	92	S	N	A	AL	FLYER	1.686E+09	1.714E+09
93	1.28330	1.575E+10	1.403E+10	1.575E+10	5.837E+07	2.8349	6.5032E+05	93	S	N	A	AL	FLYER	1.685E+09	1.710E+09
94	1.29651	1.576E+10	1.404E+10	1.576E+10	5.859E+07	2.8350	6.5032E+05	94	S	N	A	AL	FLYER	1.684E+09	1.706E+09
95	1.30972	1.577E+10	1.405E+10	1.577E+10	5.861E+07	2.8350	6.5032E+05	95	S	N	A	AL	FLYER	1.683E+09	1.703E+09
96	1.32293	1.577E+10	1.406E+10	1.577E+10	5.881E+07	2.8350	6.5032E+05	96	S	N	A	AL	FLYER	1.682E+09	1.700E+09
97	1.33614	1.578E+10	1.407E+10	1.578E+10	5.900E+07	2.8351	6.5032E+05	97	S	N	A	AL	FLYER	1.681E+09	1.697E+09
98	1.34935	1.578E+10	1.408E+10	1.578E+10	5.902E+07	2.8351	6.5032E+05	98	S	N	A	AL	FLYER	1.679E+09	1.694E+09
99	1.36256	1.578E+10	1.408E+10	1.578E+10	5.902E+07	2.8351	6.5032E+05	99	S	N	A	AL	FLYER	1.678E+09	1.691E+09
100	1.37577	1.578E+10	1.409E+10	1.578E+10	5.924E+07	2.8351	6.5032E+05	100	S	N	A	AL	FLYER	1.677E+09	1.688E+09
101	1.38898	1.579E+10	1.409E+10	1.579E+10	5.924E+07	2.8351	6.5032E+05	101	S	N	A	AL	FLYER	1.675E+09	1.685E+09

TEST 6: FINAL TIME EDIT (continued)

SCHEMATIC OUTPUT. TIME IN MICROSECS, S IN KIARS, DTNH IN NANOMSECS, DELTIM IN SECS

N	TIME	S12/SOJ1	S23/SOJ2	S34/SOJ3	S( 30)	S( 75)	S(112)	S(107)	S(224)	S(261)	JTS	DTNH	DELTIM
1	.001	.000	.000	.000	.0000	.0000	.0000	.0000	.0000	.0000	150	.001	2.134
2	.001	.000	.000	.000	.0000	.0000	.0000	.0000	.0000	.0000	150	.001	.002
3	.001	.000	.000	.000	.0000	.0000	.0000	.0000	.0000	.0000	146	.010	.052
4	.002	.000	.000	.000	.0000	.0000	.0000	.0000	.0000	.0000	150	.012	.054
5	.003	.000	.000	.000	.0000	.0000	.0000	.0000	.0000	.0000	150	.012	.056
6	.004	.000	.000	.000	.0000	.0000	.0000	.0000	.0000	.0000	150	.001	.062
7	.005	.000	.000	.000	.0000	.0000	.0000	.0000	.0000	.0000	150	1.027	.066
8	.007	.000	.000	.000	.0000	.0000	.0000	.0000	.0000	.0000	150	1.027	.076
9	.008	.000	.000	.000	.0000	.0000	.0000	.0000	.0000	.0000	150	1.027	.072
10	.011	.000	.000	.000	.0000	.0000	.0000	.0000	.0000	.0000	150	2.030	.078
11	.013	.000	.000	.000	.0000	.0000	.0000	.0000	.0000	.0000	150	2.030	.082
12	.016	.000	.000	.000	.0000	.0000	.0000	.0000	.0000	.0000	150	3.157	.082
13	.020	.000	.000	.000	.0000	.0000	.0000	.0000	.0000	.0000	150	3.157	.088
14	.025	.000	.000	.000	.0000	.0000	.0000	.0000	.0000	.0000	150	4.045	.088
15	.030	.000	.000	.000	.0000	.0000	.0000	.0000	.0000	.0000	150	4.045	.092
16	.037	.000	.000	.000	.0000	.0000	.0000	.0000	.0000	.0000	151	5.046	.094
17	.044	.000	.000	.000	.0000	.0000	.0000	.0000	.0000	.0000	151	5.046	.094
18	.054	.000	.000	.000	.0000	.0000	.0000	.0000	.0000	.0000	151	7.055	.098
19	.065	.000	.000	.000	.0000	.0000	.0000	.0000	.0000	.0000	151	7.055	.102
20	.079	.000	.000	.000	.0000	.0000	.0000	.0000	.0000	.0000	151	11.211	.110
21	.093	.000	.000	.000	.0000	.0000	.0000	.0000	.0000	.0000	152	11.211	.110
22	.107	.000	.000	.000	.0000	.0000	.0000	.0000	.0000	.0000	152	13.073	.118
23	.120	.000	.000	.000	.0000	.0000	.0000	.0000	.0000	.0000	153	13.073	.124
24	.134	.000	.000	.000	.0000	.0000	.0000	.0000	.0000	.0000	154	13.073	.124
25	.148	.000	.000	.000	.0000	.0000	.0000	.0000	.0000	.0000	154	13.073	.134
26	.162	.000	.000	.000	.0000	.0000	.0000	.0000	.0000	.0000	155	13.073	.142
27	.176	.000	.000	.000	.0000	.0000	.0000	.0000	.0000	.0000	155	13.073	.142
28	.190	.000	.000	.000	.0000	.0000	.0000	.0000	.0000	.0000	156	13.073	.156
29	.204	.000	.000	.000	.0000	.0000	.0000	.0000	.0000	.0000	156	13.073	.156
30	.218	.000	.000	.000	.0000	.0000	.0000	.0000	.0000	.0000	157	13.073	.162
31	.232	.000	.000	.000	.0000	.0000	.0000	.0000	.0000	.0000	157	13.073	.162
32	.246	.000	.000	.000	.0000	.0000	.0000	.0000	.0000	.0000	159	13.073	.170
33	.260	.000	.000	.000	.0000	.0000	.0000	.0000	.0000	.0000	159	13.073	.182
34	.274	.000	.000	.000	.0000	.0000	.0000	.0000	.0000	.0000	161	13.073	.192
35	.288	.000	.000	.000	.0000	.0000	.0000	.0000	.0000	.0000	161	14.015	.192
36	.302	.000	.000	.000	.0000	.0000	.0000	.0000	.0000	.0000	136	14.012	.206
37	.316	.000	.000	.000	.0000	.0000	.0000	.0000	.0000	.0000	136	14.012	.214
38	.330	.000	.000	.000	.0000	.0000	.0000	.0000	.0000	.0000	163	14.034	.224
39	.344	.000	.000	.000	.0000	.0000	.0000	.0000	.0000	.0000	134	14.042	.230
40	.358	.000	.000	.000	.0000	.0000	.0000	.0000	.0000	.0000	150	14.049	.236
41	.372	.000	.000	.000	.0000	.0000	.0000	.0000	.0000	.0000	150	14.049	.244
42	.386	.000	.000	.000	.0000	.0000	.0000	.0000	.0000	.0000	150	14.049	.256
43	.400	.000	.000	.000	.0000	.0000	.0000	.0000	.0000	.0000	150	14.049	.264
44	.414	.000	.000	.000	.0000	.0000	.0000	.0000	.0000	.0000	150	14.049	.274
45	.428	.000	.000	.000	.0000	.0000	.0000	.0000	.0000	.0000	150	14.049	.284
46	.442	.000	.000	.000	.0000	.0000	.0000	.0000	.0000	.0000	151	14.049	.292
47	.456	.000	.000	.000	.0000	.0000	.0000	.0000	.0000	.0000	150	14.049	.304
48	.470	.000	.000	.000	.0000	.0000	.0000	.0000	.0000	.0000	150	14.049	.312
49	.484	.000	.000	.000	.0000	.0000	.0000	.0000	.0000	.0000	150	14.049	.322
50	.498	.000	.000	.000	.0000	.0000	.0000	.0000	.0000	.0000	150	14.049	.330

TEST 6: FIRST PAGE OF STRESS HISTORIES

SCR	E	OUTPUT	TIME	S12/SOJ1	S23/SOJ2	S34/SOJ3	S(38)	S(75)	S(112)	S(187)	S(224)	S(261)	JTS	DTMH	DELTM
51		.566	15.976	0.000	0.000	0.000	0.0000	0.0000	0.0000	0.0000	0.0000	0.0000	125	1.123	.308
52		.561	15.975	0.000	0.000	0.000	0.0000	0.0000	0.0000	0.0000	0.0000	0.0000	150	1.347	3.650
53		.563	15.974	0.000	0.000	0.000	0.0000	0.0000	0.0000	0.0000	0.0000	0.0000	150	1.417	.302
54		.565	15.973	0.000	0.000	0.000	0.0000	0.0000	0.0000	0.0000	0.0000	0.0000	150	1.949	.308
55		.567	15.971	0.000	0.000	0.000	0.0000	0.0000	0.0000	0.0000	0.0000	0.0000	150	2.320	.308
56		.516	15.968	0.000	0.000	0.000	0.0000	0.0000	0.0000	0.0000	0.0000	0.0000	150	2.794	.308
57		.513	15.964	0.000	0.000	0.000	0.0000	0.0000	0.0000	0.0000	0.0000	0.0000	150	3.352	.308
58		.517	15.959	0.000	0.000	0.000	0.0000	0.0000	0.0000	0.0000	0.0000	0.0000	150	4.627	.316
59		.522	15.950	0.000	0.000	0.000	0.0000	0.0000	0.0000	0.0000	0.0000	0.0000	150	5.793	.316
60		.538	15.949	0.000	0.000	0.000	0.0000	0.0000	0.0000	0.0000	0.0000	0.0000	150	6.342	.314
61		.535	15.911	0.000	0.000	0.000	0.0000	0.0000	0.0000	0.0000	0.0000	0.0000	150	10.010	.314
62		.543	15.896	0.000	0.000	0.000	0.0000	0.0000	0.0000	0.0000	0.0000	0.0000	150	12.012	.330
63		.545	15.884	0.000	0.000	0.000	0.0000	0.0000	0.0000	0.0000	0.0000	0.0000	150	14.061	.340
64		.545	15.882	0.000	0.000	0.000	0.0000	0.0000	0.0000	0.0000	0.0000	0.0000	150	14.061	.342
65		.579	15.883	0.000	0.000	0.000	0.0000	0.0000	0.0000	0.0000	0.0000	0.0000	150	14.060	.344
66		.593	15.883	0.000	0.000	0.000	0.0000	0.0000	0.0000	0.0000	0.0000	0.0000	150	14.060	.352
67		.622	15.875	0.000	0.000	0.000	0.0000	0.0000	0.0000	0.0000	0.0000	0.0000	150	14.061	.358
68		.636	15.861	0.000	0.000	0.000	0.0000	0.0000	0.0000	0.0000	0.0000	0.0000	150	14.061	.364
69		.650	15.849	0.000	0.000	0.000	0.0000	0.0000	0.0000	0.0000	0.0000	0.0000	150	14.061	.372
70		.664	15.845	0.000	0.000	0.000	0.0000	0.0000	0.0000	0.0000	0.0000	0.0000	150	14.061	.376
71		.678	15.850	0.000	0.000	0.000	0.0000	0.0000	0.0000	0.0000	0.0000	0.0000	150	14.060	.380
72		.692	15.857	0.000	0.000	0.000	0.0000	0.0000	0.0000	0.0000	0.0000	0.0000	150	14.060	.386
73		.706	15.861	0.000	0.000	0.000	0.0000	0.0000	0.0000	0.0000	0.0000	0.0000	150	14.060	.396
74		.720	15.859	0.000	0.000	0.000	0.0000	0.0000	0.0000	0.0000	0.0000	0.0000	150	14.060	.406
75		.734	15.853	0.000	0.000	0.000	0.0000	0.0000	0.0000	0.0000	0.0000	0.0000	150	14.060	.410
76		.748	15.850	0.000	0.000	0.000	0.0000	0.0000	0.0000	0.0000	0.0000	0.0000	150	14.060	.416
77		.762	15.852	0.000	0.000	0.000	0.0000	0.0000	0.0000	0.0000	0.0000	0.0000	150	14.060	.422
78		.774	15.855	0.000	0.000	0.000	0.0000	0.0000	0.0000	0.0000	0.0000	0.0000	150	14.060	.426
79		.790	15.856	0.000	0.000	0.000	0.0000	0.0000	0.0000	0.0000	0.0000	0.0000	150	14.060	.430
80		.804	15.854	0.000	0.000	0.000	0.0000	0.0000	0.0000	0.0000	0.0000	0.0000	150	14.060	.436
81		.818	15.849	0.000	0.000	0.000	0.0000	0.0000	0.0000	0.0000	0.0000	0.0000	150	14.060	.442
82		.832	15.846	0.000	0.000	0.000	0.0000	0.0000	0.0000	0.0000	0.0000	0.0000	150	14.060	.446
83		.847	15.846	0.000	0.000	0.000	0.0000	0.0000	0.0000	0.0000	0.0000	0.0000	150	14.060	.452
84		.861	15.841	0.000	0.000	0.000	0.0000	0.0000	0.0000	0.0000	0.0000	0.0000	150	14.060	.456
85		.875	15.841	0.000	0.000	0.000	0.0000	0.0000	0.0000	0.0000	0.0000	0.0000	150	14.060	.464
86		.889	15.832	0.000	0.000	0.000	0.0000	0.0000	0.0000	0.0000	0.0000	0.0000	150	14.060	.468
87		.903	15.817	0.000	0.000	0.000	0.0000	0.0000	0.0000	0.0000	0.0000	0.0000	150	14.060	.474
88		.917	15.801	0.000	0.000	0.000	0.0000	0.0000	0.0000	0.0000	0.0000	0.0000	150	14.060	.478
89		.931	15.784	0.000	0.000	0.000	0.0000	0.0000	0.0000	0.0000	0.0000	0.0000	150	14.060	.484
90		.945	15.779	0.000	0.000	0.000	0.0000	0.0000	0.0000	0.0000	0.0000	0.0000	150	14.060	.490
91		.959	15.769	0.000	0.000	0.000	0.0000	0.0000	0.0000	0.0000	0.0000	0.0000	150	14.060	.496
92		.973	15.764	0.000	0.000	0.000	0.0000	0.0000	0.0000	0.0000	0.0000	0.0000	150	14.060	.502
93		.987	15.757	0.000	0.000	0.000	0.0000	0.0000	0.0000	0.0000	0.0000	0.0000	150	14.060	.508
94		1.000	15.746	0.000	0.000	0.000	0.0000	0.0000	0.0000	0.0000	0.0000	0.0000	150	14.060	.512
95		1.014	15.736	0.000	0.000	0.000	0.0000	0.0000	0.0000	0.0000	0.0000	0.0000	150	14.060	.518
96		1.020	15.730	0.000	0.000	0.000	0.0000	0.0000	0.0000	0.0000	0.0000	0.0000	150	14.060	.524
97		1.042	15.704	0.000	0.000	0.000	0.0000	0.0000	0.0000	0.0000	0.0000	0.0000	150	14.060	.530
98		1.056	15.700	0.000	0.000	0.000	0.0000	0.0000	0.0000	0.0000	0.0000	0.0000	150	14.060	.536
99		1.070	15.693	0.000	0.000	0.000	0.0000	0.0000	0.0000	0.0000	0.0000	0.0000	150	14.060	.540
100															

TEST 6: STRESS HISTORIES (continued)

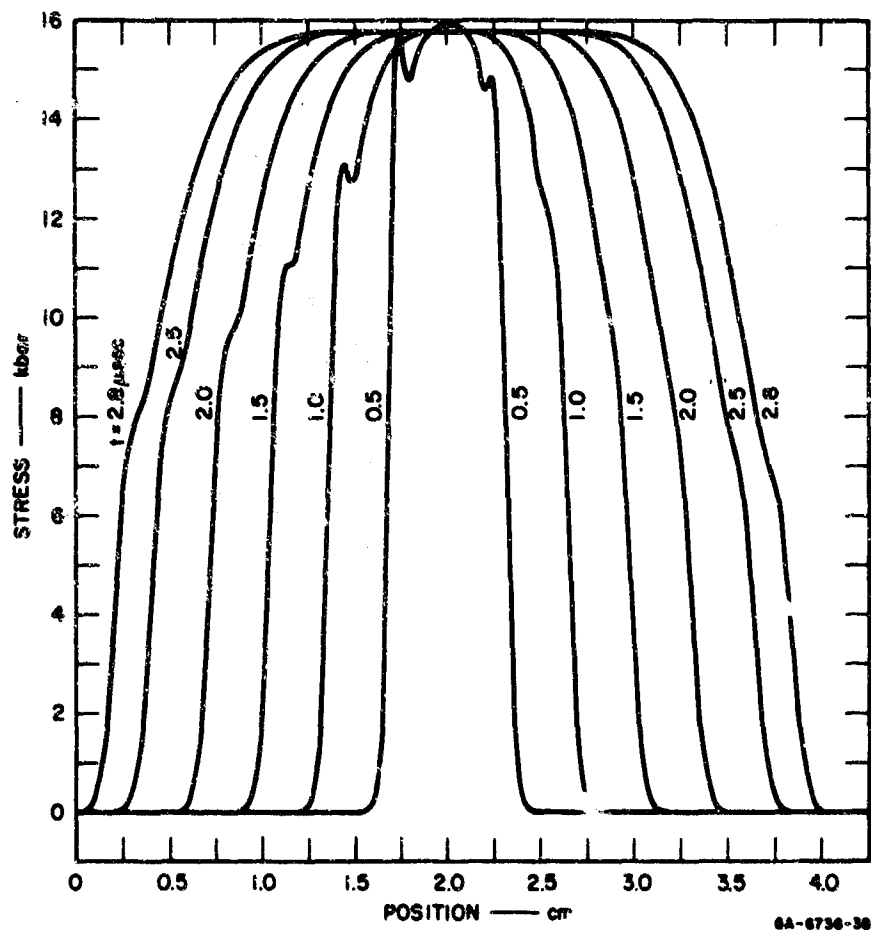


FIGURE 60 TEST 6: SUMMARY PLOT OF TIME EDITS



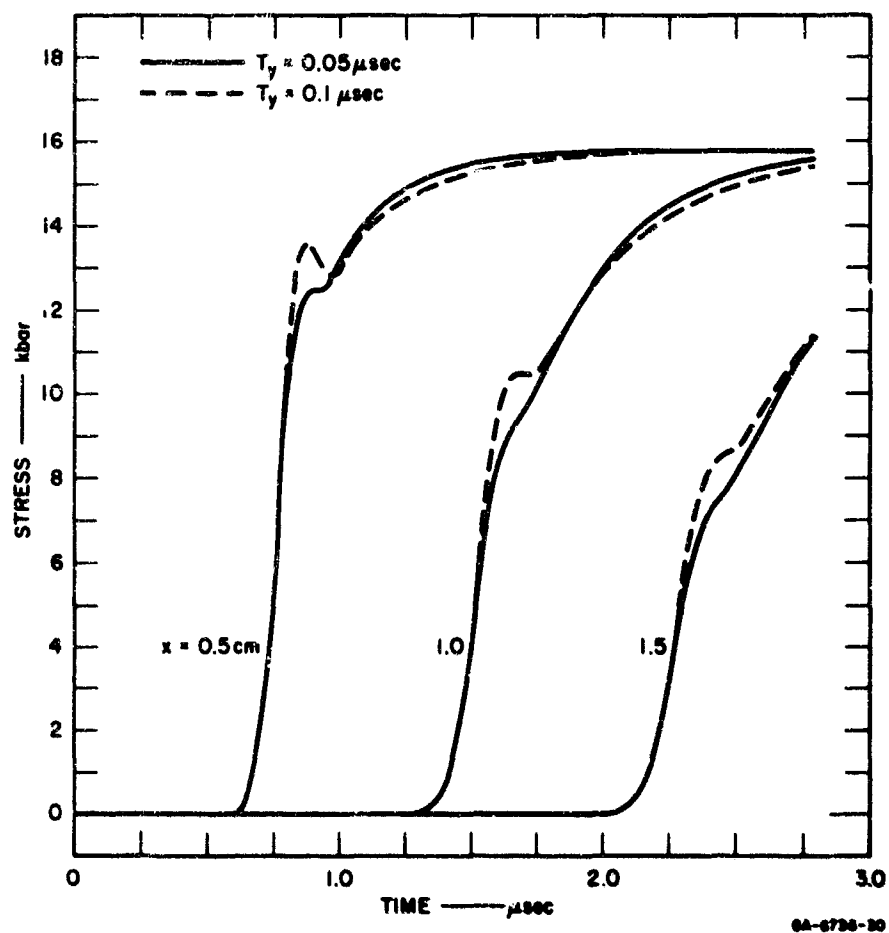


FIGURE 61 TEST 6: SUMMARY OF STRESS HISTORIES AT SIX JET LOCATIONS

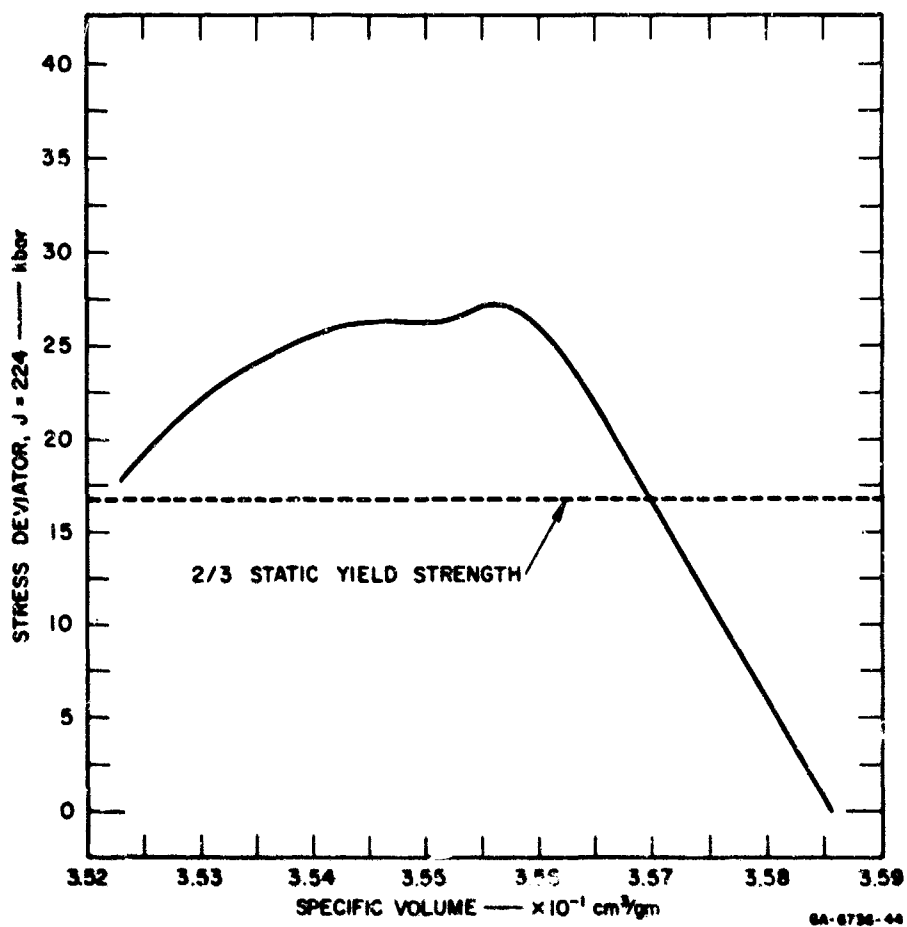


FIGURE 62 TEST 6: SAMPLE PLOT OF STRESS DEVIATOR

### 3. Listing of SRI PUFF 2

In subsequent pages the SRI PUFF 2 program elements for wave propagation calculations are listed. The program requires 51,500 words storage for loading onto a CDC 6400 and 46,500 words for execution. The program and the listings are divided naturally into two segments, the first for computations and the second for plotting. If the plotting cannot be implemented on the user's computer, then the plotting subroutines should be omitted and the call to PUFFPLOT should be removed from EDIT. (There is no other link to the plotting routines.) The program elements are included in the following order:

Main program:	SRI PUFF 2
Computational Subprograms:	EDIT
	EQST
	FMELT
	GENRAT
	HAFSTEP
	HYDRO
	JSTRESS
	POREQST
	REZONE
	SSCAL
	RELAX
	BANDRLX
	BAUSCHI
Plotting Subroutines:	PUFPLOT
	HISTORY
	HUGONIO
	TPLOTS

```

PROGRAM SRI PUFF (INPUT,OUTPUT,TAPE10=INPL,TAPE18=OUTPUT,TAPE6,
1 TAPE7,TAPE8,TAPE9,TAPE11,TAPE19,FILPPL=10000)

C
C MAIN PROGRAM * * *
C   * CALLS GENRAT TO READ DATA AND INITIALIZE ARRAYS
C   * CALLS HYDRG FOR EACH CYCLE OF CALCULATIONS
C   * SETS TIME STEP
C   * CALLS EDIT, ECTHCH, FEZCAE AS REQUIRED
C   * CALLS SCRIBE TO STORE RESULTS AND FOR TERMINAL PRINTOUT
C
REAL MATL,PU,MUN,PUP,NEP,NET
INTEGER M,PCRCLS,RINTER,SCLIC,SPALL
C MISCELLANEOUS
COMMON CEF,CKS,DAVG,DELTIM,DCLO,DRHC,CTAIA,DTA,DTAM,DU,UX,EOLC,F,
1 FIRST,J,JCYCS,JINIT,JFIN,JSMAX,JSTAR,JTS,LSLB(11),MAXPR(11),N,
2 NCYCS,NPERN,POLD,RLAST,SLAST,SPAX,TF,TIME,TJ,TS,ULAST,UCLC,
3 ALAST,XNOB,XCLC
C EQUATION OF STATE - SCLIO
COMMON COSQ(4,6),C1(6,6),C2(6),EPELT(6,5),EQSTA(6),EQSTC(6),
1 ECSTD(6),ECSTE(6),EQSTG(6),ECSTP(6),ECSTN(6),ECSTS(6),PATL(2,6),
2 MU(6),RMO(6),RMCS(6),TEAS(6,3),YACC(6),YO(6),JBNC(6),NPOR(6,2),
3 R,PUP,AMTRLS
C EQUATION OF STATE - PCREUS
COMMON AK(6),MU(6),PORA(4,3),PORB(4,2),PCRC(4,3),RMCP(6,3),
1 YACCP(4,3),DREF,RMCPV,PP,NC
C RADIATION DEPOSITION
COMMON SS(300,3),SSTOP(5),START(5),SDURP,SSTCFP,NSPEC,SSJ,JSS
C COORDINATE ARRAYS
COMMON X(300),C(300),CHL(300),DI3CC),DHL(300),EHL(300),H(300,3),
1 NEH(300),NEY(300),* (300),PHL(300),R(300),S(300),SPL(300),T(300),
2 U(300),UHL(300),VHL(300),ZHL(300)
C HALFSTEP VALUES
COMMON DM,DMLAST,CUP,EH,PH,RH,RPLAST,SH,SPLAST,UM,UHLAST,XH,XHLAST
C IDENTIFIERS
COMMON DISCPT(10),ICENT,JEDIT(2),JREZCN(15),NDATE(3),NEDIT,NEDTP,
1 NJEDIT,NR,NREZCN,NSEPRAT,NSPALL,ATEDT,ATEX,NTR(15),TEDT(50)
C CACITIC INDICATORS
COMMON IMP,LINTER,MIRROR,NORPAL,PCRCLS,RINTER,SCLIC,SPALL
C SPALL AIC RELAXATION
COMMON NSR(6),TSR(6,6),USP(50),DSP(50),LPLX,NICK,NEPH,NETH
C COMMON /PLCT/ IPLCT,IFPLOT(6),LINES,ITPLCT,ATPLOT,IFLAGT,ZNIST(9),
1 IFLAT
C
COMMON A(2500)
C
100 CALL SECONC(FIRST) & XIN=FIRST
CALL GENRAT
NRECN=NICK
CN=NCYCS,NPERN & IT=RMND(0,ATEDT-1) & NT=0 & SP=0.0
N=AB=NREZCN=1
C
C CALCULATE AND STORE HYDRODYNAMIC DATA
200 CALL HYDRG
XIM=XIN & CALL SECONC(FIRST) & DELTIM=XIN-XIM
C PERIODIC EDITS, PRINTS
IF (PCRCIN, 25) .EQ. C) ICS,ZIC 12/17
CALL TEN=FIN-FIRST
WRITE(10,971A,JSTAR,TIME,CALTEN,JTS,DTM,SPAX,JSMAX
210 IF(RMND(0,ATEDT-1).EQ.C) CALL ECTHCH 12/17
IF(PCRCIN,NEEDIT).EQ.C) CALL EDIT
C
C STORE DATA IN BUFFER
CALL SCRIBE
C
C STOP PARAMETERS
300 IF (TIME .LT. TS) GO TO 400
304 IF (N .EQ. JCYCS) GO TO 305
308 IF (N(JSMAX) .LT. C) GO TO 400
306 CALL SSTCF(2,ISWTC)
GO TO (400,500) ISWTC
C

```

MAIN PROGRAM: SRI PUFF

```

400 WRITE (10,41)
WRITE (10,40) N,JCYCS,TIME,TS,X(JSPAX),CHS,ISNTCH,CTNH
CALL EDTHN & CALL EDIT & LSLR(7)=1 & CALL SCRIBE
C      PROGRAM HALTS ON COMPLETION OF ALL DATA CHECKS
GO TO 100
C
C      TIME STEP CALCULATION
500 DTNH=AMINI(SF*CTMIN,AMAX(1.2*CTNH,.C35*SF*DTPIN))
IF (SCURN.EQ. 1.C) 530,504
C
C      COMPUTATION OF SDURN
504 SDURN=1.0
IF (TIME.LT.SSTOPM) 515,53C
515 DO 525 NS=1,ASPEC
IF ((TIME.LT.SSTOP(NS)) .AND. (TIME.GT.START(NS))) 520,525
520 SDURN=APINI(SDURN,SSTCF(NS)-START(NS))
525 CONTINUE
CTNH=AMINI(CTNH,.C.C1*SDURN)
530 CN=NCYCS=NPERR
C
C      TIME EDIT
IF (IT) 540,550,535
535 CALL ECIT INT=INT+1
IF (INT.EQ. NREZON) 537,538
537 CALL REZONE & NREZON=NREZON+1
538 CCATINUE
IF (INT.EQ. NTEDT) 54C,545
540 IT=-1 & GC TC 54C
545 IT=0
550 IF (TIME+CA*DTNH.LT.TEDIT(INT+1)) 540,555
555 NCYCS=(TEDIT(INT+1)-TIME)/CTNH+1 & CN=ACYCS
CTNH=(TEDIT(INT+1)-TIME)/CA & IT=1
540 A=N+1 & NR=NR+1
IF (DTNH.GT. 0) 200,545
545 A=N-1 & GC TC 400
C
40 FORMAT (1/ 5P N =,14.5H, JCYCS =,14. 0H, TIME =,E10.3,6H, TS =,
1 E10.3,12H, X(JSPAX) =,E10.3. 7H, CHS =,E10.2,10H, ISNTCH =13.
2 0P, CTNH =E10.3)
41 FORMAT (1/4X,26H**** CRITERIA FOR STEP ****)
09 FORMAT (5H N=15.0P, JSTAR=14.7H, TIME=E10.3,12H, CALC TIME=E10.3
1,11H SECS, JTS=,14.7H DTNH=E10.3,7P SPAX=E10.3,1H JSNAP=,14/1
&D

```

12/17

MAIN PROGRAM: SRI PUFF (concluded)





```

C
C      CALCULATE MOMENTUM OF MAIN PULSE
ENVPL=0.
209 ENVPL=ENVPL+U(JM)*.5*(JN)*(X(JP+1)-X(JP-1))
    IF (JN .LT. JSPAX) 210,211
210 IF (U(JM-1) .GT. C.) 211,212
211 IF (JN .GT. 1) 212,213
212 JM=JM-1
    GO TO 209
213 JN=JSPAX+4
C
C      CALCULATE MOMENTUM OF PRECURSOR
ENVPR=0.
214 ENVPR=ENVPR+.5*U(JM)*D(JP)*(X(JP+1)-X(JP-1))
    IF (JN .GT. JSTAR) 216,215
215 JN=JN+1
    GO TO 214
216 ENVPP=ENVPL+ENVPR
    OTPP=ENVPP/SMAX
    OTPULS=ENVPL/SPAX
C
C      CALCULATE MAXIMUM POTENTIAL PERCENTUM OF VAPOR
A=1
ENVBM=0.
DO 220 J=1,JSTAR
    IF (J .GT. JBND(IN)) P=P+1
    DE=ENH(J)-ECSTE(IN)
    IF (DE .GT. 0.) 219,221
219 UAVG=(SQRT(U(J-1)*U(J-1)+2.*DE)+SQRT(U(J)*U(J)+2.*DE))/2.
    ENVBM=ENVBM+UAVG*ZPL(J)
220 CONTINUE
221 CONTINUE
C
C      PRINT OUTPUT VARIABLES
WRITE (10,1035)
WRITE (10,1034) N,TIME,DTNH,JTS,ETOTAL,JFIN,JSTAR,JSPAX,SMAX,X(JSM
1,X),CTPP,OTPPULS,ENVNEG,ENVPCS,ENVPL,ENVPR,ENVPP,ENVBM,PCTPOS,PDTNE
26,X(1),X(JB1),X(JB2),X(JB3),X(JFIN),JRMX,RMAX,X(JRPAX)
RETURN
1035 FORMAT(15H PCPENTUP EDIT/)
1034 FORMAT (/,7X,5HCYCLE,8X,4HTIME,8X,4HDTNH,9X,3HJTS,6X,6HECTAL,8X,4
1HJFIN,7X,5HJSTAR,7X,5HJSPAX,8X,4HSMAX,4X,8HX(JSMAX),/,7I2,2E12.4,1
2I2,E12.4,3I12,2E12.4,/,8X,4HOTPP,6X,4HOTPLS,6X,6HEPVNEG,6X,6HEVP
30S,7X,5HEVPL,7X,5HEVPR,7X,5HEVPP,7X,5HEVBM,6X,6HPCPOS,6X,6HPD
4TNEG,/,10E12.4,/,8X,4HX(1),4X,8HX(JBND1),/,8HX(JBND2),4X,8HX(JBND
53),5X,7HX(JFIN),7X,5HJRMX,8X,4HRRMX,4X,8HX(JRPAX),/,5E12.4,1I2,2E
6I2.4)
C*****
C      ENTRY SCRIBE
ENTRY
C
    IF (N .EQ. 1) 250,251
250 IBUF=0. 8 NOCLUS=25
    DO 204 I=1,NJEDIT
    DO 274 IM=1,NNTALS
    IF (JEDIT(I) .LE. JBND(IN)) 206,204
204 CONTINUE
206 NJE(I)=IN
251 IF (LSUB(I)) 290,255,29C
C      STORE DATA IN BUFFER
255 IB=50+IBUF+1 8 A(IB)=N 8 A(IB+1)=TIME+1.E4 8 A(IB+17)=JTS
    A(IB+18)=DTNH+1.E9 8 A(IB+16)=DELTP 8 IB=IB+1
    NINTER = NINO(NNTALS-1,3)
    IF (NINTER .EQ. 2) GO TO 230
    DO 228 I=1,NINTER
    JB=JBND(I) 8 IB=IB+1
228 A(IB)=(S(JB)+S(JB+1))/2.*1.E-9
    IF (NINTER .EQ. 3) 224,230
230 NLEFT = 3-NINTER
    DO 223 IN=1,NLEFT
    IB=IB+1 8 JB=JEDIT(IN)

```

SUBROUTINE EDIT (continued)



```

223 A(I8)=(3(JE)-P(JE))*1.E-9
224 DO 225 I=1,4
JE=JEDIT(I) & I8=I8+1 & A(I8)=J(JE)*1.E-9 & A(I8+4)=N(JE,3)
A(I8+15)=A(JE)*1.E-9 & A(I8+27)=A(I8+39)=15(JE)-P(JE)*1.E-9
IF (D(JE) .GT. 0.) A(I8+21)=1./D(JE)
N2=NJE(I) & NSRPJ1=NSR(NJ)*1
GO TO (225,2243,2241,2241,2243,2243,2242) NSRNJ1
2241 A(I8+33)=NEN(JE) & A(I8+39)=NET(JE) & GO TO 225
2242 A(I8+33)=NEN(JE) & GO TO 225
2243 A(I8+33)=VHL(JE)*1.E-9
225 CONTINUE
IBUF=IBUF+1
IF (IBUF .EQ. MODLUS) 233,240
233 IF (UNIT,4) 233,235,500,501
235 BUFFER OUT (4,1) (A(I),A(50*MODLUS))
GO TO 270
240 IF (IBUF .EQ. 2*MODLUS) 242,270
242 IF (UNIT,4) 242,245,500,501
245 BUFFER OUT (4,1) (A(50*MODLUS+1),A(100*MODLUS))
IBUF=0
270 RETURN
C BUFFER OUT REMAINDER OF AN INCOMPLETE BLOCK
290 IF ( (IBUF .GT. 0) .AND. (IBUF .LT. PCCLLS) ) 291,299
291 IF (UNIT,4) 291,352,500,501
352 BUFFER OUT (4,1) (A(I),A(50*IBUF))
GO TO 365
355 IF (IBUF .GT. MODLUS) 360,365
360 IF (UNIT,4) 360,362,500,501
362 BUFFER OUT (4,1) (A(50*MODLUS+1),A(50*IBUF))
365 IF (UNIT,4) 365,400,500,501
400 REWIND 4
C ZERO CORNER
DO 301 I=1,2500
301 A(I)=0.
C
CALL SECOND(XSTART)
IF (IPLOT .EQ. 0) GO TO 307
C
WRITE PLOT LEADING DATA ON TAPE 7
DO 302 I=1,4
JE=JEDIT(I)
302 XJEC(I)=X(JE)
WRITE (I) N,NJEDIT,(JEDIT(I),I=1,4),(XJEC(I),I=1,4)
C BUFFER IN THE ARRAY STORED ON TAPE 6
307 INDX=0 & IBUF=MODLUS & NBUF=(N-1)/PCCLUS+1 & LENGTH=MODLUS
BUFFER IN (4,1) (A(I),A(50*MODLUS))
DO 325 NB=1,NBUF
I1=1+MODLUS*PCO(NB+1,2)
309 IF (UNIT,4) 309,309,500,501
309 IF (NB .EQ. NBUF) 310,311
C
RESET LENGTH FOR INCOMPLETE BLOCK
310 IF (MOD (N,MODLUS) .EQ. 0) GO TO 314
LENGTH=MOD(N,MODLUS) & GO TO 314
311 IF (I1 .EQ. 1) GO TO 313
312 BUFFER IN (4,1) (A(I),A(50*MODLUS))
GO TO 315
313 BUFFER IN (4,1) (A(50*MODLUS+1),A(100*PCCLLS))
314 IF (I1 .EQ. 1) WRITE (16,1041)(JEDIT(JE),JE=1,4)
315 I2=I1+LENGTH-1
C PRINT OUT OF FIRST SCRIBE HISTORIES
DO 320 I=I1,I2
DO 320 J=4,11
320 JN(J,I)=B(IJ+4,1)
WRITE (16,1040)((B(J,I),J=1,9),(B(J,I),J=10,11),
1 (B(J,I),J=12,20),I=I1,I2)
C PREPARE TAPE 19 FOR SECOND SCRIBE
IF (LMLX .GT. 1) WRITE (16) ((B(J,I),J=1,21),(B(J,I),J=22,30),I=I1,
1 I2)

```

12/17

SUBROUTINE EDIT (continued)

```

C      PREPARE TAPES FOR PLOTTING
IF (IFPLOT(2)+IFPLOT(3) .NE. 0) WRITE (7) ((B(J,I),J=1,11),I=1,12)
IF (IFPLOT(3)+IFPLOT(4)+IFPLOT(5) .NE. 0) WRITE (8) ((B(J,I),
1 J=27,32),I=1,12)
IF (IFPLOT(4) .NE. 0) WRITE (9) ((B(J,I),J=21,26),I=1,12)
IF (IFPLOT(5) .NE. 0) WRITE (11) ((B(J,I),J=33,38),I=1,12)
325 CONTINUE
REWIND 19
C      PRINTOUT OF STRESS HISTORIES (SECOND SCRIBE)
IF (LRLX .EQ. 1) GO TO 330
330 NP=(N-1)/50+1      1  NO=50
12=50
DO 345 IP=1,NP
PRINT 1091, (JED(I),JE=1,6)
IF (IP .EQ. NP) 332,340
333 IF (MOD(N,50) .EQ. 0) 340,336
336 12=MOD(N,50)
340 13=MIN(12,25)
READ(19) ((B(J,I),J=1,2), (B(J,I),J=39,50),I=1,12)
IF (12 .LE. 25) GO TO 343
READ (19) ((B(J,I),J=1,2), (B(J,I),J=39,50),I=26,12)
343 PRINT 1092, ((B(J,I),J=1,2), (B(J,I),J=39,44),I=1,12)
345 CONTINUE
REWIND 19
C
600 CALL SECOND(XEND)
REWIND 6 8 REWIND 7 8 REWIND 8 8 REWIND 9 8 REWIND 11
C      CALL TO PLOTTING PREPAR
IF (IPLOT .EQ. 0) GO TO 620
PRINT 499
CALL PUFPLT (INTX,JCNT)
REWIND 7 8 REWIND 8 8 REWIND 9 8 REWIND 11
620 CALL SECOND (FINAL)      8  DUR4=FINAL-FIRST
DUR=XEND-ESTART 8 DUR2=XEND-FIRST 8 DUR3=FINAL-XEND
WRITE (18,5012) DUR,DUR2,DUR3,DUR4
RETURN
C
C      STATUS CHECK PRINTS
900 IF (NB .EQ. NBUF) LENGTH=MOD(N,PCLUS)
WRITE (18,1041) NB,LENGTH 8 GO TO 600
901 IF (NB .EQ. NBUF) LENGTH=MOD(N,MODLLS)
WRITE (18,1042) NB,LENGTH 8 GO TO 600
499 FORMAT (19H PUTPLCT CALLED //)
1040 FORMAT (F5.0,F10.3,6(F5.3,F1),F5.0,F7.3,F3.3)
1041 FORMAT (18H1 SCRIBE OUTPUT, TIME IN MICROSECS, S IN KBARS, DTAM IN
1 NANOSECS, DELTIM IN SECS //
2 5H N TIME S12/SCJ1 S23/SCJ2 S34/SCJ3 S(13,
3 7H) S(13,7H) S(13,7H) S(13,7H) S(13,7H) S(13,
4 22H) JTS DTAM DELTIM)
1042 FORMAT(17H EOF ON UNIT 6 IN SCRIBE. 5H NB=12, 9H LENGTH=13)
1043 FORMAT (18H PARITY ERROR ON UNIT 6 IN SCRIBE. NB=12, 8H LENGTH=13)
1070 FCRPAT(1215)
1080 FCRPAT(1215,F10.3,15)
1090 FCRPAT(13F10.3)
1091 FCRPAT (113H1SECOND SCRIBE OUTPLY FOR ALL RELAXATION MODELS- N
1N,NT(1/CM), GAM(UNITLESS), Y,SG,PU(KILCBARS), TIME(MICROSECS) //
215X,6(17X,3HJ =,14,6X),//5H N,6X,4HTIME,6(13X,7HY CR NM,3X,7HSD,
3HT,1/15X,6(15X,5HCR PU,4X,6HCR GAP))
1092 FCRPAT (F5.0,F10.3,12E10.3)
9012 FCRPAT (17H0TIME IN SCRIBE =F10.3/17H COMPUTING TIME =F10.3/
1 17H PLOTTING TIME =F10.3/17H TOTAL TIME =F10.3)
END

```

SUBROUTINE EDIT (concluded)

```

C      SUBROUTINE EQST(EJ,DJ,PJ,NJ,CJ)
C
C      COMPUTES PRESSURE AND SOUND SPEED FOR SOLIDS
C      * MIE-GRAINEISEA FOR COMPRESSICA
C      * EXPANSION EQUATION OF STATE FOR DENSITIES LESS THAN RHGS
C
C      REAL PATL,MU,MUP,MUF
C      MISCELLANEOUS
C      COMMON CEF,CXS,DAVG,CALTIN,CCLC,CCHC,CTPIN,UTN,CTNP,DU,DX,EOLD,F,
1  FIRST,JJCYS,JINIT,JFIN,JSMX,JSTAR,JTS,LSUB(11),MAXPR(11),N,
2  NCYCS,MPEMN,POLD,PLAST,SLAST,SMAX,TF,TINE,TJ,TS,ULAST,UOLD,
3  XLAST,XNOW,XOLD
C      EQUATION OF STATE - SOLID
C      COMMON COSQ(6,6),C1(6,6),C2(6),ENELT(6,5),EQSTA(6),EQSTC(6),
1  EQSTD(6),EQSTE(6),EQSTG(6),EQSTH(6),ECSTA(6),ECSTS(6),PATL(2,6),
2  PL(6),RHQ(6),RHCS(6),TENS(6,3),YACC(6),YO(6),JBAD(6),RPCR(6,2),
3  R,MUN,MNTRL5
C      EQUATION OF STATE - PCFUS
C      COMMON AK(6),MUP(6),PORA(4,3),PORB(4,3),PORC(4,3),RMCP(6,3),
1  YACP(4,3),OREF,RHCFV,PE,AC
C
C      VJ=RHQS(NJ)/DJ & ENU=1./VJ & EPL=ENU-1.
C      IF (ENU .GE. 0.) 10,3
C      EQST FOR EXPANDED ZONES
3  ENU2=EQSTH(NJ)+41.-VJ)*VJ & TS1=EQSTE(NJ)
C      IF (ENU2 .GT. -10) 4,8
C      TS1=TS1*(1.-EXP(ENU2))
C      EN=(ENU+1.)/2. & EN2=EN+EN*EN
C      GMMU=(EQSTG(NJ)-EQSTH(NJ))*(ENU+EN/EN2+.25*EN2/EN)
C      TS2=EQSTG(NJ)+GMMU & PJ=(EJ-TS1)*DJ+TS2
C      IF (CJ .NE. 0.) 9,20
C      CSC=(EJ-TS1)*TS2+.5*GMMU+TS2*(EQSTE(NJ)-TS1)*EQSTA(NJ)+12.*VJ-1.
1  )+VJ*(PJ+TS2/DJ + 2.*MUP/(DJ+OCLO))
C      IF (CSC .LT. 0.) GO TO 30
C      CQ=CSQ+CJ*CJ & CJ=CSQ+CJ/CQ+.25*CQ/CJ & GC TC 20 12/17
C      EQST FOR COMPRESSED ZONES
10  PH=(EQSTS(NJ)+ENU+EQSTD(NJ))*ENU+EQSTC(PJ)*ENU
C      G=EQSTG(NJ)+RHCS(NJ)/DJ & PJ=PH*(1.-.5*ENU*G)+G*CJ*EJ
C      IF (CJ .NE. 0.) 11,20
C      CSQ=((3.*EQSTS(NJ)+ENU+2.*EQSTC(PJ))*ENU+EQSTC(NJ))*((1.-.5*G*ENU)
1  )/RHQS(NJ)-.5*G/DJ*PH + PJ*G/CJ + 2.*MUP/(DJ+OCLO)
C      IF (CSQ .LT. 0.) GC TC 30
C      CQ=CSQ+CJ*CJ & CJ=CSQ+CJ/CQ+.25*CQ/CJ 12/17
C      IF (LSUB(4) .GE. MAXPR(4)) GO TC 30
C      LSUB(4)=LSUB(4)+1
C      WRITE (10,110) J,N,CSC,EJ,DJ,PJ
C      RETURN
110  FORMAT (10H EQST, J=13,4H, N=14,4H, CSC=E10.3,SH, EJ=E10.3,
1  SH, DJ=E10.3,SH, PJ=E10.3)
C      END

```

SUBROUTINE EQST (complete)

```

C      FUNCTION FMELT(EJ,PJ)
C
C      COMPUTES VARIATION OF STRENGTH OR POCULUS WITH INTERNAL ENERGY
C
C      REAL MATL,MU,MUM
C      MISCELLANEOUS
C      COMMON CEF,CKS,DAVG,DELTIN,DOLD,DRHC,DTFIN,DTA,DTNH,DU,DX,ECLO,F,
1      FIRST,J,JCYCS,JINIT,JFIN,JSMAX,JSTAR,JTS,LSLB(11),MAXPR(11),N,
2      NCYCS,NPERN,POLD,RLAST,SLAST,SMAX,TF,TIME,TJ,TS,ULAST,UCLD,
3      XLAST,XNOB,XCLO
C      EQUATION OF STATE - SOLID
C      COMMON COSQ(6,6),C1(6,6),C2(6),EPELT(6,5),EQSTA(6),EQSTC(6),
1      ECSTD(6),EQSTE(6),EQSTG(6),EQSTH(6),EQSTN(6),EQSTS(6),MATL(2,6),
2      MU(6),RHO(6),RHOS(6),TENS(6,3),YACC(6),YO(6),JBND(6),NPOR(6,2),
3      N,MUM,MATPLS
C
C      IF (EJ .GE. EPELT(MJ,1)) GO TO 3C
C      IF (EJ .GT. EPELT(MJ,2)) GO TO 2C
C      IF (EJ .GT. 0.) GO TO 1C
C      FOR NEGATIVE ENERGY
C      FMELT =1.
C      RETURN
C      FOR ENERGY IN FIRST REGION
10      RR=EJ/EPELT(MJ,2)
C      FMELT=1.-RR*(1.-EMELT(MJ,4)+4.*EPELT(PJ,3)*(RR-1.))
C      RETURN
C      FOR ENERGY IN SECOND REGION
20      RR=(EMELT(MJ,1)-EJ)/(EMELT(MJ,1)-EMELT(PJ,2))
C      FMELT=RR*(EMELT(MJ,4)-4.*EMELT(MJ,5)*(RR-1.))
C      RETURN
C      FOR ENERGY ABOVE PELTING
30      FMELT=0.
C      RETURN
C      END

```

FUNCTION FMELT (complete)

```

C      SUBROUTINE GENRAT
C
C      READS INPUT DATA AND INITIALIZES ARRAYS
C      * READS INPUT CARDS
C      * COMPUTES COORDINATE LAYOUT
C      * COMPUTES RADIATION DEPOSITION FOR A RADIATION PROBLEM
C      * INITIALIZES DENSITY, ENERGY, YIELD, SCUR SPEED, TENSILE STRENGTH,
C      * CONDITION INDICATORS, PARTICLE VELOCITY
C      * PRINTS INITIAL LAYOUT
C
      REAL MATL,MU,MUN,MUP,NEM,NET
      INTEGER M,PCRCLS,PIATER,SOLIC,SPALL
      INTEGER MM
C      MISCELLANECUS
      COMMON CEF,CNS,DAVG,CELTIM,COLG,CRHC,CTPIN,CTN,DTNM,DU,DX,ECLO,F,
1 FIRST,J,JCYCS,JINIT,JFIN,JSMAX,JSTAR,JTS,LSLB(11),MAXPR(11),A,
2 NCYCS,NPERA,PCLO,PLAST,SLAST,SMAX,TF,TIME,TJ,TS,ULAST,UOLD,
3 XLAST,XNCN,XOLC
C      EQUATION OF STATE - SOLID
      COMMON COSQ(6,6),C1(6,6),C2(6),EMELT(6,5),EQSTA(6),EQSTC(6),
1 EQSTC(6),EQSTE(6),ECSTG(6),ECSTH(6),ECSTN(6),EQSTS(6),MATL(2,6),
2 MU(6),RHO(6),RHOS(6),TENS(6,3),YACD(6),YC(6),JBRD(6),NPCR(6,2),
3 M,RLM,NMTRLS
C      EQUATION OF STATE - POROUS
      COMMON AK(6),MUP(6),PORA(4,3),PCRB(4,3),PCRC(4,3),RPEC(6,3),
1 YADDP(4,3),DREF,R-CPV,MP,NC
C      RADIATION DEPOSITION
      COMMON SS(300,5),SSTCP(5),START(5),SELM,SSTOPH,NSPEC,SSJ,JSS
C      COORDINATE ARRAYS
      COMMON X(300),C(300),CHL(300),D(300),ENL(300),EHL(300),H(300,3),
1 NEM(300),NET(300),P(300),PHL(300),H(300),S(300),SPL(300),T(300),
2 U(300),UHL(300),YHL(300),ZHL(300)
C      HALFSTEP VALUES
      COMMON CH,DHLAST,CUH,EM,PH,RH,RHLAST,SH,SPLAST,UH,UHLAST,XH,DHLAST
C      IDENTIFIERS
      COMMON DISCPT(10),IDENT,JEDIT(20),JREZCA(15),ACATE(3),NEDIT,NECTH,
1 NJEDIT,NR,NREZCH,NSEPRAT,NSPALL,NTEDT,NTEX,NTR(15),VEDIT(50)
C      CONDITION INDICATORS
      COMMON INF,LIATER,PIRRCR,ACAPAL,PCRCUS,PIATER,SOLIC,SPALL
C      SPALL AND RELAXATION
      COMMON NSR(6),TSR(6,6),USP(50),XSP(50),LPLX,NICK,NEMH,METH
C
      COMMON /PLOT/ IPLOT,IFPLOT(6),LINES,ITFLCT,ATFLCT,IFLAGT,IFIST(9),
1 IFLAGJ
C
      COMMON A(2000)
      DIMENSION AC(109),AA(6,6,15),B(6,6,15),EDGE(6,6,15),EI(109),
1 RHOC(6,6),TBL(109),ACCA(6),ACE(6,6)
      DIMENSION DELFIN(6,5),DELX(6,5),TH(6,5),NCELLS(6,5),NZONES(6),
1 IEQUIV(10),RLX(6,8)
C
      EQUIVALENCE (AC,AA,C(11C)),(B,D(5C)),(EDGE,DH(29C)),
1 (EI,ENL(230)),(NMCC,M(39)),(TBL,P(75)),(NGCA,M(104)),
2 (MOZ,P(190)),(DELFIN,M(226)),(DEL,M(256)),(TH,M(206)),
3 (NCELLS,M(316)),(NZONES,M(346)),(CEF,IEQUIV)
C
      BEGIN=FIRST
100 CALL MMSSET(0.,IEQUIV,9770)
      FIRST=BEGIN
      LINTER=IRL & NORMAL=IRN & PCRCUS=IRF & PIRRCR=IRH
      PIATER=IRA & SOLIC=IRS & SPALL=IRS & ACAP=SH=END0
      LRLX=1
C      READ AND PRINT DATA
      READ 45,A1,ICENT,(DISCPT(1),I=5,10)
C      CHECK FOR END OF LAST DATA CHECK
      IF (CEF,10) 102,103
102 STOP
103 WRITE (10,31)
      CALL SCATE(CAT)
      WRITE (10,43) DAT
      WRITE (10,45) A1,ICENT,(DISCPT(1),I=5,10)
      DISCPT(1)=100 DATE = 8 DISCPT(2)=CAT
      DISCPT(3)=100 IDENT = 8 ENCODE (10,35,DISCPT(4)) IDENT

```

SUBROUTINE GENRAT

```

105 READ      59,IND,(A(I),I=1,2)
   IF (IND.EQ. 1CH ) GC TO 108
   WRITE (10,59)IND,(A(I),I=1,2)
   GO TO 105
108 BACKSPACE 10
   READ      74,A1,A2,NTEDT,A3,A4,NJEDIT,A5,A6,NREZCN,A7,A8,NSEPRAT
   WRITE(10,74)A1,A2,NTEDT,A3,A4,NJEDIT,A5,A6,NREZCN,A7,A8,NSEPRAT
   IF (NTECT.EQ. 0) GC TO 120
   NT=NINC(7,NTEDT)
   READ      76,A1,A2,(TEDIT(I),I=1,NT)
   WRITE (10,76)A1,A2,(TEDIT(I),I=1,NT)
   IF (NTECT.LE. 7) GO TO 120
   READ      79,(TEDIT(I),I=8,NTEDT)
   WRITE (10,79)(TEDIT(I),I=8,NTEDT)
120 IF (NJEDIT.EQ. 0) GC TO 125
   NJ=NINC(14,NJEDIT)
   READ      78,A1,A2,(JEDIT(I),I=1,NJ)
   WRITE (10,78)A1,A2,(JEDIT(I),I=1,NJ)
   IF (NJEDIT.LE. 14) GO TO 125
   READ      80,(JEDIT(I),I=15,NJEDIT)
   WRITE (10,80)(JEDIT(I),I=15,NJEDIT)
125 IF (NREZCN.EQ. 0) GC TO 130
   READ      70,A1,A2,(NTR(I),I=1,NREZCN)
   WRITE(10,70) A1,A2,(NTR(I),I=1,NREZCN)
   READ      78,A1,A2,(JREZCN(I),I=1,NREZCN)
   WRITE(10,78) A1,A2,(JREZCN(I),I=1,NREZCN)
130 READ      74,A1,A2,NEDTM,A3,A4,NECIT,A5,A6,NPERN,A7,A8,MAXPRN
   WRITE(10,74) A1,A2,NEDTM,A3,A4,NECIT,A5,A6,NPERN,A7,A8,MAXPRN
   IF (MAXPRN.EQ. 0) GC TO 135
   READ      78,A1,A2,(MAXPR(I),I=1,11)
   WRITE (10,78)A1,A2,(MAXPR(I),I=1,11)
135 READ      72,A1,A2,A3,JCYCS,A4,CKS,A5,TS
   WRITE (10,72)A1,A2,A3,JCYCS,A4,CKS,A5,TS
   READ      73,A1,NMTRL5,A2,MATFL,A3,UZER0,A4,IFLET
   WRITE (10,73)A1,NMTRL5,A2,MATFL,A3,UZER0,A4,IFLET
   PP=0

C      **** N-LCEP ****
C
DO 290 P=1,NMTRL5
  WRITE (10,69)
  READ      90,MATL(1,P),MATL(2,P),A1,RHCS(P),A2,NSR(M),A3,NYAM,
1  A4,NPCR(P),A5,NCON(M)
  WRITE(10,90)MATL(1,P),MATL(2,P),A1,RHCS(P),A2,NSR(P),A3,NYAP,
1  A4,NPCR(P),A5,NCON(M)
  RHO(M)=RHO5(M)

C      **** READ IN EQST VARIABLES ****
C
READ      92, A1,A2,ECSTC(M),A3,A4,EQSTI(M),A5,A6,ECSTE(M),A7,A8,
1EQSTG(M),A9,A10,EQSTH(M),A11,A12,ECSTS(P),A13,A14,ECSTN(M),A15,A16
EQSTN(M)=ECSTG(P)*RHCS(M)/ECSTE(P)
ECSTN(M)=EQSTC(M)/(EQSTG(P)*ECSTE(M)*RHCS(P))
WRITE (10,92) A1,A2,ECSTC(M),A3,A4,ECSTC(P),A5,A6,ECSTE(M),A7,A8,
1EQSTG(M),A9,A10,ECSTH(M),A11,A12,ECSTS(P),A13,A14,ECSTN(P),A15,
2A16,ECSTN(M)

C      **** READ IN VISCOSITY AND TENSILE VARIABLES ****
C
READ      92,A1,A2,CCSQ(M,A1),A3,A4,C1(P,A1),A5,A6,C2(P)
WRITE (10,92)A1,A2,CCSQ(P,A1),A3,A4,C1(P,A1),A5,A6,C2(M)
READ      92,A1,A2,TENSI(M),A3,A4,TENSI(P),A5,A6,TENSI(P,3)
WRITE(10,92) A1,A2,TENSI(P,1), A3,A4,TENSI(M,2),A5,A6,TENSI(M,3)

C      **** READ IN STRESS RELAXATION VARIABLES ****
C
C      CORRESPONDENCE OF RLX WITH MODEL AND CCMPPN VARIABLES
C


| CCMPPN | TSR(1)  | (2)  | (3) | (4)  | (5)  | (6)  | NEP | NET |
|--------|---------|------|-----|------|------|------|-----|-----|
| INPUT  | RLX(1)  | (2)  | (3) | (4)  | (5)  | (6)  | (7) | (8) |
| 1      | ANELAS. | TRLX | -   | -    | -    | -    | -   | -   |
| 2      | BAND    | Y1   | Y2  | BEE  | VP   | GEE  | EPS | AP0 |
| 3      | GILMAN  | CEE  | PMI | REE  | VP   | PMAC | -   | -   |
| 4      | 2-P Y.  | TRLX | TV  | -    | -    | -    | -   | -   |
| 5      | BALSCH. | XPO  | XP  | PUUP | YACF | -    | -   | -   |


```

SUBROUTINE GENRAT (continued)

```

C
NSRM1=NSR(P)+1
GC TC (220,210,212,212,210,210,210) NSRM1
210 READ 94,(A(I),RLX(M,I),I=1,4)
WRITE (18,94)(A(I),RLX(M,I),I=1,4)
RLX(M,5)=RLX(M,6)=C. 8 GC TC 214
212 READ 94, (A(I),RLX(M,I),I=1,8)
WRITE (18,94) (A(I),RLX(M,I),I=1,8)
214 LRLX=2
CC 216 IR=1,6
216 TSR(M,IR)=RLX(M,IR)
IF (NSR(M) .EQ. 5) TSR(M,3)=1.3333*TSR(M,3)
220 EMELT(M,1)=EMELT(M,2)=1.E20 8 EPELT(P,4)=1.
IF (NYAP .EQ. 0) GO TO 240
IF (NYAM .EQ. 2) GO TO 23C

C
C **** READ IN YIELD VARIABLES ****
C
READ 92,A1,A2,YOS, A3,A4,MU(P),A5,A6,YACD(M)
WRITE (18,92)A1,A2,YOS, A3,A4,MU(M),A5,A6,YADD(M)
Y(M)=YCS
IF (NSR(M) .NE. 5) YADD(M)=.666667*YACC(P)/(R+CS(M)*1.2-.59YCS/
1 MU(M))
MU(M)=1.333333*PL(P)
IF (NYAM .EQ. 1) GO TO 24C

C
C **** READ IN MELT VARIABLES ****
C
230 READ 76,A1,A2,(EPELT(P,I),I=1,5)
WRITE (18,76)A1,A2,(EMELT(M,I),I=1,5)

C
C **** READ IN POROUS VARIABLES ****
C
240 IF (APCR(M,1) .EQ. 0) GO TO 25C
NP=NPOR(M,1) 8 PP=NP+1 8 APCR(P,2)=PP
READ 76,A1,A2,(R+CP(I,MP),I=1,6)
WRITE (18,76)A1,A2,(RPOP(I,PP),I=1,6)
RHO(R)=RHO(P,PP)
READ 77,A1,A2,(CCSQ(M,I),I=1,5)
WRITE (18,77)A1,A2,(CCSC(P,I),I=1,5)
READ 77,A1,A2,(CI(M,I),I=1,5)
WRITE (18,77)A1,A2,(CI(P,I),I=1,5)
P2=0.
CC 245 A=1,AP
PORA(N,PP)=P1-P2
READ 92,A1,A2,P2,A3,A4,DELP,A5,A6,YACOP(N,PP)
WRITE (18,92)A1,A2,P2,A3,A4,CELP,A5,A6,YACCP(N,PP)
PGRB(N,PP)=(P2-P1)*R+CP(N+1,MP)/(R+CP(N+1,PP)-R+CP(N,MP))
PORC(N,MP)=4.*DELP*RHO(N+1,MP)*R+CP(N,PP)/(R+CP(N+1,MP)
1 -R+CP(N,PP))*2
245 CONTINUE
PORB(N,PP)=P2 8 PORC(AF,PP)=CELP
READ 92,A1,A2,AK(M),A3,A4, PLP(P),A5,A6,YOIP)
WRITE (18,92)A1,A2,AK(P),A3,A4, PUP(P),A5,A6,YC(M)
PUP(P)=1.333333*PUP(M)

C
C **** READ IN EDGE VARIABLES
C
250 IF (ACCA(M) .EQ. 0) GO TO 26C
NCONST=NCON(M)
DO 260 AC=1,NCONST
READ 94,A1,MOE(M,NC),A2,A3,RHCC(P,AC)
WRITE (18,94)A1,MOE(P,NC),A2,A3,PHCC(N,NC)
MOED=MOE(M,NC) 8 MOE1=MOED*1
MOE=MINDY(MOED) 8 MOI=MINDY(MOE1)
READ 79,A1,A2,(EDGE(M,NC,AC),NO=1,ACD)
WRITE (18,79)A1,A2,(EDGE(P,AC,PI),AC=1,ACC)
IF (ACRE .EQ. 7) GO TO 253
READ 79,(EDGE(M,AC,NO),NO=1,ACD)

```

SUBROUTINE GENRAT (continued)

```

WRITE (18,79)(EDGE(P,NC,ND),AC=8,ACE1)
253 READ 76,A1,A2,(AA(M,NC,ND),ND=1,ND1)
WRITE (18,76)A1,A2,(AA(M,NC,ND),ND=1,ND1)
IF (NOE1 .LE. 7) GC TC 256
READ 79,(AA(M,NC,ND),ND=8,NOE1)
WRITE (18,79)(AA(P,AC,ND),ND=8,ACE1)
254 READ 76,A1,A2,(B(M,NC,ND),ND=1,ND1)
WRITE (18,76)A1,A2,(B(M,NC,AC),AC=1,NC1)
IF (ACE1 .LE. 7) GO TO 240
READ 75,(B(M,NC,ND),ND=8,ACE1)
WRITE (18,79)(B(P,AC,ND),ND=8,ACE1)
260 CONTINUE
C
C      **** READ IN ZONING VARIABLES ****
C
280 READ 62,A1,AZCRES(M),A2,NCELLS(M,1),A3,A4,TH(M,1),A5,A6,DELX
1 (M,1),A7,A8,DELFIN(M,1)
WRITE (18,62)A1,AZCRES(M),A2,NCELLS(P,1),A3,A4,TH(M,1),A5,A6,DELX
1 (M,1),A7,A8,DELFIN(M,1)
IF (NZONES(M) .EQ. 1) GC TC 290
AZCN=AZCRES(P)
CO 285 N=2,NZON
READ 64,A1,A2,ACELLS(M,N),A3,A4,TH(P,N),A5,A6,DELX(M,N),
1 A7,A8,DELFIN(M,N)
285 WRITE (18,64)A1,A2,ACELLS(P,N),A3,A4,TH(P,N),A5,A6,DELX(M,N),
1 A7,A8,DELFIN(M,N)
290 CONTINUE
C
C      **** END OF N-LOOP****
C
C      **** CALCULATE ZONING AND INITIALIZE CELL COORDINATES ****
C
X(1)=0.
J = 1
DO 390 P=1,NTALS
NZON=NZONES(M)
DO 380 NZ=1,AZCA
FM=NCELLS(M,NZ) 8 RATIO=1. 8 FI=C. 8 CX=DELX(M,NZ)
IF (CX=DELFIN(M,NZ) .EQ. C.) GC TC 345
PREPARE FOR GEOMETRIC PROGRESSION OF CELLS
RATIO=DELFIN(P,NZ) 8 GC TC 360
PREPARE FOR ARITHMETIC PROGRESSION OF CELLS
345 IF (CX .NE. C.) GC TC 355
IF (DELFIN(M,NZ) .NE. C.) GO TO 35C
DX=TH(M,NZ)/FM 8 GC TC 36C
OX=2.*TH(M,NZ)/FM-DELFIN(M,NZ)
350 FI=2.*(TH(M,NZ)/FM-OX)/(FI-1.)
355 JN=J+ACELLS(P,NZ) 8 J1=J+1
360 CO 365 I=J1,JN
X(1)=X(1-1)+CX
CX=RATIO*CX+FI
365 J=JN 8 JNAD(P)=J 8 J=J+1
380 X(J)=X(J-1)
JINIT=1 8 JFIN=J
IF (NATPL .NE. C) GC TO 500
C
C***** RADIATION DEPOSITION
C
READ 54,A1,NSPEC,A2,A3,ANGLE
WRITE (18,54)A1,NSPEC,A2,A3,ANGLE
ANGLE=CCS(ANGLE/57.2957795)
CC 465 NS=1,NSPEC
READ 60,(A(1),I=1,6)
WRITE (18,60)(A(1),I=1,6)
READ 10,A1,MMNU,A2,NBB,A3,NBBB,A4,START(AS),A5,SSTOP(AS)
WRITE (18,10)A1,MMNU,A2,NBB,A3,NBBB,A4,START(AS),A5,SSTOP(AS)
SSTOP=MAX(SSTOP,SSTOP(AS))
IF (NBBB .NE. C) GC TC 47C
IF (MMNU .EQ. 0) GO TO 42C
NBB=1 8 TEMP=1.
C
C      ARBITRARY SPECTRUM INPUT
C
READ 76,A1,A2,PLNR
WRITE(18,76) A1,A2,PLUX

```

SUBROUTINE GENRAT (cc. invud)



```

DC 415 NH=1,AMNU
READ 11,A1,A2,TBL(NH),A3,A4,EI(NH),A5,A6
WRITE(10,11)A1,A2,TBL(NH),A3,A4,EI(NH),A5,A6
415 EI(NH)=EI(NH)*ANGLE*FLUX
NR=1 1 GC TC 430
C
C      BLACK BODY INPUT
420 APAC=NBE 8 NH=109
IF (NS.NE.1) GC TO 424
READ 60,(AI1),I=1,8)
WRITE (10,60)(AI1),I=1,8)
READ 12,(TBL(NH),NH=1,109)
WRITE (10,12)(TBL(NH),NH=1,109)
NR=1
424 READ 92,A1,A2,TEMP,A3,A4,ECAL
WRITE (10,92)A1,A2,TEMP,A3,A4,ECAL
ECAL=ECAL*ANGLE
CO 428 NH=1,109
EI(NH)=ECAL*.01*(1.-.9*(NH/100))
C
C      COMPUTATION OF ABSORPTICA COEFFICIENT - AC
430 JBEG=1
DO 440 P=1,APTRLS
CO 433 NP=1,109
AC(NH)=0.
ACCAST=ACON(NH)
CO 445 NC=1,NCONST
NEDG=1
CO 445 NP=1,NMNL
IF (NEDG.GT. ACE(P,AC)) GC TC 440
IF (ECGE(NH,NC,NEDG).GT. TBL(NH)*TEPP) GC TC 440
NEDG=NEDG+1 8 GC TC 438
440 AC(NH)=AC(NH)+AC(NH,NC)*AA(NH,NC,NEDG)*(TBL(NH)*TEPP)*BIP(NH,NEDG
1 )/ANGLE
445 CONTINUE
C
C      DISTRIBUTE ENERGY INTO CELLS
JBNDP=JBND(NH)-1
CO 455 J=JBEG,JBNDP
ESLR=0.
CX=X(J+1)-X(J)
DO 450 NH=1,AMNU
IF (EI(NH).LT. 1.E-20) GO TO 450
EIZ=EI(NH)*(1.-EXP(-1.*AC(NH)*CX))
EI(NH)=EI(NH)-EIZ
ESUM=EIZ+ESUM
450 CONTINUE
SS(J,NS)=ESUM*.10007/RND(NH)/DX/(ESSTCP(NS)-START(NS))+SS(J,NS)
455 JBEG=JBND(NH)+1
NR=NR+1
IF (NR.LE. NRAJ) GO TO 424
C
C      END OF NSPEC LOOP
465 CONTINUE 8 GO TO 500
C
C      ARBITRARY POSITION
470 READ 70,(AC1),I=1,7),EI(1)
WRITE (10,70)(AC1),I=1,7),EI(1)
READ 70,A1,A2,IAC(N),P=1,APTRLS)
WRITE (10,70)A1,A2,IAC(P),P=1,APTRLS)
JBEC=1
DO 480 P=1,APTRLS
JBACP=JBAD(P)-1
CO 475 J=JBEG,JBNDP
CX=X(J+1)-X(J)
EIZ=EI(1)*(1.-EXP(-AC(N)*CX))
EI(1)=EI(1)-EIZ
SS(J,1)=EIZ*.10007/RND(NH)/DX/(ESSTCP(NS)-START(NS))
475 JBEG=JBAD(NH)+1
480 JBEC=JBAD(NH)+1
C
C      **** READ IN PLOTTING CONTROLS ****
C
500 DO 502 I=1,6
502 IFPLCT(I)=0
PRINT 65
IF (IFPLCT=IFPLCT-1) 500,503,105
503 IFPLC=IFPLCT(1)+IFPLCT(2)-1 8 IFPLCT(3)+IFPLCT(4)+IFPLCT(5)+6
IFPLCT=15 8 IFPLCT=5+IFPLCT 8 IFPLCT=2+IFPLCT

```

SUBROUTINE GENRAT (continued)

```

CO 504 I=1.9
INIST(I)=1
GO TO 500
509 REAC 20,A1,(IFPLCT(I),I=1,6),A2,LINES
PRINT 20,A1,(IFPLCT(I),I=1,6),A2,LINES
IF (IFPLCT(I) .EQ. C) GO TO 510
REAC 21,A1,A2,ITPLCT,A3,NTPLCT,A4,IFLAGI
PRINT 21,A1,A2,ITPLCT,A3,NTPLCT,A4,IFLAGI
510 IF (IFPLCT(I) .EQ. C) GO TO 500
READ 22,A1,A2,(IHIST(I),I=1,6),A3,(IHIST(I),I=7,9),A4,IFLAGJ
PRINT 22,A1,A2,(IHIST(I),I=1,6),A3,(IHIST(I),I=7,9),A4,IFLAGJ

C
C      CHECK FOR THE END OF DATA DECK
500 REAC 60,A1
IF (ECF,10) 600,503
503 WRITE (10,55)
505 READ 60,A1
IF (ECF,10) 100,505

C
C      **** INITIALIZE CONDITION,DENSITY,TENSILE AND YIELD VARIABLES ****
C
600 J=C
CO 630 P=1,NMTRLS
YOM=Y0(P)=.66667*Y0(P)
EJ=0. 8 CJ=5.E5
IF (NPORE(M,1) .NE. C) GO TO 601
NM=SCALE 8 PUM=PU(M) 8 DCLD=RVC(P)
CALL ECSTIEJ,RHOM(M),PJ,P,CJ)
GO TO 602
601 NM=POROUS 8 DCLD=DREF*NHC(M) 8 NC=1 8 F=1. 8 PJ=C.
CALL PCREGSTIEJ,RHC(M),PJ,P,NPCF(2,2),CJ)
602 JN=JNCH(M)
JL=J+1
CC 610 J=J1,JN
CML(J)=CJ1=CJ
DML(J)=CJ1=RHC(M)
X(J,1)=PM
H(J,2)=AORPAL
H(J,3)=2
T(J)=TENSIN,1)
YHL(J)=YOM
ZHL(J)=Q(J)*(X(J+1)-X(J))
ASPM=ASPM+1
CO 70 (410,41C,4C5,4C6,610,41C,6C7) ASPM
605 NEPIJ=RLX(P,7) 8 NETIJ=RLX(M,8) 8 CC TC 61C
606 NHEIJ=RLX(M,5) 8 NETIJ=0. 8 CC TC 610
607 NCP(J)=NUC(M)
610 CONTINUE
H(J,2)=RINTER
T(J)=TENSIN,3)
H(J,3)=LATER
630 CONTINUE
H(J,2)=H(J,2)+SFALL
ETAM=1.E-12
IF (NATPL) 819,700,600

C
C***** DEPOSITION EDIT
C
700 WRITE (10,14) ICISCT(I),I=1,1C)
JSEG=1 8 ALL(CCI)=C.
CO 704 P=1,NMTRLS
JNCH=JNCH(M)
CO 703 J=JSEG,JNCH
H(J)=H(J+1)-H(J)
EPG=0.
CO 702 AS=1,NSPT
EPG=SSIJ,NSJ*(1,STOPIN)-1*PARTIN)+EPG
C
C      TEST FOR SETTING JSTAR
IF (EPCREQSIG(M) .GT. 1.ETI JSTAR=J
C
C      STORE ENERGY (ERGS/GP), CALORIES AND SUM OF CALORIES IN -A-
H(J+500)=EPG 8 H(J+1000)=EPG*(4.186E)
H(J+1500)=H(J+1000)+ZHL(J)+H(J+1400)
703 CONTINUE 8 JSEG=JNCH(M)+1
704 CONTINUE

```

SUBROUTINE GENRAT (continued)

```

P=K-J1-1
710 J2=PIAC(JFIN-1,500K,JEND(P))
WRITE (18,15) (J,A(J),K(J),A(J+500),A(J+1000),VPL(J),C(J),D(J),
1 T(J),ZHL(J),MATL(1,M),MATL(2,M),(P(J),I=1,3),J,J=J1,J2)
IF (J2 .EQ. JFIN-1) GO TO 500
J1=J2+1
IF (J2 .NE. 500K) GO TO 710
K=K+1 & WRITE (18,14) (DISCPT(I),I=1,10)
710 IF (J2 .NE. JEND(M)) GO TO 710
M=M+1 & WRITE (18,69) & GO TO 710
C
C ***** INITIALIZE VELOCITY *****
800 JFIN2=JEND(MATL)
DO 810 J=1,JFIN2
810 L(J)=LHL(J)-UZERO
JSTAR=JFIN2+3 & SCLRN=1. & GO TO 810
815 H(1,2)=PIRCA & JSTAR=3 & SCLPP=1.
U(1)=.5*UZERO
C
C ***** VELOCITY EDIT *****
810 WRITE (18,16) (DISCPT(I),I=1,10)
DO 820 J=1,JFIN
820 A(J)=K(J+1)-K(J)
M=K-J1-1
825 J2=PIAC(JFIN-1,500K,JEND(P))
WRITE (18,17) (J,A(J),K(J),L(J),ZHL(J),C(J),T(J),ZHL(J),
1 MATL(1,M),MATL(2,M),(H(J),I=1,3),J,J=J1,J2)
IF (J2 .EQ. JFIN-1) GO TO 500
J1=J2+1
IF (J2 .NE. 500K) GO TO 830
K=K+1 & WRITE (18,16) (DISCPT(I),I=1,10)
830 IF (J2 .NE. JEND(M)) GO TO 825
M=M+1 & WRITE (18,69) & GO TO 825
900 CALL SECND(TWIX) & CUR=TWIX-FIRST
WRITE (18,18) CUR
WRITE (18,41)
RETURN
C
10 FORMAT (A7,13,A7,13,A7,13,AP,2X,E10.3,AE,4X,E10.3)
11 FORMAT (3A7,A5,E10.3)
12 FORMAT (8E10.3)
14 FORMAT (H1,1CAIC//
1 J DX A(J) EPC SLPCL VPL(J) C(J) 1310
2 D(J) T(J) ZHL(J) PATERAL CCAC J
3 /IC2H CM CM ERGS/GP CALS DYN/CP2 CM/S
4EC GM/CM3 DYN/CM2 CM/CM2 1
15 FORMAT (14, 9E10.3,2X,2A10.3(12,R11,15)
16 FORMAT (H1,10-10//
1 J DX A(J) U(J) VPL(J) C(J) C(J) 131H
2 T(J) ZHL(J) PATERAL CCAC J
3 /IC2H CM CM CM/SEC DYN/CM2 CM/SEC GM/C
4M3 DYN/CM2 GP/CP2 1
17 FORMAT (14, 8E10.3,2X,2A10.3(12,R11,15)
18 FORMAT (20H TIME TO COMPLETE GENRAT IS FIC.3,9H SECONDS.)
20 FORMAT (A10,4(1H,12),A9,11)
21 FORMAT (A10,2(AE,12))
22 FORMAT (2A10,4(15,A5,3(15,A8,12))
31 FORMAT (H1,25X,350-0000 SRI PUFF 1 (2ACC VERSION) 0000 /)
35 FORMAT (11C)
41 FORMAT (1H1)
43 FORMAT (17H DATE = A10)
44 FORMAT (2A4,12,2(A1,12),4X,4A,14,2(12,12))
45 FORMAT (A10,11C,6A1C)
54 FORMAT (A8,12,2A4,E10.3)
58 FORMAT (7A5,E10.3)
59 FORMAT (A1,A4,7A1Q)
60 FORMAT (8A1C)
61 FORMAT (7A10,2A5)
62 FORMAT (A8,12,A5,15,2(2A5,E10.3))
64 FORMAT (A8,A7,15,3(2A5,E10.3))
69 FORMAT ( )

```

SUBROUTINE GENRAT (continued)

```

70  FORMAT (1H0)
72  FORMAT (3A10,I10,2(A10,E10.3))
73  FORMAT (2(A10,I10),A10,E10.3,A10,I10)
74  FORMAT (4(2A5,I10))
76  FORMAT(2A5,7E10.3)
77  FORMAT (2A5,5F10.4)
78  FORMAT(2A5,14I5)
79  FORMAT(10X,7E10.3)
80  FORMAT(10X,14I5)
82  FORMAT (3A10,F10.3,4(A8,I2))
92  FORMAT(4(2A5,E10.3))
94  FORMAT (4(A8,2X,E10.3))
95  FORMAT(38HOERRR ENCOUNTERED READING INFLY DATA.)
    END

```

SUBROUTINE GENRAT (concluded)

```

C      SUBROUTINE HAFSTEP
C      (INCLUDES ENTRY HSTRESS)
C      * CALLED BY HYDRC TO COMPUTE X, L, C, E, R, S, P FOR THE
C      * HALFSTEP POINT BETWEEN J AND J+1
C
C      REAL MATL,MU,MUM,MUP,NEM,NET,MECH
C      INTEGER X,PGRELS,MINTER,SCLIC,SPALL
C      MISCELLANEOUS
C      COMMON CEF,CKS,DANG,DELYIN,DOLD,DRHC,DTAIN,CTA,CTAH,DU,DX,EOLD,F,
1 FIRST,J,JCYCS,JINIT,JFIN,JSMAX,JSTAR,JTS,LSLB(11),MAXPR(11),N,
2 NCYCS,NPERN,POLD,RLAST,SLAST,SMAX,TF,TIME,TJ,TS,ULAST,UCLD,
3 XLAST,XNCH,XCLD
C      EQUATION OF STATE - SOLID
C      COMMON COSQ(6,6),C1(6,6),C2(6),EPELT(6,5),EQSTA(6),EQSTC(6),
1 ECSTC(6),ECSTE(6),EQST(6),EGST(6),ECSTN(6),ECSTS(6),MATL(2,6),
2 PU(6),RHO(6),RHCS(6),TEAS(6,3),YACC(6),YO(6),JBNC(6),NPOR(6,2),
3 P,MUM,NMTRL
C      EQUATION OF STATE - POROUS
C      COMMON AK(6),MUP(6),PORA(4,3),PCP(4,3),PGRC(4,3),RHOP(6,3),
1 YACCP(4,3),DREF,RHCPV,PF,AC
C      RADIATION DEPOSITION
C      COMMON SS(300,5),SSTOP(5),START(5),SCURP,SSTCFP,ASPEC,SSJ,JSS
C      COORDINATE ARRAYS
C      COMMON X(300),C(300),CHL(300),D(300),DML(300),EHL(300),H(300,3),
1 NEM(300),NET(300),P(300),PHL(300),R(300),S(300),SPL(300),T(300),
2 U(300),UHL(300),YHL(300),ZHL(300)
C      HALFSTEP VALUES
C      COMMON CH,DHLAST,CU,EF,PF,RF,RPLAST,SH,SPLAST,UH,UHLAST,XH,XHLAST
C      IDENTIFIERS
C      COMMON DISCP(10),ICENT,JEDIT(20),JREZON(15),ADATE(3),MEDIT,AEDIT,
1 NJEDIT,NR,JREZON,NSEPRAT,NSPALL,ATEDT,ATEX,NTR(5),TECIT(50)
C      CONDITION INDICATORS
C      COMMON INF,LINTER,MIRROR,NORMAL,PGRELS,MINTER,SOLID,SPALL
C      SPALL AND RELAXATION
C      COMMON NSRI(6),TSRI(6,6),LSP(50),DSP(50),LRLX,NICK,NEMH,NETH
C
C      DIMENSION L(10)
C      GO 1 I=1,10
1      L(I)=0
C      CC=0.0
C      DX=X(J+1)-X(J) & EOLD=EHL(J) & UHM=.5*(U(J)+U(J+1))
C      DCLD=DHL(J) & G2=0.
C      IF (C(J+1)*C(J)+U(J+1)*U(J)+C2(M)*C2(M)*EC(C)) 7.6
6      G2= C2(M)*ABS(C(J+1)-C(J))*RHC(M)/(C(J+1)*C(J)+DCLD)
7      IF ((1.5*DTN-DTNH)*(1.5*DTN-DTA)) 15,10,10
10      LH=UHL(J)-.5*(DTAH+CTN)/DX+G2*(R(J+1)-R(J))/DOLD
C      GO TO 18
15      UH=UHM+.5*(DTN/DX+G2)*(R(J+1)-R(J))/ECLC
18      CHL(J)=DH+ZHL(J)/(LX+.5*DTN*(U(J+1)-C(J)))-DCLD*G2*(U(J+1)-U(J))
C      UHL(J)=LH
C      XH=.5*(X(J+1)+X(J))+.2*DTN*(LH+UH)
C      EHL(J)=EH=EOLD+.5*(R(J+1)+R(J))*1./DH-1./DCLD)+SSCALH(J)
C      HSTRESS ENTRY AND STRESS COMPUTATION
C      ENTRY HSTRESS
C      F=PELT(EH,M)
C      IF (DM) 20,20,25
20      PRINT 110,A,J,DH,TIME
C      CALL ECDUMP & LSUB(7)=1 & N=N-1 & CALL SCRIBE & STOP
C      COMPUTE CLC VALUE OF SC
25      SDH=SPL(J)-PHL(J) & TF=1.+EH*EQSTA(P) & DREF=CH*TF
C      ESTABLISH ROUTE
C      IF (HIJ,1) .NE. POROUS) GO TO 50
C      IF (F .GT. 0.) GO TO 40
C      UNCONSOLIDATED
C      MUM=0. & CALL ECST(EH,DH,PHL(J),P,CC)
C      L(3)=52
C      SDH=RH=0.
C      IF (PHL(J) .LT. 0.) 37,39
37      PHL(J)=SML(J)=0. & GO TO 50
39      HIJ,1)=SOLID & L(4)=39 & GO TO 53
C      SELECT POROUS REGION
40      RHOPV=F*(RHCP(3 ,PP)-RHCS(P))+RHCS(M)/TF
C      L(3)=40

```

SUBROUTINE HAFSTEP

```

43 IF (DH .GT. RHOPV) 49,43
NC=0
L(4)=43
45 NC=NC+1
IF (DREF .GT. RHOP(NC+1,MP) .AND. NC .LT. NPOR(M,2)) 45,60
C SOLID
49 H(J,1)=SOLID
50 MUH=MU(M)*F
CALL EQST(EH,DH,PHL(J),M,CHL(J))
L(5)=50
53 YADDH=YADDH(M) $ NC=5
IF (NPOR(M,1)) 55,55,54
54 DREF=AMAX1(DREF,RHOP(5,MP))
IF (DREF-RHOP(6,MP)) 67,55,55
55 COT=COSQ(M,6) $ CIT=C1(M,6)
L(6)=55
GO TO 70
C POROUS
60 CALL POREQST (EH,DH,PHL(J),M,MP,CHL(J))
L(5)=60
YADDH=YADDH(M,MP)
67 COT=COSQ(M,NC)+(COSQ(M,NC+1)-COSQ(M,NC))*(DREF-RHOP(NC,MP))
1 / (RHOP(NC+1,MP)-RHOP(NC,MP))
CIT=C1(M,NC)+(C1(M,NC+1)-C1(M,NC))*(DREF-RHOP(NC,MP))
1 / (RHOP(NC+1,MP)-RHOP(NC,MP))
L(6)=67
C VELOCITY GRADIENT AND TIME STEP PARAMETERS
70 DUH=-2.*(DH-DOLD)*(X(J+1)-X(J))/(DH+DOLD)*DTNH
DUHM=AMIN1(DUH,0.) $ CS=CHL(J)-DUH/2.
CF=CIT-COT*DUHM/CS $ CEF=CS*(1.+CF*(1.+5*CF))
C DEVIATOR STRESS
IF (NSRM) .EQ. 0) GO TO 78
DRHO=DH-DOLD $ DAVG=(DH+DOLD)/2.
SDH=SDH $ COEF=MU*DRHO/DAVG $ MEOW=2.*MUH
NSRM=NSRM(M) $ DNUM=MUM
GO TO (73,74,74,73,75) NSRM
73 CALL RELAX(SDH,H(J,3),YHL(J),SDO,DTNH,TSR(M,1),DRHO,COEF,YADDH,N,
1 J,TSR(M,2),YO(M),NSRM)
GO TO 80
74 CONTINUE
CALL BANDRLX(SDH,H(J,3),YHL(J),SDO,DTNH,DRHO,COEF,MEOW,YADDH,N,J,
1 TSR(M,1),TSR(M,2),TSR(M,3),TSR(M,4),TSR(M,5),TSR(M,6),NEM(J),
2 NET(J),NSRM)
GO TO 80
75 CALL BAUSCHI(H(J,3),SDO,SDH,YHL(J),YO(M),YADDH,DRHO,COEF,TSR(M,1),
1 TSR(M,2),MUH,N,J,DAVG,TSR(M,3),TSR(M,4))
CJ=CHL(J) $ CSQ=CJ*CJ+AMAX1(0.,MUM-DMUM)/DAVG
CQ=CSQ+CJ*CJ $ CHL(J)=CSQ*CJ/CQ+.25*CQ/CJ
GO TO 80
78 SDH=SDH+2.*MUM*(DH-DOLD)/(DH+DOLD)
L(7)=78
IF (ABS(SDH) .LT. YHL(J)*F) GO TO 80
YHL(J)=AMIN1(ABS(SDH),YHL(J)+YADDH*ABS(DH-DOLD))
SDH=SIGN(YHL(J)*F,SDH)
L(8)=79
C RESULTANT STRESS
80 SHL(J)=PHL(J)+SDH $ RH=SHL(J)-.5*CF*CS*DUHM*(DH+DOLD)
90 IF (INSEPRAT .GE. 0) GO TO 100
IF (TRH .LT. 0.) .AND. (F .EQ. 0.) 95,100
95 RH=PHL(J)-SHL(J)+SDH=0.
100 IF (LSUB(3) .GE. MAXPR(3)) GO TO 120
LSUB(3)=LSUB(3)+1
WRITE (18,5000) J,N,EH,DH,PHL(J),SDH,(L(1),1-1,8)
WRITE (18,5001) CHL(J),CS,CEF,COT,CIT,RH
120 RETURN
150 FORMAT (20H STOP IN HAFSTEP, N=14,4H, J=14,4H, D=E10.3,
1 7H, TIME=E10.3)
5000 FORMAT (15H HAFSTEP, J=13,4H, N=14,4H EH=E10.3,4H DH=E10.3,
1 4H PH=E10.3,5H SDH=E10.3,3H L=8I3)
5001 FORMAT (6H C=E10.3,5H, CS=E10.3,4H, CEF=E10.3,4H, COT=E10.3,
1 6H, CIT=E10.3,5H, RH=E10.3)
END

```

SUBROUTINE HAFSTEP (concluded)

```

SUBROUTINE HYDRC
C
C SUBROUTINE CONTROLS THE MAIN CALCULATION CYCLE
C * CONTAINS 4 PATHS -
C 1. NORMAL - COORDINATES WITHIN MATERIAL
C 2. INTERFACE - INTERFACE BETWEEN MATERIALS
C 3. INTERFACE SPALL - SEPARATED INTERFACE BETWEEN MATERIALS
C 4. SPALL - COORDINATE AT WHICH SEPARATION HAS OCCURRED
C * CALLS HALFSTEP FOR HALFSTEP CALCULATIONS AT EACH COORDINATE
C * CALCULATES X, U, D, E, AND CALLS JSTRESS TO OBTAIN STRESSES
C * CHECKS FOR SPALLING AND RECOMBINATION
C * COMPUTES MINIMUM PERMITTED TIME STEP FOR NEXT CYCLE
C
C * SET DOLD, EOLD, DU, P(I), S(I) IN PREPARATION FOR JSTRESS.
REAL MATL, MU, MUM, MUP, NEM, NET
INTEGER H, PORCLS, RINTER, SOLID, SPALL
INTEGER HJ, HJ3
C MISCELLANEOUS
COMMON CEF, CKS, DAVG, CELTIN, CCLD, CRPC, CTHIN, CTN, CTNH, DU, DX, EOLD, F,
1 FIRST, J, JCYCS, JINIT, JFIN, JSMAX, JSTAR, JTS, LSLB(11), MAXPR(11), N,
2 NCYCS, NPERN, PCLD, RLAST, SLAST, SPAX, TF, TIME, TJ, TS, ULAST, UOLD,
3 XLAST, XACH, XCLD
C EQUATION OF STATE - SOLID
COMMON COSQ(6,6), C1(6,6), C2(6), EMELT(2,5), EQSTA(6), EQSTC(6),
1 EQSTD(6), EQSTE(6), EQSTG(6), ECSTH(6), ECSTN(6), ECSTS(6), MATL(2,6),
2 RL(6), RHO(6), RHCS(6), TENS(6,3), YACC(6), YO(6), JBND(6), NPCR(6,2),
3 M, NUM, NMYRLS
C EQUATION OF STATE - POROUS
COMMON AK(6), MUP(6), POR(4,3), PORB(4,3), PCRC(4,3), RHCP(6,3),
1 YACCP(4,3), DREF, RMCV, PF, AC
C REACTION DEPOSITION
COMMON SS(300,5), SSTOP(5), START(5), SCURP, SSTCP, NSPEC, SSJ, JSS
C COORDINATE ARRAYS
COMMON X(300), C(300), CHL(300), D(300), DHL(300), EHL(300), H(200,3),
1 NEM(300), NET(300), P(300), FHL(200), PE(200), S(300), SP(300), T(300),
2 U(300), UHL(300), YHL(300), ZHL(300)
C HALFSTEP VALUES
COMMON CH, DHLAST, CLF, EP, PH, RH, RLAST, SH, SHLAST, UH, UHLAST, XH, XHLAST
C IDENTIFIERS
COMMON DISCPT(10), IDENT, JEDIT(20), JREZCN(15), KDATE(3), NEDIT, NEDTM,
1 NJEDIT, NR, NREZCN, NSEPRAT, NSPALL, NTEDT, NTEX, NTRI(15), TEDIT(50)
C CONDITION INDICATORS
COMMON INF, LINTER, MIRROR, NORMAL, PORCLS, RINTER, SOLID, SPALL
C SPALL AND RELAXATION
COMMON NSRI(6), TSR(6,6), USP(50), XSF(50), LRLX, NICK, NPH, NEYH
C
C DIMENSION L(10)
C
C CALL SECOND(XNOW) & DUR=XNOW-FIRST & DT=DTMIN+1.
C SMAX=0.
C
C OUTER HYDRC LOOP
DO 1000 NN=1, NCYCS
TIME=TIME+DTNH
JSPALL=0
M=MP=0
DO 900 J=JINIT, JFIN
IF (LSLB(11).GE. MAXPR(11)) GO TO 3
WRITE (18,5000) N, J, P(J,2)
DO 2 I=1, 10
L(I)=0
C CHECK FOR THE APPROPRIATE PATH
MOLD=X(I) & COLD=U(I) & ROLD=P(I)
IF (P(J,2) .EQ. NORMAL) GO TO 1CC
IF (P(J,2) .EQ. LINTER) GO TO 900
IF (P(J,2) .EQ. RINTER) GO TO 2CC
IF (P(J,2) .EQ. SPALL) GO TO 300
IF (P(J,2) .EQ. MIRROR) GO TO 400

```

SUBROUTINE HYDRO

```

C
C*****      NORMAL PATH WITHIN A MATERIAL      *****
C
100  IF (NSPEC .GT. 0 .OR. ABS(U(J)-U(J+1)) .GT. 1.E-3 .OR.
1    ABS(RHLAST) .GT. 1.) GO TO 102
101  UN=U(J) & RH=R(J) & XH=.5*(X(J+1)+X(J)+DTNH*U(J))
      L(1)=101
      DH=DH(J) & EH=EHL(J)
      UNEW=U(J)
      X(J)=X(J)+DTNH*U(J) & SSJ=SSCAL(J) & GO TO 800
102  CALL HAFSTEP
      L(1)=102
      DOLD=.5*(DH+DHLAST) & EOLD=.5*(EH+EHLAST)
      P(J)=.5*(PHL(J)+PHL(J-1)) & YJ=.5*(YHL(J)+YHL(J-1))
      S(J)=.5*(SHL(J)+SHL(J-1))
C      VELOCITY CALCULATION
      U(J)=UOLD-.5*DTNH*(RH-RHLAST)/(ZHL(J-1)+ZHL(J))
C      COORDINATE CALCULATION
      X(J)=X(J)+.5*DTNH*(U(J)+UOLD)
C      DENSITY CALCULATION
      D(J)=DOLD/(1+.5*DTNH*(U(J+1)-ULAST)/(X(J+1)-XLAST))
C      ENERGY CALCULATION
103  SSJ1=SSCAL(J)
      EJ=EOLD-.5*(RH+RHLAST)*(1./D(J)-1./DOLD)+SSJ+SSJ1
      SSJ=SSJ1
C      STRESS CALCULATIONS
      DU=UH-UHLAST & HJ=SORID
      IF ((H(J-1,1) .EQ. POROUS) .OR. (H(J,1) .EQ. POROUS)) HJ=POROUS
      HJ3=2
      IF (NSR(H) .EQ. 0) GO TO 106
      IF (ABS(S(J)-P(J)) .GT. YJ) HJ3=2-IFIX(SIGN(1,S(J)-P(J)))
      NSRM=NSR(H) & GO TO (106,104,104,106,105) NSRM
104  NEMH=.5*(NEM(J)+NEM(J-1)) & NETH=.5*(NET(J)+NET(J-1)) & GO TO 106
105  IL=MNO(H(J,3),H(J-1,3)) & IH=MAX0(H(J,3),H(J-1,3))
      IF ((IH-IL-1)*(IH-IL-5) .EQ. 0) .AND. (HJ3 .EQ. 2) IL=IH
      HJ3=IL
106  CALL JSTRESSIN,MP,J,EJ,HJ,HJ3,YJ
      UHL(J-1)=.025*(U(J)+UNEW+UOLD+ULAST)+.9*UHLAST
      UNEW=U(J)
      DT=(X(J+1)+U(J+1)*DTNH-X(J))/CEF
      IF(DT.LT.0.0) DT=1.0
C
C      CHECK STRESS AND SET INDICATORS FOR SPALL
C
108  IF (R(J) .GT. TJ) GO TO 800
      IF ((NSEPRAT .GE. 0) .OR. (F .GT. 0.)) GO TO 110
      R(J)=S(J)-P(J)=0. & GO TO 800
110  JFINM1=JFIN-1
      L(2)=110
      IF (NSPALL .EQ. 0) 114,111
      DO 113 I=1,NSPALL
111  DO 112 JJ=1,JFINM1
      IF (H(IJJ,2) .EQ. 1) 113,112
112  CONTINUE & NSP=H(J,2)=1 & GO TO 115
113  CONTINUE
114  NSP=NSPALL=H(J,2)=NSPALL+1
115  XSP(NSP)=X(J) & USP(NSP)=U(J)
      IF (LSUB(9) .GE. MAXPR(9)) GO TO 120
      DESC=10H SPALLED
      WRITE (18,5115) DESC,N,NH,J,NSPALL,NSP,R(J),TJ,TIME
      WRITE (18,5050) DT,R(J),S(J),C(J),D(J),T(J),U(J),UH,DH,EH,PHL(J),
1    RH,XH,L(1),I=1,5)
      WRITE (18,5051) DTMIN,DTNH,U(J+1),X(J+1),X(J),CEF
120  JSPALL=J
      R(J)=S(J)=T(J)=0.
      GO TO 800
C
C*****      INTERFACE      *****
C
C      LEFT VALUES ARE IN (J-1) CELLS AND RIGHT VALUES ARE IN (J) CELLS

```

SUBROUTINE HYDRO (continued)



```

200 MLAST=M $ MPLAST=MP $ M=M+1 $ MP= NPOR(M,2)
    L(1)=200
    CALL HAFSTEP
    SSJ=SSCAL(J)
C      FIRST ESTIMATE OF UM, HALF STEP VELOCITY AT INTERFACE
205 J1=J-1 $ J2=J-2
    UM=.5*(U(J)+U(J1))-DTNM*(R(J+1)-RLAST+.4*(RH-RHLAST))/
    1 (ZHL(J)+ZHL(J2))/6.
    SSJ1=SSCAL(J1)
    IF (LSUB(10) .GE. MAXPR(10)) GO TO 209
    LSUB(10)=LSUB(10)+1
    WRITE (18,5002) N,MLAST,M,UM,U(J),UM,UHLAST,RH,RHLAST,RLAST,R(J),
    1 R(J),R(J+1)
209 ITER=0
210 ITER=ITER+1
    S(J)=SHL(J) $ P(J)=PHL(J) $ S(J1)=SHL(J2) $ P(J1)=PHL(J2)
C
C      RIGHT SIDE ENERGY AND STRESS CALCULATIONS
    DU=2.*(UH-UM)
    DOLD=DH $ EOLD=EH
    D(J)=DH/(1.+DTNM*(UH-UM)/(X(J+1)-X(J)))
    EJ=EOLD+RH*(1./DOLD-1./D(J))+2.*SSJ
    NEMH=NEM(J) $ NETH=NET(J)
    CALL JSTRESS(M,MP,J,EJ,H(J,1),H(J,3),YHL(J))
C
C      LEFT SIDE ENERGY AND STRESS CALCULATIONS
    DU=2.*(UM-UHLAST)
    DOLD=DHLAST $ EOLD=EHLAST
    D(J-1)=DHLAST/(1.+DTNM*(UM-UHLAST)/(X(J-1)-X(LAST)))
    EJ=EOLD+RHLAST*(1./DOLD-1./D(J-1))+2.*SSJ1
    NEMH=NEM(J2) $ NETH=NET(J2)
    CALL JSTRESS(MLAST,MPLAST,J1,EJ,H(J2,1),H(J2,3),YHL(J2))
    IF (LSUB(10) .GE. MAXPR(10)) GO TO 211
    WRITE (18,5003) ITER,UM,UM1,UM2,UM3,R(J),R(J1),RJ1,RJ11,RJ2,RJ12,
    1 S(J),S(J1)
    CONTINUE
C      ITERATION TO COMPUTE INTERFACE VELOCITY AND STRESS
    IF (ITER .GT. 10) 224,213
213 RS=ABS(R(J))+ABS(R(J1))
    IF (RS .LT. 1.E6) 225,215
215 IF (ABS(R(J)-R(J1))/RS .GT. .01) 216,225
216 IF (ITER-2) 220,219,217
217 IF (ABS(RJ2-RJ12) .LT. ABS(RJ1-RJ11)) 218,219
C      MULTIPLE ITERATION ROUTE
218 UM3=UM2+(UM-UM2)*(RJ12-RJ2)/(R(J)-RJ2-R(J1)+RJ12)
    UM1=UM
    UCON=AMAX1(.2*(ABS(UH)+ABS(UHLAST)+ABS(UM1))*FLOAT(ITER**2),100.)
    UM=UM3+AMAX1(UM1-UCON,AMINI(UM3,UM1+UCON))
    RJ1=R(J) $ RJ11=R(J1) $ GO TO 210
C      2ND AND MULTIPLE ITERATION ROUTE
219 UM3=UM1+(UM-UM1)*(RJ11-RJ1)/(R(J)-RJ1-R(J1)+RJ11)
    UM2=UM
    UCON=AMAX1(.2*(ABS(UH)+ABS(UHLAST)+ABS(UM2))*FLOAT(ITER**2),100.)
    UM=UM3+AMAX1(UM2-UCON,AMINI(UM3,UM2+UCON))
    RJ2=R(J) $ RJ12=R(J1) $ GO TO 210
C      FIRST ITERATION ROUTE
220 UM1=UM
    IF ((UM-UH)*(UHLAST-UM) .EQ. 0.) 225,222
222 UM=UM-(R(J)-R(J1))/(D(J)*C(J)+D(J1)*C(J1))
    UM=AMAX1(AMINI(UM,1.10*AMAX1(UH,UHLAST)),0.90*AMINI(UM,UHLAST))
    RJ1=R(J1) $ RJ11=R(J) $ UM2=UM $ GO TO 210
224 WRITE (18,5224) N,MLAST,M
5224 FORMAT (44H 'INTERFACE ITERATIONS DID NOT CONVERGE AT N=14,
    1 12H BETWEEN M=12,7H AND M=12)
226 WRITE (18,5003) ITER,UM,UM1,UM2,UM3,R(J),R(J1),RJ1,RJ11,RJ2,RJ12,
    1 S(J),S(J1)
C      END OF INTERFACE ITERATION
C      COORDINATE CALCULATION
225 U(J)=U*J1=UOLD-2.*DTNM*(RH-RHLAST)/(ZHL(J2)+ZHL(J1))

```

SUBROUTINE HYDRO (continued)

```

      IF (N*NN .EQ. 1) U(J)=U(J1)=UM
      X(J)=X(J1)=X(J)+.5*DTNH*(U(J)+UOLD)
      DT=(X(J+1)+U(J+1)*DTNH-X(J))/CEF
      IF (DT.LT.0.0) DT=1.0
C      EQUALIZE THE STRESSES
      R(J1)=R(J)+.5*(R(J1)+R(J))
      UHL(J2)=.025*(U(J1)+UNEW+UOLD+ULAST) + .9*UHLAST
      UNEW=U(J)
C
C      CHECK STRESS AND SET INDICATORS FOR SPALL
      IF (R(J1) .LT. T(J1)) 230,800
230  HIJ,2)=SPALL
      L(2)=230
      IF (LSUB(9) .GE. MAXPR(9)) GO TO 235
      DESC=10H INT SPALL
      WRITE (18,5230) DESC,N,NN,M,MLAST,M,R(J1),T(J1),TIME
      CALL EDDIMP
235  R(J)=R(J1)=S(J)=S(J1)=T(J1)=0.
      GO TO 800
C
C*****      INTERFACE SPALL      *****
C
300  IF (J .EQ. JINIT) 330,310
310  MLAST=M & MPLAST=MP
      L(1)=310
C      LEFT SIDE
      J1=J-1 & SSJ1=SSCAL(J1)
      XLOLD=X(J-1) & ULOLD=U(J-1)
      U(J-1)=UOLD+.5*DTNH*RHLAST/ZHL(J-2)
      D(J-1)=DHLAST/(1.+DTNH*(.5*(U(J-1)+UOLD)-UHLAST)/(X(J-1)-XLAST))
      X(J-1)=XLOLD+.5*DTNH*(U(J-1)+UOLD)
      DT=1.
      UHL(J-2)=.25*(U(J-1)+UNEW+UOLD+ULAST)
      IF (J .EQ. JFIN) 900,330
C      RIGHT SIDE
330  M=M+1
      MP=MPOR(M,2)
      L(2)=330
      IF (ABS(U(J)-U(J+1)) .LT. 1.E-3 .AND. NSPEC .EQ. 0) 331,332
331  UM=U(J) & RM=R(J) & XM=.5*(X(J+1)+X(J)+DTNH*U(J))
      X(J)=X(J)+DTNH*U(J) & DT=1. & SSJ=SSCAL(J)
      DM=D(J)
      IF (J .EQ. JINIT) 800,335
332  CALL HAFSTEP
      SSJ=SSCAL(J) & UOLD=U(J) & XOLD=X(J)
      U(J)=UOLD-.5*DTNH*RH/ZHL(J)
      D(J)=DM/(1.+DTNH*(UM-.5*(U(J)+UOLD))/(X(J+1)-X(J)))
      X(J)=XOLD+.5*DTNH*(U(J)+UOLD)
      DT=(X(J+1)+U(J+1)*DTNH-X(J))/CEF
      IF (DT .LT. 0.) DT=1.
      UNEW=U(J)
C      CHECK FOR RECOMBINATION
      IF (J .EQ. JINIT) GO TO 800
335  IF (X(J) .LE. X(J-1)) 361,800
361  IF (LSUB(9) .GE. MAXPR(9)) GO TO 365
      DESC=10HINT RECOMB
      WRITE (18,5230) DESC,N,NN,M,MLAST,M,R(J-1),T(J-1),TIME
C      RESET ARRAY VARIABLES AND GO TO INTERFACE ROUTE
365  HIJ,2)=RINTER & X(J)=XOLD & X(J-1)=XOLD & U(J)=UOLD
      U(J-1)=UOLD & GO TO 205
C
C*****      SPALL WITHIN A MATERIAL      *****
C
C      LEFT VALUES ARE IN J-CELLS AND RIGHT VALUES ARE IN XSP AND USP
C
400  MSP=M(J,2) & XOLD=XSP(MSP) & UOLD=USP(MSP)
      ULOLD=U(J) & T(J)=0. & R(J)=0. & DX=X(J+1)-XOLD
      L(1)=400

```

SUBROUTINE HYDRO (continued)

```

C      LHS CALCULATIONS
U(J)=UOLD+.5*DTNH*RH/AST/ZHL(J-1)
D(J)=DHLAST/(1.+DTNH*(.5*(U(J)+UOLD)-UHLAST)/(X(J)-XLAST))
X(J)=X(J)+.5*DTNH*(U(J)+UOLD)
C      RHS CALCULATIONS
DOLD=DHL(J)  &  EOLD=EHL(J)
XH=.5*(X(J+1)+XOLD)+.25*DTNH*(U(J+1)+UOLD)
UH=.5*(U(J+1)+UOLD)+.5*DTNH*(R(J+1)/(DOLD*DX))
DHL(J)=DH+ZHL(J)/(DX+.5*DTNH*(U(J+1)-UOLD))
EHL(J)=EH+EOLD+.5*(R(J+1)+R(J))*(1./DH-1./DOLD)+SSCALH(J)
C      PREPARATION FOR HSTRESS IN SPALL
CALL HSTRESS
USP(NSP)=UOLD-.5*DTNH*RH/ZHL(J)
XSP(NSP)=XOLD+.5*DTNH*(USP(NSP)+UOLD)
D(J)=.5*(DH+DHL(J))
DT=(X(J+1)+U(J+1)*DTNH-XSP(NSP))/CEF
IF (DT .LT. 0.) DT=1.
UHL(J-1)=.25*(U(J)+UH+UOLD+ULAST)
UNEW=USP(NSP)
C      CHECK FOR RECOMBINATION AND RESET QUANTITIES AT J
IF (XSP(NSP) .LE. X(J)) 410,800
410 H(J,2)=NORMAL
L(2)=410
X(J)=.5*(X(J)+XSP(NSP))
U(J)=.5*(U(J)+USP(NSP))
D(J)=.5*(ZHL(J-1)/(X(J)-X(J-1))+ZHL(J)/(X(J+1)+DTNH*(U(J+1)-X(J)))
IF (NSP .EQ. NSPALL) NSPALL=NSP+1
IF (LSUB(9) .GE. MAXPRI(9)) GO TO 420
DESC=10HRECOMBINED
WRITE (18,5115) DESC,N,NN,J,NSPALL,NSP,R(J),TJ,TIME
WRITE (18,5050) DT,R(J),S(J),C(J),D(J),T(J),U(J),UH,DH,EH,PHL(J),
1 RH,X(J),L(1),I=1,5)
WRITE (18,5051) DTNH,DTNH,U(J+1),X(J+1),X(J),CEF
C      RETURN TO NORMAL PATH FOR STRESS CALCULATIONS
420 P(J)=S(J)=0. & DOLD=.5*(DH+DHLAST) & EOLD=.5*(EH+EHLAST)
YJ=.5*(YHL(J)+YHL(J-1))
IF (0.3*DT .GT. DTMIN) GO TO 103
DTMIN=0.3*DT & JTS=J & GO TO 103
C
C***** MIRROR AT FRONT SURFACE *****
C
500 M=M+1 & MP=NPOR(M,2)
L(1)=500
CALL HAFSTEP
DOLD=DH & EOLD=EH & DU=2.*(UH-U(J))
D(J)=DOLD/(1.+DTNH*(UH-U(J))/(X(J+1)-X(J)))
SSJ=SSCAL(J)
EJ=EOLD+RH*(1./DOLD-1./D(J))+2.*SSJ
S(J)=SHL(J) & P(J)=PHL(J)
NEMH=NEM(J) & NETH=NET(J)
CALL JSTRESS(M,MP,J,EJ,H(J,1),H(J,3),YHL(J))
R(J)=2.*R(J)-S(J)
X(J)=X(J)+DTNH*U(J)
DT=(X(J+1)+DTNH*(U(J+1)-X(J)))/CEF
UNEW=U(J)
IF (R(J) .GT. T(JFIN-1)) GO TO 800
H(J,2)=SPALL
L(2)=530
DESC=10HMIR SPALL
WRITE (18,5230) DESC,N,NN,M,M,R(J),T(JFIN-1),TIME
P(J)=R(J)-S(J)-T(JFIN-1)=0.
C
C***** END OF MIRROR PATH *****
C
800 CONTINUE
L(4)=800
C***** END OF CYCLE RESET *****
RLAST=XOLD & ULAST=UOLD & RLAST=XOLD
RHLAST=XH & UHLAST=UH & RHLAST=RH & DHLAST=DH
EHLAST=EH & SHLAST=SH

```

SUBROUTINE HYDRO (continued)

```

C
C      SMAX CALCULATION
      IF (S(J) .GT. SMAX) 820,822
820  SMAX=S(J) 8 JSMAX=J
C
C      TIME STEP CALCULATION
822  IF (DT .LT. DTMIN) 824,826
824  DTMIN=DT 8 JTS=J
826  DTP=DT
      IF (LSUB(1) .GE. MAXPR(1)) GO TO 850
      WRITE (18,5050) DT,R(J),S(J),C(J),D(J),T(J),U(J),UM,DM,EM,PHL(J),
1  RM,XM,(L(1),I=1,5)
      WRITE (18,5051) DTMIN,DTNH,U(J+1),X(J+1),X(J),CEF
      LSUB(1)=LSUB(1)+1
C
C      JSTAR CALCULATION
850  IF (ABS(U(J)) .LT. 1.E-3) 851,900
851  IF (J .GT. JSTAR) 852,900
852  JSTAR=J-1
      GO TO 990
C
C      END OF HYDRO INNER LOOP
900  CONTINUE
      JSTAR=JFIN-1
      DTN=DTNH
990  IF (JSPALL*ONSEPRAT .LE. 0) GO TO 1000
      JINIT=JSPALL 8 H(JINIT,2)=SPALL
C
C      END OF HYDRO OUTER LOOP
1000 CONTINUE
      IF (LSUB(8) .LT. MAYPR(8)) 1001,1002
1001 CALL SECOND(TWIX) 8 DUR=TWIX-XNOW
      WRITE (18,5010) N,DUR
      LSUB(8)=LSUB(8)+1
1002 RETURN
5000 FORMAT(16H)HYDRO BEGIN. N=14.3H J=14.8H H(J,2)=R1)
5002 FORMAT(12H)HYDRO, INTERFACE, N=15.4H, M=12.5H AND 12.5H, UM=
1  E10.3/ 9H U(J)=E10.3,4H UM=2E10.3,4H RM=2E10.3,
2  4H, R=4E10.3 /128H
3  ITER UM UM1 UM2 UM3 R(J) R(J-1)
4  RJ1 RJ11 RJ2 RJ12 S(J) S(J-1)
5003 FORMAT(14,12E10.3)
5006 FORMAT(18H)---IKT SPALL UM= 2E10.3,4H DU=2E10.3,4H DM=2E10.3,
1  4H RM=2E10.3,7X,3H X=2E10.3,3H U=2E10.3,3H E=2E10.3)
5010 FORMAT(22H)HYDRO COMPLETE-----M=14.22H, CALCULATION TIME IS F10.3,
1  9H SECONDS.//)
5115 FORMAT(1H ,A10.7H N, NM=214.4H, J=14.6H, NSP=213.7H, R, T=2E10.3,
1  7H, TIME=E10.3)
5230 FORMAT(1H ,A10.7H N, NM=214.4H, H=213.7H, R, T=2E10.3,7H, TIME=,
1  E10.3)
5050 FORMAT(10H)HYDRO DT=E10.3,3H R=E10.3,3H S=E10.3,3H C=E10.3,
1  3H D=E10.3,3H T=E10.3,3H U=E10.3/ 7X,4H UM=E10.3,4H DM=E10.3,
2  4H EM=E10.3,4H PH=E10.3,4H RM=E10.3,4H XM=E10.3,4H, L=514)
5051 FORMAT(10H DT=2E10.3,9H, U(J+1)=E10.3,6H, X=5=2E10.3,
1  6H, CEF=E10.3)
      END

```

SUBROUTINE HYDRO (concluded)

```

SUBROUTINE JSTRESS(MJ,MPJ,JJ,EJ,HJ,HJ3,YJ)
C
C CALL ED BY HYDRO TO COMPUTE R, S, P, AND TO SET T
C * CALLS EQST, POREQST, AND FMELT
C * TERMINATES THE PROGRAM FOR A NEGATIVE DENSITY
C
REAL MATL,MU,MUM,MUP,NL,NET,MEOM
INTEGER H,POROUS,RINTER,SOLID,SPALL
INTEGER MJ,HJ3
C MISCELLANEOUS
COMMON CEF,CKS,DAVG,DELTIM,DOLD,DRHO,DTHIN,DTN,DTNM,DU,DX,EOLD,F,
1 FIRST,J,JCYCS,JINIT,JFIN,JSNAX,JSTAR,JTS,LSUB(11),MAXPR(11),N,
2 NCYCS,NPERN,POLD,RLAST,SLAST,SNAX,TF,TIME,TJ,TS,ULAST,UOLD,
3 XLAST,XNOW,XOLD
C EQUATION OF STATE - SOLID
COMMON COSQ(6,6),C1(6,6),C2(6),EMELT(6,5),EQSTA(6),EQSTC(6),
1 EQSTD(6),EQSTE(6),EQSTG(6),EQSTH(6),EQSTN(6),EQSTS(6),MATL(2,6),
2 MU(6),RHO(6),RHOS(6),TENS(6,3),YADD(6),YO(6),JBND(6),NPOR(6,2),
3 M,MUM,MATRLS
C EQUATION OF STATE - POROUS
COMMON AK(6),MUPI(6),PORAI(4,3),PORB(4,3),PORC(4,3),RHOP(6,3),
1 YADDP(4,3),DREF,RHOPV,MP,NC
C RADIATION DEPOSITION
COMMON SS(300,5),SSTOP(5),SOURN,SSTOPM,NSPEC,SSJ,JSS
C COORDINATE ARRAYS
COMMON X(300),C(300),CHL(300),DI(300),DML(300),EML(300),HI(300,3),
1 NEM(300),NET(300),PI(300),TML(300),R(300),S(300),SHL(300),T(300),
2 U(300),UHL(300),YHL(300),ZHL(300)
C HALFSTEP VALUES
COMMON DH,DHLAST,DUM,EN,PH,RH,RHLAST,SH,SHLAST,UM,UNLAST,XH,XHLAST
C IDENTIFIERS
COMMON DISCPT(10),IDENT,JEDIT(20),JREZON(15),NDATE(3),NEDIT,NEDTH,
1 NJEDIT,NR,NRETON,NSEPRAT,NSPALL,NTEOT,NTEX,NTR(15),TEDIT(50)
C CONDITION INDICATORS
COMMON IMF,LINTER,MIRROR,NORMAL,POROUS,RINTER,SOLID,SPALL
C SPALL AND RELAXATION
COMMON NSR(6),TSR(6,6),USP(50),XSP(50),LRLX,NICK,NEMM,NETH
C
DIMENSION L(10)
DO I=1,10
L(I)=0
CC=U.O
IF (DI(JJ)) 20,20,25
PRINT 110,N,JJ,DI(JJ),TIME
CALL EDDUMP & LSUB(7)=1 & N=N-1 & CALL SCRIBE & STOP
25 SOJ=S(JJ)-PI(JJ)
F=FMELT(EJ,MJ) & TF=1.-EJ*EQSTAI(MJ) & DREF=DI(JJ)*TF
C ESTABLISH ROUTE
IF (MJ.EQ. SOLID) 50,50
IF (F.GT. 0.) GO TO 40
C UNCONSOLIDATED REGION
MUM=0. & CALL EQSTIEJ,DI(JJ),PI(JJ),MJ,CC)
L(2)=32
IF (PI(JJ).LT. 0.) 37,51
37 PI(JJ)=S(JJ)-RI(JJ)=0. & GO TO 85
C SELECT POROUS REGION
40 RHOPV=F*(RHOP(5,MPJ)-RHOS(MJ)) + RHOS(MJ)/TF
L(3)=40
IF (DI(JJ).GT. RHOPV) 50,43
43 NC=0
45 NC=NC+1
IF (DREF.GT. RHOP(NC+1,MPJ).AND. NC.LT. NPOR(MJ,2)) 45,60
C PRESSURE, SOUND SPEED, TENSILE STRENGTH IN SOLID
50 MUM=MUM(MJ)*F & CALL EQSTIEJ,DI(JJ),PI(JJ),MJ,C(JJ))
L(3)=50
51 YADD=YADD(MJ) & NC=5 & TJ=T(JJ)*F
IF (MPOR(MJ,1)) 57,57,56
56 DREF=AXAL(DREF,RHOP(5,MPJ))
L(4)=56
IF (DREF-RHOP(6,MPJ)) 67,57,57
57 GOT=COSQ(MJ,6) & C1=C1(MJ,6)
L(5)=57
GO TO 70

```

SUBROUTINE JSTRESS

```

C          PRESSURE AND TENSILE STRENGTH IN PORELS
60          CALL POREQST(EJ,C(JJ),PEJJ),PJ,PPJ,C(JJ)
          L(6)=60
          YACD=YACDP(AC,PPJ)
          TJ=0.
          IF (T(JJ) .NE. C.) 65,67
65          TJ=(TENS(MJ,2)+(TENS(MJ,1)-TENS(PJ,2))*(CREF-RHC(PJ))/
          1 (RHCPI5,PPJ)-RHC(PJ)))*F
          L(7)=65
67          COT=COSQ(MJ,NC)+(COSQ(MJ,NC+1)-CCSC(MJ,NC))*(CREF-RHOP(NC,MPJ)
          1 /(RHCPI(NC+1,PPJ)-RHOP(NC,MPJ))
          CIT=C1(MJ,NC)+(C1(MJ,NC+1)-C1(MJ,AC))*(CREF-RHCP(AC,PPJ)
          1 /(RHCPI(AC+1,PPJ)-RHCP(AC,MPJ))
          L(8)=67
C          ARTIFICIAL VISCOSITY
70          CU=APIA1(CU,0.)
          L(9)=70
          CJ=(CU*(COT-CIT)*C(JJ))*CU*(C(JJ)+DCLD)/2.
C          DEVIATOR STRESS CALCULATION
          IF (NSR(MJ) .EQ. 0) GO TO 78
          CRNO=C(JJ)-CCLC 3 CAVG=(C(JJ)+DCLD)/2.
          SDO=SDJ 8 CCEF=PI*P*DRHC/CAVG 8 PECH=2.*MUM
          NSRP=NSR(MJ) 8 CT=.5*DTNH
          GO TO (73,74,74,73,75) NSRP
73          CALL RELAX(SCJ,PJ3,YJ,SCQ,DT,TSR(MJ,1),DRHC,CCEF,YACDP,N,JJ,
          1 TSR(MJ,2),Y0(MJ),NSRP)
          GO TO 80
74          CALL BAADMLX(SDJ,PJ3,YJ,SCQ,DT,DRHC,CCEF,PECH,YACDP,N,JJ,TSR(MJ,1)
          1 ,TSR(MJ,2),TSR(PJ,3),TSR(MJ,4),TSR(PJ,5),TSR(MJ,6),NEMEJJ),
          2 NETEJJ,NSRP)
          GO TO 80
75          CALL BAUSCHI(PJ3,SCQ,SDJ,YJ,Y0(MJ),YACDP,DRHC,CCEF,TSR(MJ,1),
          1 TSR(MJ,2),MUM,N,JJ,DAVG,TSR(PJ,3),TSR(PJ,4))
          GO TO 80
78          SDJ=SDJ+2.*MUM*(D(JJ)-DCLD)/(D(JJ)+DCLD)
          IF (ABS(SDJ) .LT. YJ*F) GO TO 80
          SDJ=SIGN(MINI(ABS(SDJ)),YJ+YACDP*ABS(D(JJ)-DCLD))*F,SDJ)
C          STRESS COMPUTATION
80          SEJJ=PEJJ+SDJ 8 REJJ=SEJJ+CJ
85          IF (LSUB(2).GE.NAPRI(2)) GO TO 95
          WRITE(10,5000)NC,PJ,PPJ,CJ,SDJ,F,TJ,L(1),1-1,10)
          LSUB(2)=LSUB(2)+1
99          RETURN
5000 FORMAT(1X,JSTRESS NC=0,11,0 NJ=0,11,0 PJ=0,11,0 CJ=0,E10.3,
          1 0 SDJ=0,E10.3,0 F=0,E10.3,0 TJ=0,E10.3,0 L=0,101?)
110          FORMAT(120H STOP IN JSTRESS, N=14,4F, J=14,4F, D=E10.3,
          1 7H, TIME=E10.3)
          END

```

SUBROUTINE JSTRESS (concluded)

```

SUBROUTINE POREQST(EJ,DJ,PJ,MJ,PPJ,CJ)
C
C COMPUTES PRESSURE, BULK AND SHEAR MODULI, AND SOUND SPEED FOR
C POROUS MATERIAL
C
REAL MATL,MU,MUP,MLP
C
C MISCELLANEOUS
COMMON CEF,CKS,DAVG,DELTA,DOLD,DRHO,DTA,DTA1,DTA2,DU,DX,ECLD,F,
1 FIRST,J,JCVCS,JINT,JFIN,JSPAX,JST,JSUTS,LSLE(11),MAXPR(1),N,
2 ACVCS,NPERN,POLC,ALAST,SLAST,SPAT,TF,TEPE,TJ,TS,ULAST,UCLD,
3 PLAST,XNCH,XCLD
C
C EQUATION OF STATE - SOLID
COMMON CESC(6,6),C1(6,6),C2(6,6),EPELT(6,6),ECSTA(6),EQSTC(6),
1 ECSTD(6),ECSTE(6),ECSTG(6),ECSTH(6),ECSTI(6),ECSTS(6),MATL(2,6),
2 MU(6),RNC(6),RHCS(6),TEAS(6,3),YACC(6),VO(6),JENC(6),NPOR(6,2),
3 P,MUP,MTRLS
C
C EQUATION OF STATE - PERCUS
COMMON AK(6),MUP(6),PCRA(4,3),PCRB(4,3),PCRC(4,3),RHOP(6,3),
1 YACCP(4,3),DREF,RHOPV,MP,NC
C
C
C DIMENSION L(10)
C DO 2 I=1,3
2 L(I)=0
C CC=0.0
C IF (NC-NPOR(MJ,1)) 12,20,65
12 P2=P2+PCRA(MJ,PPJ)*(1.-RHOP(MJ,PPJ)/DREF)
1 (PORB(MJ,PPJ)+PORC(MJ,PPJ)*(PMCF(MJ,PPJ)/DREF-1.))
P1=PCRA(2,PPJ)
L(1)=12
CC TO 30
C
C (DENSITY LIES IN THE LAST POROUS REGION BEFORE SOLID)
20 CALL ECST(EJ,RHOPV,PJCIAT,PJ,CC)
C
C (SIMPLIFY EXPRESSIONS AND COMPUTE PRESSURE ALONG THE CURVE)
PAF=PORA(MJ,PPJ)*F DA=RNC(MJ,PPJ)/TF
PCF=4.*PORC(MJ,PPJ)/F*(RHOPV-DN)*(RNCV/DJ-1.)
P2=PAF+RHOPV/(RHOPV-DN)*(1.-DN/DJ)*(PJC1AT-PAF+PCF)
NC=RHOP(MJ,2) P1=PORA(MJ,PPJ)
L(1)=20
C
C COMPUTE BULK PRESSURE AND SELECT MINIMUM
30 RATIO=AKIN(1.,ANAT1((P2-P1)/(PCRB(4,PPJ)-P1),C.))
MUM=(MUP(MJ)+MUP(PJ)-MUP(PJ))*RAT1(C)*F
BULK=(AK(MJ)+ECSTC(MJ)-AK(MJ))*RAT1(C)*F
PBULK=P1+BULK*(DJ-DCLD)/(1.5*(DJ-DCLD))+ECSTAIN(MJ)*EJ-DCLD
IF (PBULK-CT. P2) GO TO 45
IF (NC-LEQ. NPOR(MJ,1)) PBULK=ANAT1(PJC1AT*(1.-RNCV/DJ)/(RNCV-
1 RNC(MJ)/TF),PBULK)
L(2)=40
PJ=PBULK 1 GO TO 50
45 PJ=P2
L(2)=45
C
C SOUND SPEED CALCULATION
50 CS=(BULK*(MUM)/(1.5*(DJ-DCLD)))
IF (CS-CT. 0.) 57,65
57 CG=CSQ*CG*CG 1 CJ=CSQ*CG*CG+.25*CG/CG
L(3)=57
60 IF (LSUB(1).GE. MAXPR(1)) GO TO 65
65 WRITE (10,110) J,N,MJ,PPJ,NC,CJ,DJ,CJ,PJ,P2,PBULK,MUM,MUP,CGF,
1 RHOPV,DOLD,TP,ECLD,CEC,AT(1),P(1,3)
1 (SUB(1)-LSUB(1)) * 2
65 CONTINUE
RETURN
110 FORMAT (11H POREQST J=13,3H N=14,3H P=212,4H AC=12,4H EJ=E1C.3,
1 4H DJ=E10.3,4H CJ=E10.3,3H P=E10.3,4H MOD=E10.3/51,2H D=E10.3,
2 4H TP=E10.3,4H ECLD=E10.3,3H CSC=E10.3,3H L=313)
END

```

SUBROUTINE POREQST (complete)

```

C      SUBROUTINE REZONE
C
C      INCREASES CELL SIZES TO GIVE MORE UNIFORM DISTRIBUTION
C      * STARTS REZONING AT JREZON AND WORKS TOWARD JINIT
C      * DOES NOT DISTURB LOCATION OF INTERFACES, JEDITS, OR SPALLS
C
C      REAL MATL,MU,MUM,MUP,NEM,NE
C      REAL MASS,MOM,MASLAST,MOMLAST,MAGNEXT,MOMNEXT
C      INTEGER M,POROUS,RINTER,SOLID,SPALL
C      INTEGER MC,MJOLD2
C
C      MISCELLANEOUS
C      COMMON CEF,CKS,DAVG,DELTIM,DOLD,DRHO,DTN,J,DTN,DTNH,DU,DX,EOLD,F,
C      1 FIRST,J,JCYCS,JINIT,JFIN,JSMAX,JSTAR,JTS,LSUB(11),MAXPR(11),N,
C      2 JCYCS,NPERN,POLD,RLAST,SLAST,SMAX,TF,TIME,TJ,TS,ULAST,UOLD,
C      3 XLAST,XNOW,XOLD
C
C      EQUATION OF STATE - SOLID
C      COMMON COSQ(6,6),C1(6,6),C2(6,6),EMELT(5,5),EQSTA(6),EQSTC(6),
C      1 EQSTD(6),EQSTE(6),EQSTG(6),EQSTH(6),EQSTN(6),EQSTS(6),MATL(2,6),
C      2 MU(6),RHO(6),RHOS(6),TENS(6,3),YADD(6),YO(6),JBND(6),NPOR(6,2),
C      3 M,MUM,NMTRL
C
C      EQUATION OF STATE - POROUS
C      COMMON AK(6),MU(6),PORA(4,3),PORR(4,3),PORC(4,3),RHOP(6,3),
C      1 YADD(4,3),DREF,RHOPV,MP,NC
C
C      RADIATION DEPOSITION
C      COMMON SS(300,5),SSTOP(5),START(5),SDURH,SSTOPM,NSPEC,SSJ,JSS
C
C      COORDINATE ARRAYS
C      COMMON X(300),C(300),CHL(300),D(300),DHL(300),EHL(300),H(300,3),
C      1 NEM(300),NET(300),P(300),PHL(300),R(300),S(300),SHL(300),Y(300),
C      2 U(300),UHL(300),YHL(300),ZHL(300)
C
C      HALFSTEP VALUES
C      COMMON DH,DHLAST,DUH,FH,PH,RH,RHLAST,SH,SHLAST,UH,UHLAST,XH,XHLAST
C
C      IDENTIFIERS
C      COMMON DISCPT(10),IDENT,JEDIT(20),JREZON(15),NDATE(3),NEDIT,NEDTM,
C      1 NJEDIT,NR,NREZON,NSEPRAT,NSPALL,NTEDT,NTEX,NTR(15),TEDIT(50)
C
C      CONDITION INDICATORS
C      COMMON INF,LINTER,MIRROR,NORMAL,POROUS,RINTER,SOLID,SPALL
C
C      SPALL AND RELAXATION
C      COMMON NSR(6),TSR(6,6),USP(50),XSP(50),LRLX,NICK,NEMH,NETH
C
C      DIMENSION CC(20),DXX(6),EC(20),HC(20,3),MASS(21),MOM(20,2),
C      1 PC(20),RS(21),SC(20),XC(20),YC(20),ANEM(20),ANET(20)
C      DIMENSION AM(20),AT(20),NEWJED(20)
C
C      CALL SECOND(XNOW)
C      JREZON=NREZON-MIN0(JREZON(NREZON),JFIN)
C      IF (JREZON(NREZON) .LE. JINIT) GO TO 900
C      IF (TIME+DTNH .LT. SSTOPM) GO TO 900
C      IF (TIME-.5*DTNH .GT. SSTOPM) GO TO 2
C      TIME=TIME+DTNH & SDURH=C.
C      DO 1 J=JINIT,JFIN
C      1 EHL(J)=EHL(J)+SSCALH(J)
C      TIME=TIME+DTNH & SDURH=1.
C      JLAST=JREZON(NREZON)-1 & M=0 & NJ=1
C
C      SECTION 1 LOCATE JREZON WITH RESPECT TO MATERIAL AND JEDITS
C
C      M=M+1
C      IF (JREZON(NREZON)-JBND(M)-216,5,3
C      5 JLAST=JLAST-1
C      6 MASLAST=ZHL(JLAST)
C      MOMLAST=0.5*MASLAST*(J(JLAST)
C      RSLAST=.5*MASLAST*(R(JLAST)+R(JLAST+1)) & TLAST=T(JLAST)
C      DO 10 I=1,NJEDIT
C      10 NEWJED(I)=JEDIT(I)
C      ** SET JOLD, THE OLD COORDINATE VALUE, AND JNEW, THE NEW VALUE
C      ** REZONING OCCURS FOR CELLS BETWEEN JOLD AND JLAST. MIDCELL
C      ** QUANTITIES ARE SET FOR JLAST-1 WHILE COORDINATE QUANTITIES ARE
C      ** SET FOR JLAST.
C      JOLD=JNEW JLAST-1 & NCEL=NPART-0

```

SUBROUTINE REZONE



```

LOC=11
WRITE (18,5000) LOC,JOLD,JNEW,JLAST,M,NJ,MCEL,NPART          PRINT
C ** SET DX (CELL DIMENSION) AND XN (COORD TO LEFT OF NEW CELL) FOR
C ** FIRST GROUP OF CELLS TO BE REZONED
XN=X(JLAST-1) & DX=X(JLAST)-(M
M=M-1 & DXX(M)=DX
IF (M.EQ. 1) GO TO 13
DO 12 I=1,M
12 DXX(I)=DXX(M)*SORT(EQSYC(I)*RHOS(M)/(EQSYC(M)*RHOS(I)))
13 WRITE (18,5015) (I,DXX(I),I=1,M)          PRINT
C
C ** SAVE NEM AND NET AT JEDITS FOR RADIATION DEPOSITION PROBLEMS
IF (INSPEC.EQ. 0) GO TO 50
DO 30 I=1,NJEDIT
JE=JEDIT(I)
AM(I)=NEM(JE)
30 AT(I)=NET(JE)
C
C SECTION 2 - FIND REZONABLE SET OF CELLS
C
C TERMINATION OF REZONABLE SET OF CELLS AT AN INTERFACE (PART 1)
50 IF (M-1) 790,130,52
52 IF (JOLD-JBND(M-1)-1) 790,60,130
60 NPART=1 & MJOLD2=M(JOLD,2) & GO TO 500
100 JLAST=JOLD-1
C ** RETURN WITH JNEW SET TO JBND(M-1)
C CHECK WHETHER JEDITS COINCIDE WITH JBND(M-1) OR JBND(M-1)+1
DO 103 NJ=1,NJEDIT
IF (JOLD.NE. JEDIT(NJ)) GO TO 103
NEWJED(NJ)=JNEW+1
GO TO 105
103 CONTINUE
105 DO 108 NJ=1,NJEDIT
IF (JOLD-1.NE. JEDIT(NJ)) GO TO 108
NEWJED(NJ)=JNEW
GO TO 125
108 CONTINUE
125 M(JNEW+1,2)=MJOLD2 & X(JNEW)=X(JNEW+1)
M=M-1 & JBND(M)=JNEW & TLAST=T(JOLD-1) & JNEW=JNEW-1
JOLD=JOLD-2 & XN=X(JOLD)
LOC=125
WRITE (18,5000) LOC,JOLD,JNEW,JLAST,M,NJ,MCEL,NPART          PRINT
GO TO 50
C
C TERMINATION AT A SPALL WITHIN MATERIAL (PART 5)
130 IF ((M(JOLD,2).EQ. SPALL).OR. (M(JOLD,2).EQ. NORMAL)) 155,132
132 NPART=5 & NSP=M(JOLD,2) & XSAVE=X(JOLD) & USAVE=U(JOLD)
X(JOLD)=XSP(NSP) & U(JOLD)=USP(NSP) & GO TO 500
140 JLAST=JOLD & USP(NSP)=U(JNEW+1)
XSP(NSP)=X(JNEW+1) & X(JOLD)=XSAVE & U(JOLD)=USAVE
C RETURN WITH JNEW=COORD TO LEFT OF SPALL, JOLD=COORD AT SPALL
M(JNEW+1,2)=NSP
DO 142 NJ=1,NJEDIT
IF (JOLD.NE. JEDIT(NJ)) GO TO 142
NEWJED(NJ)=JNEW
GO TO 145
142 CONTINUE
145 JOLD=JOLD-1
LOC=145
WRITE (18,5000) LOC,JOLD,JNEW,JLAST,M,NJ,MCEL,NPART          PRINT
GO TO 50
C
C TERMINATION AT INITIAL BOUNDARY (PART 2)
155 IF(JOLD-JINIT) 790,160,255
160 NPART=2 & GO TO 500
200 DO 205 NJ=1,NJEDIT
IF (JOLD.NE. JEDIT(NJ)) GO TO 205
NEWJED(NJ)=JNEW+1
GO TO 800

```

SUBROUTINE REZONE (continued)

```

205 CONTINUE
    GO TO 800
C
C      TERMINATION OF REASONABLE SET OF CELLS AT A JEDIT (PART 3)
255 IF (NJEDIT .LE. 0) GO TO 355
    DO 264 NJ=1,NJEDIT
    IF (JOLD .NE. JEDIT(NJ)) GO TO 264
    NPART=3
    GO TO 500
264 CONTINUE
    GO TO 355
300 JOLD=JOLD-1
    NEWJED(NJ)=JNEW+1
C      ** RETURN WITH JOLD AT THE JEDIT, JNEW TO THE LEFT OF JEDIT. MIDCELL
C      ** QUANTITIES HAVE BEEN RESET UP TO JNEW+1, COORDINATE QUANTITIES
C      ** UP TO JNEW+2
    LOC=300
    WRITE (18,5000) LOC,JOLD,JNEW,JLAST,M,NJ,NCEL,NPART
    PRINT
    GO TO 50
C
C      TERMINATION WHEN NUMBER OF REASONABLE OLD CELLS IS 20 (PART 4)
355 IF ((X(JLAST)-X(JOLD))/DXX(M)-18.) 420,360,360
360 NPART=4 & GO TO 500
400 JOLD=JOLD-1
    LOC=400
C      ** RETURN WITH JOLD AT PREVIOUS LOCATION, JNEW SET AT COORDINATE TO THE
C      ** LEFT. MIDCELL QUANTITIES HAVE BEEN RESET UP TO JNEW+1, COORDINATE
C      ** QUANTITIES UP TO JNEW+2
    WRITE (18,5000) LOC,JOLD,JNEW,JLAST,M,NJ,NCEL,NPART
    PRINT
    GO TO 50
420 JOLD=JOLD-1 & GO TO 50
C
C      SECTION 3 - COMPUTE NEW CELL COORDINATES AND PROPERTIES
C
500 NQ=0
    LOC=500
    WRITE (18,5000) LOC,JOLD,JNEW,JLAST,M,NJ,NCEL,NPART
    PRINT
510 NCEL=MAX1((X(JLAST)-X(JOLD))/DXX(M)+.65,1.)
    IF ((NCEL-1)*(NQ-1) .EQ. 0) GO TO 610
C      CHECK WHETHER REGION OF LARGE CELLS LIES TO LEFT
601 DXMIN=DXX(M) & JLASTP=JLAST-1
    LOC=601
    WRITE (18,5000) LOC,JOLD,JNEW,JLAST,M,NJ,NCEL,NPART
    PRINT
    DO 603 JX=JOLD,JLASTP
    DELX=X(JX+1)-X(JX)
    IF (DELX-DXMIN) 602,602,603
602 DXMIN=DELX & JXMIN=JX
603 CONTINUE
    IF (DXMIN-.08*DXX(M)) 604,750,750
604 JX=JXMIN+1
    DO 605 I=JOLD,JXMIN
    JX=JX-1 & DELX=X(JX+1)-X(JX)
    IF (DELX-DXX(M)) 605,605,608
605 CONTINUE & GO TO 610
608 JOLD=JX+1 & NPART=N
    LOC=608
    WRITE (18,5000) LOC,JOLD,JNEW,JLAST,M,NJ,NCEL,NPART
    PRINT
    NQ=1 & GO TO 510
C
C      BEGIN COMPUTATIONS FOR NEW COORDINATES
610 NCEL=MINO(JLAST-JOLD,NCEL)
    DX=(X(JLAST)-X(JOLD))/NCEL
    XSTART=X(JLAST) & XN=XSTART-DX
C      ** XN IS NEW COORDINATE LOCATION
C      ** DX IS NEW CELL DIMENSION
    RS(1)=RSLAST
    MOM(1,1)=MOMLAST
    MASS(1)=MASLAST
    LOC=610

```

SUBROUTINE REZONE (continued)

```

WRITE (10,5002) LOC,NCEL,XSTART,DX,XN,RSLAST,MASLAST,MOMLAST PRINT
WRITE (10,5610)
MP=NPOR(M,2)
DO 650 I=1,NCEL
  RS(I+1)=MASS(I+1)=AMAVG=AMSLP1=AMSLP2=ENGVS=PS=SX=YS=0.
  HC(I,1)=SOLID
  ANEMS=ANETS=0.
  HC(I,3)=2
615 IF (JLAST .LT. 1) GO TO 625
  XEND=AMAX1(X(JLAST),XN)
  IF (XSTART-XEND) 621,621,619
619 DMASS=ZHL(JLAST)*(XSTART-XEND)/(X(JLAST+1)-X(JLAST))
  MASS(I+1)=MASS(I+1)+DMASS
  UJ=U(JLAST)
  DUOLD=U(JLAST+1)-UJ
  DXOLD=X(JLAST+1)-X(JLAST)
  XS1=XSTART+XEND-XN-XN-DX
  XS2=XSTART-XEND
  AMAVG=.5*DMASS*(UJ+DUOLD*(XSTART+XEND)/2.-X(JLAST))/DXOLD+AMAVG
  AMSLP1=DMASS/DX*1.25*DUOLD/DXOLD*XS2*(3.*XS1+XS2)
  AMSLP2=.5*DMASS*(XEND-X(JLAST))/DXOLD*XS1 + AMSLP1
  ENGVS=ENGVS+DMASS*EHL(JLAST)
  RS(I+1)=RS(I+1)+DMASS*(R(JLAST)+(R(JLAST+1)-R(JLAST))*(XSTART+
  XEND)/2.-X(JLAST))/(X(JLAST+1)-X(JLAST))
  PS=PS+DMASS*PHL(JLAST)
  SX=SX+DMASS*SHL(JLAST)
  YS=YS+DMASS*YHL(JLAST)
  CS=CS+DMASS*CHL(JLAST)
  ANEMS=ANEMS+DMASS*ANEM(JLAST)
  ANETS=ANETS+DMASS*NET(JLAST)
  XSTART=XEND
  IF (H(JLAST,1) .EQ. POROUS) HC(I,1)=POROUS
  HC(I,3)=MAX0(H(JLAST,3),HC(I,3))
621 IF (XEND .LE. XN) GO TO 625
  JLAST=JLAST-1 $ GO TO 615
625 XC(I)=XN $ DC=MASS(I+1)/DX $ EC(I)=ENGVS/MASS(I+1)
  YC(I)=YS/MASS(I+1) $ SC(I)=SX/MASS(I+1) $ PC(I)=PS/MASS(I+1)
  CC(I)=CS/MASS(I+1)
  AMSLP=AMSLP1+.5*AMAVG*AMSLP2/MASS(I+1)
  MOM(I,2)=AMAVG*AMSLP
  MOM(I+1,1)=AMAVG-AMSLP
  ANEM(I)=ANEMS/MASS(I+1) $ ANET(I)=ANETS/MASS(I+1)
  IF (HC(I,1) .EQ. SOLID) GO TO 643
  HC(I,1)=POROUS
  IF (EC(I) .GT. EMELT(M,1)) GO TO 640
  RHOPV=FHELT(EC(I),M)*(RHOP(S,MP)-RHOS(M))/(1.+EC(I)
  EQSTA(M))
  IF (DC .LT. RHOPV) GO TO 643
  HC(I,1)=SOLID $ GO TO 643
640 IF (PC(I) .GT. 0.) GO TO 643
  PC(I)=SC(I)=RS(I+1)=0.
643 K=JNEW+1-1
  LOC=643
  WRITE (10,5004) LOC,K,XC(I),DC,MOM(I,2),MOM(I+1,1),EC(I),RS(I+1),
  PC(I),SC(I),YC(I),MASS(I+1),HC(I,1)
650 XN=AMAX1(XN-DX,X(JOLD))
  T(JNEW+1)=TLAST
  DO 670 I=1,NCEL
    J=JNEW+1-1 $ CHL(J)=CC(I) $ DHL(J)=MASS(I+1)/DX
    EHL(J)=EC(I) $ PHL(J)=PC(I) $ SHL(J)=SC(I)
    YHL(J)=YC(I) $ JHL(J)=MASS(I+1) $ HJ(J,1)=HC(I,1)
    NET(J)=ANET(I) $ NEM(J)=ANEM(I)
    UJ+1=2.*(MOM(I,1)+MOM(I,2))/(MASS(I)+MASS(I+1))
    RJ+1=(RS(I)+RS(I+1))/(MASS(I)+MASS(I+1))
    T(J)=TENS(M,1) $ X(J)=XC(I) $ HJ(J,2)=NORMAL
    HJ(J,3)=HC(I,3)
670 CONTINUE
  MOMLAST=MOM(NCEL+1,1)

```

SUBROUTINE REZONE (continued)

```

      MASLAST=MASS(NCEL+1)
      RSLAST=RS(NCEL+1)      $ TLAST=T(JOLD)
      GO TO (680,680,700,700,685) NPART
680  RI(J)=RS(NCEL+1)/MASS(NCEL+1)
685  TI(J)=TLAST
      UI(J)=2.*MOMLAST/MASLAST
      MOMLAST=MASLAST=RSLAST=0.
700  CONTINUE
      LOC=700
      WRITE (18,5000) LOC,JOLD,JNEW,JLAST,M,NJ,NCEL,NPART      PRINT
      C      SET JNEW AND JLAST IN PREPARATION FOR THE NEXT ZONE CALCULATIONS
      C      JNEW=J-1      $ JLAST=JOLD
      C      RETURN TO APPROPRIATE PART OF REZONE FOR FINAL RESETTNG
      C      GO TO (100,200,300,400,140) NPART
      C
      C      RENUMBER CELLS WITHOUT REZONING
750  TI(JNEW+1)=TLAST
      LOC=750
      TLAST=T(JOLD)
      RSLAST=.5*(ZHL(JOLD)+R(JOLD)+R(JOLD+1))
      WRITE (18,5000)
752  JLAST=JLAST-1      $ DHL(JNEW)=DHL(JLAST)
      EHL(JNEW)=EHL(JLAST)      $ PHL(JNEW)=PHL(JLAST)
      SHL(JNEW)=SHL(JLAST)      $ YHL(JNEW)=YHL(JLAST)
      CHL(JNEW)=CHL(JLAST)      $ ZHL(JNEW)=ZHL(JLAST)
      HI(JNEW,1)=HI(JLAST,1)      $ HI(JNEW,2)=HI(JLAST,2)
      MASNEXT=ZHL(JLAST)
      UI(JNEW+1)=(2.*MOMLAST+MASNEXT*UI(JLAST+1))/(MASLAST+MASNEXT)
      MASLAST=MASNEXT
      MOMLAST=.5*MASLAST*UI(JLAST)
      RI(JNEW+1)=R(JLAST+1)
      TI(JNEW)=TI(JLAST)      $ X(JNEW)=X(JLAST)
      NEH(JNEW)=NEH(JLAST)      $ NET(JNEW)=NET(JLAST)
      HI(JNEW,3)=HI(JLAST,3)
      I=JNEW      $ JNEW=JNEW-1
      WRITE (18,5003) LOC,I,X(I),DHL(I),UI(I+1),EHL(I),R(I+1),PHL(I),
1  SHL(I),YHL(I),TI(I),ZHL(I),HI(I,1)
      IF (JLAST=JOLD) 790,755,752
      C      ** JNEW IS TO LEFT OF LAST RENUMBERED CELL. JLAST=JOLD, THE LAST
      C      ** OLD COORDINATE RENUMBERED.
755  CONTINUE
      LOC=755
      WRITE (18,5000) LOC,JOLD,JNEW,JLAST,M,NJ,NCEL,NPART      PRINT
      GO TO (760,760,300,400,755) NPART
760  RI(JNEW+1)=R(JLAST)
765  UI(JNEW+1)=2.*MOMLAST/MASLAST
      TI(JNEW+1)=TI(JLAST)
      MOMLAST=MASLAST=RSLAST=0.
      LOC=760
      WRITE (18,5000) LOC,JOLD,JNEW,JLAST,M,NJ,NCEL,NPART      PRINT
      GO TO (100,200,300,400,140) NPART
      C
      C      ERROR MESSAGE
      C
790  WRITE (18,1000) NPART,JOLD,JNEW,JLAST,NJ,JEDIT(NJ),M,JBNDD(M)      PRINT
      CALL EDDUMP      $ LSUB(7)=1      $ CALL SCRIBE      $ STOP
      C
      C      ENDING ROUTINE - INTERFACE AND BOUNDARY ADJUSTMENTS
      C
800  JINIT=JNEW+1      $ HI(JINIT,2)=HI(JOLD,2)
      IF (HI(JINIT,2) .EQ. SPALL) RI(JINIT)=SI(JINIT)=PI(JINIT)=0.
      DO 810 J=JINIT,JPIN
      UML(J)=.5*(UI(J)+UI(J+1))
      SJ(J+1)=.5*(SHL(J)+SHL(J+1))
      PJ(J+1)=.5*(PHL(J)+PHL(J+1))
810  C(J)=CHL(J)
      DO 820 M=1,NMTRLS
      JB=JBNDD(M)      $ HI(JB,2)=LINTER
      SI(JB)=SHL(JB-1)

```

SUBROUTINE REZONE (continued)

```

      S(JB+1)=SM(JB+1)
      P(JB)=PM(JB-1)
      P(JB+1)=PM(JB+1)
      IF (H(JB+1,2) .EQ. SPALL) 815,816
815  R(JB+1)=R(JB)=0.  & GO TO 820
816  R(JB+1)=R(JB)=.5*(R(JB+1)+R(JB))
      U(JB+1)=U(JB)=(U(JB)*ZML(JB-1)+U(JB+1)*ZML(JB+1))/(ZML(JB-1)+
1  ZML(JB+1))
820  CONTINUE
      DO 825 I=1,NJEDIT
825  JEDIT(I)=NEWJED(I)
      IF (INSPEC .EQ. 0) GO TO 840
      DO 830 I=1,NJEDIT
      JE=JEDIT(I)
      NEM(JE)=AN(I)
830  NET(JE)=AT(I)
840  CALL EDIT
      CALL EDDUMP
900  CONTINUE
      CALL SECOND(TWIX)  & DUR=TWIX-XNOW
      WRITE (18,5010) JINIT,DUR
      RETURN
1000 FORMAT (25H ERROR IN REZONE, NPART=I3,6H JOLD=I3,6H JNEW=I3,
1  7H JLAST=I3,4H NJ=I3,11H JEDIT(NJ)=I3,3H M=I3,9H JEND(M)=I3)
5000 FORMAT (13H REZONE, LOC=I3,7H, JOLD=I3,7H, JNEW=I3,8H, JLAST=I3,
1  4H, M=I3,5H, NJ=I3,7H, NCEL=I3,8H, NPART=I3)
5002 FORMAT (13H REZONE, LOC=I3,7H, NCEL=I3,9H, XSTART=E10.3,5H, DX=,
1  E10.3,5H, XN=E10.3,9H, RSLAST=E10.3,10H, MASLAST=E10.3,
2  10H, NOMLAST=E10.3)
5003 FORMAT(2I5,10E10.3,3X,R1)
5004 FORMAT (2I5,1P10E10.3,3X,R1)
5010 FORMAT(19HOEND REZONE, JINIT=I3,17H, TIME IN REZONE=E10.3,5H SECS)
5015 FORMAT(21H REZONE, DXX VALUES ,6I18,F9.6)
5610 FORMAT (120H LOC J PC XC OC MOM(I,2) MOM(I+1,1)
1  EC RS(I+1) PC SC YC MASS(I+1) HC(I,1)
2)
5750 FORMAT (120H LOC J X DML U(I+1) FHL
1  R(I+1) PHL SHL YML T ZML HT(I,1)
2)
      END

```

385\*

SUBROUTINE REZONE (concluded)

```

C      FUNCTION SSCALH
C      (INCLUDES ENTRY SSCALH)
C      COMPUTES RADIANT ENERGY FOR DEPOSITION IN EACH CELL DURING THE
C      HYDRODYNAMIC COMPUTATIONS
C      * SSCALH COMPUTES FOR COORDINATE POINTS
C      * SSCALH COMPUTES FOR HALFSTEP POINTS AND INITIALIZES ENERGY IN
C      NEW ZONES
C
C      REAL MATL,MU,NUM,MUP,NEM,NET
C      INTEGER H
C
C      MISCELLANEOUS
C      COMMON CEF,CKS,DAVG,DELTIM,DOLD,DRHO,DTMIN,DTN,DTNH,DU,DX,EDLD,F,
1      FIRST,J,JCYCS,JINIT,JFIN,JSMAX,JSTAR,JTS,LSUB(11),MAXPR(11),N,
2      NCYCS,NPERN,POLD,RLAST,SLAST,SMAX,TF,TIME,TJ,TS,ULAST,UOLD,
3      XLAST,XNOW,XOLD
C      EQUATION OF STATE - SOLID
C      COMMON COSQ(6,6),C1(6,6),C2(6),EMELT(6,5),EQSTA(6),EQSTC(6),
1      EQSTD(6),EQSTE(6),EQSTG(6),EQSTH(6),EQSTN(6),EQSTS(6),MATL(2,6),
2      MU(6),RHO(6),RHOS(6),TENS(6,3),YADD(6),YO(6),JBND(6),NPOR(6,2),
3      M,MUM,NMTRLS
C      EQUATION OF STATE - POROUS
C      COMMON AK(6),MUP(6),PORA(4,3),PORB(4,3),PORC(4,3),RHOPI(6,3),
1      YADDP(4,3),DREF,RHOPV,MP,NC
C      RADIATION DEPOSITION
C      COMMON SS(300,5),SSTOP(5),START(5),SDURM,SSTOPM,NSPEC,SSJ,JSS
C      COORDINATE ARRAYS
C      COMMON X(300),C(300),CHL(300),D(300),DHL(300),EHL(300),H(300,3),
1      NEM(300),NET(300),P(300),PHL(300),R(300),S(300),SHL(300),T(300),
2      U(300),UHL(300),YHL(300),ZHL(300)
C
C      DIMENSION L(10)
C
C      SSCAL=0.
C      IF (NSPEC*(SDURM-1.) .EQ. 0.) RETURN
C      IF (TIME-.5*DTNH .GT. SSTOPM) RETURN
C      DO 1 I=1,10
1      L(I)=0
C      L(1)=5
C      ENERGY ADDITION AT COORDINATE POINTS
10      DO 20 I=1,NSPEC
C      IF ((TIME-START(I))*(TIME-.5*DTNH-SSTOP(I)) 12,20,20
12      SSCAL=SSCAL+.5*SS(I)*AMIN1(AMIN1(.5*DTNH,TIME-START(I)),
1      SSTOP(I)-TIME+.5*DTNH)
20      CONTINUE
C      GO TO 70
C      ENTRY FOR HALFSTEP CALCULATIONS
C      *****
C
C      ENTRY SSCALH
C      SSCAL=0.
C      IF (NSPEC .EQ. 0) RETURN
C      IF (JS .GT. JSS) GO TO 50
C      IF (SDURM .EQ. 1.) RETURN
C      IF (TIME-DTNH-.5*DTN .GT. SSTOPM) RETURN
C      DO 42 I=1,10
42      L(I)=0
C      L(1)=40
C      ENERGY ADDITION IN ACTIVE ZONES - HALF STEP
C      DO 44 I=1,NSPEC
C      IF ((TIME-.5*DTNH-START(I))*(TIME-DTNH-.5*DTN-SSTOP(I)) 46,48,48
46      SSCAL=SSCAL+SS(JS,I)*AMIN1(SSTOP(I),TIME-.5*DTNH)-
1      AMAX1(START(I),TIME-DTNH-.5*DTN)
48      CONTINUE
C      GO TO 70
C      ENERGY ADDITION FOR NEW ZONES
50      JSS=JS
C      L(2)=50
C      DO 60 I=1,NSPEC
C      IF (TIME-.5*DTNH .LT. START(I)) GO TO 60
C      SSCAL=SSCAL+SS(JS,I)*AMIN1(SSTOP(I),TIME-.5*DTNH)-START(I)
60      CONTINUE
70      IF (LSUB(6) .GE. MAXPR(6)) GO TO 75
C      WRITE (10,5000) SSCAL,L(1),L(2)
C      LSUB(6)=LSUB(6)+1
75      RETURN
5000  FORMAT(5X,6HSSCAL=F10.4,3H L=2I3)
C      END

```

FUNCTION SSCAL (complete)

```

SUBROUTINE RELAX(SD,ICON,YCLD,SDC,DT,TRLX,CRO,COEF,YAD,N,J,TY,
1YNGT,IASR)
C THIS VERSION CONTAINS STRESS RELAXATION MODELS 1 AND 4
DIMENSION JK(20)
KKK=0
ICOR=ICON & YNEB=YCLD & L=0
IN=PAXO(2,IASR)/2
IF (ICON.EQ.2)18,1
C INITIAL CONDITION OUTSIDE OF ELASTIC ZONE
1 L=1 & GO TO (4,2)IN
2 XPY=EXP(-DT/TY)
KKK=KKK+1
JK(KKK)=2
YNEB=YNGT+(YCLD-YACT)*XPY+ABS(COEF)*TY/CT*(1.-XPY)*.5*(1.+SIGN(1.,
ICRO)*SIGN(1.,SDC))
YAVG = (YNEB+YCLD)/2. & YSTAR = SIGN(YAVG,SDC) & GO TO 5
4 YSTAR = SIGN(YCLD,SDC)
KKK=KKK+1
JK(KKK)=4
5 XPO=EXP(-DT,TRLX)
KKK=KKK+1
JK(KKK)=5
SD = YSTAR + (SDC-YSTAR)*XPO + COEF*TRLX/DT*(1.-XPO)
C CHECK IF DEVIATOR CROSSES INTO ELASTIC ZONE. IF SO, RECALCULATE RELAXATION
IF (ABS(SD).GT.YNEB.AND.SIGN(1.,SD).EQ.SIGN(1.,SDC))30,6
6 TC = (SIGN(YNEB,SDC)-SDC)/(SD-SDC)*DT & L=2
KKK=KKK+1
JK(KKK)=6
GO TO (5,7)IN
7 YNEB=YNGT+(YCLD-YACT)*EXP(-TC/TY)
KKK=KKK+1
JK(KKK)=7
YAVG = (YNEB+YCLD)/2. & YSTAR = SIGN(YAVG,SDC)
9 XPO = EXP(-TC/TRLX)
KKK=KKK+1
JK(KKK)=9
SD=YSTAR+(SDC-YSTAR)*XPO+COEF*TRLX/DT*(1.-XPO)+CCEFC*(D1-TC)/DT
C CHECK IF DEVIATOR CROSSES OVER INTO OTHER SIDE OF ZONE
IF (ABS(SD).GT.YNEB)11,10
10 ICOR = 2 & L=3 & GO TO 25
11 IF (SIGN(1.,SD).EQ.SIGN(1.,SDC))30,12
C RECALCULATE TIME DURING WHICH RELAXATION OCCURS
12 TK = (SD-SIGN(YNEB,SDC))/(SD-SIGN(YNEB,SDC))*(CT-TC) & L=4
KKK=KKK+1
JK(KKK)=12
GO TO (25,13)IN
13 XPY=EXP(-TK/TY) & YNOLD=YNEB
YNEB=YNGT+(YNEB-YACT)*XPY+ABS(COEF)*TY/CT*(1.-XPY)
YAVG = (YNEB+YNOLD)/2. & YSTAR = SIGN(YAVG,SD) & GO TO 25
C NOW CONSIDER INITIAL CONDITIONS INSIDE ELASTIC ZONE
18 SD = SDC + CCEF
KKK=KKK+1
JK(KKK)=18
C CHECK IF DEVIATOR CROSSES ZONE BOUNDARY
IF (ABS(SD).GT.YCLD)19,35
C CHANGE CONDITION VARIABLE AND RECALCULATE DEVIATOR WITH RELAXATION
19 YSTAR = SIGN(YCLD,SD) & L=5 & TK = (SD-YSTAR)/(SD-SDC)*DT
KKK=KKK+1
JK(KKK)=19
GO TO (25,20)IN
20 YNEB=YNGT+ABS(CCEF)*TY/DT*(1.-EXP(-TK/TY))
KKK=KKK+1
JK(KKK)=20
YAVG = (YNEB+YNGT)/2. & YSTAR = SIGN(YAVG,SD)
25 ICOR = 2 - IFIX(SIGN(1.,SD))
KKK=KKK+1
JK(KKK)=25
SD = YSTAR + CCEF*TRLX/DT*(1.-EXP(-TK/TRLX))
30 GO TO (31,35)IN
C RECALCULATE YIELD STRENGTH TO ACCOUNT FOR STRAIN HARDENING
YNEB = AMINI(ABS(SD),YCLD+YAD*ABS(ICRO))
KKK=KKK+1
JK(KKK)=31

```

SUBROUTINE RELAX.

```

      IF (YNEW.EQ.ANS(SD)) 32,35
32  ICCA=2  & L=L+10
      KKK=KKK+1
      JK(KKK)=32
35  CONTINUE
      KKK=KKK+1
      JK(KKK)=35
49  CALL SSMTCH(3,ISMTCH)
      KKK=KKK+1
      JK(KKK)=49
      GO TO (50,40)ISMTCH
50  PRINT 100, N, J, L, ICOR, ICON, SDC, SD, YOLD, YNEW, CCEF
      PRINT 81,(JK(I), -1, KKK)
40  YOLD=YNEW
      RETRN
81  FORMAT (15X PATH IN RELAX 2415)
100  FORMAT(3H N=,I3,3H J=,I3,6H PATH ,I2,6H ICCA=,I1,1H-,I1,4H SD=,
1E11.4,4H TO ,E11.4,2H,5HYOLD=,E ,4,4H TO ,E11.4,6H CORF=,E11.4)
      ENC

```

SUBROUTINE RELAX (concluded)



```

SUBROUTINE BANDRLX(SC, YNOT, SEC, CT, CRC, CCEF, MECH, YAO, N, J, T1, T2
1, BEE, VM, GEE, EPS, AP, AT, IASR)
C THIS VERSION CONTAINS BOTH BANC AND GILMAN RELAXATION MODELS
C FOLLOWING TABLE GIVES CORRESPONDENCE OF COMMON, BANDRLX VARIABLES
C COMMON NS: TSRI(1) (2) (3) (4) (5) (6) NEM NET
C BANC 2 T1 T2 BEE VP GEE EPS NM NT
C GILMAN 3 CEE P-T BEE VM BNPC - NM GAP
C NOTE. MECH=MUM, YAO=YADD, IASR=NSR
C NEM AND NET ARE PCRIE AND TOTAL DISLOCATIONS
C GAM IS PLASTIC SHEAR STRAIN
C JK IS A PATH INDICATOR
C DIMENSION JK(20)
C REAL MECH, NM, NT, NMC, NTO
C KKK=0
C ICCR = ICON & YNOTG=YNOT
C ATC = AT & NPO = AP & SC=SDC
C AT=4
C L=0 & ENT=FLOAT(NT) SIT=0
C SIGNA = SIGN(1., SEC)
C IF(ICON.EQ.2)1,1C
C INITIAL CONDITIONS INSIDE ELASTIC ZONE
1 SD=SDC+CCEF
C KKK=KKK+1
C JK(KKK)=1
C IF (ABS(SD).GT.YNOT)2,35
C DEVIATOR LEAVES ELASTIC ZONE. CALCULATE RELAXATION
2 L = 1
C KKK=KKK+1
C JK(KKK)=2
C S = .5*(ABS(SDC+CCEF)-YNOT)
C DELT = (SC-SIGN(YNOT,CCEF))/(SC-SDC)*DT
C SIGNM = SIGN(1., CCEF)
C ENT=1. & SC=SDC
C GO TO 4C
C INITIAL CONDITION OUTSIDE OF ELASTIC ZONE
10 L=2
C KKK=KKK+1
C JK(KKK)=10
C IT=IT+1 & SDI=SC+CCEF/(2.*ENT)
C S=ABS(SDI)-YNOT & DELT=DT/ENT
C IF(S.LE.0.)10,11
C AVERAGE DEVIATOR REMAINS OUTSIDE ELASTIC ZONE. CALCULATE RELAXATION
11 L=3
C KKK=KKK+1
C JK(KKK)=11
C IF(SIGNA.EQ.SIGN(1., SDI))10,17
13 IF(ABS(SD).GT.YNOT)14,16
14 L=4
C KKK=KKK+1
C JK(KKK)=14
C IF(SIGN(1., SC).EQ.SIGNM)15,16
C DEVIATOR REMAINS OUTSIDE ELASTIC ZONE AFTER RELAXATION
15 L=5
C KKK=KKK+1
C JK(KKK)=15
C IF(IT.EQ.NET) 30,10
16 SD=SDI-CCEF/(2.*ENT)
C KKK=KKK+1
C JK(KKK)=16
17 L=6
C KKK=KKK+1
C JK(KKK)=17
C DEVIATOR REENTERS ELASTIC ZONE. RECALCULATE RELAXATION
18 S = .5*(ABS(SDI)-YNOT) & YSTAR = SIGN(YACT, SEC)
C KKK=KKK+1
C JK(KKK)=18
C DELT=(YSTAR-SDI)/COEF*DT
C GO TO 4C
19 SD=SD+CCEF/ENT*FLOAT(NT-IT)
C KKK=KKK+1
C JK(KKK)=19
C IF (ABS(SD).GT.YNOT)21,20
20 ICCR = 2

```

SUBROUTINE BANDRLX



```

103 FORMAT(3H N=,I3,3H J=,I3,3H L=,I2,4H IC=,I1,1H=,I1,4H SD=,E10.3,
13H = ,E10.3,3H C=,E10.3,3H Y=,E10.3,5H CAP=,E10.3,1H=,E10.3,
24H NM=,E10.3)
110 FORMAT (3H J=,E10.3,1H ARC=,E10.3,5H XPC=,E10.3,5H CRC=,E10.3,
16H DELT=,E10.3)
199 FORMAT (25H ERROR IN BANDRLX,INSR = 15,5H, L = 15)
      ENC

```

SUBROUTINE BANDRLX (concluded)

```

SUBROUTINE BAUSCHI (I,SDC,SD,Y,YNOT,YAC,CRC,CCEFL,XPO,XP,MUL,N,J,
1RC,MU,YADF)
REAL MU,MUL,MUU
DIMENSION JL(20)
KKK=0
DO 90 K=1,20
90 JL(K)=0
DY=YAD $IOR=I $YOR=Y $COEF=CCEFL $EMU=DY $SDAV=0. $MU=MUL
CCEFU=CCEF*MUU/MU
IF(1.LE.2) GO TO 3
DY=YADF*YAC $MU=MUL*MUU $COEF=CCEFU
KKK=KKK+1
JL(KKK)=0
3 SD=SDC+CCEF
KKK=KKK+1
JL(KKK)=3
GO TO (10,5,10,10,59,10) I
5 IF(XPO.GE.1.E2)6,1
C DETERMINE EFFECTIVE SHEAR MODULUS AND STRESS DEVIATOR FOR INITIAL LOADING
1 EMU=MU*(DY*RC-MU)*(ABS(SDC/Y))**XFC
KKK=KKK+1
JL(KKK)=1
SDAV=AMIN1(Y,SDC+CCEF*EMU/MU/2.)
EMU=MU*(DY*RC-MU)*(ABS(SDAV/Y))**XFC $SD=SDC+CCEF*EMU/MU
6 IF(SD.GE.Y)2,7
7 IF(CRO.LT.0.)8,30
8 MU=PLL*MUU $DY=YADF*YAC $CCEF=CCEFU $GO TO 20
2 Y=AMIN1(ABS(SD),Y+(SD-Y)/(SD-SDC)*DY*ABS(CRC)) $SC=SIGN(Y,SD) $I=1
KKK=KKK+1
JL(KKK)=2
GO TO 30
C STRAIN HARDENING PATH
10 IF(1.SIGN(1,IFIX(DRC)),EQ.2-1)11,15
11 IF(ABS(SD).GT.Y)12,30
12 Y=AMIN1(ABS(SC),Y+Y*ABS(DRC)) $SD=SIGN(Y,SD) $GO TO 30
15 I=1+3 $MU=MUL*MUU $CY=YADF*YAC $CCEF=CCEFU $GO TO 20
C BAUSCHINGER EFFECT PATH
18 IF(1.EQ.4.AND.CRO.GT.C.CRC.I.EQ.6.AND.CRC.LT.C.)19,20
19 I=10-I
KKK=KKK+1
JL(KKK)=19
20 EMU=MU*(DY*RC-MU)*(ABS(1.5+.5*SIGN(1.,CRC)*SDC/Y))**XP
KKK=KKK+1
JL(KKK)=20
SD=SDC+CCEF*EMU/MU
SDAV=AMAX1(-Y,(SD+SDC)/2.)*FLOAT(3-1/2)*AMIN1(Y,(SD+SDC)/2.)*FLOAT
1(1/2-2)
EMU=MU*(DY*RC-MU)*(ABS(1.5+.5*SIGN(1.,CRO)*SDAV/Y))**XP
SC=SDC+CCEF*EMU/MU
IF(ABS(SD).GE.Y)22,30
22 Y=AMIN1(ABS(SC),Y+(SC-SIGN(Y,SD))/(SD-SDC)*DY*ABS(DRC))
KKK=KKK+1
JL(KKK)=22
SC=SIGN(Y,SD) $I=I-MAX0(I,4)
30 CALL SSMTCH(3,ISMTCH)
KKK=KKK+1
JL(KKK)=30
GO TO (40,50)ISMTCH
40 PRINT 80,N,J,1CR,I,SDC,SD,YOR,Y,CCEF,EMU,CRC,SDAV
PRINT 81,(JL(K),K=1,KKK)
50 RETURN
99 PRINT 100,1,N,J $ RETURN
80 FORMAT(3H N=,I3,3H J=,I3,3H I=,I1,1H -,I1,4H SD=,E10.3,4H YC ,E10.3
1,3H Y=,E9.3,4H YC ,E9.3,6H CCEF=,E10.3,4H MU=,E9.3,5H DRC=,E9.2,6H
2 SDAV=,E10.3)
81 FORMAT (17H PATH IN BAUSCHI 2315)
100 FORMAT(15H M IS hRCAG, M=,I2,3H N=,I3,3H J=,I3)
END

```

2500\*

SUBROUTINE BAUSCHI (complete)

```

      SUBROUTINE PUFLOT(NTEXP,IDENTP)
C     THIS SUBROUTINE DIRECTS THE PLOTTING PROCEDURE
      COMMON IDENT,N,NJEDIT,JEDIT(6),XJED(7)
      COMMON /PLOT/ IPLOT,IFPLOT(6),IDUM(14)
      CALL SECOND (BEG)
      NTEX=NTEXP $IDENT=IDENTP
      A'TIME=10H L. SEAMAN $ CHARGE=10H6736-2 $ XTEN=6HX-3587
      C' XEROX
      CALL HEADER (ANAME,CHARGE,XTEN)
      IF (IFPLOT(1).EQ.0) GO TO 1
      CALL TPLOTS(NTEX)
      PRINT 20
1     READ (7) N,NJEDIT,(JEDIT(I),I=1,6),(XJED(I),I=1,6)
      N=MIN0(N-2,1000)
      IF (IFPLOT(2).EQ.0) GO TO 2
      CALL HISTORY $PRINT 21
2     IF (IFPLOT(3)+IFPLOT(4)+IFPLOT(5).EQ.0) GO TO 5
      CALL HUGONIO $ PRINT 22
5     CALL SECOND (END) $ DUR=END-BEG $ PRINT 25, DUR
      RETURN
20    FORMAT(14H TPLOTS CALLED)
21    FORMAT(15H HISTORY CALLED)
22    FORMAT(15H HUGONIO CALLED)
25    FORMAT(13H TIME TO COMPLETE PLOTTING IS , F10.3,8H SECONDS)
      END

```

MAIN PLOTTING SUBROUTINE: PUFLOT (complete)

```

SUBROUTINE HISTORY
C THIS ROUTINE PRODUCES STRESS VERSUS TIME HISTORIES FOR JEDITS AND INTERFACES
COMMON IDENT,N,NJEDIT,JEDIT(6),XJED(6),S(1000,6),SIF(1000,3),
ITLABEL(3),SLABEL(3),TITLE(3)
COMMON /PLOT/ IPLOT,IFPLOT(6),LINES,IDUM(3),ING(9),IFLAG
DIMENSION T(1000),SEQV(1000,9)
EQUIVALENCE (S,SEQV)
SMAX=SMIN=0.0 $ IFS=0 $ JT=0 $ ORIG=0.
IF (IFLAG.LT.0) IFS=1 $ IFLAG=ABS(IFLAG)
DO 2 I=1,N
READ (7) T(I),(SIF(I,J),J=1,3),(S(I,J),J=1,6)
DO 2 J=1,9
IF (ING(J).EQ.0) GO TO 2
SMAX=AMAX1(SMAX,SEQV(I,J)) $ SMIN=AMIN1(SMIN,SEQV(I,J))
2 CONTINUE
THAX=T(N) $ TMIN=T(1) $ MARK=0 $ BLANK=0
C INDIVIDUAL HISTORIES PLOTTED
ENCODE (30,212,TLABEL)
DO 30 J=1,9 $ JN=J-6
IF (ING(J).EQ.0) GO TO 30
IF (J.EQ.6) GO TO 8
ENCODE (30,211,SLABEL)
ENCODE (30,210,TITLE),JN,IDENT
GO TO 9
8 ENCODE (30,213,TITLE),XJED(J),IDENT
ENCODE (30,214,SLABEL),JEDIT(J)
JT=JT+1 $ JAD=J-JT
9 PRINT 240,(TITLE(M),M=1,3),TMIN,TMAX,SMIN,SMAX
CALL LINSET(TMAX,TMIN,SMAX,SMIN,TLABEL,SLABEL,TITLE,LINES)
IPEN=0
DO 10 I=1,N
IF (ABS(SEQV(I,J)).GT.1E-3*SMAX) IPEN=1
CALL LINPLT(T(I),SEQV(I,J),MARK,IPEN)
10 CONTINUE
CALL PENEND
30 CONTINUE
IF (IFLAG.LE.1) GO TO 90
C SEVERAL JEDITS PLOTTED ON ONE GRAPH
ENCODE (30,211,SLABEL)
ENCODE (30,214,TITLE),IDENT
PRINT 240,(TITLE(M),M=1,3),TMIN,TMAX,SMIN,SMAX
CALL LINSET(TMAX,TMIN,SMAX,SMIN,TLABEL,SLABEL,TITLE,LINES)
CALL LINPLT (ORIG,ORIG,MARK,BLANK)
L=1 $ K=0 $ IFLAG=MIN0(IFLAG,NJEDIT)+JAD
DO 60 J=1,IFLAG
IF (ING(J).EQ.0) GO TO 60
IF (J.EQ.0) IFLAG GO TO 42
DO 35 IO=1,5
IF (ING(J+IO).NE.0) GO TO 42
CONTINUE $ PRINT 250,J $ RETURN
42 M=L
DO 55 I=M,N
IF (K.EQ.0.AND.S(I,J).LT.1E-3*SMAX) GO TO 55
K=1 $ IF (J.EQ.0) IFLAG GO TO 54
IF (L.NE.M) GO TO 44
IF (S(I,J+IO).GT.1E-3*SMAX) L=I
44 IF (IFS.EQ.1) 48,46
46 IF (S(I,J).LT.1.05*S(I,J+IO)) GO TO 56
48 IF (I.EQ.N) GO TO 56
56 CALL LINPLT (T(I),S(I,J),MARK,IPEN)
55 CONTINUE $ GO TO 60
56 CALL LINPLT (T(I),S(I,J+IO),MARK,BLANK)
60 CONTINUE
CALL PENEND
90 RETURN
210 FORMAT (17H INTERFACE STRESS 11,0H, IDENT=14)
211 FORMAT(30H STRESS (KILOBARS) )
212 FORMAT(30H TIME (MICROSECONDS) )
213 FORMAT (11HISTORY, X=F7.4,0H CM, ID=14)
214 FORMAT(15HSTRESS IN CELL ,13,12H (KILOBARS) )
215 FORMAT(26H HISTORIES AT JEDITS ID =,14)
240 FORMAT (17H PLOT-- ,3A10,4H T=,F8.4,4H TO ,F8.4,4H S=,F9.4,4H TO ,
IF9.4)
250 FORMAT (24H COMBINED PLOT ERROR, J=,11)
END

```

PLOTTING SUBROUTINE: HISTORY (complete)

```

SUBROUTINE HUGONIC
C THIS ROUTINE PRODUCES GRAPHS OF STRESS, RESULTANT STRESS, AND DEVIATORIC
C STRESS VERSUS SPECIFIC VOLUME
COMMON IDENT,N,NJEDIT,JEDIT(6),XJED(6),S(1000,6),V(1000,3),
ISLABEL(3),VLABEL(3),TITLE(3),VMAX(3),VMIN(3),VPMAX(3),VPMIN(3)
COMMON /PLOT/ IPLOT,IFPLOT(6),LINES,IDUM(13)
DIMENSION VP(1000,3)
DO 1 I=1,N
1 READ (6) (V(I,J),J=1,3),(VP(I,J),J=1,3)
MARK=0 & L=1
ENCODE (30,210,VLABEL)
DO 5 J=1,3
VMAX(J)=VMIN(J)=V(I,J) & VPMAX(J)=VPMIN(J)=VP(I,J)
DO 5 I=2,N
VMAX(J)=AMAX1(VMAX(J),V(I,J)) & VPMAX(J)=AMAX1(VPMAX(J),VP(I,J))
VMIN(J)=AMIN1(VMIN(J),V(I,J)) & VPMIN(J)=AMIN1(VPMIN(J),VP(I,J))
5 CONTINUE
IF(IFPLOT(3).EQ.0) GO TO 30
IF(IFPLOT(2).NE.0) GO TO 10
C READ STRESS FROM TAPE
DO 8 I=1,N
8 READ (7) TI,(S(I,J),J=1,6),F1,F2,F3
10 NP=MIN0(NJEDIT,IFPLOT(L+2))
SMAX=SMIN=0
DO 12 J=1,NP
DO 12 I=1,N
SMAX=AMAX1(SMAX,S(I,J)) & SMIN=AMIN1(SMIN,S(I,J))
12 CONTINUE
C PLOT HUGONIQTS
DO 20 J=1,NP
GO TO (21,22,23) L
21 ENCODE (30,211,SLABEL) JEDIT(J) & GO TO 25
22 ENCODE (30,212,SLABEL) JEDIT(J) & GO TO 25
23 ENCODE (30,213,SLABEL) JEDIT(J)
25 ENCODE (30,215,TITLE)XJED(J),IDENT
IF(J.GT.3) GO TO 17
PRINT 240,(TITLE(M),M=1,3),VMIN(J),VMAX(J),SMIN,SMAX
CALL LINSET(VMAX(J),VMIN(J),SMAX,SMIN,VLABEL,SLABEL,TITLE,LINES)
DO 15 I=1,N & IPEN=MIN0(I-1,1)
15 CALL LINPLT(V(I,J),S(I,J),MARK,IPEN) & GO TO 20
17 K=J-3
PRINT 240,(TITLE(M),M=1,3),VPMIN(K),VPMAX(K),SMIN,SMAX
CALL LINSET(VPMAX(K),VPMIN(K),SMAX,SMIN,VLABEL,SLABEL,TITLE,LINES)
DO 18 I=1,N & IPEN=MIN0(I-1,1)
18 CALL LINPLT(VP(I,K),S(I,J),MARK,IPEN)
20 CALL PENEND
GO TO (30,40,50) L
30 IF (IFPLOT(4).EQ.0) GO TO 40
C READ RESULTANT STRESS FROM TAPE
L=2 & DO 32 I=1,N
32 READ (9) (S(I,J),J=1,6)
GO TO 10
40 IF(IFPLOT(5).EQ.0) GO TO 50
C READ DEVIATORIC STRESS FROM TAPE
L=3 & DO 42 I=1,N
42 READ (11) (S(I,J),J=1,6)
GO TO 10
50 RETURN
210 FORMAT (30H SPECIFIC VOLUME (CM3/GRAM) )
211 FORMAT (15HSTRESS IN CELL ,I3,12H (KILOBARS) )
212 FORMAT (19HRESULTANT STRESS J=,I3,8H (KBARS))
213 FORMAT (19HSTRESS DEVIATOR, J=,I3,8H (KBARS))
215 FORMAT (8HHUGONIC X=F7.4,11H CM, IDENT=I4)
240 FORMAT (7H PLOT-- ,3A10.4H V=,F8.5,4H TC ,F8.5,4H S=,F9.4,4H TO ,
IF9.4)
END

```

PLOTTING SUBROUTINE: HUGONIC (complete)

```

      SUBROUTINE TPLOTS(NTX)
C----- THIS ROUTINE PRODUCES STRESS VERSUS DISTANCE GRAPHS FOR DESIRED TEDITs
      COMMON IDENT,X(300,15),S(300,15),XLABEL(3),YLABEL(3),TITLE(3),
      INPT(15),XJB(6)
      COMMON /PLOT/ IPLOT,IFPLOT(6),LINES,IT,NT,IFLAG,IDUM(10)
      NT=MIN0(NT,15) $LT=MIN0(4*EX,IT+NT-1) $ IG=0
      MARK=0 $ IPEN=1 $ IBLANK=0 $ IFS=0 $ SMA=SMI=0,
      IF (IFLAG,LT,0) IFS=1 $ IFLAG=IABS(IFLAG)
C   INDIVIDUAL TEDITs PLOTTED
      ENCODE (30,211,XLABEL)
      DO 100 I=1,NTX
      READ (7) NTED,NC,TIME,NPTS $NPTS1=NPTS+1
      IF (IT,LE,NTED,AND,NTED,LE,LT)10,90
10    IG=IG+1 $ NPT(IG)=NPTS
      DO 13 IP=1,NPTS
      READ (7) X(IP,IG),S(IP,IG),R
      IF (IP,EQ,1) 11,12
11    XMIN=X(IP,IG) $ SMA=SMIN=S(IP,IG)
      IF (IG,EQ,1) XMIN1=XMIN $ GO TO 13
12    XMAX=X(IP,IG)
      SMA=AMAX1(SMA,S(IP,IG)) $ SMIN=AMIN1(SMIN,S(IP,IG))
13    CONTINUE
      ENCODE (30,210,TITLE)IG,TIME,IDENT
      ENCODE (30,212,SLABEL)NC
      SMA=AMAX1(SMA,SMA) $ SMI=AMIN1(SMI,SMIN)
      PRINT 240,(TITLE(M),M=1,3),XMIN,XMAX,SMI,SMA
      CALL LINSET (XMAX,XMIN,SMA,SMI,XLABEL,SLABEL,TITLE,LINES)
      CALL LINPLT(X(1,IG),S(1,IG),MARK,IBLANK)
      DO 15 IP=2,NPTS
15    CALL LINPLT (X(IP,IG),S(IP,IG),MARK,IPEN)
      READ (7) NM,(XJB(M),M=1,6)
      IF (NM,LE,0) GO TO 80
      DO 70 M=1,NM $ XB=XJB(M)
      CALL LINPLT(XB,SMI,MARK,IBLANK)
      SINCR=(SMA-SMI)/75. $ SB=SMI
      DO 70 IN=1,75 $ INK=MOD(IN,2) $ SB=SB+SINCR
70    CALL LINPLT (XB,SB,MARK,INK)
80    CALL PENEND $ GO TO 100
90    DO 91 IP=1,NPTS1
91    READ (7)
100   CONTINUE
      IF (IFLAG,LE,1) GO TO 150
C   SEVERAL TEDITs PLOTTED ON ONE GRAPH
      IF (IG,LT,2) GO TO 145
      IGPLT=MIN0(IFLAG,IG)
      IBEG=1
105   ENCODE (30,220,TITLE)IBEG,IGPLOT,IDENT
      ENCODE (30,221,SLABEL)
      PRINT 240,(TITLE(M),M=1,3),XMIN,XMAX,SMI,SMA
      CALL LINSET(XMAX,XMIN,SMA,SMI,XLABEL,SLABEL,TITLE,LINES)
      CALL LINPLT(X(1,1),S(1,1),MARK,IBLANK)
      LP=MP=1
      DO 130 L=IBEG,IGPLOT
      MP=NPT(L)
      DO 120 IP=MP,NP
      IF (IFS,EQ,1) 120,115
      IF (LP,NE,MP,OR,L,EQ,IG)GO TO 120
      IF (S(IP,L),LT,.9*SMA,AND,S(IP,L+1),GT,(S(IP,L)+1.05)) LP=IP
120   CALL LINPLT (X(IP,L),S(IP,L),MARK,IPEN)
      IF (L,EQ,IG) GO TO 130
      CALL LINPLT (X(LP,L+1),S(LP,L+1),MARK,IBLANK)
      MP=LP
130   CONTINUE
      CALL PENEND
      IF (IGPLOT,GE, IG-1) GO TO 150
      IBEG=IGPLOT+1 $ IGPLT=IGPLOT+MIN0(IFLAG,IG-IGPLOT)
      GO TO 105
145   PRINT 146
150   RETURN
146   FORMAT (23H ONLY ONE TEDIT GRAPHED)
150   FORMAT (15HTEDIT,12,1H,F7.4,11H MUSECS ID=14)
151   FORMAT (13H POSITION (CENTIMETERS) )
152   FORMAT (15HSTRESS AT CYCLE,14,11H (KILOBARS))
153   FORMAT (16H TEDITs 12,6H THRU 12,8H, IDENT=14)
154   FORMAT (13H STRESS (KILOBARS) )
155   FORMAT (17H PLOT-- ,3A10,4H X=,F8.4,4H TO ,F8.4,4H , ,F9.4,4H TO ,
      IF9.4)
      END

```

PLOTTING SUBROUTINE: TPLOTS (complete)



## APPENDIX II

### QUASI-STATIC AND ACOUSTIC DATA

#### 1. Introduction

As an adjunct to the dynamic measurements, a series of quasi-static acoustic measurements were made to assist in characterizing the metals studied. The purposes of these tests were to determine:

- the quasi-static moduli and yield strength,
- the variation of quasi-static properties with specimen thickness,
- the difference in quasi-static properties measured parallel and transverse to the direction of rolling,
- the effect of testing speed on the quasi-static properties, and
- the effect of the sign of the loading (tension or compression) on the properties.

For these purposes an extensive test program was laid out for the five alloys under study. The scope of the quasi-static experiments is partially indicated by the listing of specimens in Tables 13 and 14. Both tensile and compression tests were performed. Some compression tests were conducted on all three directions (parallel and transverse to rolling, and thickness) of the material. Tensile tests were conducted over a wide range of thicknesses and at three testing rates for one thickness.

#### 2. Test Descriptions

##### a. Tensile Tests

The tensile tests were conducted on the usual dog-bone-shaped test specimens instrumented with either strain gages or an extensometer. Two sets of tests were performed: one series at several thicknesses but a constant testing speed of 0.05 in./in./min. and a second series at a single thickness but three testing speeds (0.5, 0.05, and 0.005 in./in./min). The second series was instrumented with both longitudinal and transverse strain gages so that Poisson's ratio could be determined.

The tests were generally conducted with a continuous recording of load and deflection so that Young's modulus, the yield strength, ultimate strength, and breaking strength could be determined.

Table 13

## ALUMINUM: NUMBERS OF SPECIMENS TESTED

Alloy	Thickness (in.)	Compression			Tensile	
		P.*	Tr. <sup>†</sup>	Th. <sup>‡</sup>	p.*	Tr. <sup>†</sup>
6061-T6	1/16				2	2
	1/8			2	2	2
	3/16				2	2
	1/4	3	3	2	(9)	(9)
	3/8				2	2
	1/2	2	2	4	2	2
	3/4				1	1
	1-1/4	1	1	3	1	1
2024-T8	1/16				2	2
	3/32				2	2
	1/8			2	2(9)	2(9)
	3/16				2	2
	1/4	3	2	2		
	3/8				2	2
	1/2	2	2	3	2	2
	3/4				1	1
	1-1/4	1	1	4	1	1

Parenthetical numbers refer to tests conducted at three testing speeds.  
Other tests were conducted at a single speed.

\* Parallel to rolling.

† Transverse to rolling.

‡ Thickness direction.

Table 14

## TITANIUM: NUMBERS OF SPECIMENS TESTED

Alloy	Thickness (in.)	Compression			Tensile	
		P *	Tr <sup>†</sup>	Th <sup>‡</sup>	P *	Tr <sup>†</sup>
Type 50A	1/16				1	1
	1/8			1	(3)	(3)
	3/16	1	1		1	1
	3/8	1	1	2	1	1
	3/4	1	1	3	1	1
	1	1	1	4	1	1
Ti-6Al-4V	1/16				1	1
	1/8			4	(3)	(3)
	1/4		1	4	1	1
	3/4	1	1	3	1	1
	1-1/8	1	1	4	1	1
Ti-13Cr-11V-3Al	1/16				1	1
	1/8			4	(3)	(3)
	1/4	1	1	3	1	1
	3/4	1	1	3	1	1
	1-1/8	1	1	4	1	1

Parentetical numbers refer to tests conducted at three testing speeds.  
Other tests were conducted at a single speed.

\* Parallel to rolling.

<sup>†</sup> Transverse to rolling.

<sup>‡</sup> Thickness direction.

#### b. Compression Tests

The compression tests were conducted on dog-bone-shaped specimens similar to those for tension tests and at the rate of 0.05 in./in./min. The thick portions at the ends of the specimens were provided to give lateral support to prevent buckling. The specimens were instrumented either with an extensometer or a pair of longitudinal strain gages.

The tests were conducted until buckling occurred or until the capacity of the machine was reached. It is believed that all the exhibited yield data represent yielding of the material and not premature buckling.

#### c. Thickness Compression

Specimens about 1 inch thick were manufactured for determining properties in the thickness direction. The specimens were formed by stacking together a number of 1 inch square coupons from each sheet of material. Strain was measured with an extensometer recording the overall compression of the specimen. These specimens were loaded at 0.05 in./in./min.

The load-deflection curves show an initial soft portion as the coupons comprising the specimen are being brought into contact, then a straight elastic region, and finally yielding. Post-yield behavior was not interpreted for these tests.

#### d. Acoustic Tests

Dilatational and shear velocities were measured on 1 inch square coupons from each of the materials. The tests were performed for the thickness direction on all specimen thicknesses, and in all three directions on specimens over 1 inch thick.

### 3. Results of Quasi-Static Tests

A total of 234 static tests was conducted on specimens of the three titanium and two aluminum alloys to characterize the materials. Average magnitudes of the elastic properties determined from the test program are listed in Tables 15 and 16, and the results of the parameter studies are given in Tables 17 and 18. For the titanium there was considerable variability among results from samples of different thicknesses; the

Table 15

## TITANIUM DATA FROM STATIC TESTS (AVERAGE VALUES)

Alloy	Young's Modulus* kbar (psi x 10 <sup>3</sup> )	Plastic Modulus† kbar (psi x 10 <sup>3</sup> )	Yield Strength‡ kbar (psi x 10 <sup>3</sup> )	Ultimate Strength§ kbar (psi x 10 <sup>3</sup> )	Poisson's Ratio
Type 50A	1070 (15,500)	66 (960)	3.5 (50)	4.1 (65)	0.26
Ti-6Al-4V	1210 (17,500)	7 (100)	9.5 (138)	9.6 (139)	0.29
Ti-13Cr-11V-3Al	1040 (15,100)	6 (80)	9.3 (135)	9.4 (136)	0.27

\* Coefficient of variation (standard deviation/mean value) about 2 percent for samples of a single thickness.

† Slope of line from yield point to 1 percent strain. Highly variable; negative values were obtained from alloy Ti-13Cr-11V-3Al in many tests.

‡ An offset of 0.2 percent.

§ Obtained from peak of stress-strain curve before decrease to breaking.

Table 16

## ALUMINUM DATA FROM STATIC TESTS (AVERAGE VALUES)

Alloy	Young's Modulus * kbar (psi x 10 <sup>3</sup> )	Plastic Modulus † kbar (psi x 10 <sup>3</sup> )	Yield Strength ‡ kbar (psi x 10 <sup>3</sup> )	Ultimate Strength § kbar (psi x 10 <sup>3</sup> )	Poisson's Ratio
6061-T6	710 (10,300)	103 (1490)	2.8 (40.7)	3.1 (45.1)	0.32
2024-T8	745 (10,800)	32 (460)	4.4 (63.6)	4.9 (71.0)	0.33

\* Coefficient of variation about 1 percent for specimens of a single thickness.

† Average slope of stress-strain curve from yield to 1 percent strain.

‡ 0.2 percent offset; coefficient of variation up to 1.6 percent for one thickness and direction of rolling, up to 6 percent for all thicknesses.

§ Coefficient of variation of 0.7 percent or less for one thickness and direction of rolling, 3 percent or less for all thicknesses.

Table 17

## STATIC TEST PARAMETER VARIATION FOR TITANIUM

Parameter varied	Young's Modulus, E	Yield Strength, <sup>*</sup> Y	Ultimate Strength, U
Thickness	Marked variation among samples of different thicknesses with a trend toward decreasing modulus with increasing thicknesses	Marked variation among samples of different thicknesses, but no apparent trend attributable to thickness	Marked variation among samples of different thicknesses, but no apparent trend attributable to thickness
Parallel vs transverse to direction of rolling	No significant effect	50A: 20%-30% higher for parallel 6-4: slightly higher for transverse 13-11-3: no significant difference	No significant difference
Tension vs compression	No significant effect	2%-3% higher for compression	(No ultimate strength observed in compression)
Strain rates: 0.005, 0.05, or 0.5 in./in. min	No effect	50A: 13% increase from lowest to highest rate 6-4: 6.5% increase 13-11-3: 4% increase	50A: 9% increase from lowest to highest rate 6-4: 6% increase 13-11-3: 11% increase

\* Offset of 0.2 percent.

Table 18  
STATIC TEST PARAMETER VARIATION FOR ALUMINUM

Parameter Varied	Young's Modulus E	Yield Strength, Y	Ultimate Strength, U
Thickness	No effect	6061: No effect 2024: 10% increase through range of thicknesses	6061: No effect 2024: 10% increase through range of thicknesses
Parallel vs transverse to direction of rolling	No effect	6061: 4% higher parallel 2024: No effect	No effect
Tension vs compression	No significant effect	6061: 4% higher in tension 2024: No effect	(No ultimate strength observed in compression)
Strain rates: 0.005, 0.05, or 0.5 in./in./min.	No effect	No effect	6061: 2% increase with strain rate 2024: No effect

\* Offset of 0.2 percent.



coefficients of variation (standard deviation/mean value) of the yield strength  $Y$  and ultimate strength  $U$  were usually about 5 percent and in some cases 10 percent. This difference is attributed to real variations among specimens, despite the special care taken in acquiring material of controlled quality. The aluminum exhibited a coefficient of variation of 1 to 2 percent for tests at a single thickness and 3 to 6 percent for tests at all thicknesses.

#### 4. Elastic Constants from Acoustic Velocity Measurements

Acoustic velocity measurements were made with samples of the aluminum and titanium materials to determine the elastic constants of the materials at nominally zero stress levels. The tests were conducted by transmitting longitudinal (compressional) and shear pulses through thin specimens and measuring the transit times. These transit times were then used to compute Young's modulus  $E$  and Poisson's ratio  $\nu$  for each material.

The equations used to determine the elastic constants are the usual ones for linearly elastic, homogeneous, isotropic materials. The samples did not qualify as isotropic because their properties were different in the three principal directions: parallel to rolling, transverse to rolling, and in the thickness direction. These differences were small however, and were neglected in the analysis. This neglect is testament to the assumption that wave propagation in one direction is but slightly affected by anisotropy in the other two directions. With the assumption of isotropy we can compute longitudinal and shear acoustic velocities  $C_L$  and  $C_S$  from the travel times of the waves through the samples. These sound velocities are related to the elastic constants as follows:

$$C_L = \sqrt{\frac{E}{\rho} \frac{(1 - \nu)}{(1 - 2\nu)(1 + \nu)}} \quad (106)$$

$$C_S = \sqrt{\frac{E}{\rho} \frac{1}{2(1 + \nu)}} \quad (107)$$

where  $\rho$  is the material density. Equations (106) and (107) can be solved for  $E$  and  $\nu$ , obtaining

$$\nu = \frac{(C_L/C_S)^2 - 2}{2(C_L/C_S)^2 - 2} \quad (108)$$

$$E = 2(1 + \nu) C_S^2 \rho \quad (109)$$

$$E = \frac{(1 - 2\nu)(1 + \nu)}{(1 - \nu)} C_L^2 \rho \quad (110)$$

The measured acoustic velocities and the elastic constants derived therefrom are exhibited in Table 19 for the five alloys tested.

The elastic constants calculated from the sound velocities are not directly proportional to these velocities but are related in a complex manner to the square of the velocities. Because of this complicated relationship, it is not obvious how the uncertainties in the measured velocities contribute to uncertainties in the elastic constants. The following analysis represents an attempt to define the uncertainties in those constants, based on estimated uncertainties in the measured velocities.

The probability distributions for the longitudinal and shear wave velocities were assumed to be normal for convenience in the analysis and for lack of a better assumption. The probability density functions for all the variables are certainly continuous functions. For simplicity in the analysis, however, we approximated distributions of the velocities by a small number of points with equal probability. The points were selected so that the means and standard deviations of the discrete and continuous distributions were equal. Selected points were obtained by dividing the continuous distribution into 10 intervals of equal probability, that is, with equal areas under the probability distribution curve. With this formulation we obtained 10 discrete, equally probable values for each of the two wave velocities. We can combine these to form 100 equally probable values for each of the elastic constants  $E$  and  $\nu$ . The resulting values of  $E$  and  $\nu$  form discrete approximations to

Table 19  
ACOUSTIC VELOCITY MEASUREMENTS

Alloy	Dilatational Velocity (mm/μsec)			Avg.	Shear Velocity (mm/μsec)			Avg.	Elastic Constants		Density (g/cm <sup>3</sup> )
	Direction				Direction				ν	E (kbar)	
	thick.	longit.	trans.		thick.	longit.	trans.				
Aluminum											
6061-T6	6.41	6.48	6.48	6.44	3.18	3.04	3.17	3.15	0.337	725	2.709
2024-T8	6.43	6.38	6.38	6.41	3.17	3.14	3.12	3.16	0.339	745	2.785
Titanium											
Type 50A	6.13	6.12	6.02	6.13	3.13	3.00	2.99	3.10	0.328	1175	4.507
Ti-6Al-4V	6.28	6.14	6.26	6.23	3.27	3.26	3.23	3.24	0.314	1240	4.424
Ti-13Cr-11V-3Al	5.62	5.98	5.97	5.72	2.80	2.79	2.80	2.80	0.332	1025	4.839

the desired continuous distributions. Calculations were made using nominal values for  $C_L$  and  $C_S$ .

The coefficients of variation (standard deviation divided by mean value) of  $C_L$  and  $C_S$  were assumed to be 1 and 2 percent respectively. The resulting coefficients of variation for  $E$  and  $\nu$  are given in Table 20. The mean values of both the elastic constants coincide with those computed from the mean values of  $C_L$  and  $C_S$ . The coefficients of variation are somewhat larger than those for either  $C_L$  or  $C_S$ . In general, we can probably obtain  $E$  and  $\nu$  with somewhat less precision than we can obtain either of the sound velocities.

Table 20

ILLUSTRATION OF VARIABILITY OF ELASTIC CONSTANTS  
DERIVED FROM ACOUSTIC MEASUREMENTS

Measurement*	Mean	Coefficient of Variation <sup>†</sup> (%)
$C_L$ (mm/ $\mu$ sec) <sup>‡</sup>	6.0	1
$C_S$ (mm/ $\mu$ sec) <sup>‡</sup>	3.0	2
$E$ (kbar) <sup>§</sup>	720	3.14
$\nu$ <sup>§</sup>	0.333	2.81

\*  $C_L$  and  $C_S$  are arbitrary; density was taken as 3 g/cm<sup>3</sup>.

<sup>†</sup> Coefficient of variation = standard deviation/mean.

<sup>‡</sup> Assumed.

<sup>§</sup> Computed.

## 5. Titanium Properties Tests by the Manufacturer

The manufacturer, Titanium Metals Corporation of America, supplied a list of test data for each thickness of the titanium alloys. Chemical analyses showed about 0.11 percent O for all three types and 0.02 percent N in Ti-13Cr-11V-3Al titanium and 0.01 percent N in the other two types. The tensile test values supplied are shown in Tables 21, 22, and 23. For the Type 50A (pure alpha) titanium, three samples of each thickness were tested and all values reported in Table 19. The variation of yield among the three samples at each thickness was studied. The coefficient of variation (standard deviation/mean value) at each thickness varied from 5 to 12%. There was a clear trend toward decreasing yield strength with increasing thickness; average yield values varied from 54,000 psi down to 47,000 psi.

Only average strengths from several tests were reported for Ti-6Al-4V and Ti-13Cr-11V-3Al titanium. However, these were differentiated by direction of rolling. For the Ti-6Al-4V alloy, the yield strength was consistently 3000 to 4000 psi higher when tested transverse to the direction of rolling than for parallel to rolling. There was a clear trend of decreasing strength with increasing thickness. The Ti-13Cr-11V-3Al alloy was also stronger in the transverse direction than parallel to the rolling direction. The yield data of this alloy varied considerably from sheet to sheet so that no trend of strength variation with thickness could be established.

Table 21

### MANUFACTURER'S DATA FOR TYPE 50A TITANIUM

Thickness (in.)	Yield Strength (psi x 10 <sup>3</sup> )	Ultimate Strength (psi x 10 <sup>3</sup> )	Elongation (%)
0.0625	56.0, 40.8, 57.3	70.6, 68.7, 71.8	28.0, 26.5, 28.0
0.125	49.9, 48.1, 58.1	66.4, 65.8, 66.8	27.0, 27.0, 29.0
0.1875	47.6, 60.7	72.8, 72.5	26.5, 27.0
0.375	46.5, 44.3, 50.3	68.5, 67.2, 70.2	32.5, 31.0, 34.0
0.750	44.5, 40.8, 49.1	65.0, 63.8, 66.4	36.0, 35.0, 37.0
1.0	46.5, 42.9, 52.3	68.0, 65.5, 69.6	54.5, 53.0, 56.5
Average	49.7	68.0	34.6

Table 22

## MANUFACTURER'S DATA FOR Ti-6Al-4V TITANIUM

Thickness (in.)	Yield Strength		Ultimate Strength		Elongation	
	Parallel	Transverse*	Parallel	Transverse*	Parallel	Transverse*
	(psi x 10 <sup>3</sup> )		(psi x 10 <sup>3</sup> )		%	
0.0625	134.7	137.7	141.5	146.0	14.0	12.0
0.125	132.5	144.7	136.6	145.7	15.0	15.0
0.250	133.7	138.0	139.1	142.6	16.0	14.5
0.750	126.8	130.9	134.3	137.4	15.0	15.5
1.125	121.9	126.1	129.3	131.9	13.5	16.5
Average	129.9	135.5	136.2	140.7	14.7	14.7

\* Parallel and transverse refer to the direction of rolling.

Table 23

## MANUFACTURER'S DATA FOR Ti-13Cr-11V-3Al TITANIUM

Thickness (in.)	Yield Strength		Ultimate Strength		Elongation	
	Parallel	Transverse*	Parallel	Transverse*	Parallel	Transverse*
	(psi x 10 <sup>3</sup> )		(psi x 10 <sup>3</sup> )		%	
0.0625	126.5	135.7	131.7	138.8	20.0	14.5
0.125	129.8	132.2	135.2	137.7	21.0	17.5
0.250	130.6	137.8	141.1	146.8	24.0	12.0
0.750	126.8	132.0	131.8	139.6	24.0	16.5
1.125	125.3	129.5	132.3	136.6	18.5	13.5
Average	127.8	133.4	134.4	139.9	21.5	14.8

\* Parallel and transverse refer to the direction of rolling.

## 6. Discussion of Quasi-Static and Acoustic Results

The elastic properties of aluminum developed from the quasi-static tests agree with those from the acoustic tests to within 1 or 2 percent. A similar comparison for the titanium alloys shows that the values of Young's modulus agree within 3 percent for the Ti-6Al-4V and Ti-13Cr-11V-3Al alloys but that the acoustic modulus is 10 percent high for type 50A. This difference may indicate that the modulus decreases gradually with loading instead of maintaining a constant modulus up to the yield point. The values of Poisson's ratio derived from the acoustic tests are up to 20 percent higher than those derived from the quasi-static tests: this disagreement has not been explained.

A comparison of the manufacturer's test results and our data shows that there is good agreement for yield and ultimate strength for type 50A titanium. Our values for yield strength are about 3 percent higher for the Ti-6Al-4V and Ti-13Cr-11V-3Al alloys but the two sets of values for ultimate strength agree very well.

Our yield strength data on Ti-6Al-4V are about 25 percent below those of Maiden and Green (Ref.8) for the same range of strain rate. This difference suggests that there were important differences in the metals tested by the two organizations, although both sets had the same nominal composition and were fully annealed. The increase in the yield strength was about 3 percent per decade of strain rate according to the results of both organizations.

Our results for 6061-T6 agree with those of Maiden and Green (Ref.8) in exhibiting a yield strength of 41,000 psi and no strain rate effect.

The quasi-static measurements have shown that the aluminum alloys are not strain-rate-dependent in the range of testing speeds used. The titanium alloys show a rate-dependence of strength. This rate effect could lead to a variation of the Hugoniot elastic limit in shock experiments. The noted sample-to-sample variability in properties strongly suggests that any test series should be conducted on material of a single sheet.

AFWL-TR-69-96

This page intentionally left blank.



# REFERENCES

1. Malvern, L. E.; "Propagation of Longitudinal Waves of Plastic Deformation in a Bar of Material Exhibiting a Strain-Rate Effect," Trans. ASME, 73, 203-208 (1951).
2. Zener, C.; Elasticity and Anelasticity of Metals, Univ. of Chicago Press, Chicago, Illinois, 1948.
3. Taylor, J. W.; Rice, H. H.; "Elastic-Plastic Properties of Iron," J. Appl. Phys., 34 (2), 364-371 (1963).
4. Lubliner, J.; "A Generalized Theory of Strain-Rate-Dependent Plastic Wave Propagation in Bars," J. Mech. Phys. Solids, 12, 59-65 (1964).
5. Gilman, J. J.; "Microdynamics of Plastic Flow at Constant Stress," J. Appl. Phys., 36 (9), 2772-2777 (1965).
6. Taylor, J. W.; "Dislocation Dynamics and Dynamic Yielding," J. Appl. Phys., 36 (10), 3146-3150 (1965).
7. Dorn, J. E.; Mitchell, J.; Hauser, F.; "Dislocation Dynamics," Exper. Mech., 5, 353-362 (1965).
8. Maiden, C. J.; Green, S. J.; "Compressive Strain-Rate Tests on Six Selected Materials at Strain Rates from  $10^{-3}$  to  $10^4$  In/In/Sec.," J. Appl. Mech., 33 Series E (3), (1966).
9. Ahrens, T. J.; Duvall, G.; "Stress Relaxation behind Elastic Shock Waves in Rocks," J. Geophys. Res., 71 (18), 4349-4360 (1966).
10. Butcher, B. M.; Munson, D. E.; The Application of Dislocation Dynamics to Impact Induced Deformation Under Uniaxial Strain, SC-DC-67-1402, Sandia Corporation, Albuquerque, New Mexico, April 1967.
11. Johnson, J. N.; Shock Waves in Stress-Relaxing Solids, Ph.D. Thesis, Dept. of Physics, Washington State University, Pullman, Washington, July 1966.
12. Band, W.; unpublished private communication to Johnson, described in Ref. 11.

13. Anderson, G. D.; Alverson, R. C.; Murri, W. J.; Hanagud, S. V.;  
Stress Relaxation in the Shock Compression of Solids, Stanford  
Research Institute, Tech. Rept. No. AFWL-TR-67-24, Contract AF 29(601)-  
7119, May 1967.
14. Wilkins, M. L.; "Le Calcul de la Resistance Dynamique d'un Matériau,"  
IUTAM Symposium on High Dynamic Pressure, Dunod, Paris, 1963.
15. Morland, L. W.; "The Propagation of Plane Irrotational Waves Through  
an Elastoplastic Medium," Phil. Trans. of the Royal Society, Series A  
(1997), 251, 341-383 (June 1959).
16. Al'tshuler, I. V.; Kormer, S. B.; Brazhnik, M. I.; Vladimirov, L. A.;  
Speranskaya, M. P.; Funtikov, A. I.; "The Isentropic Compressibility  
of Aluminum, Copper, Lead, and Iron at High Pressures," Soviet  
Physics JETP (translation), II (4), 766 (1960).
17. Curran, D. R.; "Nonhydrodynamic Attenuation of Shock Waves in  
Aluminum," J. Appl. Phys., 34 (9), 2677 (1963).
18. Barker, L. M.; Lundergan, C. D.; Herrman, W.; "Dynamic Response of  
Aluminum," J. Appl. Phys., 35 (4), 1203-1212 (1964).
19. Buckley, S. N.; Entwistle, K. M.; "The Bauschinger Effect in Super-  
Pure Aluminum Single Crystals and Polycrystals," Acta Metallurgica,  
4, 352 (1956).
20. Jones, O. E.; Holland, J. R.; "Bauschinger Effect in Explosively  
Loaded Mild Steel," J. Appl. Phys., 35 (6), 1771 (1964).
21. Butcher, M.; Canon, J. R.; "Influence of Work-Hardening on the  
Dynamic Stress-Strain Curves of 4340 Steel," Amer. Inst. Aeron.  
Astro. J., 2, (12), 2174 (1964).
22. Erkman, J. O.; Christensen, A. B.; Fowles, G. R.; Attenuation of  
Shock Waves in Solids, Stanford Research Institute, Tech. Rept.  
No. AFWL-TR-66-12, Contract AF29(601)-6734, May 1966.
23. Barker, L. M.; "Fine Structure of Compressive and Release Wave Shape  
in Aluminum Measured by the Velocity Interferometer Technique,"  
Behavior of Dense Media under High Dynamic Pressures Symposium,  
Gordon and Breach, New York, 1968, p. 483.

24. Richtmyer, R. D.; Morton, K. W.; Difference Methods for Initial-Value Problems, 2d Ed., Interscience Publishers, New York, 1967.
25. Von Neumann, J.; Richtmyer, R. D.; "A Method for the Numerical Calculation Of Hydrodynamic Shocks," J. Appl. Phys., 21, 232 (1950).
26. Seaman, L.; Linde, R. K.; Distended Material Model Development, Final Report, SRI Project 6586, AFWL-TR-68-143, Contract No. F29601-67-C-0073, August 1968.
27. Brodie, R. N.; Hormuth, J. E.; The PUFF 66 and P PUFF 66 Computer Programs, Research and Technology Division, Air Force Weapons Laboratory, Kirtland Air Force Base, New Mexico, May 1966.
28. Kolsky, H.; Stress Waves in Solids, Dover Publications, Inc., New York, 1963.
29. Duvall, G. E.; Stress Waves in Inelastic Solids, Springer-Verlag, Berlin, 1964, p. 20.
30. Linde, R. K.; Schmidt, D. N.; "Measuring the Submicrosecond Response of Shock Loaded Materials," Rev. Sci. Inst., 37 (1), 1 (1966).
31. Doran, D. G.; Measurement of Shock Pressures in Solids, in High Pressure Measurement, A. A. Giardini and E. C. Lloyd, eds., Butterworths, Washington, D.C., 1963.
32. Ahrens, T. J.; Rosenberg, J. T.; Ruderman, M. H.; Dynamic Properties of Rocks, Final Report, Stanford Research Institute, Project FGU 4816, DASA 1868, September 1966.
33. Keough, D. D.; Procedure for Fabrication and Operation of Manganin Shock Pressure Gages, Final Report, Stanford Research Institute, AFWL-TR-68-57, Contract AF29(601)-68-C-0038, August 1968.
34. Rice, M. H.; McQueen, R. G.; Walsh, J. M.; "Compression of Solids by Strong Shock Waves," Solid State Physics, Vol. 6, ed., F. Seitz and D. Turnbull, Academic Press, New York, 1958.
35. Fuller, P. J. A.; Price, J. H.; "Dynamic Pressure Measurements to 300 Kilobars with a Resistance Transducer," British J. Appl. Phys., 15, (1964).

36. Keough, D. D.: Pressure Transducer for Measuring Shock Wave Profiles, Final Report, Stanford Research Institute Project 3713, DASA Contract No. DA-49-146-XZ--96, November 1964.
37. Keough, D. D.; Wilkinson, W.: Manganin Wire Shock Transducer Investigation, Final Report, Stanford Research Institute, Project GSU 5344, AFWL-TR-65-170, Contract AF29(601)-6681, December 1965.
38. Van Horn, K. R.; ed., Aluminum (Vol. I, Ch. 5; Vol. III, Ch. 9), American Society for Metals, Metals Park, Ohio, 1967.
39. American Standards Association, Alloy and Temper Designation System for Wrought Aluminum, Report No. ASA H35.1-1962, 1962.
40. Private communication from M. H. Rice of Los Alamos Scientific Laboratory, 1968.
41. Fowles, G. R.; "Shock Wave Compression of Hardened and Annealed 2024 Aluminum," J. Appl. Phys., 32, (8), 1475-1487 (1961).
42. Molchanova, E. K.; Phase Diagrams of Titanium Alloys, translated from Russian by Holbreich et al., Israel Program for Scientific Translations, Jerusalem, 1965.
43. Properties of Ti-6Al-4V, Titanium Engineering Bulletin No. 1, Titanium Metals Corporation of America, Los Angeles, February 1965.
44. Properties of Ti-13V-11Cr-3Al, Titanium Engineering Bulletin No. 9, Titanium Metals Corporation of America, Los Angeles, undated.
45. Harmon, E. L.; "Basic Titanium Metallurgy," DMIC Memorandum 215, Defense Metals Information Center, Battelle Memorial Institute, Columbus, Ohio, September 1966.
46. McQueen, R. G.; Marsh, S. P.; "Equation of State for Nineteen Metallic Elements from Shock-Wave Measurements to Two Megabars," J. Appl. Phys. 31 (7), 1253 (1960).
47. Walsh, J. M.; Rice, M. H.; McQueen, R. G.; Yarger, F. L.; "Shock Wave Compressions of Twenty-Seven Metals. Equations of State of Metals," Phys. Rev. 108 (2), (1957).

48. Isbell, W. M.; Froula, W. H.; Christman, D. R.; "Hugoniot Equation of State and Release Wave Structure of Alpha Titanium to 65 Kbar," Presented at Winter Annual Meeting, American Physical Society, San Diego, December 1968.
49. Jamieson, J. C.; "Crystal Structures of Titanium, Zirconium, and Hafnium at High Pressures," Science, 140, 72-73 (1963).
50. Deribas, A.; Mogilevsky, M.; Sobolenko, T.; "The Effect of Shock and Detonation Waves on the Properties of Some Metals and Alloys," Behavior of Dense Media under High Dynamic Pressures Symposium, Gordon and Breach, New York, 1968.
51. Wong, J. Y.; Linde, R. K.; DeCarli, P. S.; "Dynamic Electrical Resistivity of Iron: Evidence for a New High Pressure Phase," Nature, 212 (5155), 713-714 (1968).

UNCLASSIFIED

Security Classification

## DOCUMENT CONTROL DATA - R &amp; D

(Security classification of title, body of abstract and indexing annotation must be entered when the overall report is classified)

1. ORIGINATING ACTIVITY (Corporate author) Stanford Research Institute Menlo Park, California 94025		2a. REPORT SECURITY CLASSIFICATION UNCLASSIFIED	
2b. GROUP			
3. REPORT TITLE CLASSIFICATION OF MATERIALS BY SHOCK PROPERTIES			
4. DESCRIPTIVE NOTES (Type of report and inclusive dates) May 1967-March 1969			
5. AUTHOR(S) (First name, middle initial, last name) L. Seaman; R. F. Williams; J. T. Rosenberg; D. C. Erlich; R. K. Linde			
6. REPORT DATE November 1969	7a. TOTAL NO. OF PAGES 298	7b. NO. OF REFS 51	
8a. CONTRACT OR GRANT NO. F29601-67-C-0087	9a. ORIGINATOR'S REPORT NUMBER(S) AFWL-TR-69-96		
b. PROJECT NO. 5710	9b. OTHER REPORT NO(S) (Any other numbers that may be assigned this report) Contractor's No.: SRI Project PGU 6736		
c. Subtask No. RAS 1114			
d.			
10. DISTRIBUTION STATEMENT This document is subject to special export controls and each transmittal to foreign governments or foreign nationals may be made only with prior approval of AFWL (WLRX), Kirtland AFB, NM, 87117. Distribution is limited because of the technology discussed in the report.			
11. SUPPLEMENTARY NOTES		12. SPONSORING MILITARY ACTIVITY AFWL (WLRX) Kirtland AFB, NM 87117	
13. ABSTRACT (Distribution Limitation Statement No. 2) A new experimental technique was developed for determining loading and unloading stress-volume paths directly from gage measurements; theoretical models were formulated for stress relaxation and the Bauschinger effect; Hugoniot information was generated from impact experiments on aluminum alloys, titanium alloys, and a woven quartz-phenolic; and the new experimental technique and Bauschinger calculations were applied to the aluminum alloys. The new experimental technique provides for measurement of complete loading and unloading paths rather than the discrete Hugoniot or release points previously obtained. The technique is applicable to the examination of nonsteady-state, nonisentropic flow, yield point phenomena, strain-hardening, the Bauschinger effect, and strain-rate (or stress-relaxation) effects. The technique is based on the entire stress or particle-velocity records obtained from a series of gages embedded in a specimen. Four stress relaxation models were implemented in the SRI PUFF wave propagation code, and computations were made to obtain representative results. The Bauschinger model implemented in the SRI PUFF code exhibits the smooth unloading adiabat and high rarefaction velocity observed in our experiments on 6061-T6 and 2024-T8 aluminum alloys. Experiments with Ti-50A, Ti-6Al-4V, and Ti-13Cr-11V-3Al titanium served to map Hugoniots from 15 to 750 kbar, indicate Hugoniot elastic limits, and show an alpha <sup>1</sup> to omega phase transformation at 50 kbar. Preliminary experiments on a three-dimensional woven quartz phenolic resulted in Hugoniot data from 10 to 200 kbar and indicated a shock-wave structure that is very different from that observed in homogeneous solids.			

DD FORM 1473  
1 NOV 55UNCLASSIFIED  
Security Classification